INVESTIGATIONS OF HEAT POWERED EJECTOR COOLING SYSTEMS

By

XIANGJIE CHEN

BEng, MSc

Thesis submitted to the University of Nottingham

for the degree of Doctor of Philosophy

OCTOBER 2013

ABSTRACT

In this thesis, heat powered ejector cooling systems was investigated in two ways: to store the cold energy with energy storage system and to utilize low grade energy to provide both electricity and cooling effect. A basic ejector prototype was constructed and tested in the laboratory. Water was selected as the working fluid due to its suitable physical properties, environmental friendly and economically available features. The computer simulations based on a 1-D ejector model was carried out to investigate the effects of various working conditions on the ejector performance. The coefficients of performance from experimental results were above 0.25 for generator temperature of 115°C-130 °C, showing good agreements with theoretical analysis. Experimental investigations on the operating characteristics of PCM cold storage system integrated with ejector cooling system were conducted. The experimental results demonstrated that the PCM cold storage combined with ejector cooling system was practically applicable. The effectiveness-NTU method was applied for characterizing the tube-in-container PCM storage system. The correlation of effectiveness as the function of mass flow rate was derived from experimental data, and was used as a design parameter for the PCM cold storage system. In order to explore the possibility of providing cooling effect and electricity simultaneously, various configurations of combined power and ejector cooling system were studied experimentally and theoretically. The thermal performance of the combined system in the range of 0.15-0.25 and the turbine output between 1200W-1400W were obtained under various heat source temperatures, turbine expansion ratios and condenser temperatures. Such combined system was further simulated with solar energy as driving force under Shanghai climates, achieving a predicted maximum thermal efficiency of 0.2. By using the methods of Life Saving Analysis, the optimized solar collector area was $30m^2$ and $90m^2$ respectively for the system without and with power generation. The environmental impacts and the carbon reductions of these two systems were discussed.

ACKNOWLEGEMENTS

I would like to express my sincere appreciations to my supervisors, Prof. Saffa Riffat and Dr. Yuehong Su for their invaluable guidance and supports throughout my research work. I would like to extend great gratitude to Dr. Siddig Omer and Dr. Mark Worall for their academic contributions and practical helps in this research.

I would also like to thank the group of technicians at the Department of Architecture and Built Environment, especially Mr. David Oliver, Mr. David Taylor and Mr. Robert Clarke, without their dedicated helps the experimental works could not be carried out smoothly.

My special gratitude extends to my husband Dr. Zhengxu Wang, my mother and all my great friends. The research work would not be fulfilled without their love, help and contributions.

Dean of Engineering Scholarship, University of Nottingham is highly acknowledged.

CONTENT

NOMENCLATURE

Symbol	Term	Unit
A	Area	m^2
COP	Coefficient of performance	
c_p	Specific heat	kJ/(Kg ^{o}C)
E_x	Heat exchanger effectiveness	
f	Thermodynamic relationship of H_2O refrigerant	
F	Thermodynamic relationship of CO_2 refrigerant	
G	Solar energy irradiation	W/m^2
h	Specific enthalpy	kJ/kg
$\dot{m}$	Mass flow rate	kg/sec
M	Mach number	
P	Static pressure	Pa,Bar
Q	Heat energy	kW
R	Ideal gas constant	
s	Specific entropy	kJ(kg K)
T	Temperature	°C
U	Heat loss coefficient	W/m^2k
V	Volume	m^3
v	Mean steam velocity	
W	Mechanical work	kW

Greeks

α	Ratio between energy provided by exhausted gas and cooling capacity of the evaporator
β	Turbine expansion ratio
λ	Turbine extraction ratio

ω	Entrainment ratio, secondary flow to primary flow
γ	Nozzle area ratio
η	Efficiency
$(\tau\alpha)_e$	Effective transmittance-absorbance product
ζ	Solar collector heat removal factor

Subscripts

a	Ambient condition
aux	Auxiliary heat input
b	Boiler
b-in	Boiler inlet (from turbine)
c	Condenser
cl	Solar collector
com	Compressor
d	Diffuser
e	Evaporator
ej	Ejector cycle
exh	Exhaust gas
gc	Gas-cooler
hyb	Hybrid system
H-in	Chilled water inlet
H-out	Chilled water outlet
isen	Isentropic process
in	Inlet of heat transfer fluid/inlet of the tank
m	Mixing chamber
n	Nozzle

o	Outlet of heat transfer fluid/outlet of the tank
p	Primary flow
pum	Pump
s	Secondary flow
sb	Sub-cooler
st	Cold storage rate/cold discharge rate
t-in	Turbine exhaust inlet
t-out	Turbine exhaust outlet
ta	Tank
tu	Turbine
tot,st	The sum of storage rate which means storage capacity
vc	Vapour compression system

LIST OF FIGURES

LIST OF TABLES

Chapter 1 Introduction

This thesis reports the working performances of various kinds of heat powered ejector cooling systems. Research developments and progresses in ejector technology have been reviewed and updated. The system performances under different working conditions were analyzed theoretically and experimentally. The measured COPs from experiments demonstrated good agreements with the simulation results. The research innovations are focusing on the following several parts: firstly, with the aim to use the ejector to sub-cool the vapour compression system, a novel hybrid ejector and CO_2 vapour compression system was proposed and simulated. Secondly, a novel PCM energy storage system integrated with ejector cooling system was experimentally studied as a method of conserving and utilizing the cold energy from the ejector. Thirdly, aiming at provide both cooling and electricity, a combined power and ejector cooling system was tested with two different configurations. The experimental results of this combined system provided guidance for further system optimization and numerical simulation. Lastly, solar energy was chosen as a renewable energy source to drive the system. Computer programmes were developed to simulate the system performance with hourly changing solar radiation. The economic analysis and environment impact assessment of the combined system were presented.

1.1 Background of ejector cooling system

With the growing concerns about the aggravating primary energy shortage and increasing energy demand, the energy consumption of buildings is at a critical stake. Application of intensive energy conservation methods has stabilized the energy requirements for heating systems. However, the energy consumption for cooling system is still significant. In Europe, the air-conditioned office, commercial and industrial buildings occupy total volume of about 20 million cubic meters[1]. Meanwhile, the energy consumed by space

cooling accounts for 25% of energy costs by buildings [2]. Since the cooling systems are mostly powered by primary energy, such great energy dissipation will be equivalent to 2754 Mtonnes green house gas emissions every year[3].

The current air-conditioning market is dominated by electrically-powered mechanical vapour compression units. Although vapour compression system offers higher system performance, the issues associated with this system have been raised. Due to the significant cooling demands during summer times, the electricity requirements from the vapour compression system always cause huge pressure on the electricity grid. Since most of the power is generated by the combustion of primary energy source (such as fossil fuel or coal). This not only poses threats on the increasingly aggravating energy situation in the world, but also produces green house gases. Moreover, the conventional vapour compression systems use CFCs, HCFCs, and HFCs as working fluids, which have very high global warming potentials (GWP). The possible leakage of such refrigerants can cause global warming and the depletion of ozone layer.

The aggravating energy situations and associated global warming problems have aroused great attentions among researchers during past few decades. To reduce energy consumption as well as the carbon dioxide emissions have become the main focal points for energy intensive industries. Developing more energy efficient and environmental benign cooling systems is therefore the key point for scientific researches.

Ejector cooling system has aroused great interests among researchers during past few decades due to a number of advantages. Firstly, in the commonly used vapour compression system, the refrigerant has to be compressed to higher pressure, requiring in the mechanical energy consumption in the compressor. In the ejector cooling system, the secondary flow can be entrained by the high temperature primary fluid. Thus the pressure of the evaporator can be lifted without consuming mechanical energy.

Secondly, ejector features very few moving parts and less vibration compared with the vapour compression system. This enables simplicity in construction and low maintenance costs. Ejector cooling system is therefore considered as the most promising refrigeration technology.

Thirdly, water can be used as the working fluid in the ejector cooling system. The ozone crisis has caused a major stir in the air conditioning industry and has triggered a reconsideration of the refrigerants in use. Compared with other commonly used refrigerants (HFCs, CFCs, and hydrocarbon fluids), water is inexpensive and has minimal environment impact (zero ozone depletion and global warming potential). Hence, using water as the refrigerant in the ejector cooling system will prevent further damage to the ozone layer.

Moreover, the utilization of low-grade thermal energy (such as industrial waste heat or solar energy) in the ejector cooling system is of great economic and environmental significance. According to [4], the total industrial waste heat is expected to increase dramatically year by year. It is estimated to be 1000 MW by 2010. If not used properly, such great amount of thermal energy could only be emitted to the environment, which exacerbates the global warming problem. Another kind of low-grade energy, solar energy is recommended by the International Energy Agency as "an indigenous, inexhaustible, sustainable and most import-independent resource". In the tropical and subtropical areas, the cooling loads and solar radiation share the same pattern and both reach the summit at summer times. This enables the possibility of driving the ejector cooling system by solar energy. Thus, using low grade energy to power the ejector cooling system could not only meet the rising cooling demands, but also reduce the consumption of primary energy.

Furthermore, the integration of ejector with other systems brings new features to the cooling system and makes it more attractive and competitive. One application is to combine the ejector cooling system with energy storage system. The energy storage system will store

the excessive energy from the evaporator and release it when it is required. If the system is powered by electricity, the peak cooling demand during summer seasons can be shifted to off-peak period or night times to bridge the gap between energy generation and consumption. If the system is run by renewable energy source (such as solar energy or industrial waste heat), the stored energy could be used to provide cooling effect when the energy source is not adequate. The integrated system can therefore operate in a more stable and flexible way with reduced primary energy costs.

Another application is the combined power and ejector cooling system. Such system could not only offer cooling effect, but also generate electricity in the meantime. In some tropical areas, the power generation capacity is still very low. The abundant solar energy throughout the year offers huge potentials for electricity production. If the combined system could be further designed to gear with the electricity grid, the tight power supply during peak hours could be substantially alleviated.

Therefore, the ejector cooling system powered by low grad energy can provide the cooling effect in an environmental friendly and economically feasible way. The combined systems add innovative features to the ejector, with the possibility of energy conservation and power generation. Such characteristics bring new attractions and arouse research interests for the ejector cooling system.

1.2 Research objectives and methodology

This research work investigates various kinds of ejector cooling systems, which could supply cooling effect in sustainable ways. The main research innovations are based on the cold side and the hot side of the systems. From the cold side, the cooling effect provided by the evaporator could be used in two novel ways. One way is to store the excessive cold energy from the evaporator in a designed storage system, and re-use it whenever required. Another way is to explore the potential of sub-cooling vapour compression system with the ejector by

a hybrid ejector and CO_2 vapour compression system. From the hot side, explore the possibility of utilizing low grade energy (such as solar energy or industrial waste heat) to drive the ejector. In the rural tropical area where the solar energy is abundant throughout the year and the electricity generation capacity is very low, a solar-driven combined power and ejector cooling system could be applied to offer both electricity and cooling effect. Based on these concepts, the project will pursue:

1) To investigate the working performance of the ejector cooling system

Computer modelling was carried out on single ejector cooling system. The system was demonstrated and tested experimentally under various operation conditions, i.e. the generator temperatures, condenser temperatures, evaporator temperatures and nozzle exit positions. For boiler temperature of 115-130°C, evaporator temperature of 5-10°C and condenser pressure below 60mbar, the measured COPs were in the range of 0.2-0.5, which showed good agreement with the simulation results.

2) To explore the possibility of sub-cooling vapour compression system with the ejector

A novel hybrid ejector and CO_2 vapour compression system was introduced. The purpose of the hybrid system was to sub-cool the vapour compression sub-system using the cooling effect provided by the ejector. Thermodynamic simulations of two sub-systems and the hybrid system were presented and compared.

3) To store the cold energy from the evaporator with energy storage system

From the cold side, PCM storage system was integrated with the evaporator to store the cold energy. Experiments were conducted under various operation conditions, i.e, heat

transfer fluid with different flow rates, different heat transfer methods. Effectiveness-NTU methods were applied for characterizing the cold storage system.

4) To power the system with solar energy

From the hot side, solar energy was modelled as the main driving force for ejector cooling system under the summer climatic conditions in Shanghai, China. The intermittent characteristics of solar energy were simulated with hourly changing solar radiation inputs. Different solar collector areas and tank sizes were investigated. The life cycle saving analysis was performed to optimize the system.

5) To investigate the possibility of combined power and ejector cooling system

When the energy source is abundant to power the ejector, the excessive energy can be used to drive a turbine which can convert low grade energy into electricity. Based on existing ejector cooling system, two different configurations were investigated experimentally. The testing results provided guidance for the simulation process of the combined system, which carried out with various heat source temperatures, turbine expansion ratios and condenser temperatures. The performance of the combined system driven by solar energy was simulated numerically under hourly changing solar energy. The results of economic analysis and environmental impact assessment were presented.

1.3 Structure of thesis

This thesis is organized in eight chapters, including:

Chapter 2 Literature reviews

This chapter reviews recent development in relevant technical areas, including the performance characterization of ejector cooling system, ejector geometric optimization, various system performance enhancement methods for ejector cooling system and the

integration of combined power and ejector cooling system. Recent development in PCM thermal storage system is discussed as well. The innovations and shortcomings of these technologies are compared and addressed.

Chapter 3 Simulation of ejector cooling system and case study of hybrid ejector and vapour compression system

In chapter 3, the working performance of the ejector cooling system under various operation conditions (generator, condenser and evaporator temperatures) with five different working fluids (water, methanol, ethanol, HFE7000 and HFE7100) are simulated and compared. With the aim to use the ejector to sub-cool the vapour compression system, a novel hybrid ejector and CO_2 vapour compression cooling system is proposed. Thermodynamic simulations of two sub-systems and the hybrid system are presented. The performance of hybrid system is compared with each of the single system.

Chapter 4 Experimental investigations of ejector cooling system

Experimental investigations of ejector cooling system are carried out under various operating conditions. The system performances of ejector cooling system under various generator temperatures, condenser pressures and evaporator temperatures are tested. The effects of nozzle exit plan on the system performance are disused. The experimental results are compared and verified with simulation outcomes.

Chapter 5 Experimental investigations of PCM cold storage system integrated with ejector cooling system

In chapter 5, experimental investigations on the operating characteristics of cold storage system integrated with ejector cooling system are described. In order to enhance the heat transfer between the PCM and heat transfer fluid (HTF), two tube configurations (with and without fins) are tested and compared. The performance parameters, such as the temperature inside the PCM container, inlet and outlet temperature of HTF, cold storage rate and cold

storage capacity are measured at various mass flow rates. Effectiveness-NTU (number of transfer unit) methods are applied for characterizing the cold storage system.

Chapter 6 Theoretical and experimental investigations of combined power and ejector cooling system

Two different configurations of combined power and ejector cooling system are tested experimentally. Based on the experimental outcomes, computer simulation of the combined system is conducted. The system performances of five different working fluids are simulated. Thermal performance of the combined system and the turbine output are analyzed under various heat source temperatures, turbine expansion ratios and condenser temperatures.

Chapter 7 Modelling and economic analysis of solar-driven ejector cooling system with and without the power generation system in Shanghai

With solar energy as the main driving force, a computational model is developed to perform hourly simulations of solar-driven ejector cooling system with and without power generation under the climatic condition of Shanghai. Various evacuated solar collector areas and storage tank volumes are compared. Life Saving Analysis is applied to optimize the system dimension in order to determine the least cost method to meet the energy demands. The environmental impacts and the carbon reductions of these two systems are discussed.

Chapter 8 Conclusion

This chapter includes the summary and conclusions of the research works. Potential research works on the relevant topics are also suggested.

Chapter 2 Literature Review

Ejector was first invented by Sir Charles Parsons around 1901 for removing air from a steam engine's condenser [5]. Since then, the researches on ejector technology are broad and productive. A great number of ejector models have been proposed and optimized in order to investigate the mixing process of primary fluids and secondary fluid. In the late 20^{th} century, research emphases have been placed on the enhancement of system performance. Recent few decades have seen great developments in the integration of ejector with other systems.

This chapter reviews recent decade's development in relevant technical areas, including the performance characterization of ejector cooling system, ejector geometric optimization, various system performance enhancement methods for ejector cooling system and the integration of combined power and ejector cooling system. Recent developments in PCM thermal storage system are discussed as well. Finally, the working principles and representative case studies of two other cooling cycles (desiccant and absorption) are reviewed. The advantages and disadvantages of these cooling cycles are summarized and compared with ejector cooling cycle.

2.1 Ejector cooling System

Conventional vapour compression cooling cycles are usually driven by electricity. Power generation requires huge consumption of primary energy, often in the form of coal and fossil fuel. This results in air pollution and emission of green house gases, and posing threats to the environment. Ejector cooling systems are more attractive compared with vapour compression system. It can be powered by the low-grade thermal energy, helping to save primary energy and reduce CO_2 emission. Furthermore, with the advantage of simplicity in construction and low maintenance costs, ejector cooling system is considered as the most reliable cooling technology.

However, due to its relatively low coefficient of performance, ejector cooling system has yet to achieve a dominant position in the market of cooling system. In order to promote the use of ejector in cooling, many researchers have been engaged in enhancing the performance of ejector system. Based on the published review paper [6], this section summarizes research progress and development in ejector technology in the last decade, with emphasis on the various combinations of ejectors with other cycles.

2.1.1 Performance characterization of ejector cooling system

A schematic view of a typical ejector is shown in Figure 2-1. Normally, an ejector consists of four principal parts, the primary nozzle, the mixing chamber, the ejector throat and the subsonic diffuser. High pressure primary fluid, expands and accelerates through the primary nozzle, it fans out with supersonic speed to create a very low pressure region at the nozzle exit plane and hence in the mixing chamber. The high-velocity primary stream entrains the secondary fluid into the mixing chamber. The combined streams are assumed to be completely mixed at the end of the mixing chamber and the flow speed is supersonic. A normal shock wave is then produced within the constant-area section, creating a compression effect, and the flow speed is reduced to subsonic value. Further compression of the fluid is achieved as the combined streams flow through the subsonic diffuser section.

Several parameters are used to describe the performance of an ejector. The working performance of cooling system is often measured by the coefficient of performance (COP), defined as the ratio between the cooling capacity at the evaporator and energy input at the boiler and pump.

$$\text{COP} = \frac{\text{Cooling effect at the evaporator}}{\text{Energy input at the boiler and pump}} = \frac{Q_e}{Q_b + W_{pum}}$$

Where, Q_e and Q_b are the cooling capacity at the evaporator and energy input to the generator, and W_{pum} is work consumed by the mechanical pump.

As the energy input at the pump is usually negligible (typically less than 1% of the generator heat input), it is often not taken into account, and the COP is then calculated as the ratio of the cooling capacity at the evaporator and the heat input at the boiler.

$$COP = \frac{Q_e}{Q_b}$$

For cooling applications, the most important parameters are defined in terms of entrainment and expansion ratios. The entrainment ratio (ω) is the mass flow rate of secondary flow to primary flow. The expansion ratio is defined as the ratio of primary pressure to secondary pressure. The entrainment ratio is related to the energy efficiency of a cooling cycle and the expansion ratio limits the temperature at which heat can be rejected. For a given primary pressure and secondary pressure, the highest entrainment ratio will be achieved when compression ratio is minimised.

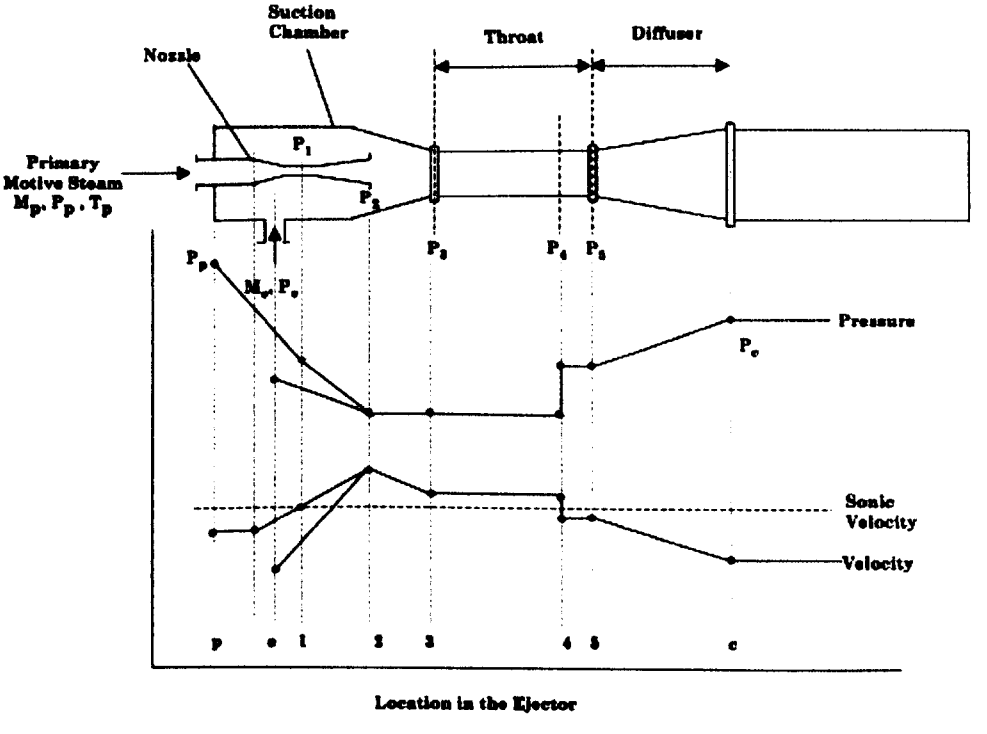

Figure 2-1 Schematic diagram of a typical supersonic ejector[7]

2.1.1.1 Operating Conditions

The operating conditions at various points (boiler, condenser and evaporator) are important parameters which affect the ejector's working performance.

The experimental studies carried out on the ejectors refrigerator [8] showed that, at each setting of boiler and evaporator operating condition, the operation of the ejector can be categorized into three regions (as shown in Figure 2-2): double choked flow in the mixing chamber, primary chocking flow and reversed flow. When the ejector is operated under the "critical condenser pressure", COP and cooling capacity remain constant. Further increase in condenser pressure above the critical condenser pressure moves the thermodynamic shock wave into the mixing chamber and prevents secondary flow from reaching sonic velocity. Upstream conditions can now be transmitted downstream, which results in a reduction in secondary flow, entrainment ratio and COP. Eventually, secondary flow drops to zero, the ejector loses its function and primary flow will reverse back into the evaporator.

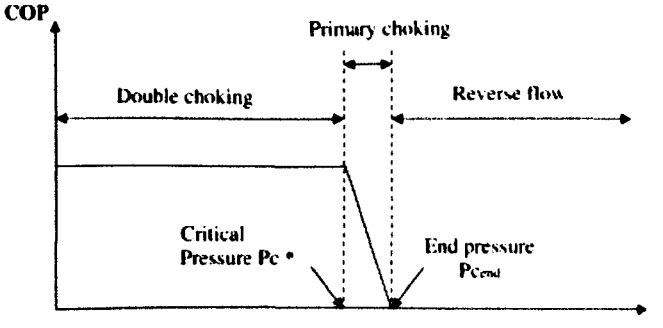

Figure 2-2 Operational modes of an ejector [7]

Recent years, many researchers have been focused on analyzing the effect of various operation conditions on the ejector working performance. Some of the representative works have been summarized in Table 2-1.

Table 2-1 Experimental results of ejector cooling system under different operating conditions

Reference	Cooling capacity	Working fluid	T_e(°C)	T_c(°C) or P_c	T_b(°C)	COP	Conclusion
Chunnanond and Aphornratana[9]	3kW	water	5-15	22-36	110-150	0.28-0.48	1) A decrease in the boiler pressure caused the cooling capacity and COP to rise and the critical condenser pressure was reduced. 2) An increase in the evaporator pressure increased the critical condenser pressure, cooling capacity and COP, which sacrificed with the desired cooling temperature.
Selvaraju and Mani[10]	0.5kW	R134a	2-13	26-38	65-90	0.03-0.16	1) $COP_{critical}=-0.375976R_d-0.284386R_c+0.242682\Phi+0.933787$ (R_d=driving pressure ratio, R_c=compression ratio, Φ=ejector area ratio) 2) For given condenser and evaporator temperatures, every ejector with particular configuration has an optimum boiler temperature, at which the maximum COP can be obtained.
Sankarlal and Mani[11]	2kW	ammonia	5-15	30-36	62-72	0.12-0.29	COP increased with increase in expansion ratio and decreased in compression ratio
Chaiwongsa and Wongwises [12]	1.8kW-3kW	R134a	8-16	26.5-38.5	50-60	0.3-0.48	Cooling capacity varied inversely with the heat sink(where condenser rejects heat to the cold water) temperature while it varied identically with the heat source(where evaporator is supplied by using hot water) temperature
Yapıcı et al. [13]	2kW	R123	0-14	108kPa-142kPa	83-103	0.12-0.39	1) Optimum nozzle exit position was 5mm outwards from the mixing chamber 2) Generator temperature higher than 97°C resulted in constant cooling capacity but lower COP.
Ma et al. [14]	5kW	water	6-13	25mbar-65mbar	84-96	0.17-0.32	1) Increase the boiler temperature does not always accompany by increase in system efficiency. Maximum cooling capacity was found at boiler temperature around 90°C. 2) Spindle can help to control ejector's primary flow and achieve fine tuning for system operation.

2.1.1.2 Working fluids

The choice of the appropriate working fluid plays an indispensable role in the design of the ejector cooling system.

Based on their chemical composition, the working fluids can be classified into the following categories:

(1) Halocarbon group, e.g. R11, R113, R114, R134a, R245ca, R245fa and R152a.

(2)Hydrocarbon group, e.g. methane (R50), ethane (R170), propane (R290), cyclopropane (RC270), butane (R600), isobutene (R600a), and ethylene glycol.

(3) The compound refrigerants, e.g. R407a, R407b, and R410a.

(4) Natural refrigerants, e.g. air, water (R718), carbon dioxide (CO_2) and ammonia (R717).

The ozone crisis has caused a major stir in the cooling industry and has triggered a critical look at the refrigerants in use. Commercial widely used working fluids, such as CFCs, HCFCs and HFCs, allow more ultraviolet radiation into the earth's atmosphere by destroying the protective ozone layer and thus contributing to the greenhouse effect and global warming.

Hence, many working fluids suggested in previous work for ejector are now, forbidden due to their environmental effects, such as R11, R12, R113, or R114. New refrigerants are now studied, for example, halocarbon compounds (R134a, R152a, R245fa, etc) and hydrocarbon compounds (R290, R600, R600a), carbon dioxide (R744) and ammonia. The basic physical properties of the mostly studied refrigerants have been summarized in Table 2-2.

Table 2-2 Physical properties of working fluids for ejector cooling system

	Boiling point at 1atm (°C)	Pressure at 100 °C (KPa)	Molecular mass (Kg/kmol)	Latent heat at 0 °C (KJ/Kg)	Global warming potential (GWP)	Ozone depletion potential (ODP)	Wet/dry vapour	Reference
R123	27.9	787	152.39	176.8	0.02	0.016	Dry	[13, 15-19]
R141b	32.1	677	116.9	129.4	0.15	0	Dry	[20-27]
R134a	-26.1	3972	101.03	190.9	0.26	0.020	Wet	[10, 12, 15, 22, 25, 28-37]
R600a	-0.5	2016	58.12	374.3	<10	0.043	Dry	[28, 38-40]
R290	-42.1	2332	44.1	357.2	3	0	Wet	[28]
R718b(water)	100.0	101	18.02	2257.0	0	0	Wet	[8, 9, 14, 41-44]
R717(ammonia)	-33.34	6264	17.03	1369	0	0	Dry	[11, 15, 45-47]

Cizungu et al.[15] simulated the ejector refrigerator with various refrigerants, including R123, R134a, R152 and R717. It was found that, for the same ejector at condenser temperature of 35°C and evaporator temperature between -6°C and 15°C, R134a and R512a were suitable for 70–85°C heat sources and ammonia was suitable for the heat source temperature higher than 90°C.

An analysis of ejector refrigerator with environmental friendly refrigerants was implemented by Selvaraju et al. [28]. Comparisons on performance of ejector with five working fluids, R134a, R152a, R290, R600a and R717 were made. Among those selected refrigerants, R134a proved to yield a better performance and higher critical entrainment ratio. A similar experimental analysis on a solar assisted ejector cooling system was presented by Nehdi et al. [21] with R134a, R141b, R142b, R152a, R245fa, R290, R600 and R717 as refrigerants. Comparative calculations showed that R717 offered the highest COP followed by

R152a, R134a and R290. However, simulation carried out by Roman[38] with low ecological impact refrigerants indicated that R290 demonstrated better performance, which followed by R152a and R134a, and hydrocarbon refrigerant R600a and R600 at the end.

R245fa and R123 were taken as refrigerants by Eames et al. [48] and Yapici et al. [13] in experimental studies on ejector refrigerators, respectively. The results indicated that both R245fa and R123 were practical working fluids for jet-pump cooling systems.

A solar-driven ECS with R600a as refrigerant was studied by Pridasawas et al. [39]. And COP of the cooling subsystem was about 0.48. Boumaraf et al. [40]carried out a simulation programme on an ECS, with R142b and R600a as refrigerants. It was demonstrated that R142b produced better performance of the system. As R142b is a heavier fluid than R600a, this further supported the conclusions made by Holton et al. [49] that an ejector performed better with high molecular weight fluid.

Using water as the working fluid for an ejector refrigerator provides many advantages. Its extremely high heat of vaporization causes a low circulation rate for given cooling capacity. Therefore, low mechanical power is required for the pump. Water is inexpensive and has minimal environment impact (zero ozone depletion and global warming potential). However, there are some drawbacks. Using water as a refrigerant limits the cooling temperature to above 0°C and the system must be under vacuum condition. Moreover, water has very large specific volume at typical evaporator conditions and to minimize the pressure loss, pipe diameter must be large to accommodate the large volume flow rate. Recently, Butterworth et al. [41] studied the feasibility of using high-pressure water as driving fluid in an ejector cooling system. With the high-pressure water available from vertical pipelines in deep mine shafts, he concluded that the system performance improved as the motive water pressure increased.

2.1.2 Recent development in ejector geometric optimization

In order to make the ejector system more economically attractive, a number of researches have investigated the optimization of the ejector geometry on system performance.

2.1.2.1 Area Ratio

An important non-dimensional factor affecting ejector performance is the area ratio γ between primary nozzle and constant area section. Flow emerges from the primary nozzle and maintains its definition as primary fluid for some distance. The secondary fluid is entrained into the region between the primary fluid and the ejector wall. If an ejector of fixed primary pressure, secondary pressure and nozzle geometry is considered, increasing the mixing section area will result in a greater flow area for the secondary stream. The entrainment ratio will therefore increase but since the compression work available from the primary flow is unchanged, the ejector is unable to compress to higher discharge pressures.

Researchers have carried out theoretical and experimental investigations to analyze the effect of area ratio of ejector's working performance, which is summarized in Table 2-3.

Table 2-3 Results on the ejector's area ratio with different working conditions

Reference	Method	Working fluid	Area ratio	COP	T_e(°C) or P_e	T_c(°C) or P_c	T_b(°C) or P_b	Conclusion
Yapici et al. [13]	Experiment	R123	6.5-11.5	0.29-0.41	10°C	125kPa	83-103°C	1) The optimum area ratio nearly linearly increased with the generator temperature in the studied range. 2) For a given ejector area ratio, there existed an optimum generator temperature at which maximum COP was obtained for the ejector cooling system.
Jia et al.[29]	Experiment	R134a	2.74-5.37	0.14-0.35	4.43bar	7.8bar	17.5-16.5bar	1) Optimum area ratio was found between 3.69 and 4.76, with maximum COP in the range of 0.24 to 0.30. 2) For given operating conditions, the cooling capacities were related to area ratios as well as nozzle diameters while COPs depend only on area ratios.
Cizungu et al.[45]	Numerical modelling	Ammonia	4-12	0.24-0.34	4.5°C	32°C	80-130°C	There exited a quasi linear dependence between γ_A and the driving pressure ratio (pressure ratio of boiler to condenser).
Varga et al.[42]	CFD modelling	Water	13.5-26.4	0.18-0.38	10°C	4.25-5.63kPa	70.1-101kPa	By changing the spindle position, the effective nozzle area can be adjusted and an optimal γ_A can be adjusted with a single ejector.
Ma et al. [14]	Experiment	Water		0.17-0.32	10°C	25mbar-65mbar	84-96°C	

2.1.2.2 Nozzle Exit Position (NXP)

The nozzle exit position (NXP) inwards or outwards the mixing chamber is known to affect both the entrainment and pressure lift ratio of ejectors. In the experimental studies [9, 12, 17] and CFD simulations [20, 50-54], it was demonstrated that moving the nozzle exit into the mixing chamber reduced COP and cooling capacity. Recently, Eames et al. [48] found a clear optimum of the entrainment ratio (40% increase) at 5mm from the entrance of the entrainment chamber. In this case the ejector tail was designed by the constant momentum rate change (CMRC) method and R245fa was used as working fluid. Similar conclusions can be found from numerical investigations carried out by Varga et al. [55] and Zhu et al. [56]. CFD modelling results from Varga et al. [55] indicated that an optimum entrainment ratio of 0.33 can be achieved when NXP was 60mm downstream. Zhu et al. [56] reported that the optimum NXP was not only proportional to the mixing section throat diameter, but also increased as the primary flow pressure rises. The authors also pointed out that the ejector performance was very sensitive to the converging angle θ of the mixing section. When NXP was within its optimum range, the optimum θ was in the range of 1.45-4.2°. A relative larger θ was required to maximize ejector performance when the primary flow pressure rised.

In contrast, CFD analyses of Rusly et al. [20] and Pianthong et al. [8] showed that NXP only had a small influence on entrainment ratio. In the first case, a 20% variation in NXP was considered in an ejector using R141b as working fluid. Compared to the base model, moving the nozzle towards the constant area section caused λ to decrease, while moving it in the other direction λ remained practically unchanged. The authors claimed that the optimum NXP of 1.5 diameters of the constant area section produced better performance. Pianthong et al. [8] varied NXP in the range of -15 to 10mm from the mixing chamber inlet. The entrainment ratio increased slightly as NXP was moved further from the inlet section.

Optimum primary nozzle position or converging angle cannot be predefined to meet all operating conditions. When the operating conditions are different from the design point, the NXP should be adjusted accordingly to maximize the ejector performance. An ejector with movable primary nozzle can provide a flexible NXP when the conditions are out of the design point. This was first presented by Aphornratana and Eames[57]. Recently Yapici et al. [13] carried out an experimental investigation on an ejector refrigerator with movable primary nozzle. The author concluded that the optimum primary nozzle exit should be -5mm from the mixing chamber inlet.

Due to the varying nature of the operation conditions as well as the different ejector geometries, no general agreement can be achieved among various researches.

2.1.3 Solar-driven ejector cooling system

With the ability of harnessing solar energy, the solar-driven ejector cooling system is less energy demanding and more environmental friendly in comparison with conventional vapour compression cooling system. However, due to the intermittent feature of solar energy, the unstable heat gains from solar sources inherently affect the operation of solar-driven ejector cooling system. Thus, thermal storage system integrated with solar-driven ejector cooling system is becoming a hot research topic.

2.1.3.1Conventional solar-driven ejector cooling system

Conventional solar-driven ejector cooling system has been widely studied during past decade. Heat from the solar collector is carried by the intermediate medium and transferred to the refrigerant by the boiler. The heat transfer mediums should have the boiling point higher than the possible temperature in the system, low viscosity and good heat transfer properties.

Recent years' experimental and theoretical simulation results on solar-driven ejector cooling system are summarized in Table 2-4.

Table 2-4 Operating conditions and system performances of solar-driven ejector systems

Reference	Area	Solar radiation (w/m^2)	Cooling capacity (kW)	Working fluid	T_e(°C)	T_c(°C)	T_b(°C)	Solar collector area (m^2)	COP
Varga et al. [43]	Mediterranean countries	800	5	water	5-15	30-35	90-110	50	0.1-0.55
Alexis and Karayiannis [30]	Athens	536-838	-	R134a	-10-0	32-40	82-92	-	0.035-0.199
Ersoy et al. [18]	Turkey	178.3	3.2	R123	12	30	85	21	0.197
Pridasawas and Lundqvist [39]	Bangkok	600-900	3.5	R600a	5-15	5°C above ambient	70-120	50	0.35-0.48
Vidal et al. [22]	Brazil	-	10.5	R141b	8	32	80	80	0.39
Huang et al. [23]	-	700	10.5	R141b	8	32	90	68	0.5

2.1.3.2 Solar-driven ejector cooling system with thermal storage system

During some adverse weather conditions, the cooling capacity provided by available solar energy cannot be essentially matched with the cooling demand. Taken this into consideration, energy storage technology was applied in solar-driven ejector cooling system. Two kinds of thermal storage are considered: hot storage-high temperature energy from the solar collectors, and cold storage-low temperature energy from the evaporator.

Guo and Shen[58] numerically investigated a solar-driven air conditioning system with hot storage for office buildings. With generator temperature of 85°C, evaporator temperature of 8°C and condenser temperature varying with ambient temperature, the average COP was 0.48. It was concluded that the system could save approximately 75% of the electricity used for conventional air conditioning under Shanghai's climatic conditions.

In contrast, Pridasawas and Lundqvist[39] reported that the size of the hot storage tank didn't improve significantly the performance of the system. Hence, cold storage was

recommended by Bejan et al. [59]. Diaconu et al. [60] analysed a simulation on solar-assisted ejector cooling system with cold storage over one year in Algeria. Compared to that without cold storage, the annual energy removal of the system with cold storage achieved higher values. In order to provide better compliance with varying ambient conditions, a variable geometry ejector with cold storage was investigated by Dennis et al. [61]. The annual cooling simulation results concluded that a variable geometry ejector was able to increase system COP by 8-13% compared to a fixed geometry ejector. The modelling further showed that the solar collector area may be decreased if a cold storage was used.

Worall et al. [96] and Eames et al. [62, 63]carried an experimental investigation of a novel ejector cooling cycle with thermal ice storage system (as shown in Figure 2-3). Ice was formed in the evaporator vessel under normal operation and acted as a coolth storage medium. The low evaporator temperature resulted in a relatively low COP of 0.162 during experiments.

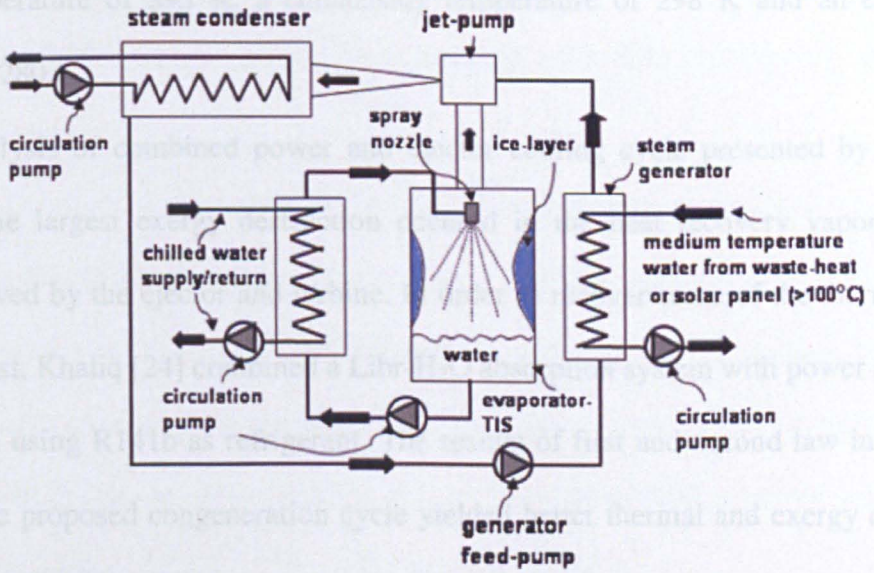

Figure 2-3 Schematic diagram of ejector cooling system with thermal ice storage [61]

2.1.4 Combined power and ejector cooling system

Recently, many combined power and cooling cycles have been proposed to make better use of low grade heat sources. Zhang and Lior [64] discussed the combined power and cooling cycles with both parallel and series-connected configurations. However, the system

operated at temperatures about 450 °C, which is incompatible with low temperature heat sources.

Similarly, Alexis et al.[65] studied a combined power and ejector cooling cycle in which extracted steam from the turbine in Rankine cycle was used to heat the working fluid in an independent steam ejector cooling cycle. Rankine cycle and steam ejector cooling cycle produced electrical power and cooling capacity, respectively. Computer modelling results showed that when the ratio between electrical power and heat transfer rate was varied between 0.1 and 0.4, the ratio between electrical power and cooling capacity was varied between 0.23 and 0.92.

A combined power and ejector cooling system with R245fa as working fluid was presented by Zheng et al. [66]. Simulation results showed that a thermal efficiency of 34.1%, an effective efficiency of 18.7% and an exergy efficiency of 56.8% could be obtained at a generator temperature of 395 K, a condensing temperature of 298 K and an evaporating temperature of 280 K.

Exergy analysis of combined power and ejector cooling cycle presented by Wang[67] showed that the largest exergy destruction occured in the heat recovery vapor generator (HRVG) followed by the ejector and turbine. In order to recover some of the thermal energy from the exhaust, Khaliq [24] combined a Libr-H_2O absorption system with power and ejector cooling system using R141b as refrigerant. The results of first and second law investigation showed that the proposed congeneration cycle yielded better thermal and exergy efficiencies than the cycle without absorption system. However, no experimental results were available.

Godefroy et al. [68] designed a small CHP-ejector trigeneration system which combined heat and power (CHP) to drive an ejector cooling cycle. The system (shown in Figure 2-4) consisted of a CHP unit and an ejector cooling cycle. The design had been tested and validated by a model based on the real fluid properties. The results showed that this system

offered an overall efficiency around 50% and would have an almost neutral effect on overall CO_2 emissions.

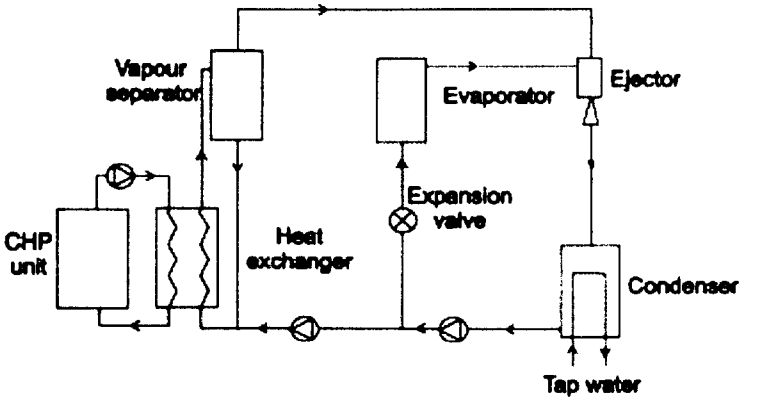

Figure 2-4 Schematic diagram of a CHP-ejector system [66]

2.1.5 Multi-ejector cooling system

Although the single stage ejector cooling system is simple, it is difficult to keep the system running at optimum conditions due to the variation of working conditions. Ambient temperatures above design conditions or lower generator temperatures often lead to operational difficulties. Attempts have been made to solve this problem by using multi-components ejectors.

A schematic view of a solar-powered bi- ejector cooling system designed by Shen et al. [69] is shown in Figure 2-5. In this system, an ejector (injector) replaces the mechanical pump to promote pressure of the liquid condensate and conveys the condensate back to the generator. The authors studied the performance of this system with different refrigerants using numerical modelling. The result showed the best overall system COP achieved was 0.26 with R717 as the refrigerant.

In the proceeding work, Wang and Shen[70] took considerations of the effect of injector structures on the system performance. And the previous 1-D flow model was replaced by a new injector thermodynamic model considering the real fluid's thermal properties. They concluded that an optimum COP of 0.132 was achieved.

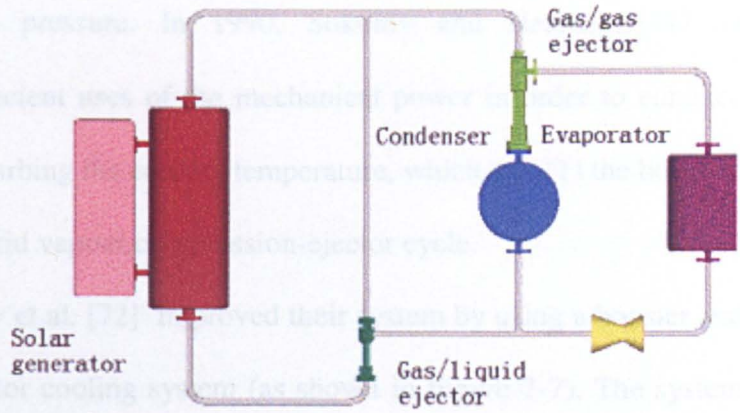

Figure 2-5 Schematic diagram of solar-powered bi-ECS [67]

Yu et al. [32] proposed an ejector cooling system with an additional liquid-vapour ejector pump, as shown in Figure 2-6. This additional ejector pump was applied to entrain the mixing vapour from the ejector, which acts as secondary flow for ejector pump. In this case, the backpressure of the ejector can be reduced by the ejector-pump, and then the entrainment ratio and COP of the system could be increased. Simulation results showed that, compared with conventional ejector cooling system at same working conditions, the COP was increased by 57.1% and 45.9%, with R152a and R134a respectively as refrigerants.

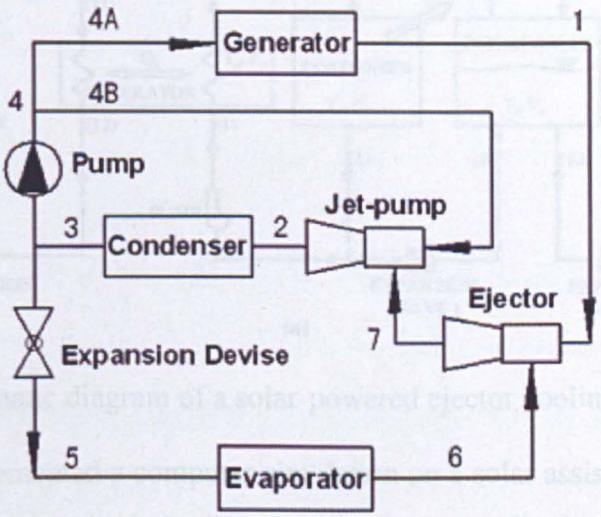

Figure 2-6 Schematic diagram of an ejector cooling system with additional ejector pump [30]

2.1.6 Application of ejector cooling system combined with other systems

Since the system performance of ejector cooling system is determined by ejector entrainment ratio and operating conditions, one way to enhance the performance is to increase

the secondary flow pressure. In 1990, Sokolov and Hearshgal[71], introduced new configurations of efficient uses of the mechanical power in order to enhance the secondary pressure without disturbing the cooling temperature, which are: (1) the booster assisted ejector cycle and (2) the hybrid vapour compression-ejector cycle.

Recently, Sokolov et al. [72] improved their system by using a booster and inter-cooler in a solar-powered ejector cooling system (as shown in Figure 2-7). The system consisted of a conventional compression and ejector sub-cycles with an intercooler as an interface between them. The system operated at 4°C evaporator temperature and 50°C condenser temperature, with cooling capacity of 3.5kW. The overall system COP could reach up to 0.5. The group later revised their work [73] by substituting the refrigerant of R114 with R142b. The results indicated that R142b provided higher efficiency than that operating with R114.

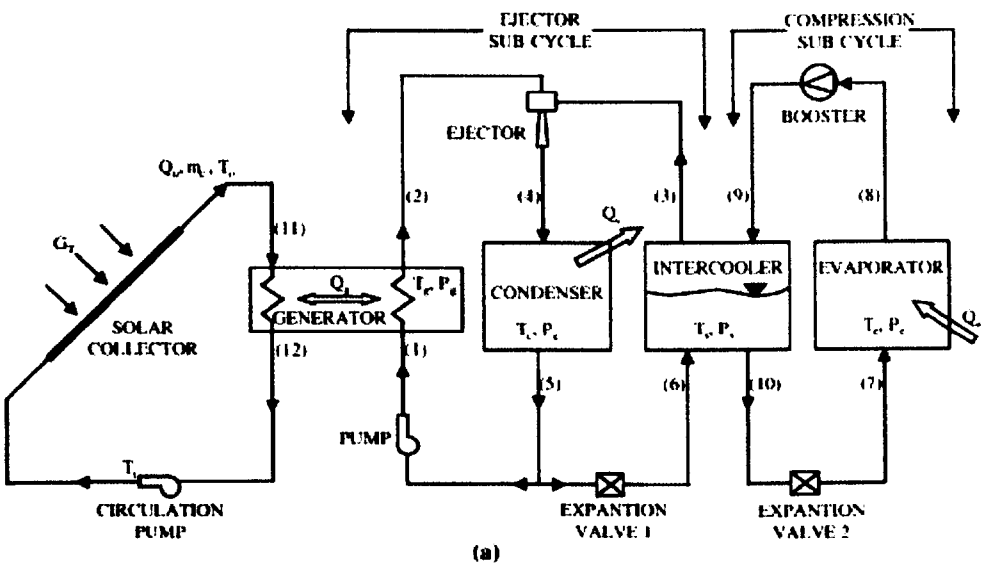

Figure 2-7 Schematic diagram of a solar-powered ejector cooling system [70]

Vidal et al. [22] implemented a computer simulation on a solar assisted combined ejector-compression system. The mechanical compression cycle and the thermal driven ejector cycle were performed with two different refrigerants, R134a and R141b respectively. The final optimum results showed that an intercooler temperature of 19 °C resulted in a solar fraction of

the system of 82% and a COP of 0.89 for the combined cycle. A 10.5 kW cooling capacity was achieved with the flat plate collector area of 105 m^2.

Zhu et al. [74] proposed a hybrid vapour compression cooling system which combined with an ejector cooling cycle(as shown in Figure 2-8). The ejector cooling cycle was driven by waste heat from the condenser in the vapour compression cooling cycle. The additional cooling capacity from the ejector cycle was directly input to the evaporator of the vapour compression cooling cycle. Simulation results showed that COP increased by 5.5% with R152a and 8.8% with R22 compared with the basic system. However, no experimental results were available to validate these.

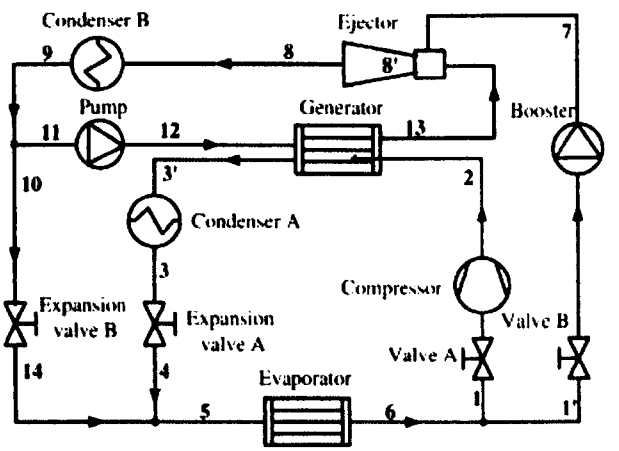

Figure 2-8 Schematic diagram of a cooling system with the integrated ejector [72]

2.2 Thermal energy storage system

Thermal energy storage is perhaps as old as civilization itself. Since history recorded, human beings were able to conserve food with the help of fresh ice. In the new century, the intense energy situation still remains to be the global question. Effectively conserving and re-using the energy therefore becomes an urgent matter.

Thermal energy storage can store excessive energy which would otherwise be wasted, and bridge the gap between energy generation and consumption. The mismatch between supply and demand can therefore be mitigated. Peak hour cooling requirements during day time can be shifted to off peak periods. Moreover, energy storage can also improve system

performance and reliability by reducing peak load and allowing systems to work within an optimal range.

Over past few decades, a variety of energy storage system based on the phase change material (PCM) has aroused practical interests. As an example, latent heat storage system is widely studied as it can provide high energy storage density during phase change within a very narrow temperature range.

2.2.1 Phase change materials (PCM)

Thermal energy can be stored as sensible or latent energy by heating or cooling a certain amount of material. In sensible energy storage system, energy is stored/released by heating/cooling a liquid or solid storage material through a heat transfer interaction. The amount of energy input to a sensible heat system is related to the mass of storage material and its heat capacity as well as the temperature difference of the storage medium between its initial and final states.

Latent heat involves the change of a substance from one phase to another at a fixed temperature. In latent thermal storage systems, energy is stored during the phase change (e.g. melting, evaporating and crystallization). Due to the specific heat of a typical medium and the high enthalpy change during phase change, the latent heat change is usually greater than the sensible heat change for a given system size.

Hence, latent heat storage is more attractive because of its high energy storage density. Phase change materials are such kind of widely used latent heat storage system which can absorb or release large quantities of energy at a constant temperature by undergoing a change of phase. Moreover, compared with sensible heat storage, latent heat storage system using PCM can result in a significant reduction in storage volume.

2.2.2 Classification of PCMs

PCMs can be categorized as organic, inorganic and eutectic materials, as shown in Figure 2-9. Generally, inorganic compounds are almost twice volumetric latent heat storage capacity (250-400kg/dm^3) than that of the organic compounds (128-200kg/dm^3).

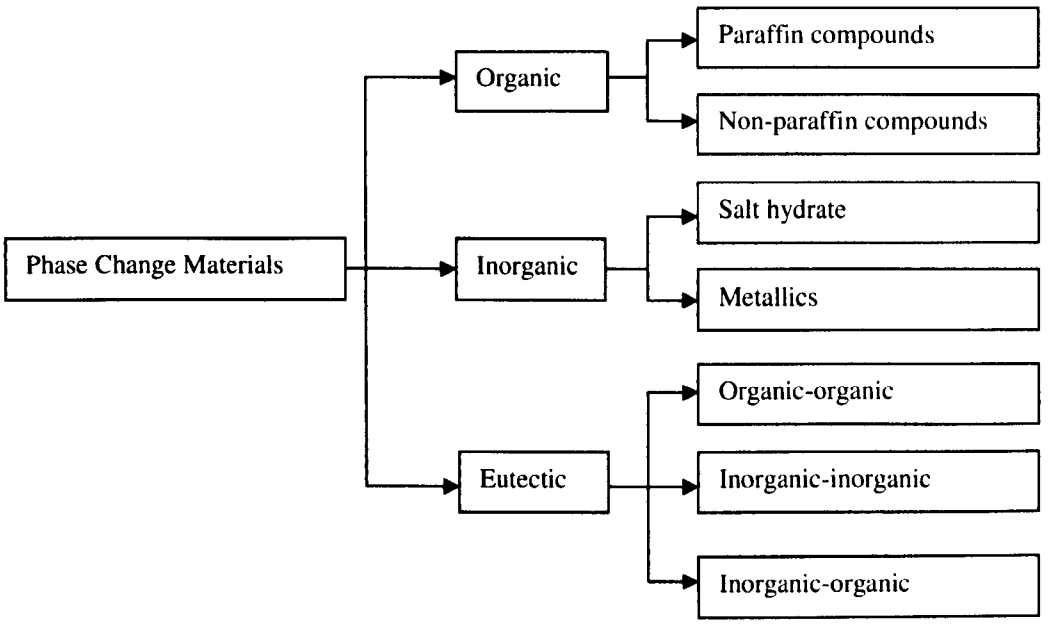

Figure 2-9 Classification of PCMs

2.2.2.1 Organic PCMs

Organic materials are further described as paraffin and non-paraffin. Organic materials include congruent melting, which means that melting and freezing can occur repeatedly without phase segregation and consequent degradation of their latent heat of fusion. Another feature of organic materials is its ability of self nucleation, which means that the materials can crystallize themselves with little or no supercooling and usually non-corrosiveness.

2.2.2.2 Inorganic PCMs

Inorganic materials are further classified as salt hydrate and metallic. Inorganic compounds have a high latent heat per unit mass and low in cost in comparison to organic compounds and are non-flammable. However they suffer from decomposition and supercooling which further can affect their phase change properties.

2.2.2.3 Eutectics

An eutectic is a minimum-melting composition of two or more components, each of which melts and freezes congruently forming a mixture of the component crystals during crystallization.

2.2.3 PCM cold storage heat transfer enhancement methods

The cold storage capacity of PCM depends significantly on the thermal conductivity, which is relatively low for most of the materials. Various heat transfer enhancements have been studied, which can be classified as the following categories: (1) adding metallic particles with higher thermal conductivity than the PCM, as studied by Chen et al. [75] with metal agents and Fukai et al. [76] with carbon fibres; (2) macro and micro encapsulating the PCM as proposed by Alvarado et al.[77], Diaconu at al. [78], Inaba et al. [79], Zhang et al.[80]; (3) using a PCM–graphite composite material as studied by Martin et al.[81] ; and (4) using finned tubes with different configurations as presented by Erek et al. [82] and Ermis [83].

2.2.3.1 Nucleating agents

The effects of different nucleating agents on the super-cooling phenomenon during ice formation were analyze and reported experimentally by Chen et al.[75]. Three different metal agents, iron ore, iron chips and silver iodide were tested with mass percentage varied from 0.005 % to 10%. Since the crystal structure of silver iodide is very similar to that of ice, the comparison among three types of agents indicated that it had the best effect in facilitating nucleation.

Unlike other metals (aluminium, copper, nickel etc) which selectively compatible with some of the PCMs, carbon fibres are strongly resistant to corrosion and chemical attack. Carbon fibres were used to enhance the thermal conductivities of TES[76]. Two different enhancement methods, mixing carbon fibres randomly with PCM and employing a fibre brush whose direction coincided with the HTF, were experimentally investigated. The results showed that brush types were superior to the rand one in terms of enhancement technique.

2.2.3.2 Graphite composite material

Graphite matrix is used to overcome the low heat transfer rates, because of the following advantages: (a) The anisotropy of the graphite allows to address the heat transfer in the direction of interest. (b) The graphite matrix occupies only a small space so that the energy storage density remains very close to its value for the PCM alone. (c) The matrix introduces no corrosion problems, and (d) It is commercially available.

J. Marin [81] studied a thermal energy system for storing cold from outside air during the night and using it during the day for air conditioning. In order to study the effect on heat transfer enhancement of graphite matrix, the authors focused on the experimental and numerical comparisons of the differences of encapsulating in flat plates paraffin alone or embedding with a graphite. It was concluded that embedded PCM with a porous matrix of graphite could noticeably reduce power consumption and response time.

2.2.3.3 Encapsulated PCM

Zhou et al. [84, 85] have investigated numerically the thermal behaviour of a building in Beijing, which includes shape-stabilized phase change materials (SSPCM) plates as inner linings of the walls and the ceiling. The results indicate the thermal storage effect of SSPCM plates, which improves the indoor thermal comfort level and saves about 47% of normal-and-peak-hour energy use and 12% of total energy consumption in winter in Beijing.

2.2.3.4 Finned tubes

Erek et al. [82] carried out numerical and experimental investigations on an energy storage system with a finned tube system. It was found that several factors affected the solidification process around finned tube, which included the flow Reynolds number, the Stefan number, the fin diameter and fin spacing. The numerical data proved to be in good agreement with experimental results. Following this, Ermis and Erek et al. [83] studied the same heat storage system by using an artificial neural network (ANN) algorithm. Numerical results compared

with the previous experimental results [82] showed a better agreement with experimental data than previous numerical model results.

2.2.4 Integrations of PCM cold storage with cooling systems

Most of the experimental [86, 87] and numerical works [79, 88, 89] on PCM cold storage system are concentrated on the properties of thermal storage system. As designed to store the coldness, its operating conditions are greatly related to the cooling system. However, few researches have focused on the working characteristics of PCM cold storage system integrated with cooling system.

Diaconu [90] carried out a simulation of a solar assisted ejector air conditioning system with cold storage. Two types of system configurations (as shown in Figure 2-10) with and without secondary storage units were studied and compared. The author concluded that configuration B yielded better performances with respect to energy usage. However, the assumption made inside the simulation which required the COP of ejector cycle remained constant during operation is not feasible in real situation.

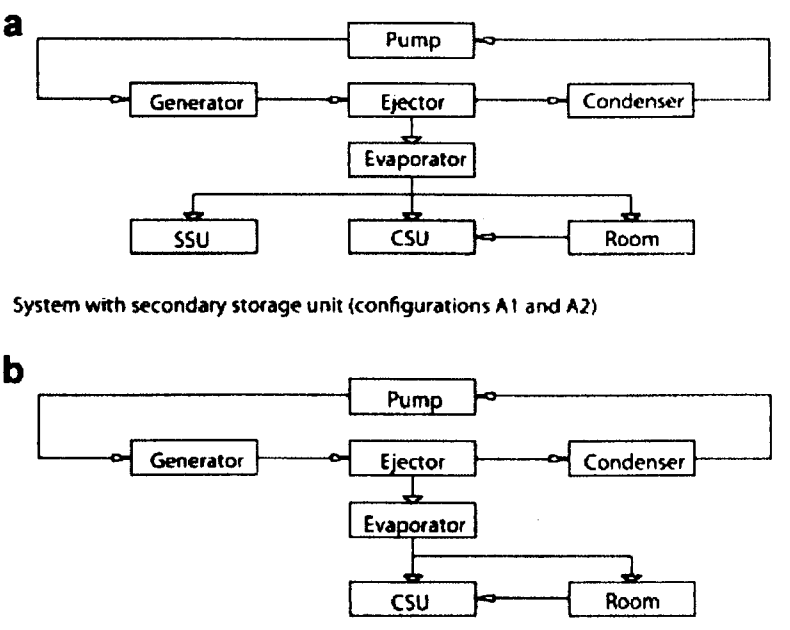

Figure 2-10 System configurations (a) with secondary storage unit (b) without secondary storage unit [82]

Fang et al. [91] experimentally investigated a cool storage air-conditioning system with spherical capsules packed bed (as shown in Figure 2-11).The system consisted of air-conditioning mode, cool storage mode and cool discharge mode. The experimental results indicated that the cool storage air-conditioning system with spherical capsules packed bed had better performances and can stably work during charging and discharging period.

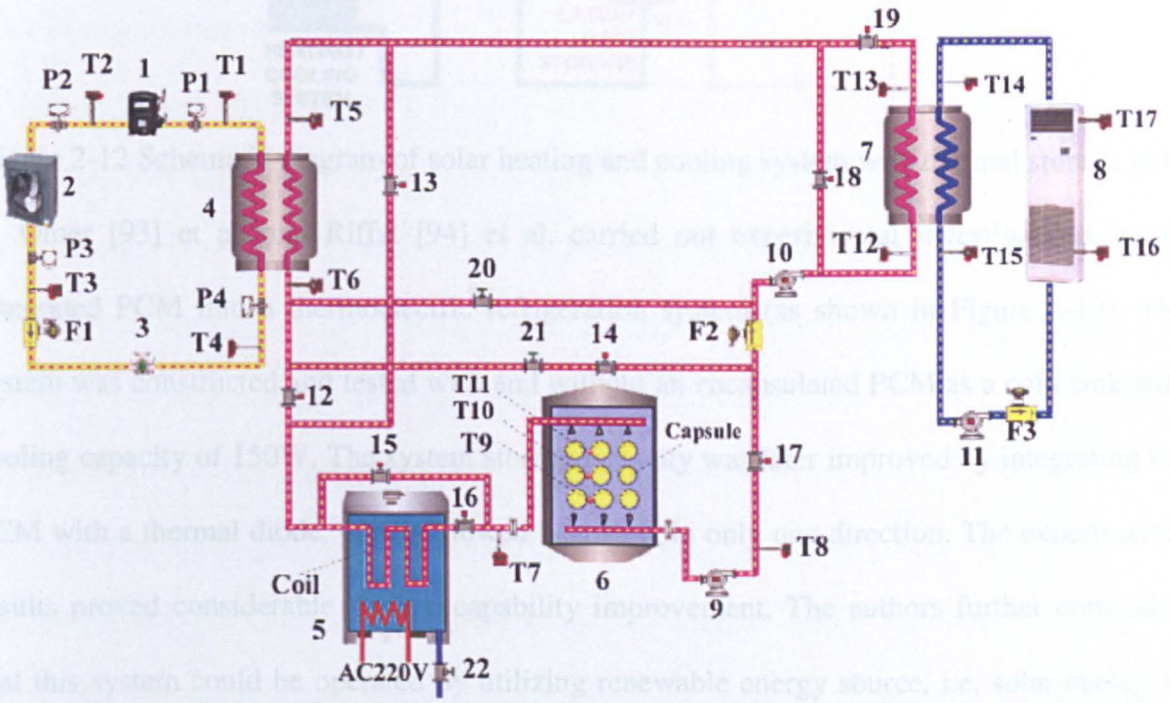

Figure 2-11Schematic diagram of cool storage air-conditioning system with spherical capsules packed bed [89]

Helm et al. [92] carried out an experimental investigation on a solar heating and cooling absorption system with PCM cold storage system (as shown in Figure 2-12). The PCM storage system integrated with coolant loop, was charged during the operation of solar cooling system and discharged during off-peak operation or night time. The results showed that the latent heat storage provides a 10 times higher volumetric storage density in comparison to a conventional water heat storage, with the latent heat storage capacity of 10 kW.

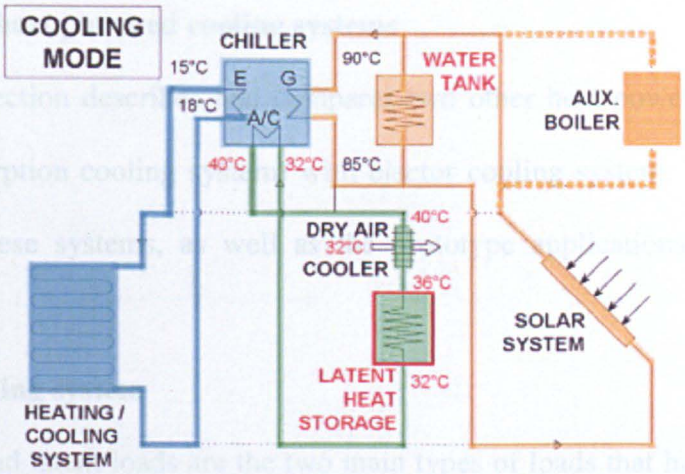

Figure 2-12 Schematic diagram of solar heating and cooling system with thermal storage [84]

Omer [93] et al. and Riffat [94] et al. carried out experimental investigations which integrated PCM into a thermoelectric refrigeration system (as shown in Figure 2-13). The system was constructed and tested with and without an encapsulated PCM as a cold sink with cooling capacity of 150W. The system storage capacity was later improved by integrating the PCM with a thermal diode, which allowed heat flow in only one direction. The experimental results proved considerable storage capability improvement. The authors further concluded that this system could be operated by utilizing renewable energy source, i.e, solar energy to produce DC electricity.

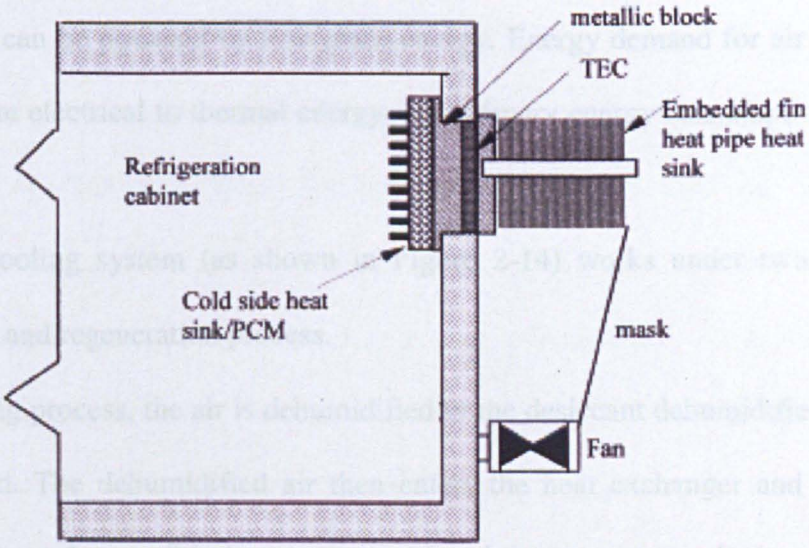

Figure 2-13 Schematic diagram of a thermoelectric refrigeration system integrated with PCM [85]

2.3 Comparison of heat powered cooling systems

The following section describes and compares two other heat powered cooling systems (desiccant and absorption cooling system) with ejector cooling system. The advantages and disadvantages of these systems, as well as the prototype applications are compared and summarized.

2.3.1 Desiccant cooling system

Sensible loads and latent loads are the two main types of loads that have to be considered in the design and operation of the cooling system. In traditional vapour compression system, the latent heat is removed by cooling the air below its dew point. This deep cooling process result in two forms of energy consumption on the cooling system, 1) the energy consumed to cool the air from the supply temperature down to the dew point, and 2) the energy needed to reheat the air from that temperature to its supply temperature.

These two types of energy consumption can be avoided by introducing a system which can dehumidify the incoming air. Desiccant cooling system is such a kind of system, in which the solid or liquid desiccant materials can absorb the moisture in the air by the pressure difference between the ambient air and the desiccant surface. More importantly, desiccant cooling system can be powered by low grade energy. Energy demand for air conditioning is thus shifted from electrical to thermal energy, and primary energy consumption is reduced as well.

Desiccant cooling system (as shown in Figure 2-14) works under two processes: the cooling process and regeneration process.

In the cooling process, the air is dehumidified in the desiccant dehumidifier, and the latent heat is removed. The dehumidified air then enters the heat exchanger and an evaporative cooling unit, where the sensible heat is extracted and the temperature is dropped to meet the indoor air requirement.

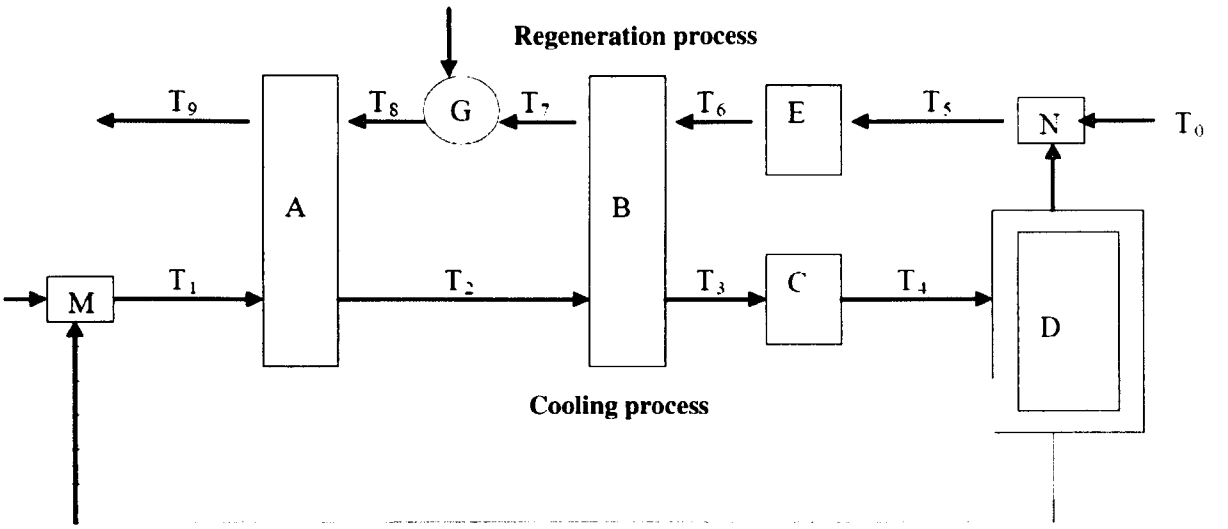

Figure 2-14 Schematic diagram of desiccant cooling system

(A: desiccant dehumidifier; B: heat exchanger; C, E: evaporative cooler; D: space required to be cooled; M, N: mixed air; G: generator)

In the regeneration process, low grade energy is used to provide the heat for regeneration, which increases the temperature/pressure of the desiccant material. The moisture that the desiccant has absorbed during the sorption process is removed by the pressure difference between the ambient air and the desiccant surface. After that, the desiccant material can be utilized in next cycle.

2.3.1.1 Solar powered desiccant cooling systems

Experimental investigation was carried out on a solar powered desiccant cooling system by Henning et al. [95]. A COP of 0.6 and solar fraction of 76% was achieved in the experiment. Similar experiments were conducted by Halliday et al. [96] in the UK. The authors concluded that a 70% reduction in gas consumption could be achieved by incorporating solar coils into the desiccant system. Recently, a PV façade and PV sheds were used as the heat supply for a desiccant cooling system in Spain [97]. The study results proved that a solar fraction of 75% and the average COP of 0.518 can be achieved for the cooling system during summer season.

A prototypes of a LiCl/water desiccant system driven by solar energy was built and tested by Gommed and Grossman [98]. The average dehumidification capacity reached 16kW with solar collector area of $20m^2$. Two methods of storage were involved in this prototypes-hot water storage and cooling storage in regenerated desiccant. The experimental results showed a thermal COP of 0.8 with regeneration temperature 65-100 °C and cooling water temperature 22-27 °C.

2.3.1.2 Hybrid VC and desiccant cooling system

In conventional VC system, the moisture has to be condensed by cooling the incoming air below its dew point temperature. The condensed air has to be reheated to the supply temperature before it enters into the room. Such process consumes more energy and the system operates at reduced COP. In order to improve the system performance, a hybrid system with a VC cycle for sensible cooling and a liquid desiccant cycle for latent heat removal is studied by many researchers.

In this system, the incoming air will pass through the desiccant solution, which lowers the relative humidity of process air in order to help the evaporative cooler to function more effectively. Therefore, the hybrid VC and desiccant cooling system can significantly reduce the size of conventional VC system and enhance its COP. Moreover, since the cooling of the incoming air below its dew point is avoided, the temperature of evaporation can be raised up to 15°C from its practical level of 5 °C for conventional VC cycle. This will substantially improve the COP of hybrid system as well.

Analysis of the hybrid VC and desiccant cooling system was performed by Yadav [99]. The study indicated that 80% of energy can be saved when latent heat load consist 90% of the total heat load. Similar experiments were conducted by Jia et al. [100]. The authors stated that compared with conventional VC system, the hybrid system saved 38% electrical energy at the ambient temperature of 30°C and relative humidity of 55%.

2.3.1.3 Hybrid sorption and desiccant cooling system

In order to recover the heat rejected from the condenser of the absorption cooling system, a solid desiccant dehumidifier integrated with a solar driven absorption system was proposed by Fathalah et al. [101]. Numerical simulation was conducted on this hybrid system, and the results showed an overall COP of 1.2 (which is 53% higher than that for the absorption cooling system) with a cyclic duration of 15 minutes.

A hybrid adsorption cooling and liquid desiccant dehumidification system was reported by Ma et al. [102]. In the hybrid system, the sensible heat load is handled by solar adsorption cooling and VC cooling system. The condensing water at 80°C was used to regenerate a liquid desiccant dehumidification system, which removed the latent heat load. The simulation results indicated that 45% of performance enhancement could be achieved by this system compared with conventional VC system at latent load of 30%.

2.3.1.4 Gas turbine cycle integrated with desiccant-based evaporative cooling system

In order to improve the system performance, a desiccant evaporative cooling system integrated with a gas turbine cycle was proposed by Zadpoor and Golshan [103]. Performance enhancement comparisons have been made between this system and those of direct/indirect evaporative cooling system in different climatic conditions. The authors concluded that, although the power output from this system was better than other methods, the additional performance improved caused by desiccant-based cooling method is limited. Specific NOx emission was reported to be decreased by using this technique.

2.3.1.5 Advantages and disadvantages of desiccant cooling system

Advantages:

1) The possibility of utilising low grade energy (solar energy, industrial waste heat)
2) In the desiccant cooling system, no compression work is required. With the only usage of pump and fan, the electricity consumption is around 1/3 of that by conventional VC system.

3) Water can be used as the refrigerant in desiccant cooling system, which is more environmental friendly compared with other CFCs refrigerants used in conventional VC system.
4) The desiccant dehumidifier extends the climatic applicability scope of the evaporative cooling to the hot and humid zones.
5) The dehumidifier can help to eliminate the pollutants and bacteria from the air, which improves the indoor air quality significantly.

Disadvantages:

1) Desiccant cooling system is impracticable in the areas where the ambient relative humidity is too high. For in this condition, the regeneration temperatures required will be excessive.
2) High investment costs, difficult control, and poor dynamic properties, since cooling capacity is limited by air humidification.
3) Inorganic salts used as desiccant material can cause corrosive problem of air ventilation pipes. The prevention of leak and corrosion of the liquid desiccant in air handling unit should be addressed.

2.3.2 Absorption cooling system

The process of absorption cooling (shown in Figure 2-15) involves binary working fluids, the refrigerant and the absorbent.

The pressure difference between the liquid refrigerant in the evaporator and the poor solution (absorbent and refrigerant) in the absorber causes the vapour evaporation in the evaporator, which reduce the temperature of the remaining refrigerant in the evaporator and produces cooling effect. As the vapour is absorbed in the absorber, the solution becomes more dilute. This is called the absorption process.

The regeneration process happens when the solution in the absorber is too concentrated to continue with the absorption process, and the refrigerant has to be separated from the diluted

solution. Low grade heat (solar energy or industrial waste heat) is applied to the generator to dry the refrigerant from the solution. The refrigerant vapour will be condensed in the condenser by exchanging heat with the surroundings. And the condensed refrigerant will enter into the evaporator to complete another cycle.

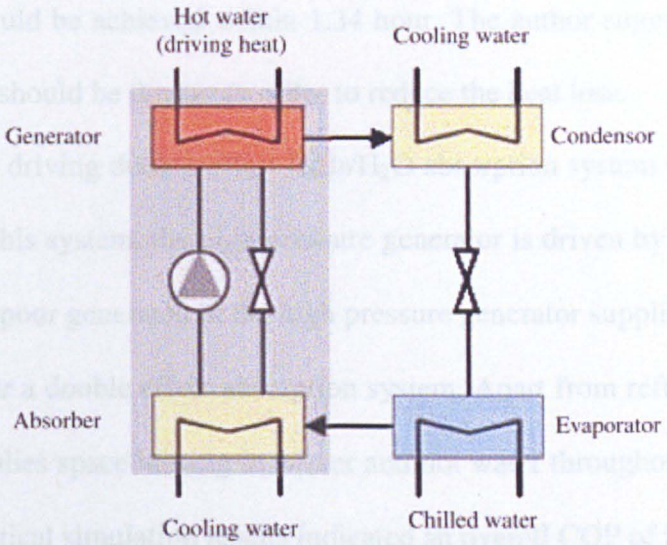

Figure 2-15 Schematic diagram of absorption cooling process

Case studies

Sozen et al. [104] developed and tested a solar powered absorption cooling system with NH_3/H_2O as working fluid. A parabolic solar collector was applied to this prototype and supplied high temperature water around 100°C to drive the generator. The experimental results showed COP in the range of 0.58 to 0.6 with evaporator temperature from -10°C to 10°C and generator of 90°C.

A similar prototype with NH_3/H_2O as working pairs was proposed by Francisco et al. [105]. Instead of using cooling tower, the condenser and absorber were air-cooler by natural ventilation. The utilization of parabolic solar collector in the climatic condition in Spain provided the water temperature over 150°C. The simulation results expected COP between 0.3 and 0.5. However, due to the difficulty to maintain a uniform operation during the experiments, the measured COP was lower than 0.05.

Experimental investigation of a solar powered LiBr/H_2O absorption system in Madrid was proposed by Syed et al. [106]. Flat plate solar collectors with area of 50m^2 were implemented. The experimental results concluded that with peak solar irradiation of 969w/m^2, generation and absorption temperature of 57-67 ℃ and 32-36 ℃, 5.13kW cooling capacity and average COP of 0.34-0.42 could be achieved within 1.34 hour. The author suggested that the storage tank insulation layer should be thicker in order to reduce the heat loss.

A novel solar/gas driving double-effect LiBr/H_2O absorption system was presented by Liu and Wang [107]. In this system, the high-pressure generator is driven by natural gas and solar energy. The water vapour generated in the high pressure generator supplied energy to the low-pressure generator for a double effect absorption system. Apart from refrigeration in summer, this system also supplies space heating in winter and hot water throughout the year for family daily use. The theoretical simulation results indicated an overall COP of 0.7.

Advantages

1) As the working pairs, LiBr/ H_2O has two outstanding features, which are non-volatility (a rectifier is eliminated) and high heat of vaporization of water. Other new working fluids, including binary mixture using inorganic salt are of interest for researchers.
2) The working fluids for absorption system are mainly liquid, inside which the heat transfer methods are conduction and convention. Convention is more predominantly, which offers higher heat transfer coefficient.

Disadvantages

1) The two main working pairs (LiBr/H_2O and NH_3/H_2O) of absorption system have their own disadvantages. The material cost of LiBr is relatively high, which renders a high initial cost for the system. Although NH_3 is much cheaper, its volatility requires a rectifier in the system. The toxicity of NH_3 makes it less applicable for domestic use.

2) For single stage absorption system, the cooling effect is intermittent as the process can not be done simultaneously.

3) When normal solar collector can not provide sufficient heat source temperature. Mulit effect absorption cooling system is applied to improve system performance. Concentrated parabolic solar collector has to be used to increase the heat source temperature to higher value (around 150 °C), and the initial cost will increases. For mulit effect absorption system, corrosion rate may be increased due to high temperature operation.

4) Special attention has to be made on $LiBr/H_2O$ absorption system. LiBr is prone to crystallization when the temperature of solution is lower than the saturation temperature, which causes the blockage of the pipework and heat exchanger.

2.3.3 Comparisons of heat driven cooling systems

Table 2-3 summarize the pros and cons of the three cooling systems. Compared with absorption system, ejector cooling system only needs four simple components (evaporator, condenser, generator and ejector), so it is easy to construct with relatively low installation costs. While absorption system is relatively complicated, involving the regenerator, rectifier and several heat exchangers. All the reactive vessels and pipes have to be thin enough to avoid corrosion.

Desiccant cooling system can only provide cooling effect with temperature around 5-15°C. In comparison, ejector cooling system can work with a wider range of cooling temperature, even below zero degree, which extends its application to refrigeration area.

Thus, due to its simplicity, low initial cost and relatively wide cooling scope, ejector cooling system is chosen as the main focus point in this research.

Table 2-5 Summary of advantages and disadvantages of heat driven cooling systems

Heat driven cooling systems	Desiccant	Absorption	Ejector
Advantage	Water as environmental friendly fluid, can be used as refrigerant	Proper selection of working pairs can help to achieve high heat of vaporization ($LiBr/H_2O$)	Water as environmental friendly fluid, can be used as refrigerant
	Dehumidifier can help to eliminate the pollutants and bacteria from the air, which improves the indoor air quality significantly	Convention is the main heat transfer methods for liquid refrigerant, which offers higher heat transfer coefficient.	Simplicity in construction, low initial cost and maintenance requirement
Disadvantage	Impracticable in the areas where the ambient relative humidity is too high	For single stage absorption system, the cooling effect is intermittent as the process can not be done simultaneously	Can only work under design conditions (ie, at certain evaporator and condenser temperature ranges)
	Inorganic salts used as desiccant material can cause corrosive problem of air ventilation pipes	For LiBr/H2O working pairs, LiBr is corrosive in nature. In case of the ammonia system, ammonia is corrosive to copper.	
	High investment costs, difficult control, and poor dynamic properties	High initial cost	
Heat source temperature (°C)	50-80	80-120	80-120
COP	0.4-0.8	0.3-0.7	0.3-0.4

2.4 Conclusions

This chapter reviews the recent technology developments of ejector cooling system, cold storage system and heat driven cooling systems. The reviewed research and development were broad based and productive, concentrating on performance enhancement methods, combinations of ejector cooling system with other systems, integrations of cold storage system with cooling system and comparisons between heat driven cooling systems.

The following conclusions can be drawn from the reviewed works:

Research developments of ejector cooling system were investigated, which focused on design fundamentals, refrigerants selection and system optimization. Geometric investigation revealed that area ratio and nozzle exit position were the most widely investigated parameters. Refrigeration comparisons concluded that R143a and R142b were proved to yield better performance than other working fluids. As the most environmentally friendly and economically available refrigerant, water had been widely used and tested as refrigerant for ejector refrigeration system. The investigations of combining ejector cooling system with other systems (Rankine cycle, vapour compression systems, etc) were carried out in many researches. However, most of those studied were limited to numerical analysis, with few experimental results available. With the aim to utilize renewable energy source, solar driven ejector cooling system had been widely studied. Due to the intermittent characteristic of solar energy, the system performance was hardly stable. Thus the combination of energy storage in the solar-driven ejector cooling system remains to be the research topic in this field. Combined power and ejector cooling systems were proposed by researchers. A thermal efficiency between 0.3 and 0.5 was reported. The research works were mainly focused on the system modelling, which were not validated with experimental results.

Energy storage techniques were reviewed. Various categories of phase change materials as well as different heat transfer enhancement methods were compared and analyzed. The

investigations of cold storage system integrated with cooling system demonstrated that previous works were mainly focused on the theoretical analysis, with few experimental works available. Hence, the experimental investigation of cold storage system integrated with ejector cooling system would be of novelty for research work in this area.

The final section of this chapter reviews three kinds of heat driven cooling systems, i.e, desiccant, absorption and ejector cooling system. The basic working principles were described and the main research outcomes were demonstrated in the case studies. The advantages and disadvantages of these cooling systems were analyzed and compared. Due to its simplicity, low initial cost and relatively wide cooling scope, ejector cooling system is chosen as the main focus point in this research.

Chapter 3 Simulation of Ejector Cooling System and Case Study of Hybrid Ejector and CO_2 Vapour Compression System

This chapter conducts computer simulations based on the simplified 1-D ejector model. The working performances of single ejector cooling system under various operation conditions (generator, condenser and evaporator temperatures) were simulated. Five different working fluids, water, methanol, ethanol, HFE7000 and HFE7100 were chosen as the refrigerants for comparison. The system performances, environmental impacts and safety issues of these refrigerants were compared. Due to its zero global warming potential and availability, water was chosen as the working fluid for the ejector cooling system.

Investigations into the vapour compression system revealed that a lower gas cooler outlet temperature could contribute to higher system performance. The CO_2 vapour compression sub-system was therefore coupled with the ejector, whose cooling effect was used to sub-cool the vapour compression system. The simulation case study of this novel hybrid ejector and CO_2 vapour compression cooling system was presented. In the hybrid system, significant performance improvement (around 22% for ejector and 45% for vapour compression system) could be identified compared with individual sub-systems.

3.1 Ejector cycle simulation

3.1.1 Ejector theory

The performance of an ejector can be defined in terms of the entrainment ratio ω or mass flow ratio, which is the ratio between the secondary and the primary fluid mass flow rates:

$$\omega = m_s / m_p \qquad \text{Eq. (3.1)}$$

The performance of ejectors can be predicted using one-dimensional compressible flow theory. The first model was presented by Keenan [108] to analysis air ejector. It was a one-

dimensional model based on ideal gas dynamic in conjunction with the principles of conservation of mass, momentum and energy. Later Munday and Bagster [109] extended the theory to include a constant-pressure mixing chamber and a diffuser. However, heat and friction losses were ignored. Eames [44] modified Keenan's model and included irreversibilities associated with the primary nozzle, mixing chamber and diffuser.

The simulation is carried out based on the model presented by Eames[44]. The governing equations are presented in the following subsections.

3.1.2 Ejector design analysis

The analysis is based on the steady-state and steady-flow equations of energy, momentum and continuity as follows:

The energy conservation equation for a one-dimensional adiabatic process between inlet and outlet of a horizontal plane is:

$$\sum m_i \left(h_i + \frac{v_i^2}{2}\right) = \sum m_e \left(h_e + \frac{v_e^2}{2}\right) \qquad \text{Eq. (3.2)}$$

Momentum equation:

$$P_i A_i + \sum m_i v_i = P_e A_e + \sum m_e v_e \qquad \text{Eq. (3.3)}$$

Continuity equation:

$$\sum \rho_i v_i A_i = \sum \rho_e v_e A_e \qquad \text{Eq. (3.4)}$$

Where, m is the mass flow (kg/sec), h is specific enthalpy (kJ/kg), v is velocity (m/s), P is pressure (Pa), ρ is density (kg/m^3) and A is area (m^2).

3.1.3 Simplifying assumptions made in the analysis

With reference to Figure 3-1, the following simplified assumptions are made for the one-dimensional analysis:

1) Vapour behaves as perfect gas.

2) Ejector walls are adiabatic.

3) Friction losses were introduced by applying isentropic efficiencies to the primary nozzle, diffuser and mixing chamber.

4) The primary and secondary fluids were supplied at zero velocity at section i and section o respectively. The velocity at diffuser outlet 3-3 is assumed to be zero.

5) At section 1-1 where the two streams first meet, the static pressure was assumed to be uniform.

6) Mixing of the two streams was complete before a normal shock wave occurred at the end of the mixing chamber 3-3.

3.1.4 Theory description

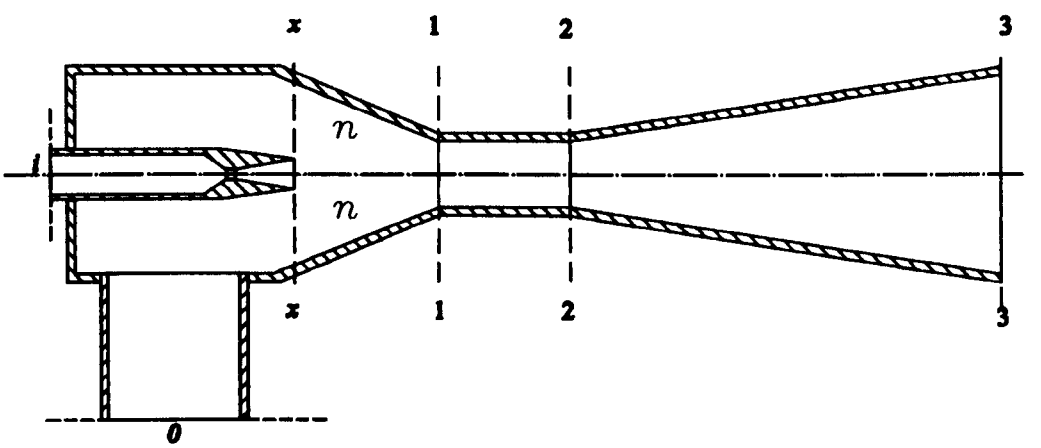

Figure 3-1 Schematic representation of an ejector

3.1.4.1 Diffuser outlet section 3-3

The temperature for the primary flow and secondary flow, and the outlet flow of the diffuser are assumed as stagnation temperature. Applying the energy equation between the inlet of the ejector (the primary and secondary flow) and the outlet stagnation:

$$\dot{m}_p h_i + \dot{m}_s h_o = (\dot{m}_p + \dot{m}_s) h_3 \qquad \text{Eq. (3.5)}$$

The specific enthalpy is defined as

$$h = c_{PV} T \qquad \text{Eq. (3.6)}$$

where, c_{PV} is the specific heat of vapour at constant pressure, T is the absolute temperature.

Combine equation Eq. (3.1), Eq. (3.5) and Eq. (3.6), and rearranging gives:

$$T_i + \omega T_o = (1 + \omega)T_3 \qquad \text{Eq. (3.7)}$$

Eq. (3.7) indicated that the outlet stagnation temperature is determined by the inlet temperatures of primary and secondary flow and the entrainment ratio.

3.1.4.2 Primary and secondary streams at nozzle exit plane (section x-x)

High-pressure primary stream enters primary (supersonic) nozzle, through which it expands to produce a low pressure at the exit plan x-x. The high-velocity primary stream entrains the secondary fluid into the mixing chamber. During this process, fiction loss of the primary nozzle is considered by applying an isentropic efficiency η_p to the equation. Apply the energy equation between i-x and o-x to primary flow and secondary flow respectively:

$$\dot{m}_p h_p = \dot{m}_{px}(h_{px} + \eta_p v_{px}^2/2) \qquad \text{Eq. (3.8)}$$

$$\dot{m}_s h_s = \dot{m}_{sx}(h_{sx} + v_{sx}^2/2) \qquad \text{Eq. (3.9)}$$

The inlet mass flow rate $m_p$and outlet mass flow rate m_{px} of the primary nozzle remain the same, which further gives the primary and secondary flow velocities at section x-x:

$$v_{px} = \sqrt{2\eta_p(h_p - h_{px})} \qquad \text{Eq. (3.10)}$$

$$v_{sx} = \sqrt{2(h_s - h_{sx})} \qquad \text{Eq. (3.11)}$$

Specific heat at constant pressure is defined as

$$c_{PV} = \frac{kR}{k-1} \qquad \text{Eq. (3.12)}$$

Where, R is the ideal gas constant and k is the isentropic index of compression and expansion.

The isentropic relationship between pressure and temperature ratios between states 1 and 2 is given by:

$$\frac{T_1}{T_2} = \left(\frac{P_1}{P_2}\right)^{\frac{k-1}{k}} \qquad \text{Eq. (3.13)}$$

The speed of sound at local static temperature is

$$c = \sqrt{kRT} \qquad \text{Eq. (3.14)}$$

The local Mach number is defined as

$$M = \frac{V}{C} \qquad \text{Eq. (3.15)}$$

The relation between the pressure ratio across the nozzle and Mach number at the exit of the nozzle is given as

$$M_{px} = \sqrt{\frac{2\eta_p}{(k-1)}\left(\left(\frac{P_i}{P_x}\right)^{\frac{k-1}{k}} - 1\right)} \qquad \text{Eq. (3.16)}$$

Similarly to the primary nozzle, the Mach number of the secondary fluid at the nozzle exit plane is given as

$$M_{sx} = \sqrt{\frac{2}{(k-1)}\left(\left(\frac{P_o}{P_x}\right)^{\frac{k-1}{k}} - 1\right)} \qquad \text{Eq. (3.17)}$$

When the secondary flow is entrained from the evaporator, irreversible losses would occur at the boundary where the evaporator is connected with the ejector profile. This is not mentioned in previous literature. Considering the dynamic flow pattern of such flow, the losses associated with the secondary flow will lead to reduced entrainment ratio, and hence lower system performance.

3.1.4.3 Mixing process (between section n and section 2)

Applying the momentum equation with ideal lossless mixing between primary nozzle exit plane (section n) and the exit of mixing chamber (section 2):

$$P_n A_n + \dot{m}_p v_{px} + \dot{m}_s v_{sx} = P_2 A_2 + (m_p + m_s) v_2 \qquad \text{Eq. (3.18)}$$

The mixing process between primary and secondary fluids is assumed all to occur between section n-n and section 2-2 at constant pressure ($P_n = P_2$) and where the cross-sectional areas of expanded flow (section n-n) from the nozzle exit and exit of the mixing chamber (section2-2) are assumed to be equal ($A_n = A_2$).This is based on the assumption described by Chunnanond and Aphornratana [9] that the primary flow expands through the

primary nozzle and fans out into the mixing chamber with some "expansion angle". Section n identifies the cross section of such expanded flow.

Therefore

$$\dot{m}_p v_{px} + \dot{m}_s v_{sx} = (\dot{m}_p + \dot{m}_s) v_1 \qquad \text{Eq. (3.19)}$$

This relation describes fully idealized mixing process. It is modified by including η_m as efficiency for the whole mixing chamber to make it more realistic:

$$\eta_m(\dot{m}_p v_{px} + \dot{m}_s v_{sx}) = (\dot{m}_p + \dot{m}_s) v_1 \qquad \text{Eq. (3.20)}$$

Thus the velocity of the mixed fluid at section 1 can be expressed as

$$v_1 = \eta_m \left(\frac{\dot{m}_p v_{px} + \dot{m}_s v_{sx}}{\dot{m}_p + \dot{m}_s}\right) = \eta_m \left(\frac{v_{px} + \omega v_{sx}}{1+\omega}\right) \qquad \text{Eq. (3.21)}$$

Equation Eq. (3.21) can be written in terms of the Mach number:

$$M_1^* = \frac{\eta_m (M_{px}^* + \omega M_{sx}^* \sqrt{\tau})}{\sqrt{(1+\omega\tau)(1+\omega)}} \qquad \text{Eq. (3.22)}$$

Where, τ is defined the ratio of inlet stagnation temperatures,

$$\tau = \frac{T_0}{T_i} \qquad \text{Eq. (3.23)}$$

Where the relation between M and M* is given as

$$M^* = \frac{\sqrt{(k+1)M^2/2}}{\sqrt{1+(k-1)M^2/2}} \qquad \text{Eq. (3.24)}$$

3.1.4.4 Mixed stream after shock wave

At some distance in the mixing chamber, a transverse shock wave is induced creating a compression effect. Across this point, the velocity of mixed stream sudden drops to sonic value[9]. The Mach number of the mixed fluid after the shock wave is obtained from

$$M_2 = \frac{M_1^2 + 2/(k-1)}{\left[\frac{2k}{k-1}\right] M_1^2 - 1} \qquad \text{Eq. (3.25)}$$

The pressure lift ratio across the shock wave is obtained as follows:

$$\frac{P_2}{P_1} = \frac{1+kM_2^2}{1+kM_1^2}$$ Eq. (3.26)

3.1.4.5 Pressure lift ratio across the subsonic diffuser

Further compression of the mixed fluid is achieved as it passes through the subsonic diffuser. It is assumed that the flow speed is reduced to zero at the end of the diffuser (section 3-3). The pressure lift ratio across the diffuser can be obtained from

$$\frac{P_3}{P_2} = \left[\frac{(k-1)\eta_d M_2^2}{2} + 1\right]^{\frac{k}{k-1}}$$ Eq. (3.27)

Where, η_d is the isentropic efficiency of the diffuser. The critical pressure lift ratio across the ejector is then found from Equation Eq. (3.28). The assumption of constant pressure mixing from x to 1, gives $P_x = P_1$, therefore the critical pressure lift ratio is

$$\frac{P_3}{P_o} = \left(\frac{P_3}{P_2}\right)\left(\frac{P_2}{P_x}\right)\left(\frac{P_x}{P_o}\right) = N_S^*$$ Eq. (3.28)

The static pressure P_x at the nozzle exit plane x is unknown. Following an iterative scheme presented by Eames et al. [43], the optimum critical pressure lift ratio can be obtained by varying a range of assumed entrainment ratios.

3.1.5 Simulation of single ejector cooling system

The equations were programmed in Engineering Equation Solver (EES). The properties of working fluids were computed by the program from internal fundamental equations of state and correlations. With the entrainment ratio as an input, varying the assumed P_1/P_0 yields a maximum discharge pressure, which can be considered as the most critical condenser conditions for ejector design.

Efficiency constants for the primary nozzle η_p, diffuser η_d and momentum loss η_m are chosen as 0.85, 0.8 and 0.9 respectively, as described by Eames et al. [44].

3.1.5.1 Comparisons of various working fluids

The performance of the ejector system depends not only on the ejector geometry and operating conditions, but also on the property of the working fluid. A wide variety of refrigerants are available that are suitable for use in an ejector. A selection of natural and synthetic refrigerants was evaluated for their performances, environmental impacts and safety.

Simulations are carried out for five refrigerants that could be used in the ejector refrigeration system. Three natural refrigerants (Water, methanol and ethanol) and two synthetic refrigerants (HFE7000 and HFE7100) were chosen. The variations in entrainment ratio with condenser temperature were compared at evaporator temperature of 20°C and generator temperature of 120°C respectively.

Figure 3-2 illustrates the variations of entrainment ratio with respect to condenser temperatures for five different working fluids. It can be seen that for condenser saturation temperature at 35°C, entrainment ratio for water, ethanol, methanol, HFE7100 and HFE7000 was 0.54, 0.66, 0.70, 0.75 and 0.80, respectively. For a given condenser temperature, HFE7000 showed the highest entrainment ratio, followed by HFE 7100 and methanol, while water yielded the lowest value.

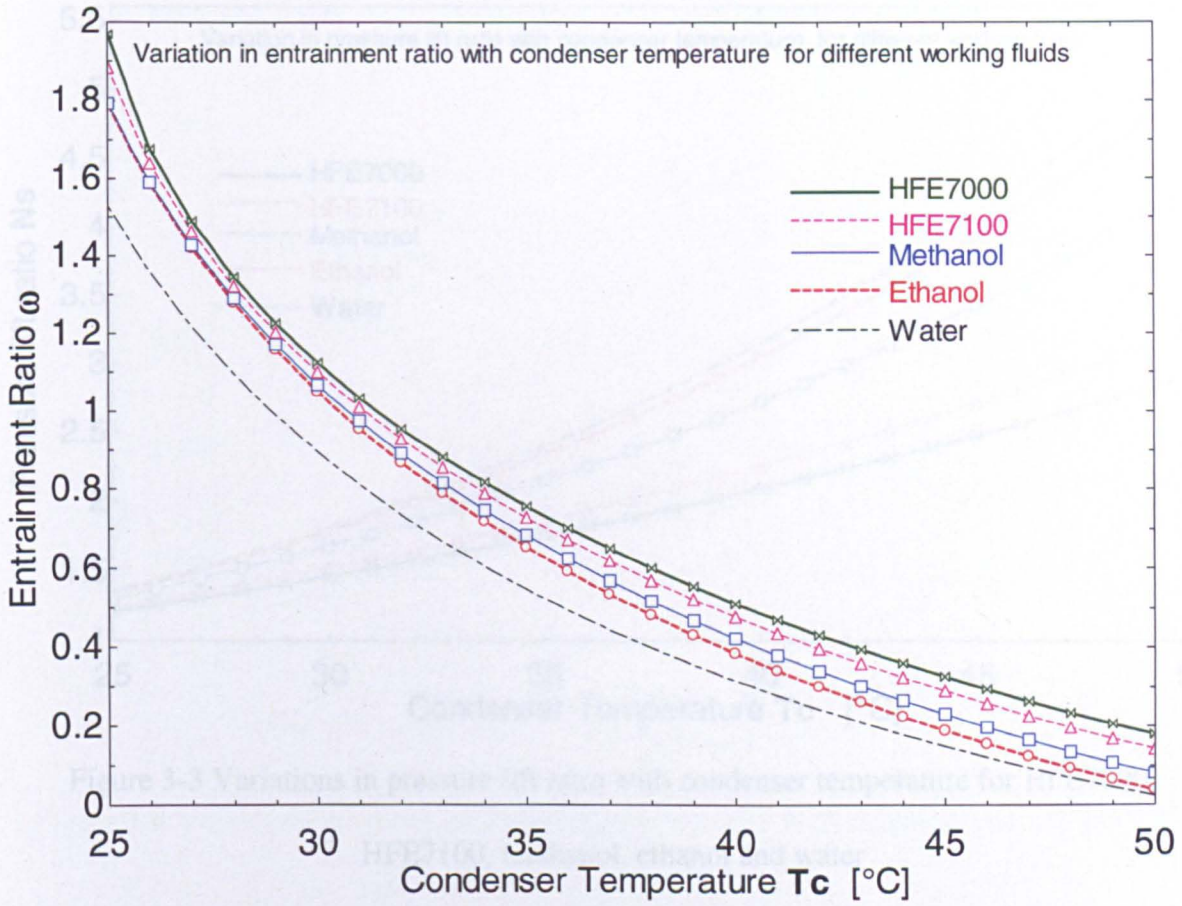

Figure 3-2 Variations in entrainment ratio with condenser temperature for HFE7000, HFE7100, methanol, ethanol and water

Figure 3-3 shows the variations of pressure lift ratio with condenser saturation temperatures for the five refrigerants. Pressure lift ratio is the ratio of condenser pressure to evaporator pressure. A refrigerant with a high pressure lift ratio uses much of the input energy to re-compress the mixture, with less being used to entrain the secondary stream. It can also be observed in Figure 3-3 that the pressure lift ratio is lowest for HFE7000 and highest for water. This means that the lower curves (HFE fluids) in Figure 3-3 have more potential to entrain secondary stream. These fluids therefore yielded higher entrainment ratio, as manifested in Figure 3-2.

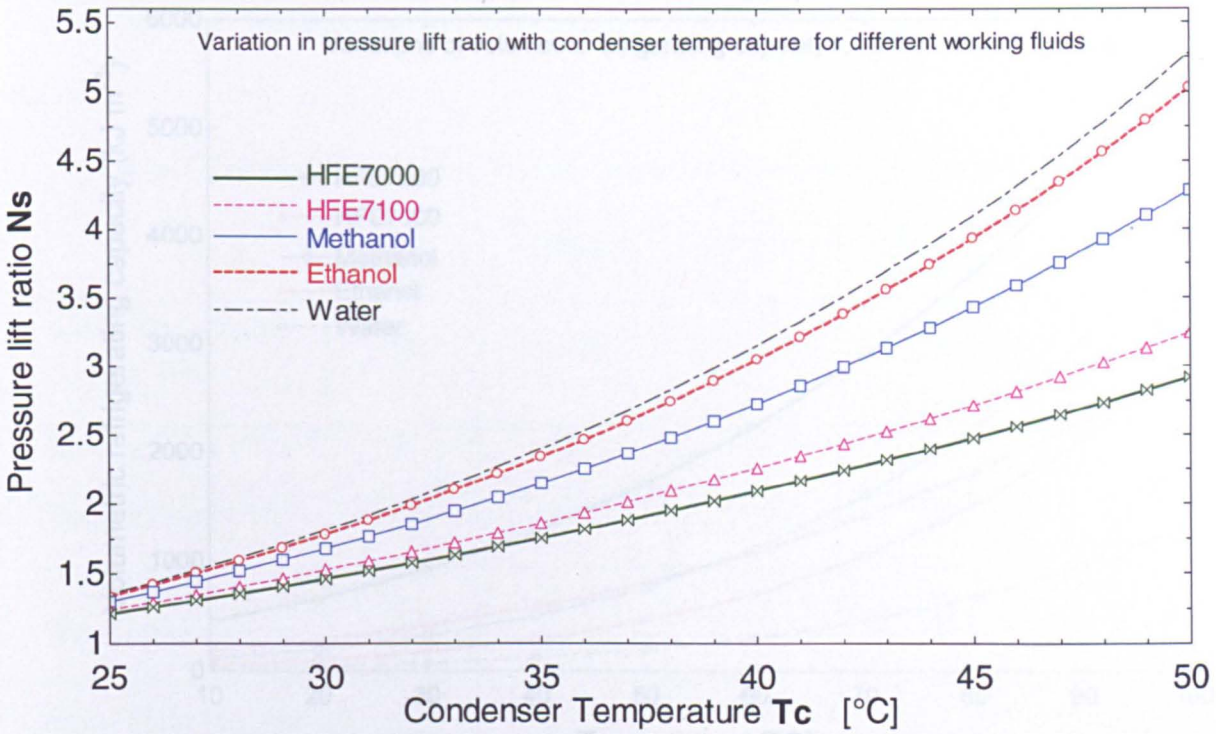

Figure 3-3 Variations in pressure lift ratio with condenser temperature for HFE7000, HFE7100, methanol, ethanol and water

Another useful indicator for the selection of proper refrigerant is volumetric refrigerating capacity, which is defined as the ratio of the latent heat of vaporisation to the vapour density. It can be used to compare the relative size of components such as heat exchangers of the different refrigerants. Figure 3-4 shows the variations in volumetric refrigerating capacity with temperatures for water, methanol, ethanol, HFE7000 and HFE7100.

As shown in Figure 3-4, HFE7000 showed the highest volumetric refrigerating capacity and water showed the lowest. A Refrigerant with higher volumetric refrigerating capacity means that for a given cooling capacity, the heat exchanger required can be more compact or for a given space or volume, the possible cooling capacity can be increased. Hence, in order to satisfy with the same cooling requirements, the largest heat exchanger has to be used in water based ejector cooling system.

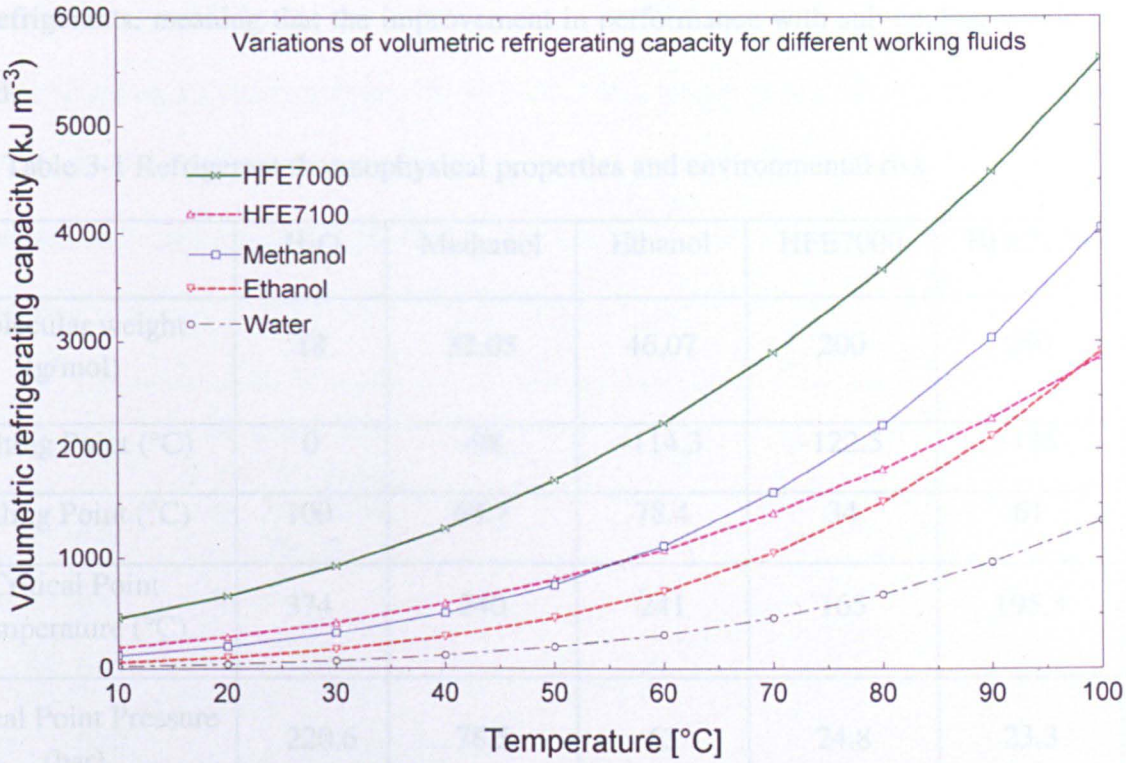

Figure 3-4 Variations in volumetric refrigerating capacity with temperature for HFE7000, HFE7100, methanol, ethanol and water

Table 3-1compares the refrigerants with respect to their thermophysical properties and safety. As concluded from the previous comparisons, the HFE refrigerants have better performance in terms of COP and are not flammable, explosive or toxic. However, they have a high GWP. EU directive 2006/40/EC restricts the use of refrigerants for air-conditioning system to a GWP of less than 150. Therefore a target GWP of less than 150 would rule out the HFE refrigerants. Of the alcohol based refrigerants considered, methanol is highly flammable and highly toxic, and so the hazards of using it in transport refrigeration are very high. Ethanol is flammable and toxic in large quantities, but its containment could be safely managed if adequate precautions are taken. It has a low GWP and good thermophysical properties and so is a good candidate for air-conditioning systems. Water is the safest and least damaging to the environment but its thermophysical properties are poor compared to the

other refrigerants, meaning that the improvement in performance with sub-cooling would be reduced.

Table 3-1 Refrigerant thermophysical properties and environmental risk

	H_2O	Methanol	Ethanol	HFE7000	HFE7100
Molecular weight (g/mol)	18	32.05	46.07	200	250
Melting Point (°C)	0	-98	-114.3	-122.5	-135
Boiling Point (°C)	100	64.7	78.4	34	61
Critical Point Temperature (°C)	374	240	241	165	195.3
Critical Point Pressure (bar)	220.6	78.5	63	24.8	23.3
Explosive limits	No	6-36%	3.3-24.5%	No	No
Flammable	No	Highly	yes	No	No
Toxic	No	Highly	If consumed in large amounts	No	No
GWP100	-	3	3	350	320

3.1.5.2 Effect of various operating conditions

The proper selection of working fluids is the first step towards better system performance. Ejector working conditions, such as generator temperature, evaporator temperature and condenser temperature, also place important roles on the ejector performance. The objective of this section is to analysis the impacts of these conditions with respect to ejector working performance.

Figure 3-5 shows the variation of system performance with respect to evaporator temperatures under generator temperatures of 110°C-130°C and condenser saturated

temperature fixed at 35°C. It can be seen that the COP increases considerably as the evaporator temperature changes from 5°C to 20°C. The reason is that more secondary flow will be entrained as evaporator temperature increases, which will result in a better system performance and cooling effect. However, this has to sacrifice with the desired cooling temperature.

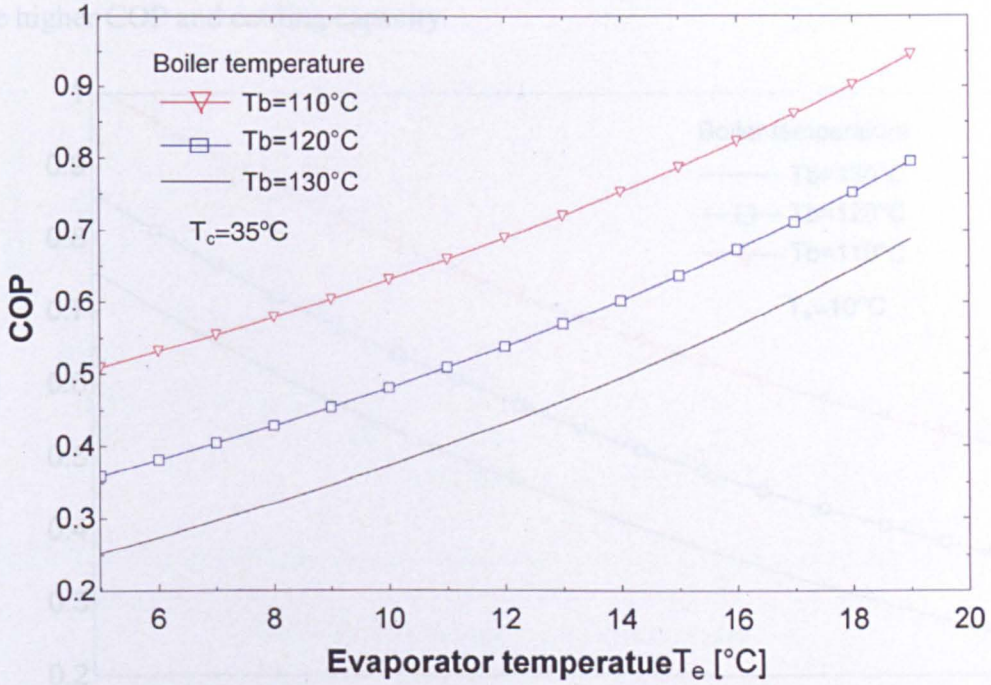

Figure 3-5 Variations of COP with evaporator temperature under different generator temperatures (T_c=35°C)

Figure 3-6 depicts the variations of system performance with respect to condenser temperature under generator temperature of 110°C-130°C and evaporator temperature fixed at 10°C. It can be seen that the COP decreases remarkably as the condenser temperature increases from 25°C to 40°C. The reason is that, when condenser temperature increases, the back pressure at the ejector exit goes up. This will consumes more input energy to re-compress the mixture, with less being used to entrain the secondary stream, which consequently leads to the reduced entrainment ratio and COP. If fixing the condenser temperature at 35°C, it could be found that COP decreased as the boiler temperature increased from 110°C to 130°C. This conclusion is only suitable for a particular ejector with defined

geometry and fixed evaporator and condenser temperature. According to Chunnanond and Aphornratana [9], when an ejector is operated with lower boiler temperature, a smaller primary mass flow will leave the primary nozzle with lower speed. This caused the expanded wave to fan out with smaller momentum. Since the mixing area of the mixed flow remains unchanged, higher secondary flow will be entrained from the evaporator. Thus, the system will have higher COP and cooling capacity.

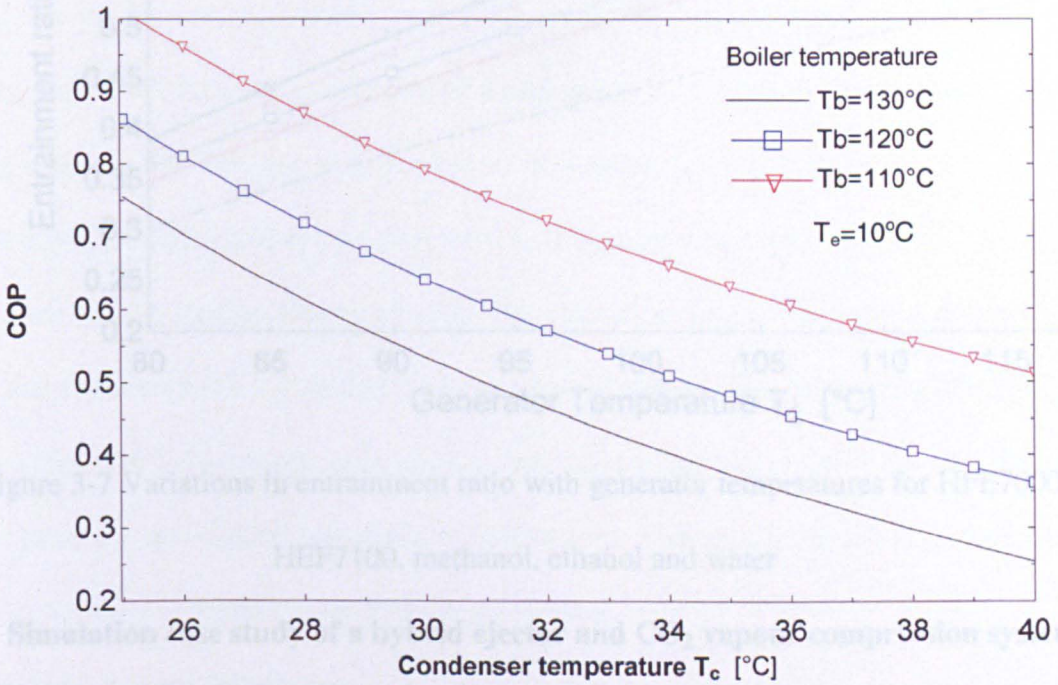

Figure 3-6 Variations of COP with condenser temperature under various generator temperatures (T_e=10°C)

Figure 3-7 shows the variations of entrainment ratio with generator temperatures. The curves in this diagram are different from these in Figure 3-6, which represent the optimized value of a certain ejector. Instead any point on the curves in Figure 3-7 represents a particular ejector at its designed condition. With evaporator temperature at 10°C and condenser temperature at 35°C, the entrainment ratio increases as the boiler temperature rises from 80°C to 120°C. A cycle designed to operate at higher boiler temperature would require an ejector with larger area ratio than another cycle.[44] This will result in higher driving pressure ratio

across the ejector system and hence more secondary flow is entrained, which causes the cooling capacity and COP to rise.

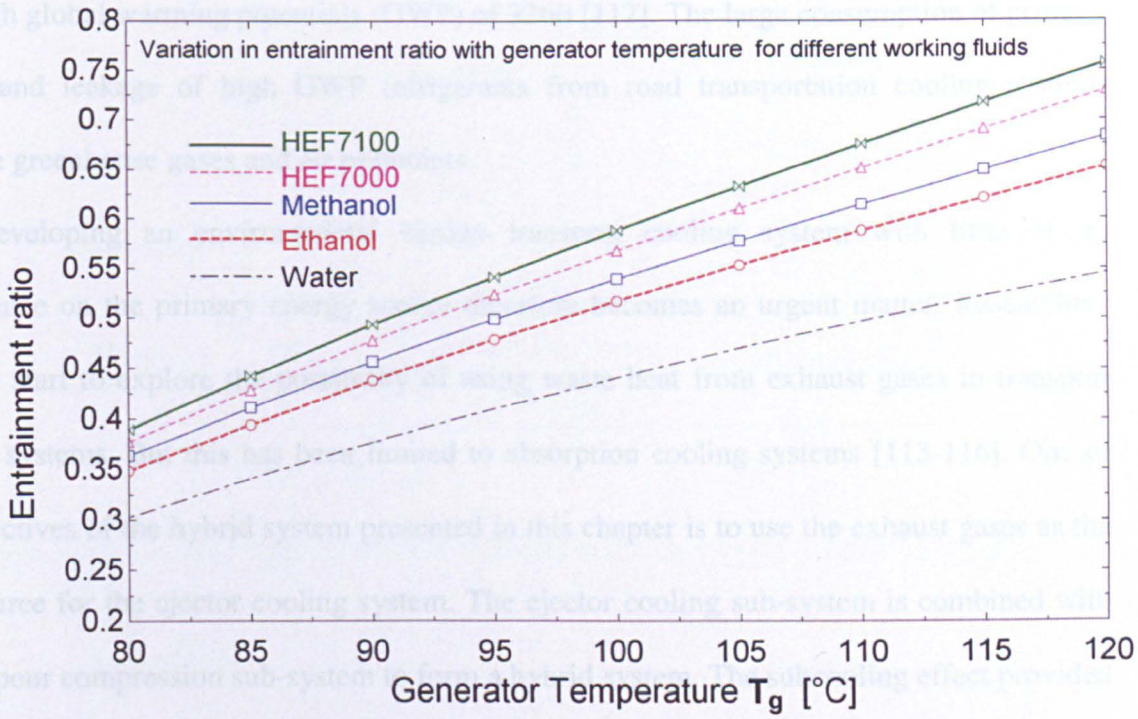

Figure 3-7 Variations in entrainment ratio with generator temperatures for HFE7000, HEF7100, methanol, ethanol and water

3.2 Simulation case study of a hybrid ejector and CO_2 vapour compression system

Recent years' researches have laid emphasis on combining the ejector cycle with other systems, with the aims to improve the system performance of either the ejector cycle or other systems. This section theoretically analyzes a novel hybrid ejector and CO_2 vapour compression system.

3.2.1 Introduction

In the era of economic globalisation, the distances between the location of food production and retailing shops are increasing dramatically. Food transportation vehicles, therefore, require effective cooling systems which can maintain a given temperature for food preservation. According to DEFRA [110], the energy consumed to store and preserve food during road transportation accounts for 10% to 25% of the total energy used in refrigerated

vehicles [111]. Moreover, the leakage of total refrigerant charge can range from 10% to 37% per annum [111]. One of the most common refrigerants in transport systems is R404a, with very high global warming potentials (GWP) of 3260 [112]. The large consumption of primary energy and leakage of high GWP refrigerants from road transportation cooling systems generate greenhouse gases and air pollutants.

Developing an environmental benign transport cooling system with little or no dependence on the primary energy source therefore becomes an urgent matter. Researchers recently start to explore the possibility of using waste heat from exhaust gases in transport cooling systems. But this has been limited to absorption cooling systems [113-116]. One of the objectives of the hybrid system presented in this chapter is to use the exhaust gases as the heat source for the ejector cooling system. The ejector cooling sub-system is combined with CO_2 vapour compression sub-system to form a hybrid system. The subcooling effect provided by the ejector to CO_2 vapour compression sub-system consequentially reduces the energy consumption by the vapour compression sub-system. Theoretical simulation results for the hybrid system are presented in the following sections.

3.2.2 Hybrid system description

Figure 3-8 shows a simplified system diagram of the hybrid ejector and CO_2 Vapour compression (VC) cooling system. The typical operating conditions and corresponding P-h and T-s diagrams of the two sub-systems are shown in Figures 3-9 and Figure 3-10. The CO_2 VC sub-system is shown by the dash lines and the ejector sub-system is shown by the solid lines. Water is selected as the working fluid in the ejector sub-system.

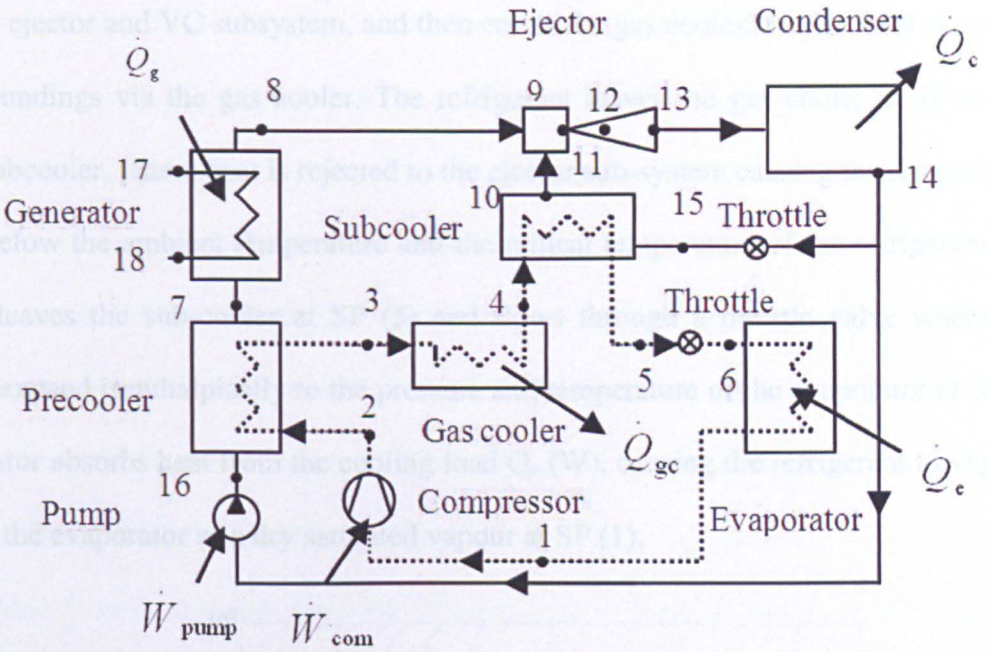

Figure 3-8 Schematic diagram of hybrid ejector and CO_2 vapour compression system

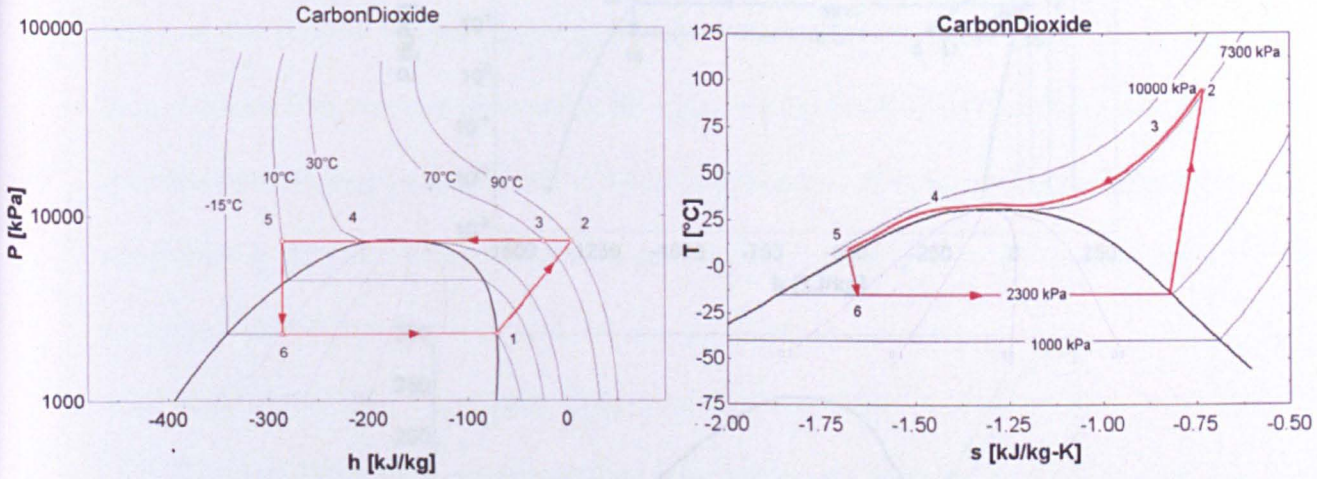

Figure 3-9 P-h and T-s diagrams of the vapour-compression CO2 cycle

In the CO_2 VC sub-system, the refrigerant leaves the evaporator at state point SP (1) and its pressure is increased by the compressor to SP (2). It is assumed that the refrigerant was compressed and losses are taken into account by assuming an isentropic coefficient of 0.8. The refrigerant will not condense in the supercritical region and so it is assumed to be cooled at constant pressure and with a temperature glide from SP (2) through to SP (5). The refrigerant leaves the precooler at SP (3) at a lower temperature, due to the heat transfer

between the ejector and VC subsystem, and then enters the gas cooler. Further heat is rejected to the surroundings via the gas cooler. The refrigerant leaves the gas cooler at SP (4) and enters the subcooler, where heat is rejected to the ejector sub-system causing the refrigerant to be cooled below the ambient temperature and the critical temperature of the refrigerant. The refrigerant leaves the sub-cooler at SP (5) and flows through a throttle valve where it is assumed to expand isenthalpically to the pressure and temperature of the evaporator at SP (6). The evaporator absorbs heat from the cooling load Q_e (W), causing the refrigerant to vaporise and leaving the evaporator as a dry saturated vapour at SP (1).

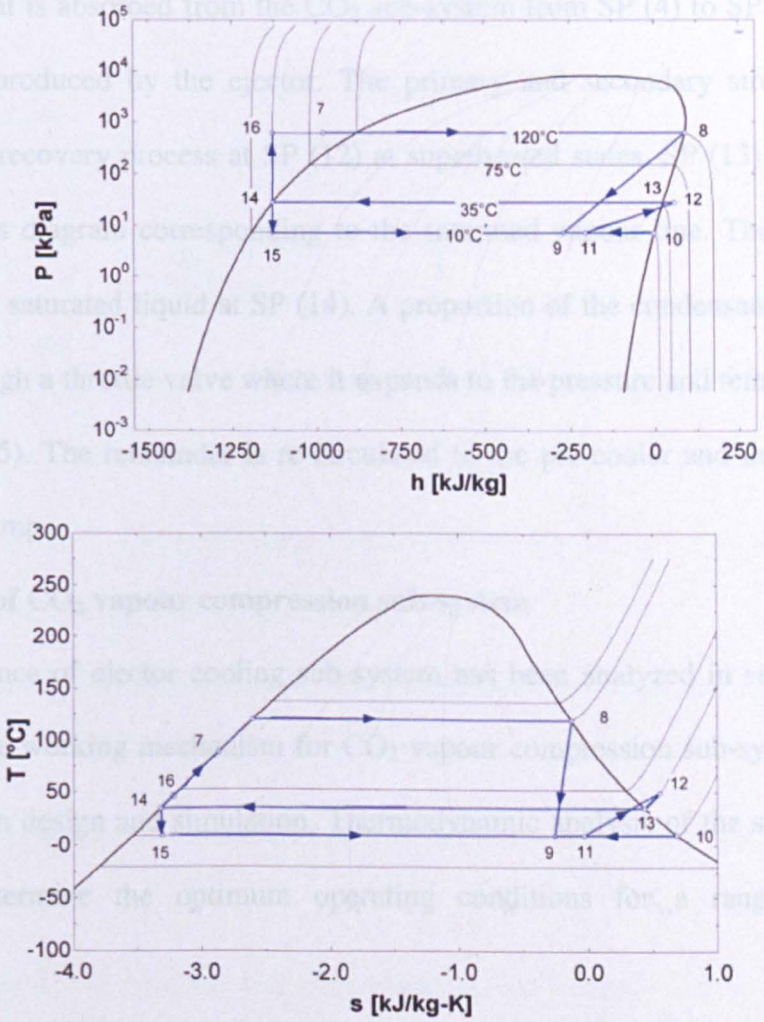

Figure 3-10 P-h and T-s diagrams of sub-cooler ejector-pump cycle

In the ejector sub-system shown in Figure 3-8, liquid refrigerant at SP (14) is pumped at constant temperature to a pressure corresponding to the pre-cooler pressure at SP (16). The

refrigerant enters the pre-cooler where heat is transferred from the CO_2 VC sub-system corresponding to SP (2-3), causing sensible heat increase of the refrigerant. The refrigerant leaves the pre-cooler at SP (7). It then enters the boiler, where heat from the exhaust gas of the engine is used to vaporize the refrigerant, and leaves the exhaust heat exchanger as a dry saturated vapour at SP (8). The vapour expands through a convergent-divergent nozzle and leaves the nozzle at SP (9). The stream is known as the primary flow. At the exit from the nozzle, the primary flow creates a low pressure region which entrains vapour surrounding the nozzle and induces flow from the subcooler. The flow from the subcooler is known as the secondary flow. Heat is absorbed from the CO_2 sub-system from SP (4) to SP (5) to balance the cooling effect produced by the ejector. The primary and secondary streams mix and undergo a pressure recovery process at SP (12) at superheated states. SP (13) represents the point on the process diagram corresponding to the saturated vapour line. The refrigerant is then condensed to a saturated liquid at SP (14). A proportion of the condensate is returned to the sub-cooler through a throttle valve where it expands to the pressure and temperature of the sub-cooler at SP (15). The remainder is re-circulated to the pre-cooler and the exhaust heat exchanger by the pump.

3.2.3 Exploitation of CO_2 vapour compression sub-system

The performance of ejector cooling sub-system has been analyzed in section 3.1. The understanding of the working mechanism for CO_2 vapour compression sub-system is crucial to the hybrid system design and simulation. Thermodynamic analysis of the sub-system was carried out to determine the optimum operating conditions for a range of ambient temperatures.

3.2.3.1 CO_2 vapour compression system description

As shown from Figure 3-11, the CO_2 VC sub-system consists of an evaporator that absorbs heat, Q_e, from the load causing boiling of the two phase refrigerant to a dry saturated

condition at exit. A compressor does work W_c, to raise the pressure of the refrigerant from the evaporator to the gas cooler operating pressure. Above the critical temperature, discharge pressure can be controlled independently of temperature. State 2 indicates to the pressure and temperature that optimises the COP for the given operating conditions. In this case the discharge pressure was approximately 8750kPa and the discharge temperature was 92°C. The process 2-3 operates above the critical point and so heat Q_{gc} is rejected at constant pressure but with reduction in temperature from 92°C to 35°C. The exit temperature from the gas cooler was assumed to be 35°C, which is a peak North European summer ambient temperature.

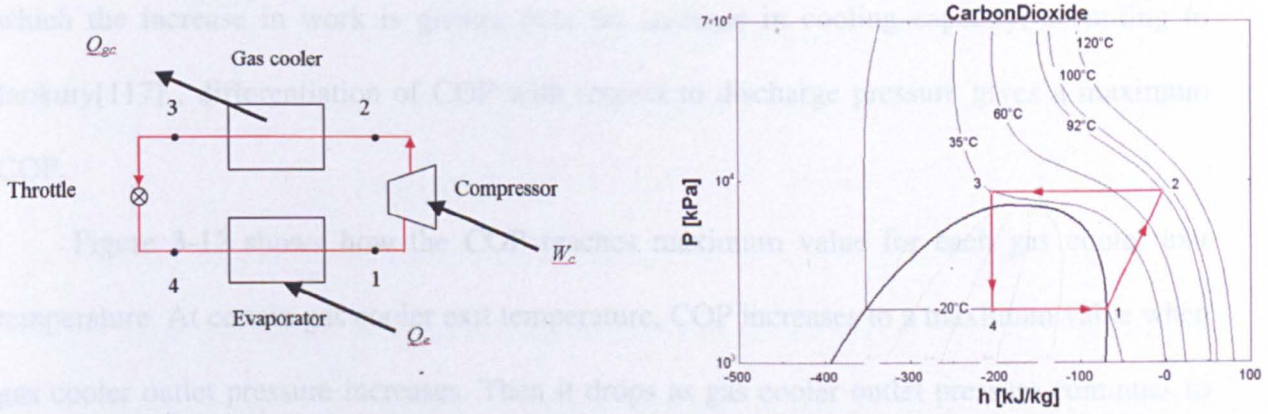

Figure 3-11 Transcritical CO_2 vapour-compression cycle and p-h diagram of the process

The cycle is based on the following assumptions:

1) The refrigerant is assumed to be compressed with isentropic efficiency of 0.8 (process 1-2).

2) The refrigerant is assumed to pass through the throttle isenthalpically (process 3-4).

3) Losses due to frictions and temperature differences across heat exchangers are assumed to be neglected.

3.2.3.2 Thermodynamic analysis of CO_2 vapour compression system

Thermodynamic analysis of the sub-system cycle has been carried out to determine the optimum operating conditions for a range of ambient temperatures. A number of simulations were carried out to investigate the relationship between discharge pressure, COP and gas cooler exit temperature. At a constant evaporator temperature of -10°C, gas cooler exit temperatures of 35°C, 40°C, 45°C and 50°C are used and the discharge pressure is varied parametrically for each simulation to obtain the results.

Inspection of the p-h diagram in Figure 3-11 shows that as the discharge pressure increases, the isotherms become steeper and closer together. Thus a point is reached above which the increase in work is greater than the increase in cooling capacity, according to Inokuty[117] , differentiation of COP with respect to discharge pressure gives a maximum COP.

Figure 3-12 shows how the COP reaches maximum value for each gas cooler exit temperature. At certain gas cooler exit temperature, COP increases to a maximum value when gas cooler outlet pressure increases. Then it drops as gas cooler outlet pressure continues to rise. The optimum discharge pressure is higher at higher gas cooler exit temperatures and the optimum COP decreases with increasing optimum discharge pressure. The optimized discharge pressures were then used to determine the performance at a gas cooler exit temperature of 35°C and 50°C, representing typical North European and Southern European summer ambient temperatures. The optimum discharge pressure, COP and discharge temperature at a gas cooler exit temperature of 35°C were found to be 8750kPa, 2.02 and 92°C, respectively. In comparison, these values were found to be 14500kPa, 1.26 and 135°C at gas cooler exit temperature of 50 °C, respectively. It could be concluded from Figure 3-12 that a lower gas cooler outlet temperature could contribute to a higher performance of CO_2 vapour compression sub-system.

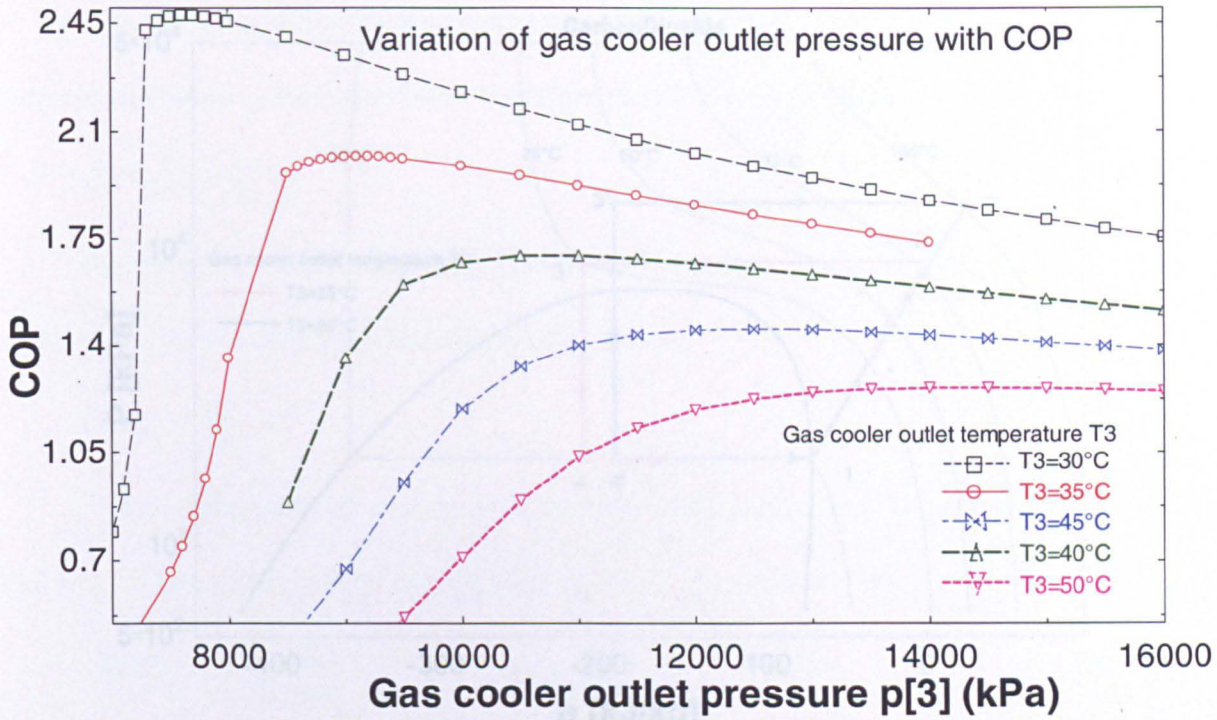

Figure 3-12 Variations of COP with compressor discharge pressure at gas cooler temperature of 35°C, 40°C, 45°C and 50°C

Figure 3-13 shows how an increase in gas cooler exit temperature causes a reduction in refrigeration effect and an increase in compressor work, thus reducing COP. One method of improving the performance of the CO_2 vapour compression sub-system is to further cool the refrigerant at the gas cooler exit so that the temperature at point 3 is below the ambient temperature. Hence, the evaporator of the ejector cooling sub-system is positioned at the outlet of the gas cooler and functions as a gas cooler in the hybrid system, to provide sub-cooling effect for CO_2 vapour compression sub-system.

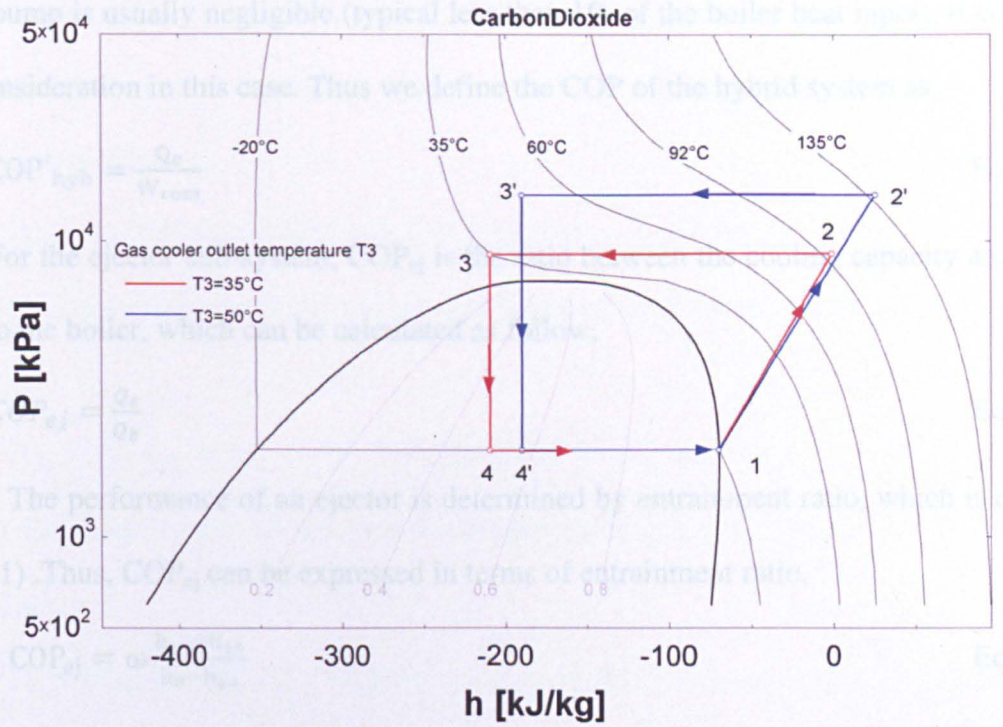

Figure 3-13 p-h diagram of process at gas cooler outlet temperature of 35°C and 50°C

3.2.4 Simulation of hybrid ejector and CO_2 vapour compression cooling system

3.2.4.1 Performance parameters

The thermodynamic performance of a cooling cycle is measured by the coefficient of performance (COP), defined as the ratio of the cooling capacity to the total energy input to drive the cycle. Generally the energy input in the hybrid system takes into considerations of the boiler heat input, the power consumption of the compressor and pump. Therefore the COP of the hybrid system can be defined as,

$$COP_{hyb} = \frac{Q_e}{W_{com}+W_{pum}+Q_b} \qquad \text{Eq. (3.29)}$$

An important feature of the hybrid system is the use of waste heat to drive the ejector sub-system. Sokolov and Hershgal [20] showed that if the heat driving the ejector was from waste heat or renewable sources, then the economic cost is low or zero. So we could define a COP that reflected the economic benefits of exploiting the waste heat. Since the power input

at the pump is usually negligible (typical less than 1% of the boiler heat input), it is not taken into consideration in this case. Thus we define the COP of the hybrid system as,

$$COP'_{hyb} = \frac{Q_e}{W_{com}} \qquad \text{Eq. (3.30)}$$

For the ejector sub-system, COP_{ej} is the ratio between the cooling capacity and the heat input to the boiler, which can be calculated as follow,

$$COP_{ej} = \frac{Q_e}{Q_b} \qquad \text{Eq.(3.31)}$$

The performance of an ejector is determined by entrainment ratio, which is defined in Eq. (3.1) .Thus, COP_{ej} can be expressed in terms of entrainment ratio,

$$COP_{ej} = \omega \frac{h_{10} - h_{14}}{h_8 - h_{14}} \qquad \text{Eq. (3.32)}$$

Where h_{10} and h_8 are the enthalpies at the evaporator and boiler at saturated vapour state, and h_{14} is the enthalpy at the condenser in the saturated liquid state, assuming that it is an ideal cycle.

3.2.4.2 Ejector sub-system analysis

The operation of the ejector sub-system is normally characterised by the exhaust gas heat exchanger, sub-cooler and condenser temperatures and the total refrigerant mass flow rate within the ejector sub-system. With the flow properties at SP (8), SP (10), SP (12) known, the analysis of ejector sub-system can be easily carried out.

The performance of the ejector is characterized by the conditions at SP (8), SP (10) and SP (12). The steam properties generated from exhaust gas at SP (8), entering the ejector, is given by the following saturated steam relationships:

$$T_8 = f_T(T_g),\ P_8 = f_P(T_g),\ h_8 = f_h(T_g) \qquad \text{Eq. (3.33)}$$

If the sub-cooler outlet temperature is selected, and the degree of superheating ΔT is defined, then the properties of vapour at SP (10) can be estimated from:

$$T_{10} = f_T(T_{sb}),\ P_{10} = f_P(T_{sb}),\ h_{10} = f_h(T_{sb}) \qquad \text{Eq. (3.34)}$$

The properties of the fluids at SP (8) and SP (10) are given by Eq. (3.33) and Eq. (3.34). The properties of the condensed liquid at SP (14) emerging from the condenser are determined as follows:

$$T_{14} = f_T(T_c),\ P_{14} = f_P(T_c),\ h_{14} = f_h(T_c),\ m_{14}=m_8 + m_{10} \qquad \text{Eq. (3.35)}$$

The condensate pumped to the exhaust heat exchanger increases its enthalpy at SP (16), that is

$$P_{16} = P_8,\ h_{16} = h_{14} + (P_{16} - P_{14})v_{14},\ T_{16} = T_{14},\ m_{16}=m_8 \qquad \text{Eq. (3.36)}$$

If the effectiveness of the heat exchanger Ex is assumed, the fluid in SP (7) can be derived as:

$$T_7 = (T_{16} - E_x T_2)/(1 - E_x),\ P_7 = P_8,\ h_7 = f_h(T_7, P_7),\ m_7=m_8 \qquad \text{Eq. (3.37)}$$

Through the expansion valve, the fluid pressure is reduced to the sub-cooler pressure, therefore,

$$P_{15} = P_{16},\ h_{15} = h_{14},\ T_{15} = f_T(P_{15}, h_{15}),\ m_{15}=m_{10} \qquad \text{Eq. (3.38)}$$

In order to determine the COP of ejector sub-system, energy balances at the exhaust gas heat exchanger and pump are required (assuming pump efficiency η_{Pum}=0.7):

$$Q_{exh} = m_8(h_8 - h_7),\ W_p = m_8(h_{16} - h_{14})/\eta_{Pum} \qquad \text{Eq. (3.39)}$$

In the above equations, the thermodynamic functions $f_T(), f_P()$ and $f_h()$ refer to equations for calculating the equilibrium temperature, pressure and enthalpy of H_2O refrigerant.

3.2.4.3 CO_2 VC sub-system analysis

The operation of CO_2 VC sub-system is characterized by working conditions on evaporator, sub-cooler, compressor and total mass flow rate. Referring to road vehicle cooling system, the cold space temperature is selected as $T_1 = -15°C$ and the degree of superheating is assumed to be ΔT, and the pressure and enthalpy at SP (1) can be calculated by:

$$P_1 = F_P(T_1)\ ,\ h_1 = F_h(T_1) \qquad \text{Eq. (3.40)}$$

The refrigerant leaves the evaporator and compressed to a higher pressure by the compressor. It was assumed that the refrigerant was compressed with an isentropic efficiency of 0.8. Optimum compressor discharge pressure p_2 is predetermined to be 87.5bar [118]. Therefore the following equations can be obtained:

$$h_{2,isen} = F_h(P_2, s_2 = s_1),\ w = (h_{2,isen} - h_1)/0.8,\ h_2 = h_1 + w,\ T_2 = F_T(P_2, h_2) \quad \text{Eq. (3.41)}$$

The refrigerant is assumed to be cooled at constant pressure with temperature glide from SP (2) to SP (5). The pre-cooler outlet temperature T_3 can be determined by the effectiveness of heat exchanger E_x.

$$T_3 = (1 - E_x)T_2 + E_x T_{16},\ P_3 = P_2,\ h_3 = F_h(T_3, P_3) \quad \text{Eq. (3.42)}$$

The sub-cooler inlet temperatures T_4 is set as 35°C, therefore,

$$P_4 = P_3,\ h_4 = F_h(T_4, P_4) \quad \text{Eq. (3.43)}$$

The sub-cooler is the main connection between the ejector sub-system and CO_2 VC sub-system. And the fluids properties at SP (10) and SP (15) are given by equations Eq. (3.34) and Eq. (3.38). Assuming the sub-cooler effectiveness E_x, the fluid property from the outlet of sub-cooler at SP5 is,

$$T_5 = (1 - E_x)T_4 + E_x T_{10},\ P_5 = P_4,\ h_5 = F_h(T_5, P_5) \quad \text{Eq. (3.44)}$$

Through the throttle valve, the fluid pressure is reduced to the evaporator pressure, therefore,

$$T_6 = T_1,\ P_6 = P_1,\ h_6 = h_5 \quad \text{Eq. (3.45)}$$

In order to determine the COP of CO_2 VC sub-system, energy balances at the evaporator and compressor are derived as (assuming compressor efficiency η_{com}=0.8):

$$Q_e = \mathrm{m}(h_1 - h_6),\ W_{com} = \mathrm{m}(h_2 - h_1)/\eta_{com} \quad \text{Eq. (3.46)}$$

In the above equations, the thermodynamic functions $F_T(), F_P()$ and $F_h()$ refer to equations for calculating the equilibrium temperature, pressure and enthalpy of CO_2

refrigerant. All the thermodynamic functions were determined from in-built properties using EES [119].

3.2.4.4 Simulation results and discussions

A parametric study of the performance of the hybrid system at various boiler and sub-cooler conditions was carried out for boiler temperature of 120°C, gas cooler outlet temperature of 35°C, evaporator temperature of -15°C and cooling capacity of 0.5kW.

3.2.4.4.1 Performance comparisons of hybrid ejector - CO_2 VC cycles

With the aim to analyze the performance enhancement of the hybrid system, comparisons (shown in Figure 3-14 and Figure 3-15) have been made between the performance of single systems and these in the hybrid system.

Figure 3-14 shows the improvement in system performance of the ejector sub-system in the hybrid system compared with single ejector cycle. As evaporator temperature increases from 5°C to 15°C, COP of single ejector cycle increases from 0.362 to 0.598, while COP of ejector sub-system in hybrid system improves from 0.442 to 0.730. With the same evaporator temperature at 10°C, COP improves about 22% from 0.470 of single ejector cycle to 0.584 of ejector sub-system. It is obvious that the hybrid cycle surpasses the single ejector cycle at all working conditions. One of the advantages for hybrid system is that, at high ambient conditions, the evaporator temperature could be allowed to increase and enable the ejector to operate satisfactorily. The loss in cooling due to the increase in evaporator temperature could be compensated by an increase in the secondary flow and therefore cooling capacity and COP. The implementation of hybrid system with sub-cooler (evaporator in the ejector sub-system) setting at high temperature range (25°C to 35°C) will help to make the system more efficient. However, the same evaporator temperature in conventional ejector cooling system is not applicable.

Similar performance enhancement can be found in Figure 3-15, which shows the COP of the CO_2 VC sub-system in hybrid system in comparison with single CO_2 VC cycle. The results indicated that with evaporator temperature in the range of -15°C to -6°C, COP of CO_2 VC sub-system increases from 2.99 to 4.00 (around 33.3% rise), while COP of single CO_2 VC cycle increases from 2.14 to 2.52 (around 17.8% rise). Taking the same evaporator temperature of -10°C, COP is dramatically improved around 45.2% from 2.41 of single CO_2 VC cycle to 3.5 of CO_2 VC sub-system. The reason is that with the sub-cooling degree introduced by the ejector and sub-cooler, the mechanical work consumed by compressor decreases. Moreover, the refrigerant enters the evaporator with a reduced dryness fraction and hence, the refrigeration effect is improved.

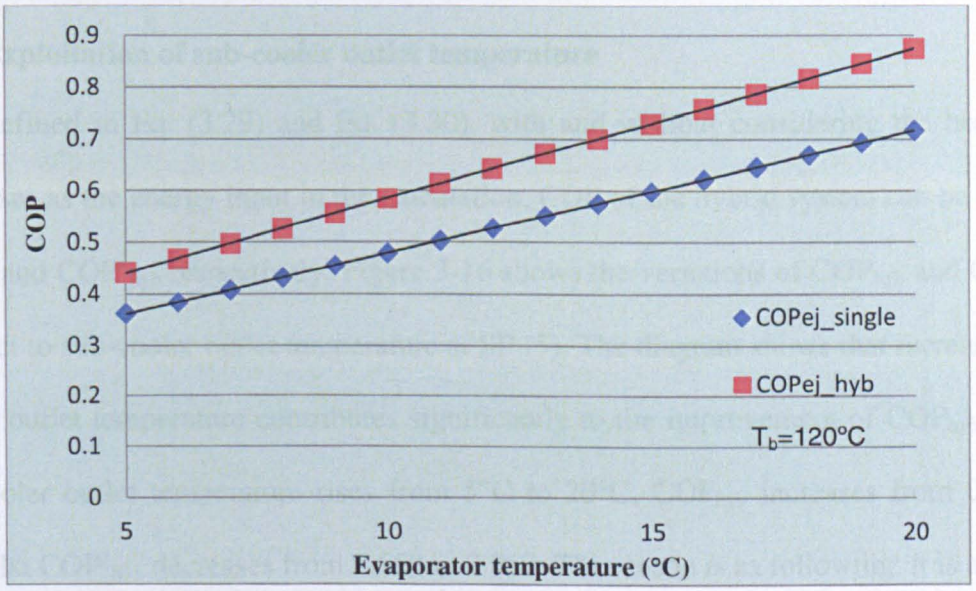

Figure 3-14 Variations in COP with respect to evaporator temperature (T_b=120°C)

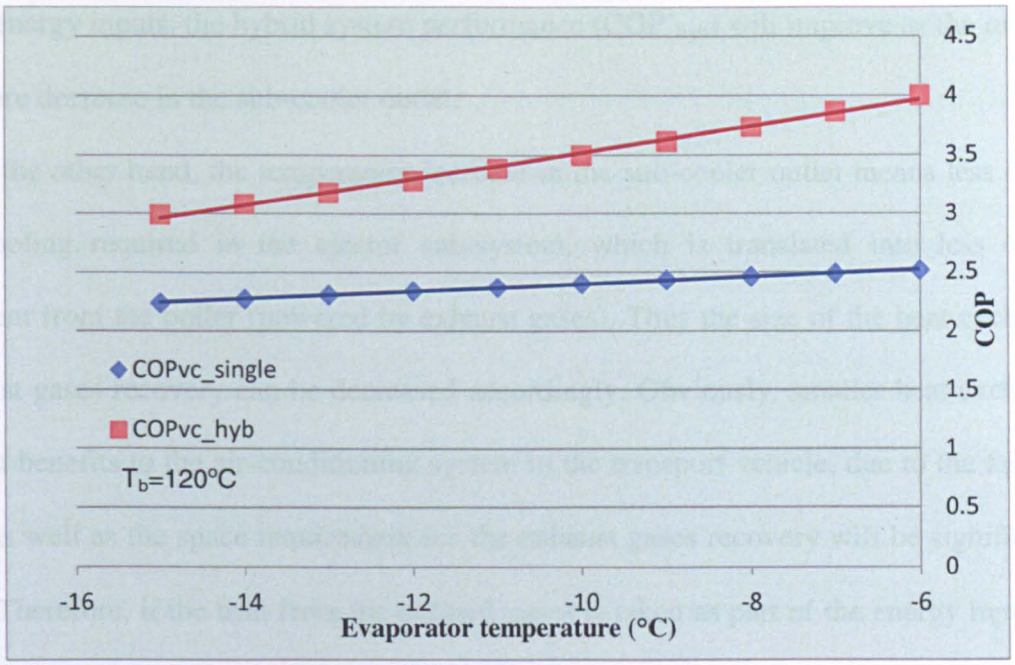

Figure 3-15 Variations in COP with respect to evaporator temperature (T_b=120°C)

3.2.4.4.2 Exploitation of sub-cooler outlet temperature

As defined in Eq. (3.29) and Eq. (3.30), with and without considering the heat from exhaust gases as the energy input in the calculation, COP of the hybrid system can be defined as COP_{hyb} and COP'_{hyb} respectively. Figure 3-16 shows the variations of COP_{hyb} and COP'_{hyb} with respect to sub-cooler outlet temperature at SP (5). The diagram shows that increasing the sub-cooler outlet temperature contributes significantly to the improvement of COP_{hyb}. When the sub-cooler outlet temperature rises from 5°C to 20°C, COP_{hyb} increases from 0.085 to 0.621, whilst COP'_{hyb} decreases from 3.659 to 2.967. The reason is as following: it is assumed that the evaporator is at a constant cooling capacity (0.5kW) and expansion through the throttle valve is isenthalpic. Therefore, a reduction in temperature at SP (5) will reduce the enthalpy at SP (6), which contributes to the increase of enthalpy difference between SP (1) and SP (6) and an enhancement in the refrigeration effect. As evaporator cooling capacity remains constant, the increase in enthalpy difference will reduce the mass flow required and thus the work done by the compressor. In this case, when considering the exhaust gases as the

cost free energy inputs, the hybrid system performance (COP'_{hyb}) will improve as the result of temperature decrease in the sub-cooler outlet.

On the other hand, the temperature increase in the sub-cooler outlet means less degree of sub-cooling required in the ejector sub-system, which is translated into less energy requirement from the boiler (powered by exhaust gases). Thus the size of the heat exchanger for exhaust gases recovery can be decreased accordingly. Obviously, smaller heat exchanger is of great benefits to the air-conditioning system in the transport vehicle, due to the fact that the cost as well as the space requirement for the exhaust gases recovery will be significantly reduced. Therefore, if the heat from the exhaust gases is taken as part of the energy input, the performance (COP_{hyb}) and the total investment cost of the hybrid system will improve as the result of temperature increase in the sub-cooler outlet.

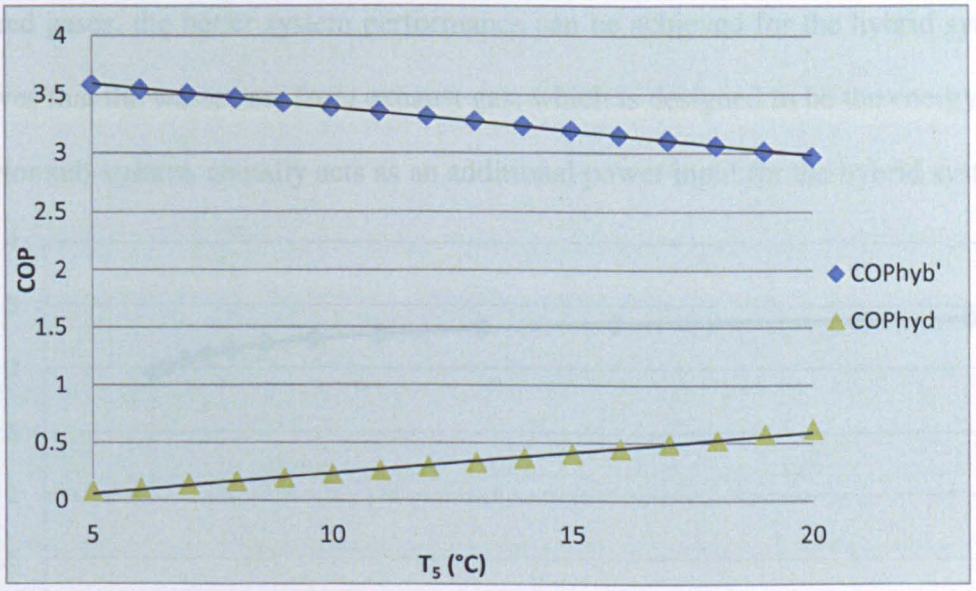

Figure 3-16 Variations in COP for sub-systems with respect to temperature at SP5

3.2.4.4.3 Exploitation of energy consumption ratio between ejector sub-system and CO_2 VC sub-system

In order to analyze the energy consumption relationship between the ejector sub-system and CO_2 VC sub-system, the ratio between energy provided by exhausted gas and cooling capacity of the evaporator α is defined. According to the test results on the exhaust system of

a four-cylinder spark-ignition vehicle engine [120], with frequency of rotation between 1500-4500 RPM, the exhaust gas power was in the range of 2-9kW. Meanwhile, cooling capacity required for vehicle air-conditioning was in the range of 2.5-6kW [121]. Hence, the ratio α between exhaust gas power and air-conditioning capacity of the vehicle is approximately in the range of 0.8-1.5.

With a boiler temperature of 120°C and the temperature at SP (5) in the range of 10°C to 20°C, the variations of system performances for ejector sub-system and hybrid system with respect to α are shown in Figure 3-17. The diagram indicates that as α increases from 0.28 to 2.38, the COP of the hybrid system (COP'_{hyb}) slightly increases from 2.97 to 3.40, approximately14.5%. Although COP'_{hyb} is limited by the degree of sub-cooling, it is still affected by the energy consumption ratio α. This means that the more energy obtained from the exhausted gases, the better system performance can be achieved for the hybrid system. It further proves that the waste heat from exhaust gas, which is designed to be the energy supply for the ejector sub-system, actually acts as an additional power input for the hybrid system.

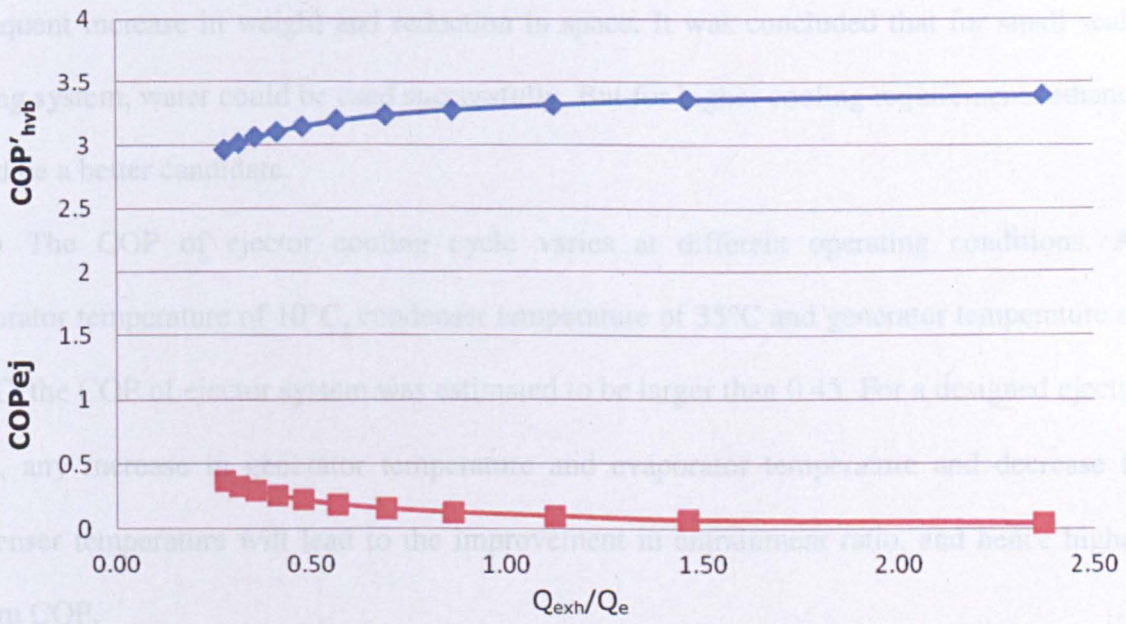

Figure 3-17 Variations in COP'_{hyb}, COP_{ej} with respect to α

3.3 Conclusion

Thermodynamic simulations were carried out on the ejector cooling system. Firstly, different refrigerants were compared to identify the most appropriate working fluid for use in the ejector system. Secondly, system performances under different working conditions were studied respectively for the ejector cycle and CO_2 VC cycle. Finally, the performance of a novel hybrid ejector and CO_2 VC system was studied by varying the temperature at both sides of the sub-cooler. Analysis of the numerical results showed the following conclusions:

1) For different working fluids, under the same operating conditions, the COP of HFE7000 and HFE7100 were relatively high, while that for water was comparatively low. Although HFE7000 and HFE7100 showed superior working performance, a global warming potential (GWP) of over 150 made them unacceptable for cooling system. Methanol and ethanol were superior to water, but methanol was highly toxic, explosive and flammable. Ethanol was much less toxic and flammable and had superior properties to water. Water was the safest but had the poorest performance and would require large heat transfer area, with the subsequent increase in weight and reduction in space. It was concluded that for small scale cooling system, water could be used successfully. But for higher cooling requirements ethanol would be a better candidate.

2) The COP of ejector cooling cycle varies at different operating conditions. At evaporator temperature of 10°C, condenser temperature of 35°C and generator temperature of 120°C, the COP of ejector system was estimated to be larger than 0.45. For a designed ejector cycle, any increase in generator temperature and evaporator temperature and decrease in condenser temperature will lead to the improvement in entrainment ratio, and hence higher system COP.

3) For the CO_2 VC cycle, an increase in gas cooler exit temperature will cause a reduction in refrigeration effect and an increase in compressor work. Hence, the optimised

discharge pressure of 8760kPa at a gas cooler exit temperature of 35°C was obtained and used to determine operating characteristics of the cycle.

4) The simulation results of hybrid ejector and CO_2 VC cooling system showed that, at boiler temperature of 120°C, evaporator temperature of 10°C, COP of hybrid system was 0.584, i,e about 22% improvement compared with COP of 0.479 for single ejector cycle. At boiler temperature of 120°C, evaporator temperature of -10°C, the COP of VC sub-system was dramatically improved around 45.2% to 3.5, compared with COP of 2.41 for single CO_2 VC cycle. Exploitation of the energy consumption ratio between ejector sub-system and CO_2 VC sub-system indicated that as the energy extracted from the exhausted gases increased, the performance of the CO_2 VC sub-system improved, and hence higher cooling capacity.

Chapter 4 Experimental Investigations of Ejector Cooling System

In this chapter, an ejector cooling system was built in the laboratory and the performance was evaluated with boiler temperatures between 115°C and 130°C, and evaporator temperatures between 5°C and 10°C. The entrainment ratio and coefficient of performance (COP) of the system were measured for all the cases. The experimental results were compared with the simulation results obtained in Chapter 3.

As reviewed in Chapter 2, researchers hold different views on the performance enhancement of the ejector under changing nozzle exit positions. No general agreement exists for the effects of nozzle exit positions. The impact of various nozzle exit positions on the system performance is therefore of great research value. Two different nozzle exit positions were tested in the experiments, and 6% COP variations were obtained.

The experimental results were obtained when ejector operated under critical pressure, while boiler temperature and evaporator temperature were at the designed values. When the ambient conditions (condenser temperature/pressure) changed, the system had to operate in different mode. Discussions were also included on how to vary the ejector working conditions so that the system performance could still be optimized under such conditions.

4.1 Description of test rig

A basic ejector cooling system consists of a generator, an ejector, a condenser, an evaporator, a circulation pump and an expansion valve. Test apparatus and schematic diagram are shown in Figure 4-1 and Figure 4-2. The high temperature and pressure vapour (point 3) gains heat (Q_b) from the external heat source, in this case from the boiler, enters the ejector and flows through a converging-diverging nozzle (known as the primary nozzle of ejector), where it expands to supersonic flow and creates a low pressure region at the nozzle exit. The

pressure difference produced by the primary flow causes the refrigerant vapour (known as secondary flow) to be entrained from the evaporator (point 5). The combined streams are assumed to be completely mixed at the end of the mixing chamber and the flow speed is supersonic. A normal shock wave is then produced within the constant-area section, creating a compression effect, and the flow speed is reduced to subsonic value. Further compression of the fluid is achieved as the combined streams flow through the subsonic diffuser section (point 6).

The fluid leaves diffuser and enters into condenser (point 7), where it is liquefied by rejecting the heat (Q_c) to ambient. Part of the condensed liquid is returned back to generator after a pressure lift by the circulation pump (point 2), while the remaining liquid enters the evaporator after undergoing a pressure reduction in the expansion valve (point 9). In the evaporator, the fluid evaporates due to the heat gain (Q_e) from the cooling space. In this way, the ejector cooling system is completed.

Detailed descriptions of the main components included in the system, test procedures are discussed in the following section.

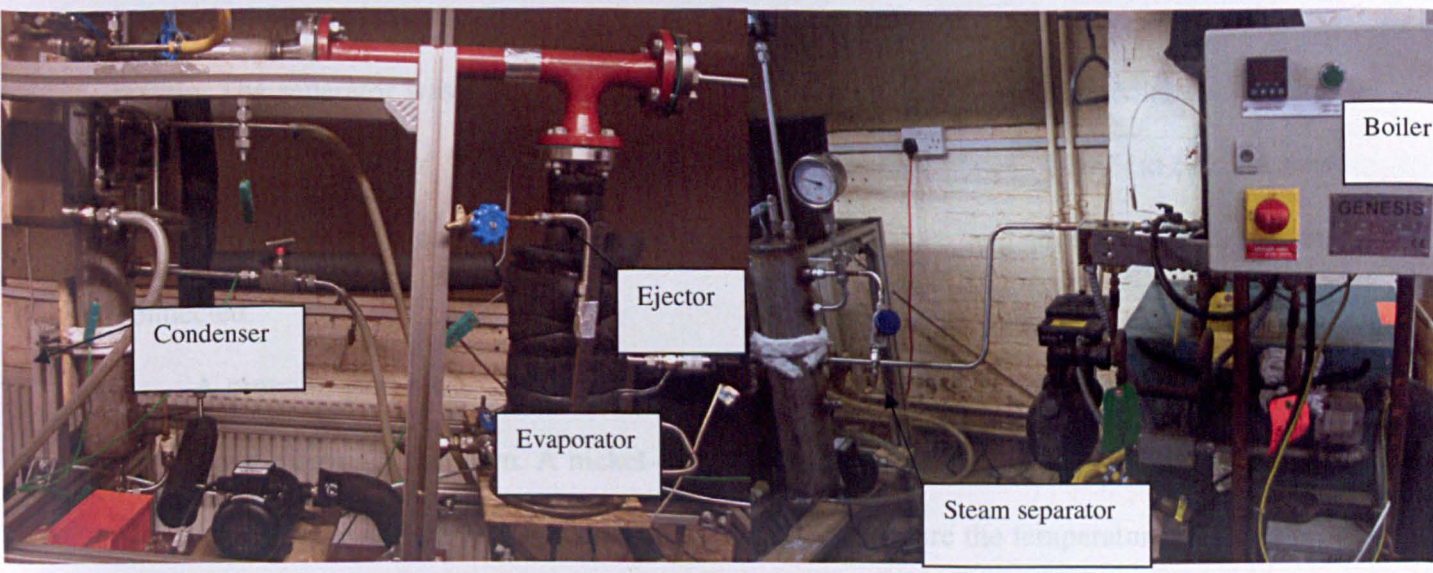

Figure 4-1 photos of ejector cooling system

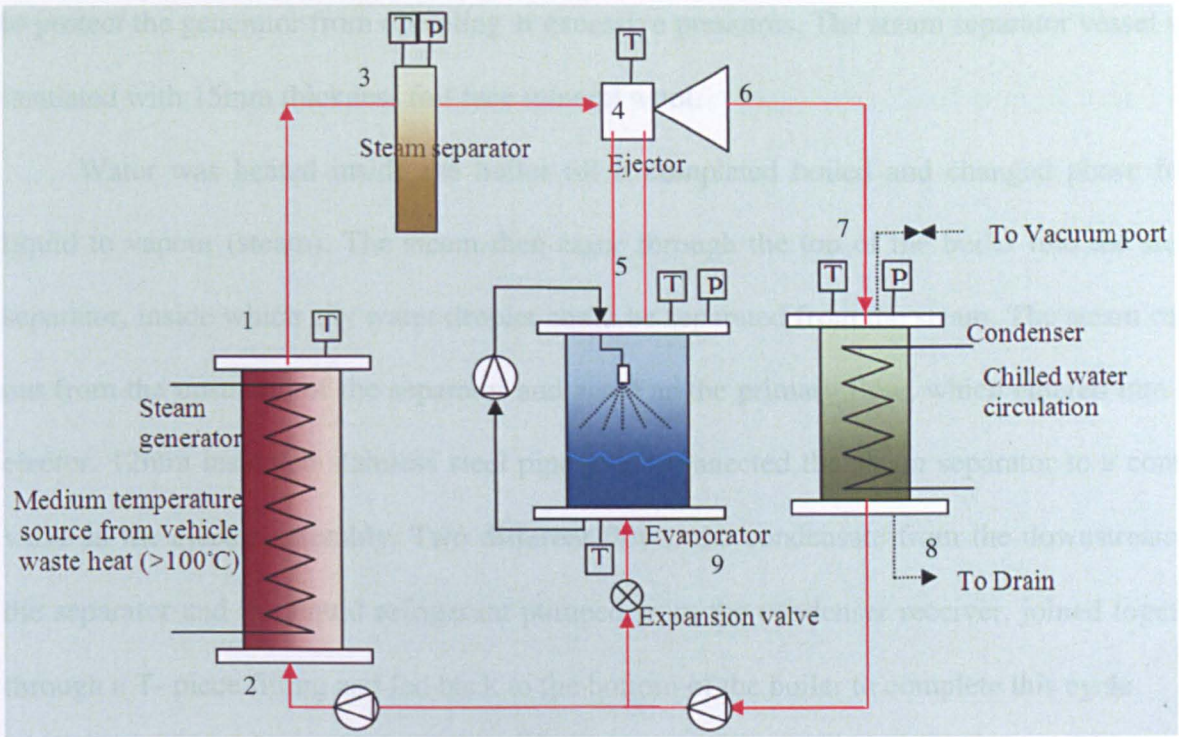

Figure 4-2 Schematic diagram of ejector cooling system

4.1.1 Boiler

A 9 kW electric boiler (as shown in Figure 4-3) was used to supply processed steam at temperatures up to 140°C. The temperature was controlled by PID controller to an accuracy of ±1°C. The stream boiler was connected to a steam drum/separator (as shown in Figure 4-4) in which liquid and vapour could be separated to eliminate liquid droplet entry to the primary nozzle. The separator was manufactured from 316 stainless steel with an internal diameter of 15cm, wall thickness of 0.35cm and a length of 100cm. End plates of 0.45cm in thickness were welded to both ends with fittings to allow temperature and pressure sensors to be connected.

A pressure gauge was fitted in the steam separator to provide pressure measurement of the vapour entering the system. A nickel-chromium/nickel-aluminium (type K) thermocouple was located in the middle part of the steam separator to measure the temperature of the steam inside the steam separator. A pressure relief valve was fitted at the top of the steam separator

to protect the generator from operating at excessive pressures. The steam separator vessel was insulated with 15mm thickness foil face mineral wool.

Water was heated inside the boiler till it completed boiled and changed phase from liquid to vapour (steam). The steam then came through the top of the boiler into the steam separator, inside which any water droplet could be separated from the steam. The steam came out from the upstream of the separator and acted as the primary flow, which entered into the ejector. 12mm insulated stainless steel pipe work connected the steam separator to a control valve in the ejector assembly. Two different flows, the condensate from the downstream of the separator and the liquid refrigerant pumped from the condenser receiver, joined together through a T- piece fitting and fed back to the bottom of the boiler to complete this cycle.

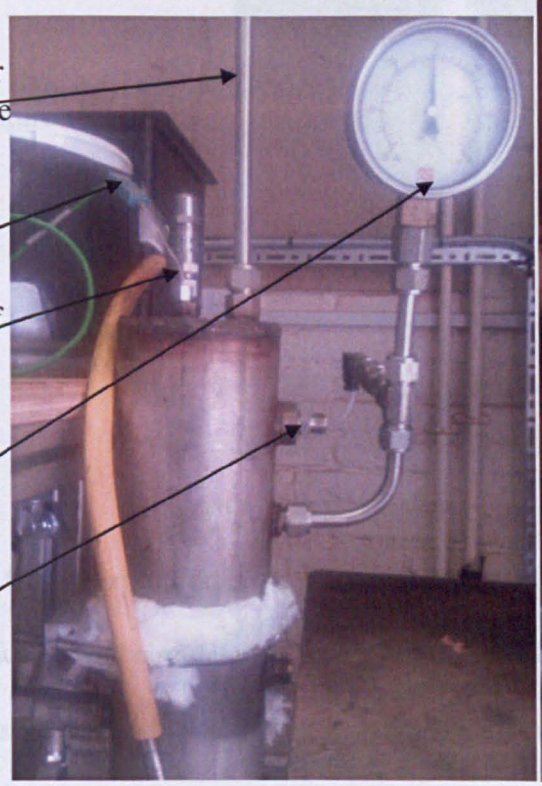

Figure 4-4 Photo of Steam separator

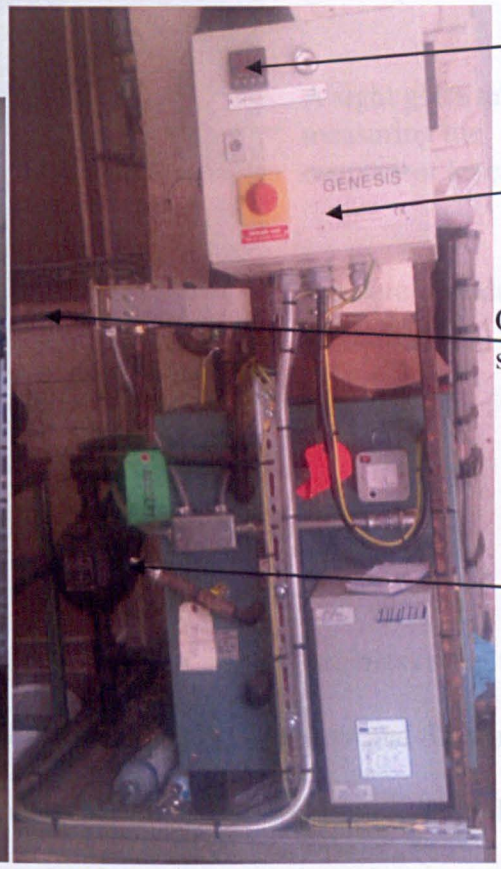

Figure 4-3 Photo of 9kW steam boiler

4.1.2 Evaporator

The evaporator (as shown in Figure 4-5) consisted of a 316 stainless steel cylindrical vessel of 20cm inside diameter, 0.35cm wall thickness and 35cm in height. The top part of the evaporator was connected to the ejector with a stainless steel tube of 100mm inside diameter. A diaphragm pump circulated water from the bottom of evaporator to a brazed plate heat exchanger (condenser), where the refrigerant absorbed a controlled heat load. In order to maintain a constant temperature inside the evaporator, the heat load was provided by room temperature water circulated by a diaphragm pump and supplied by a 10 litre water tank.

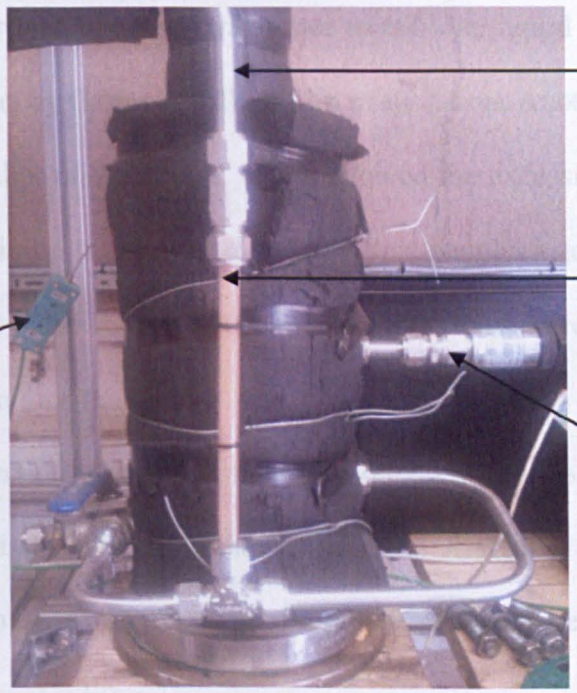

Figure 4-5 Photo of cylindrical evaporator

The flash evaporator is a cylindrical steel vessel containing a coiled stainless steel tube in which water was circulated. The evaporator vessel, 200mm inside diameter and 350mm in height was sealed at the bottom end using PTFE seals and stainless steel plates. The plates were secured to the vessel by four 20mm diameter stainless steel hexagonal fasteners, through cast iron flanges and PVC inserts. The top part of the vessel was welded with a 100mm stainless steel pipe, which connected with a 150mm diameter stainless steel plate. This plate

was linked to the suction inlet of ejector assembly with four 16mm stainless steel hexagonal fasteners using PTFE seals.

A 12mm fitting was welded at the bottom of the evaporator vessel, which acted as the liquid outlet of the vessel. The liquid was drove by a diaphragm pump and went through a control valve. It then entered into the heat exchanger, which exchanged heat with 10 litres warm water in the tank. In this way, heat load could be applied to the evaporator by warm water circulation to maintain a steady-state when testing the ejector. The warmed water came out from heat exchanger and finally sprayed back to the evaporator vessel via a spay nozzle. The spray nozzle was incorporated in the evaporator to cool the liquid water to the pressure and temperature of the vessel by flash and falling film evaporation. Another 12mm fitting was welded in the middle chamber of the vessel, which allowed the excessive water to drain out from the evaporator. This fitting was connected with 12mm stainless steel pipe, which joined with the condensate from the condenser receiver. There two flows were joined together by a T-piece and pumped back to feed the boiler.

Two nickel-chromium/nickel-aluminium thermocouples at the top and the bottom of the evaporator chamber were used to measure the temperature. A sight glass on the side of the evaporator was fitted to allow the measurement of liquid refrigerant level.

4.1.3 Condenser

The discharge from the ejector was connected to one of the upper connections of the heat exchanger 100mm hexagonal coupling. The brazed plate heat exchanger acted as the condenser (as shown in Figure 4-6), which contained 14 compact plates. The vapour was condensed in the plate heat exchanger by passing chilled water through adjacent plates in counter-flow. The condenser pressure could be adjusted by varying the chilled water flow rate. The chilled water was supplied from the laboratory at temperature ranging from 5°C to 10°C with flow rate up to 6 litre per minute. The condenser was vertically mounted with a 90°C

bend liquid outlet drop to the receiver vessel. The receiver vessel was 10cm inside diameter and 45cm height, which was fitted to the bottom of condenser. The condensed refrigerant from the receiver was joined with the liquid from the evaporator through a T-piece, and returned back through a pump to feed the boiler.

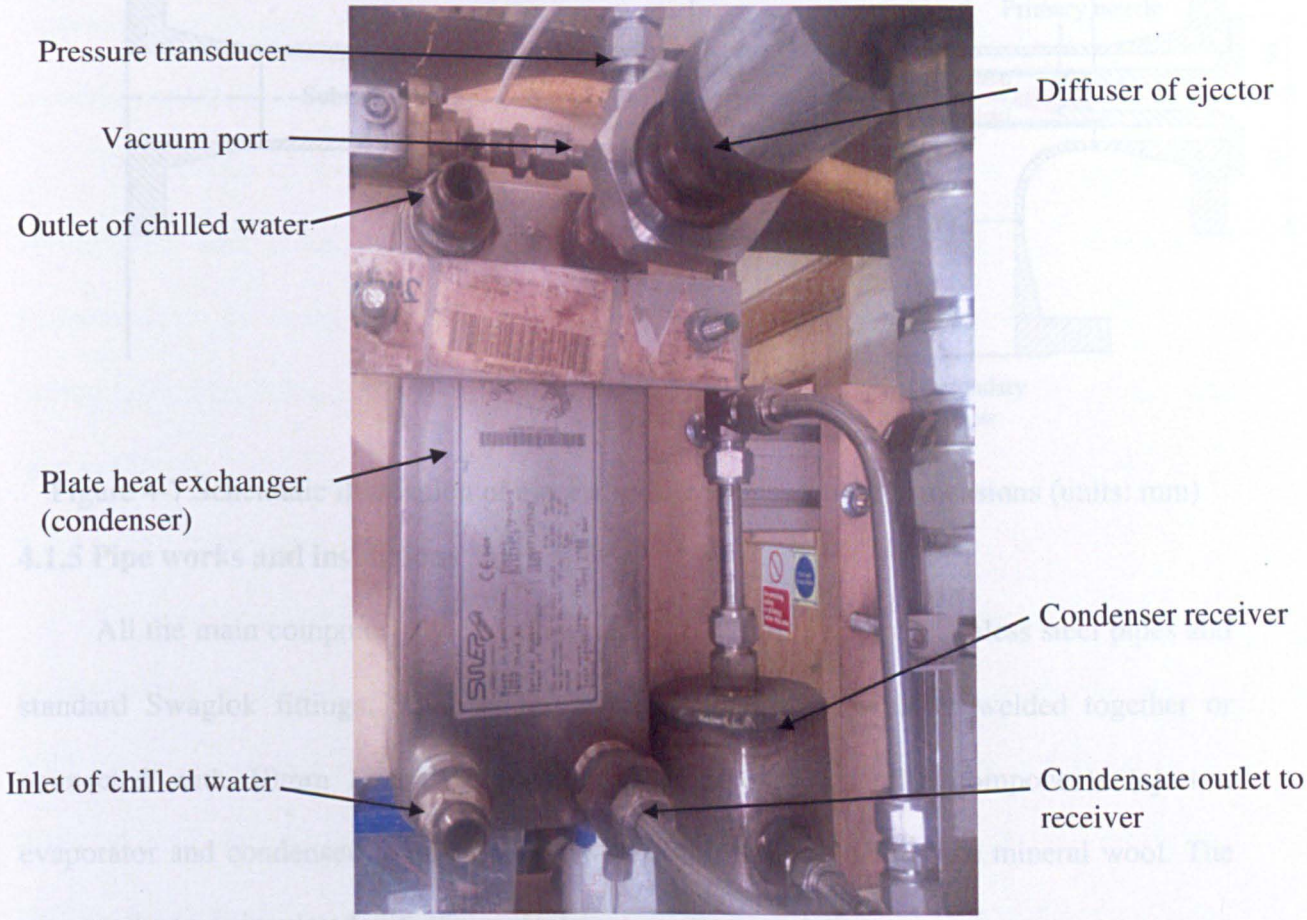

Figure 4-6 Photo of condenser

A nickel-chromium/nickel-aluminium thermocouple was used to measure the temperature, at the condensate outlet to receiver. A glass tube was connected with the receiver through 12mm fitting, which enabled the water level visualization.

4.1.4 Ejector

The ejector was designed from the one-dimensional analysis described in Chapter 3 and manufactured by Venturi Jet Pumps Ltd, UK. The main dimensions of the ejector are shown in Figure 4-7. It is well known that a typical steam ejector consists of four main parts, which

are the primary nozzle, the mixing chamber, the ejector throat and the subsonic diffuser. The primary nozzle diameter was 4.5mm and throat diameter was 1.5mm.

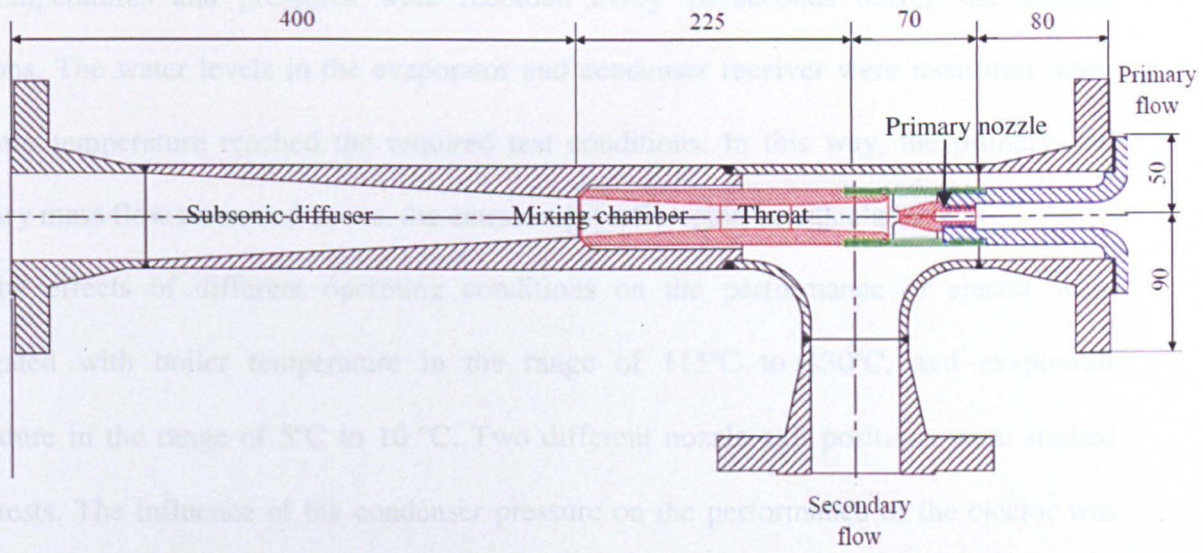

Figure 4-7 Schematic illustration of ejector profile showing main dimensions (units: mm)

4.1.5 Pipe works and insulations

All the main components were connected with 12mm Swaglok stainless steel pipes and standard Swaglok fittings. Some of the narrow sections were either welded together or connected with 10mm Swaglock stainless steel pipe works. The components (ejector, evaporator and condenser) were insulated with 20mm thickness foil face mineral wool. The pipe works were insulated with15mm thickness armflex insulation.

4.2 Experimental results and discussion

4.2.1 Test procedure

Non-condensable gases were removed by a vacuum pump from the test rig before the tests. The boiler was then switched at the required testing temperature. The water levels in the evaporator and the condenser receiver were recorded at the beginning of each test. The chilled water on the condenser side was then turned on with desired flow rate and the evaporator spray nozzle circulation pump was started. Once the steam reached the steady state, a shut-off

valve connecting the steam separator to the ejector was opened and time was recorded using a stop watch.

Temperatures and pressures were recorded every 10 seconds during the cooling conditions. The water levels in the evaporator and condenser receiver were measured when evaporator temperature reached the required test conditions. In this way, the primary and secondary mass flow rates, and hence, the entrainment ratio could be calculated.

The effects of different operating conditions on the performance of ejector were investigated with boiler temperature in the range of 115°C to 130°C, and evaporator temperature in the range of 5°C to 10 °C. Two different nozzle exit positions were studied during tests. The influence of the condenser pressure on the performance of the ejector was also evaluated.

4.2.2 Effect of nozzle exit position (NXP) on the system performance

Two different nozzle exit positions were investigated during experiments. By inserting or removing two spacers (each spacer with thickness of 2.2mm) into the primary nozzle, the NXP can be varied between 4.4mm and 0mm. With evaporator temperature of 5°C, these two different NXP were tested under boiler temperatures of 115°C to 130°C. The test results are shown in Figure 4-8 - Figure 4-11. It can be seen that as NXP moves towards the mixing chamber, the COP decreases. The critical condenser pressure, however, increases slightly. For instance, with boiler temperature of 120°C, COP decreases from 0.315 to 0.295 (around 5.9%) with nozzle moving further inside the mixing chamber. The critical condenser pressure increases about 5.7% from 35mbar to 37mbar. Since retracting of nozzle from the mixing chamber will lead to higher compression effect for the expanded secondary fluid. This enables more secondary fluid to be entrained and accelerated through the mixing chamber [9]. Hence, moving the nozzle outside the mixing chamber will lead to an increase of entrainment ratio and hence higher COP and cooling capacity.

Comparing the COP differences for NXP=0 and NXP=4.4mm from Figure 4.8-4.11, it could be found that the COP variations are 9.5%, 10.8%, 14.3% and 17.4% respectively for boiler temperature of 115°C, 120°C, 125°C and 130°C. This means that the COP differences for two nozzle positions increases as the boiler temperature rises. In real application, the performance difference for moving/not moving the nozzle from the mixing chamber will be more significant when the systems are working under higher heat source temperature.

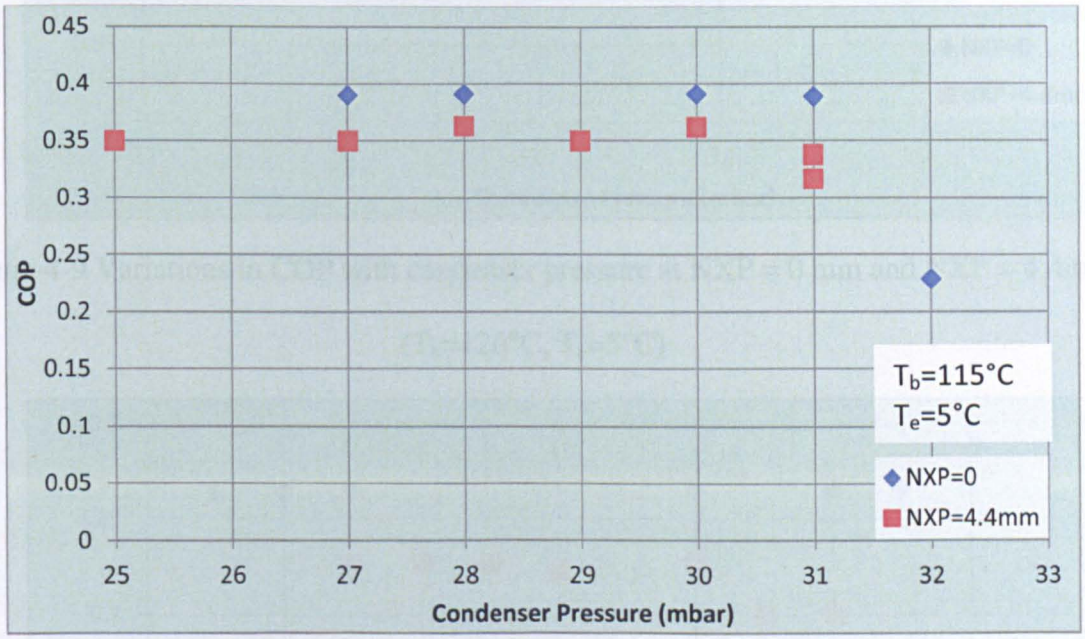

Figure 4-8 Variations in COP with condenser pressure at NXP = 0 mm and NXP = 4.4mm (T_b=115°C, T_e=5°C)

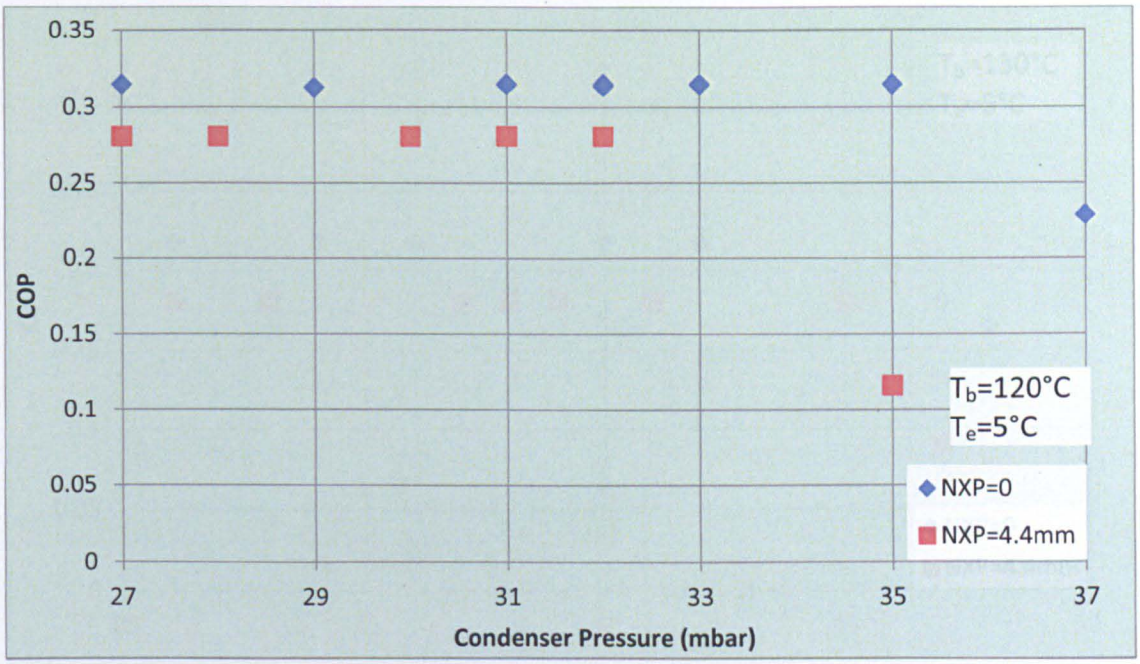

Figure 4-9 Variations in COP with condenser pressure at NXP = 0 mm and NXP = 4.4mm (T_b=120°C, T_e=5°C)

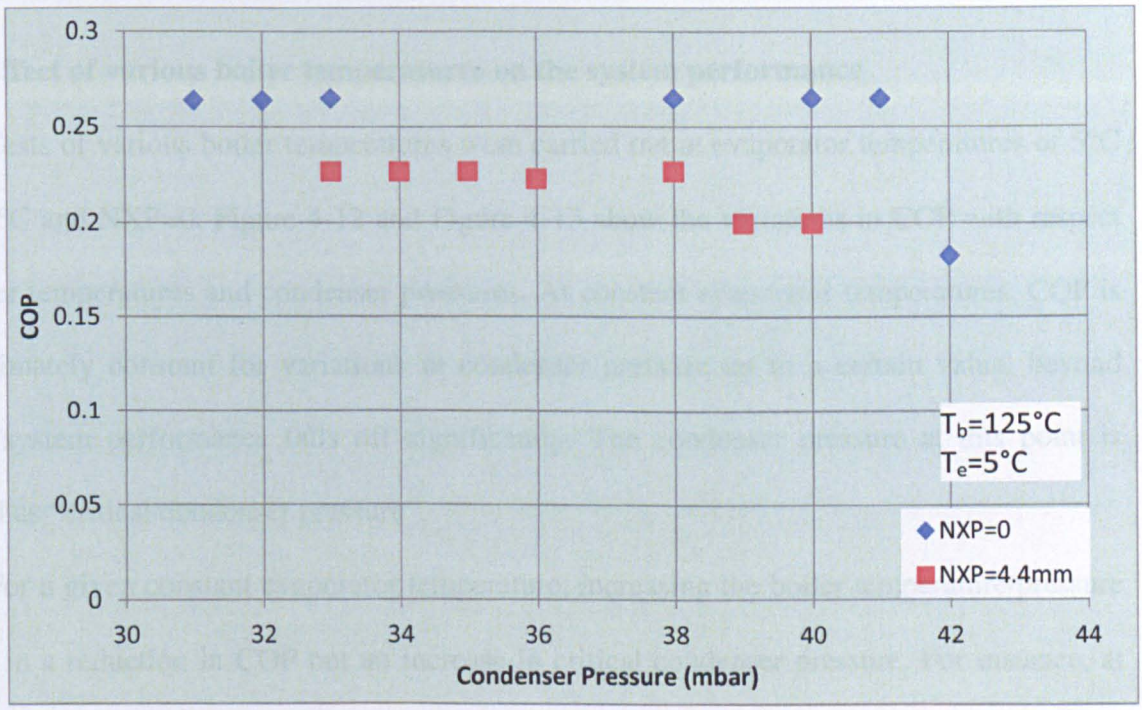

Figure 4-10 Variations in COP with condenser pressure at NXP = 0 mm and NXP = 4.4mm (T_b=125°C, T_e=5°C)

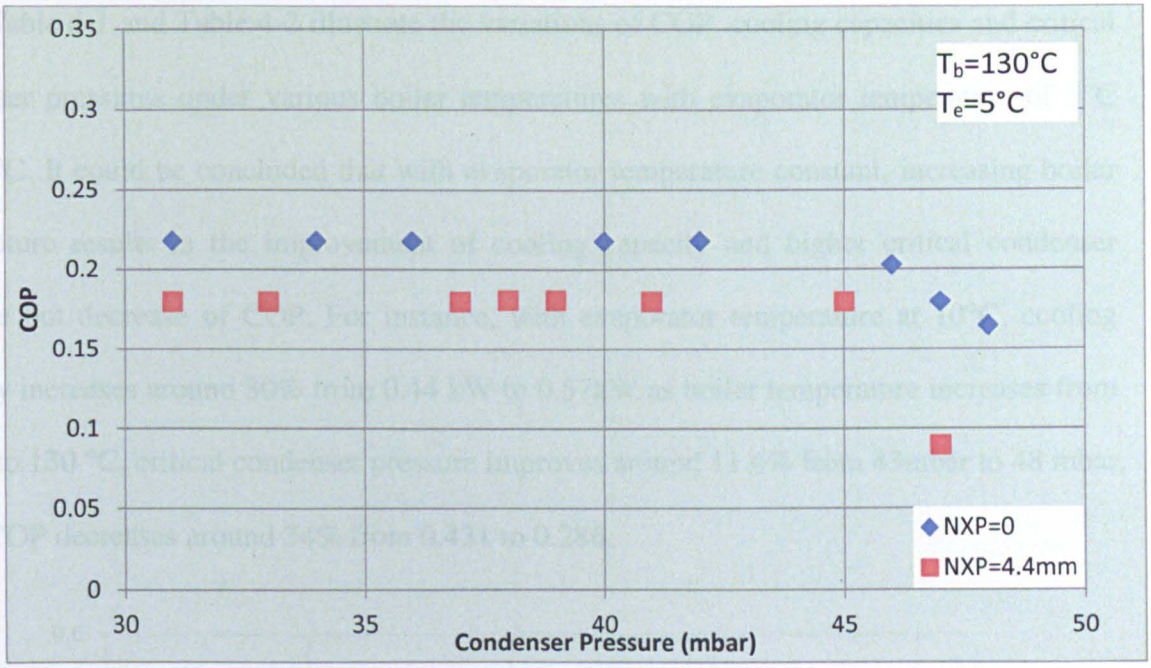

Figure 4-11 Variations in COP with condenser pressure at NXP = 0 mm and NXP = 4.4mm (T_b=130°C, T_e=5°C)

4.2.3 Effect of various boiler temperatures on the system performance

Tests of various boiler temperatures were carried out at evaporator temperatures of 5°C and 10°C and NXP=0. Figure 4-12 and Figure 4-13 show the variations in COP with respect to boiler temperatures and condenser pressures. At constant evaporator temperatures, COP is approximately constant for variations in condenser pressure up to a certain value, beyond which system performance falls off significantly. The condenser pressure at this point is defined as "critical condenser pressure".

For a given constant evaporator temperature, increasing the boiler temperature/pressure results in a reduction in COP but an increase in critical condenser pressure. For instance, at evaporator temperature of 5°C , with 10°C increase of boiler temperature from 120°C to 130°C, COP decreases from 0.315 to 0.218 (30.8%) whilst critical condenser pressure increases by 20% (from 35mbar to 42mbar).

Table 4-1 and Table 4-2 illustrate the variations of COP, cooling capacities and critical condenser pressures under various boiler temperatures with evaporator temperature of 5°C and 10°C. It could be concluded that with evaporator temperature constant, increasing boiler temperature results in the improvement of cooling capacity and higher critical condenser pressure but decrease of COP. For instance, with evaporator temperature at 10°C, cooling capacity increases around 30% from 0.44 kW to 0.57kW as boiler temperature increases from 120°C to 130 °C, critical condenser pressure improves around 11.6% from 43mbar to 48 mbar, while COP decreases around 34% from 0.431 to 0.286.

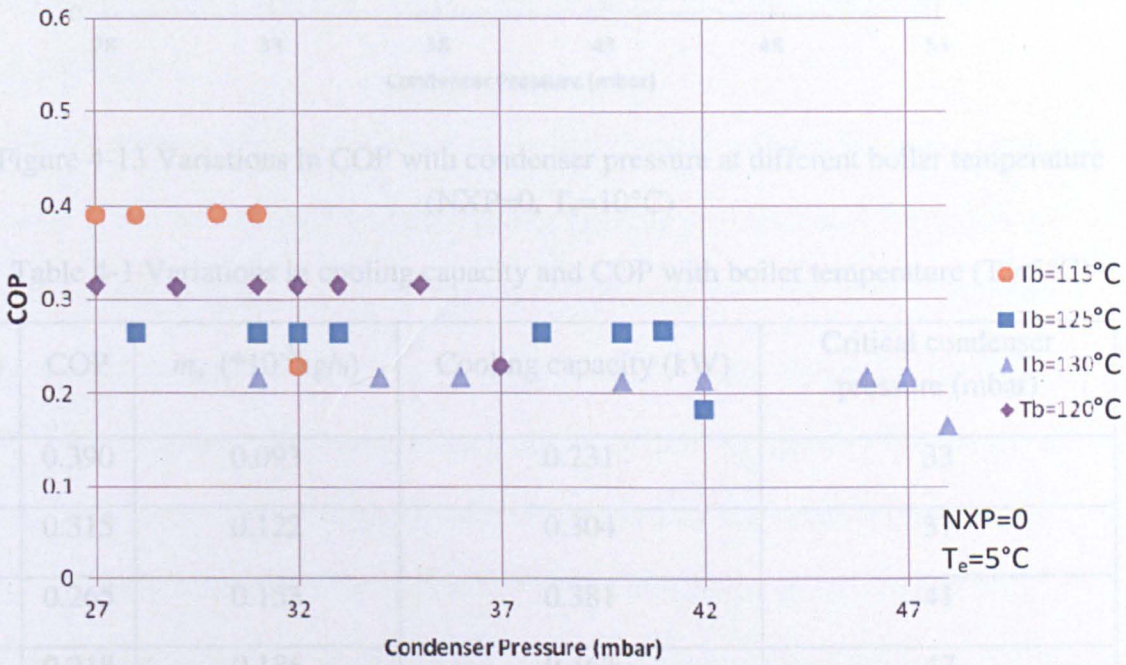

Figure 4-12 Variations in COP with condenser pressure at different boiler temperature (NXP=0, T_e=5°C)

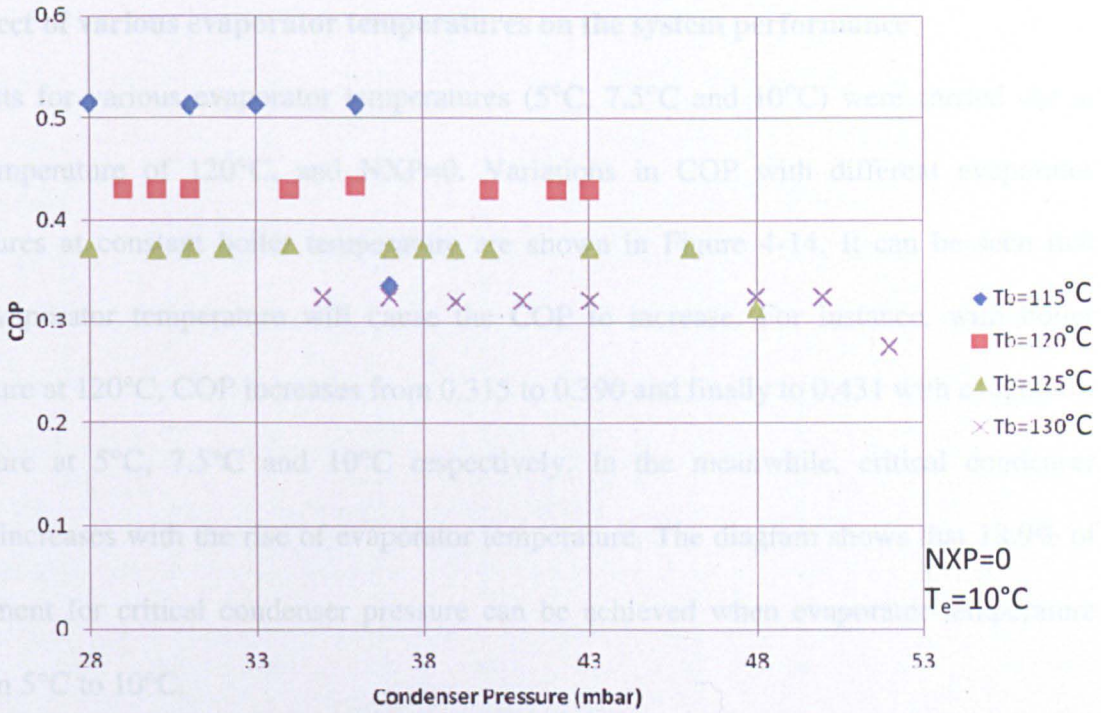

Figure 4-13 Variations in COP with condenser pressure at different boiler temperature (NXP=0, T_e=10°C)

Table 4-1 Variations in cooling capacity and COP with boiler temperature (T_e=5°C)

T_b (°C)	COP	m_s (*10^{-3}kg/s)	Cooling capacity (kW)	Critical condenser pressure (mbar)
115	0.390	0.093	0.231	33
120	0.315	0.122	0.304	37
125	0.265	0.153	0.381	41
130	0.218	0.186	0.463	47

Table 4-2 Variations in cooling capacity and COP with boiler temperature (T_e=10°C)

T_b (°C)	COP	m_s (*10^{-3}kg/s)	Cooling capacity (kW)	Critical condenser pressure (mbar)
115	0.513	0.127	0.315	37
120	0.431	0.177	0.438	43
125	0.372	0.191	0.473	48
130	0.325	0.229	0.567	52

4.2.4 Effect of various evaporator temperatures on the system performance

Tests for various evaporator temperatures (5°C, 7.5°C and 10°C) were carried out at boiler temperature of 120°C, and NXP=0. Variations in COP with different evaporator temperatures at constant boiler temperature are shown in Figure 4-14. It can be seen that higher evaporator temperature will cause the COP to increase. For instance, with boiler temperature at 120°C, COP increases from 0.315 to 0.390 and finally to 0.431 with evaporator temperature at 5°C, 7.5°C and 10°C respectively. In the meanwhile, critical condenser pressure increases with the rise of evaporator temperature. The diagram shows that 18.9% of improvement for critical condenser pressure can be achieved when evaporator temperature rises from 5°C to 10°C.

Table 4-3 demonstrates the variations of cooling capacity with respect to the evaporator temperatures. It can be indicated that the cooling capacity also increases from 0.231kW to 0.438kW (around 90.0%) as evaporator temperature increases from 5°C to 10°C respectively. Therefore, ejector cooling system will be more applicable for higher evaporator temperature.

The theoretical and experimental comparisons of cooling capacity are concluded in Table 4-3. The percentage differences between theoretical and experimental results are relatively large, which are 35.4%, 36.4% and 29.0% for evaporator temperature of 5°C, 7.5°C and 10°C respectively. Such huge differences are mainly due to the fact that some conditions are simplified in the simulation, i.e, the model is assumed to be one dimensional, the ejector system is assumed to be adiabatic. In the tests, however, the flow patterns are three dimensional and the heat losses to the ambient could not be avoided.

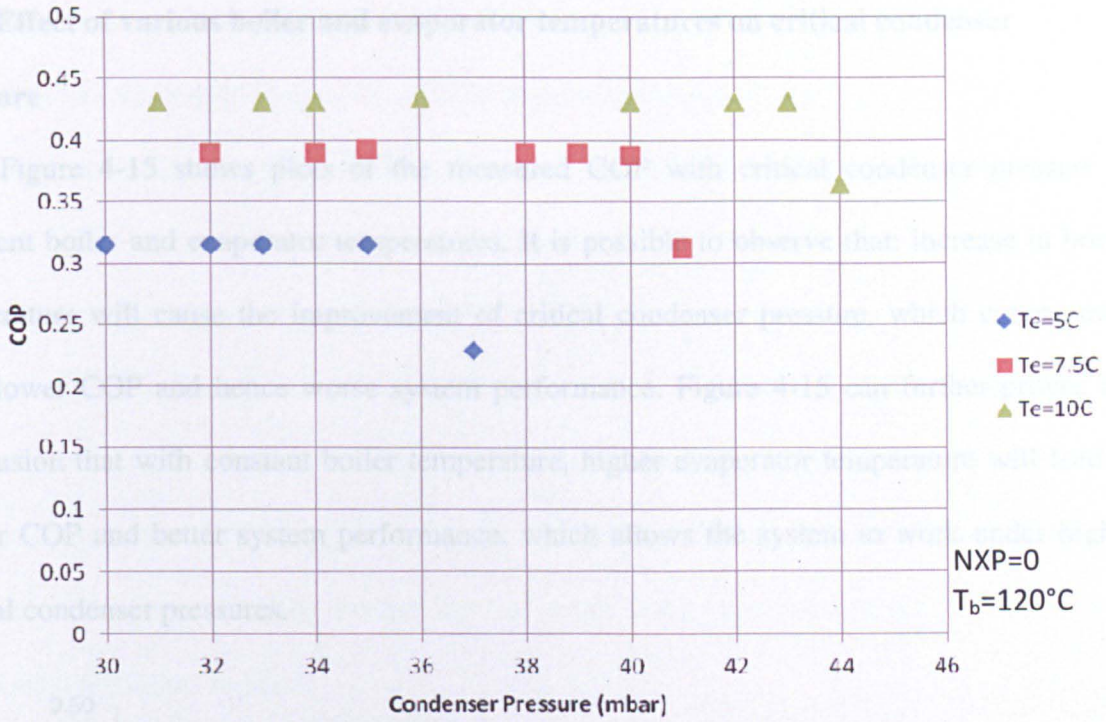

Figure 4-14 Variations in COP with condenser pressure at constant evaporator temperatures (T_b=120°C)

Table 4-3 Theoretical and experimental comparisons for cooling capacity with evaporator temperatures at 5°C, 7.5°C and 10°C (T_b =120°C)

T_e (°C)	h_f (kg/kg)	Theoretical		Experimental		% difference of theoretical and experimental cooling capacity
		m_s (*10^{-3}kg/s)	cooling capacity (kW)	m_s (*10^{-3}kg/s)	cooling capacity (kW)	
5	2489	0.144	0.358	0.093	0.231	35.37%
7.5	2482.5	0.193	0.480	0.123	0.305	36.37%
10	2477.2	0.249	0.617	0.177	0.438	28.98%

4.2.5 Effect of various boiler and evaporator temperatures on critical condenser pressure

Figure 4-15 shows plots of the measured COP with critical condenser pressure at different boiler and evaporator temperatures. It is possible to observe that: increase in boiler temperature will cause the improvement of critical condenser pressure, which compromise with lower COP and hence worse system performance. Figure 4-15 can further proves the conclusion that with constant boiler temperature, higher evaporator temperature will lead to higher COP and better system performance, which allows the system to work under higher critical condenser pressures.

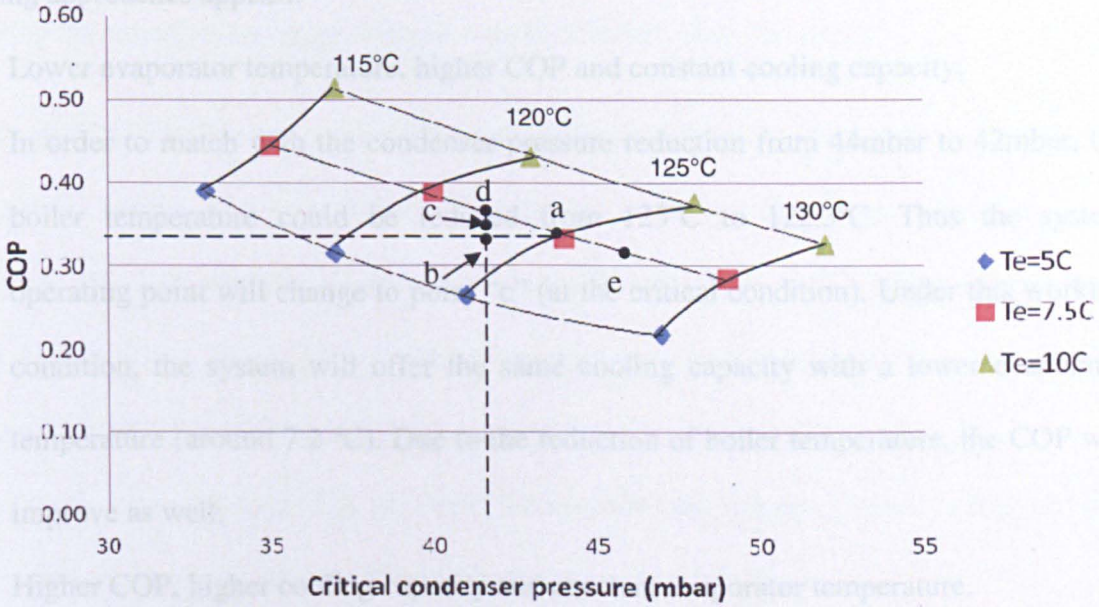

Figure 4-15 Variations in COP with critical condenser pressure at constant boiler and evaporator temperatures

4.2.6 System operation

The analyzed testing results indicate that the optimized system performance can be obtained when ejector was operated under critical pressure, while boiler temperature and evaporator temperature were at the designed values. In the following, we will discuss how to

vary the ejector working conditions so that the system performance could still be optimized when the ambient conditions (condenser temperature/pressure) change.

As shown in Figure 4-15, point "a" is the assumed ejector design condition. COP of system working at point "a" (boiler temperature of 125°C, evaporator temperature of 7.5°C and critical condenser pressure at 44mbar) was 0.333. If the condenser pressure dropped from 44mbar to 42mbar because of reduced chilled water flow rate, while the cooling capacity and COP stayed the same, the system operation point will change from "a" to "b". With the aim to enhance the system performance under the reduced condenser pressure (from 44mbar to 42mbar), the ejector cooling system has to work under another critical condition with following approaches applied:

1) Lower evaporator temperature, higher COP and constant cooling capacity;

   In order to match with the condenser pressure reduction from 44mbar to 42mbar, the boiler temperature could be reduced from 125°C to 122.3°C. Thus the system operating point will change to point "c" (at the critical condition). Under this working condition, the system will offer the same cooling capacity with a lower evaporator temperature (around 7.2 °C). Due to the reduction of boiler temperature, the COP will improve as well.

2) Higher COP, higher cooling capacity and constant evaporator temperature.

   Another way to adjust the system in order to cope with the condenser pressure drop is to keep the evaporator temperature constant at 7.5 °C, but further decrease the boiler temperature from 125 °C to approximately 121.8 °C. Under this case, the operating point would be at point "d". This would cause the improvement in the cooling capacity and COP.

On the other hand, if the ambient temperature (condenser pressure) is higher than the designed condition, the ejector will fail to operate properly at the beginning and the

evaporator temperature would be increased due to the primary flow entrained back into the evaporator. Point "e" identifies this condition. New critical condition can be reached only with higher evaporator and/or boiler temperature.

4.3 Comparisons between experimental and theoretical results

Table 4-4 and Figure 4-16 show the comparisons between experimental results and theoretical modelling results. The experimental results were found to be around 85% of the theoretical values. And the overall discrepancies between experimental and theoretical COP were from 3.3% to 15.1% (average 9.3%). It is worth noting that the experimental data were always lower than the theoretical simulation predications. This provides a guideline for modelling optimization and improvement, which deserves more attentions.

One of the possible reasons for the over-predication of simulation results compared with experimental results could be due to the fact that some conditions are simplified in the simulation. For instance, the ejector model is assumed to be one dimensional, the ejector system is assumed to be adiabatic, and the friction losses could not be better presented other than introducing several isentropic efficiencies for different ejector sections. In the tests, however, the flow patterns are in three dimensions, the friction losses could be very complicated and the heat losses to the ambient could not be avoided.

Another possible reason for the discrepancies of COP between experimental and theoretical results could be related to the measurement errors in the static pressure of the evaporator. In the tests, the evaporator was working under relatively low pressure range (0.1-1kPa). The typical percentage error of the pressure transducers was 0.05% of full scale, which was 5kPa for full scale between -1bar to 0bar. With the apparatus error so close to the measured evaporator pressure, the variations of the evaporator pressure were about 80%. The

simulation process demonstrated that a small error on the evaporator pressure would cause great differences in the ejector performance.

Table 4-4 Experimental performance of the ejector cooling system at critical condenser pressure operation

Temperature (°C)			Critical Condenser Pressure (mbar)	COP		
Evaporator	Boiler	Condenser		Experimental	Theoretical	%
5	115	26.2	33	0.390	0.411	5.38%
	120	27.8	37	0.315	0.362	14.92%
	125	29.6	41	0.265	0.29	9.43%
	130	31.4	47	0.218	0.252	11.01%
7.5	115	26.8	35	0.444	0.476	7.21%
	120	29.0	40	0.389	0.419	7.71%
	125	30.8	44	0.333	0.344	3.30%
	130	32.7	49	0.284	0.296	4.23%
10	115	27.4	37	0.513	0.553	7.80%
	120	29.6	43	0.431	0.481	11.60%
	125	31.2	48	0.375	0.424	13.07%
	130	33.5	52	0.325	0.374	15.08%

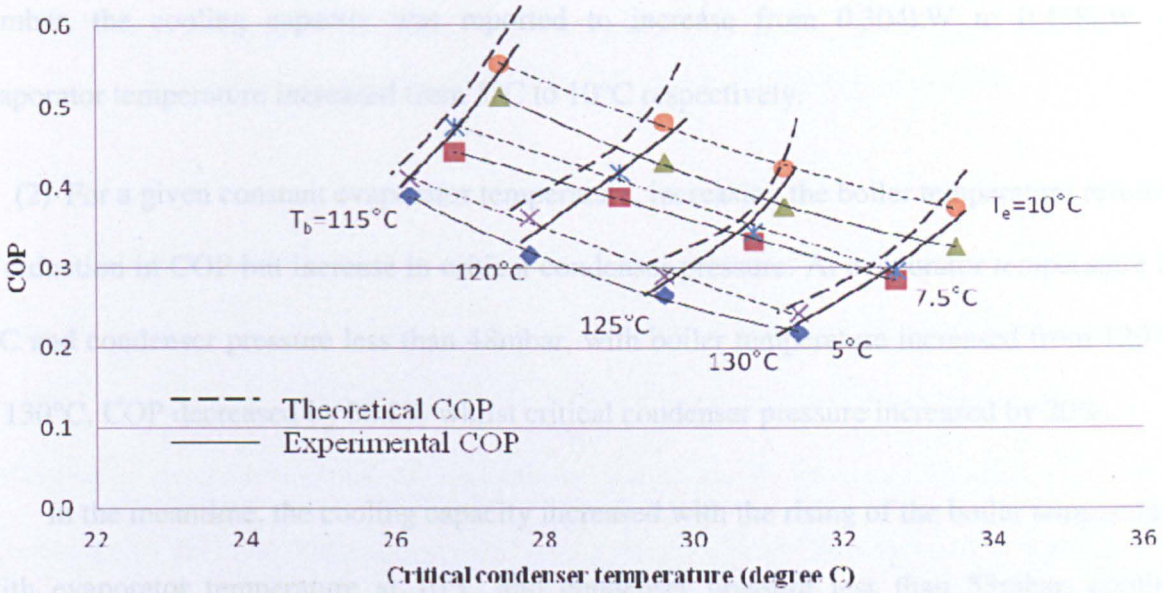

Figure 4-16 Comparison between theoretical COP predications and experimental results

4.4 Conclusions

The experimental studies on the ejector cooling system were carried out with boiler temperatures between 115°C and 130°C, and evaporator temperatures between 5°C and 10°C. The effects of various parameters on the overall ejector operation were analyzed. The following conclusions can be drawn from the experimental analysis:

(1) For a given boiler temperature, an increase in evaporator temperature improved system performance and produced a higher critical condenser pressure. With boiler temperature of 120°C and condenser pressure less than 38mbar, 36.8% COP improvement could be achieved when evaporator temperature increased from 5°C to 10°C. This further proved that in hybrid ejector and vapour compression system (Chapter 3), the ejector operating in higher evaporator temperature would contribute to an improvement in overall system performance.

It was concluded that the cooling capacity improved with the increasing of the evaporator temperature. At the boiler temperature of 120°C and condenser pressure less than

38mbar, the cooling capacity was reported to increase from 0.304kW to 0.438kW as evaporator temperature increased from 5°C to 10°C respectively.

(2) For a given constant evaporator temperature, increasing the boiler temperature resulted in reduction in COP but increase in critical condenser pressure. At evaporator temperature of 5°C and condenser pressure less than 48mbar, with boiler temperature increased from 120°C to 130°C, COP decreased by 30.8% whilst critical condenser pressure increased by 20%.

In the meantime, the cooling capacity increased with the rising of the boiler temperature. With evaporator temperature at 10°C and condenser pressure less than 53mbar, cooling capacity increased around 30% from 0.44 kW to 0.57kW as boiler temperature increased from 120°C to 130 °C.

(3) Two different nozzle exit position (NXP=0 and NXP=4.4mm) were investigated with respect to system performance. It was found that nozzle exit position only had a small influence on the system performance. When nozzle was positioned 0.44mm further inside the mixing chamber, at boiler temperature of 115°C, evaporator temperature of 5°C, 9.5% COP reduction was obtained.

(4) Experimental results were compared with the simulation results obtained from Chapter 3. The measured COPs of the system from experiments were in the range of 0.2 to 0.5, which were approximately 85% compared with the simulation results. This could be due to following two possible sources of errors: one is the simplifications assumed in the simulation model. Another reason is the measurement uncertainty of the evaporator pressure during the experiments. In order to eliminate the discrepancies between experimental and theoretical results, three dimension model which considering the friction losses and the mixing process in a dynamic way could be applied. A more accurate pressure sensor could be used in the test to minimize the test uncertainty.

Chapter 5 Experimental Investigations of PCM Cold Storage System Integrated with Ejector Cooling System

This chapter experimentally investigates the operating characteristics of cold storage system integrated with ejector cooling system. In order to enhance the heat transfer between the PCM and heat transfer fluid (HTF), two tube configurations are tested and compared. The performance parameters, such as temperature inside the PCM container, inlet and outlet temperature of HTF, cold storage rate and cold storage capacity are measured at various mass flow rates. The effectiveness-NTU (number of transfer unit) method was applied for characterizing the PCM storage system. The correlation of effectiveness as the function of ratio $\dot{m}/A$ was derived from experimental data, and was used as a design parameter for the PCM storage system.

5.1 Introduction

Thermal storage system has been extensively studied as an effective method to conserve available energy and improve the performance of cooling system. Currently, most of the conventional cooling systems are designed to be powered by electricity. Because of the high cooling requirements during mid-days, the electricity consumptions are significant, which aggravate the mid-afternoon peak load of the electricity grid. With the help of thermal storage system, the cold energy could be generated during off-peak hours with a marginal cost of the electricity. During the periods when the cooling demands are high, the stored cold energy could be released from the storage system. Thus, the peak cooling demand during summer season can be shifted to off-peak period to bridge the gap between energy generation and consumption. Furthermore, if the cooling system is designed to be powered by renewable

energy source (such as solar energy or industrial waste heat), the stored energy could be used to provide cooling effect when the energy source is not adequate. In this case, the system performance becomes more stable and less dependent on the energy source.

Thermal storage system based on the use of phase change materials (PCM) has became a focal interest of many researchers. PCM cold storage can store the energy in the form of latent heat, which offers higher energy density and smaller size of system compared with most sensible heat storage devices. The utilization of the thermal energy stored in PCM depends significantly on the thermal conductivity, which is relatively low for most of the materials. Various heat transfer enhancement methods have been studied, which take into account of adding particles with higher thermal conductivity, micro-encapsulated PCM and PCM with different fin configurations.

So far, both the numerical and experimental studies of PCM cold storage system are mainly concentrated on the material properties analysis, heat transfer enhancement investigations and various configurations of heat exchangers between PCM and HTF. The integration of PCM cold storage system with ejector cooling system is hardly reported. In order to investigate the system performance and operation characteristics, experimental investigations on a PCM cold storage system integrated with ejector cooling system were carried out in this research work. The charging and discharging performances with different flow rates of HTF were presented. Effectiveness-NTU method was applied, which provided a clear guidance for cold storage system design.

5.2 Description of test rig

A schematic diagram of the experimental system of ejector cooling system integrated with a PCM cold storage is shown in Figure 5-1. The system consists of the ejector cooling cycle, PCM cold storage charging and discharging cycle. The PCM cold storage charging unit is coupled directly with the evaporator of the ejector cooling cycle.

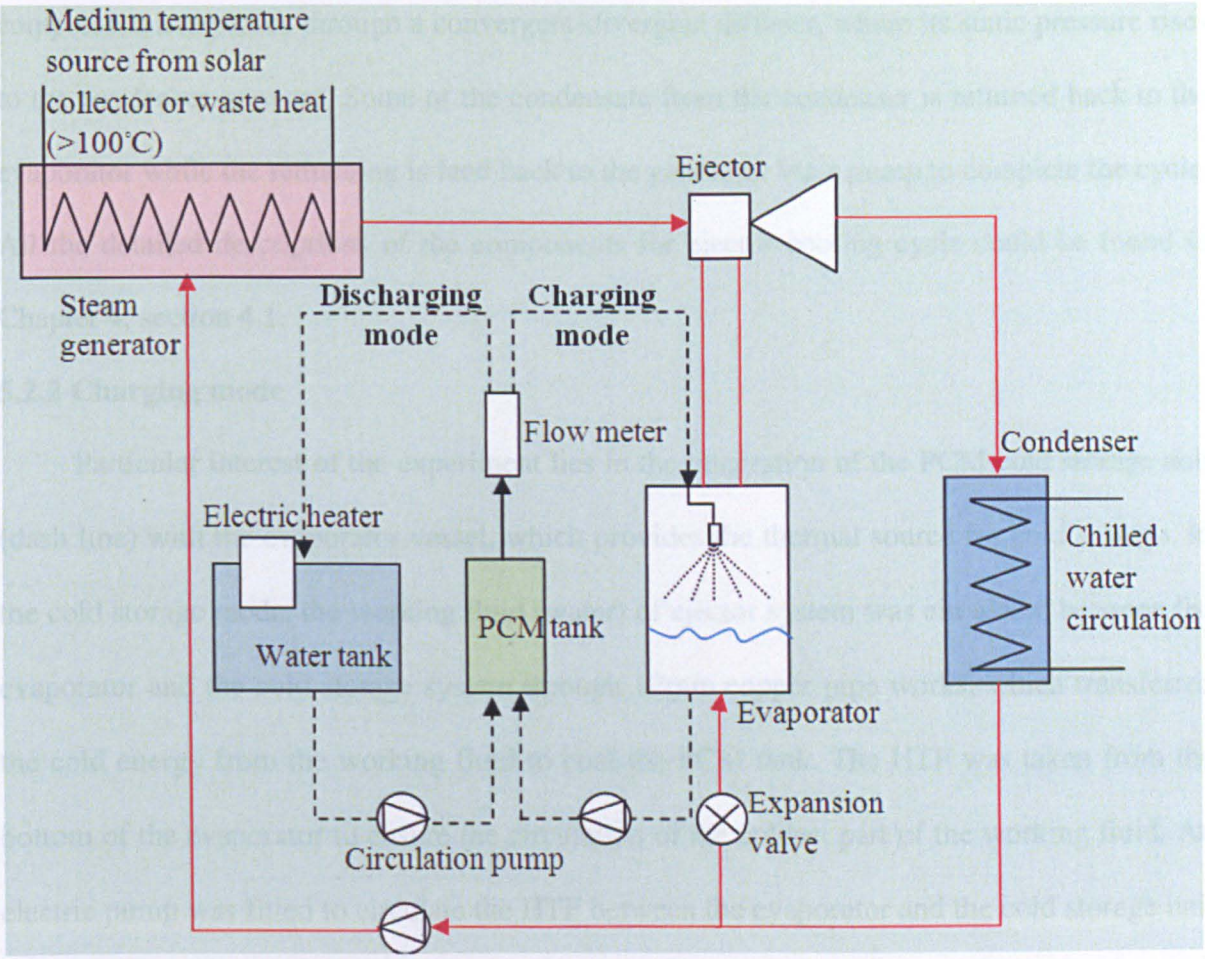

Figure 5-1 Schematic diagram of the experimental system of cold storage ejector cooling system

5.2.1 Ejector cooling cycle

The ejector cooling cycle (solid line) is composed of a steam generator, an ejector, an evaporator, a condenser and connections via pipes, heat exchangers, valves and circulation pumps. Water is used as the working fluid. The ejector cooling cycle operates as follows: High pressure steam is produced in the generator at temperature of 120°C. This steam flows through 12mm stainless pipeline into the ejector, where it enters via the primary nozzle. As the high pressure steam expands through the nozzle, its velocity is accelerated, which helps to entrain a low-pressure secondary flow from the evaporator. The entrained flow combines with the primary flow at the mixing chamber of the ejector. The combined flow is finally

compressed and passes through a convergent-divergent diffuser, where its static pressure rises to the condenser pressure. Some of the condensate from the condenser is returned back to the evaporator while the remaining is feed back to the generator via a pump to complete the cycle. All the detailed descriptions of the components for ejector cooling cycle could be found in Chapter 4, section 4.1.

5.2.2 Charging mode

Particular interest of the experiment lies in the integration of the PCM cold storage unit (dash line) with the evaporator vessel, which provides the thermal source for cold storage. In the cold storage mode, the working fluid (water) of ejector system was circulated between the evaporator and the cold storage system through 12mm copper pipe works, which transferred the cold energy from the working fluid to cool the PCM tank. The HTF was taken from the bottom of the evaporator to ensure the circulation of the coldest part of the working fluid. An electric pump was fitted to circulate the HTF between the evaporator and the cold storage unit. The HTF was feed back into the evaporator through the spray nozzle which situated on the top of the evaporator vessel. A flow meter was located vertically at the outlet of the HTF to monitor the flow rate, and a needle valve was used to control the flow rate.

1.98kg PCM S15 product (manufactured by EPS, www.epsltd.co.uk) was filled into the PCM tank. The PCM S15 physical properties are shown in Table 5-1, and the PCM tank dimensions are shown in Table 5-2. In order to enhance the heat transfer area, five pieces of copper fins (8mm * 185mm * 0.9mm) were welded to the copper tube at the distance of 25mm. The finned tube configuration is shown in Figure 5-2. In order to analysis and compare the heat transfer areas between two different tube configurations (straight tube and finned tube), packing factor (PF) was defined as the volumetric ratio between the PCM and the container as following,

$$PF = \frac{V_{pcm}}{V_{tank}} = \frac{V_{tank} - V_{tube}}{V_{tank}} \qquad \text{Eq. (5.1)}$$

5.2.3 Discharge mode

The discharge mode worked when the ejector cooling system did not operate. The solidified PCM inside the container was melted to cool the HTF (water), and the cooled HTF was transported by another circulation pump to the heat sink. An electric heater which can provide a constant temperature in the range of 20 to 70°C was positioned inside a 5 litre water container. A flow meter and a valve were fitted vertically between the heat sink outlet and the PCM container inlet to control the flow rate. The electric heater was pre-set at the testing temperature every time before the discharge test started.

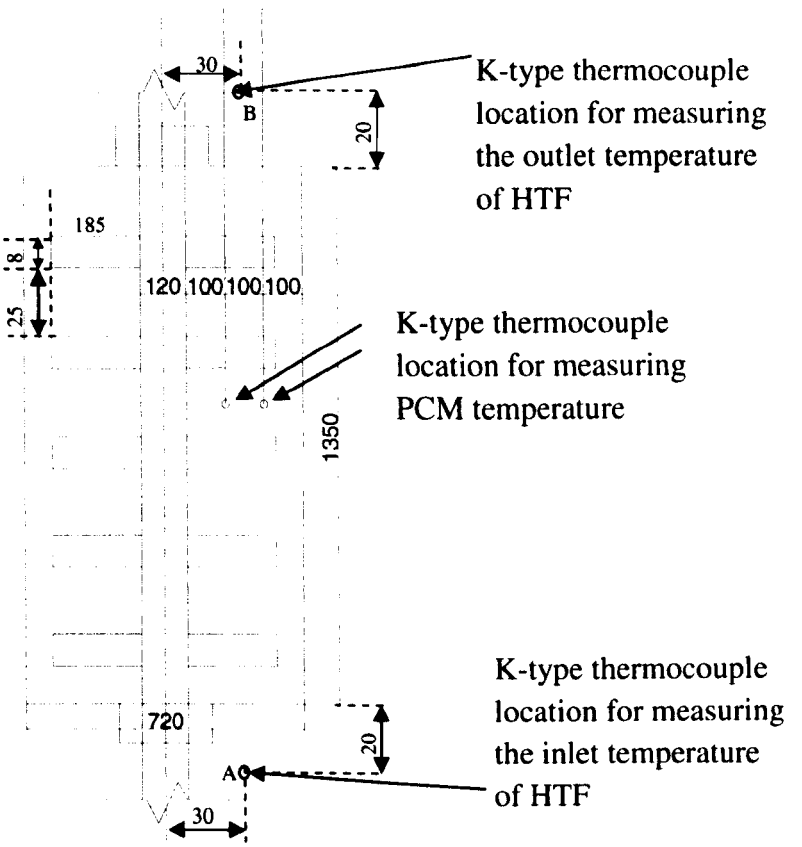

Figure 5-2 Cross section of PCM container with finned copper tube (unit: mm)

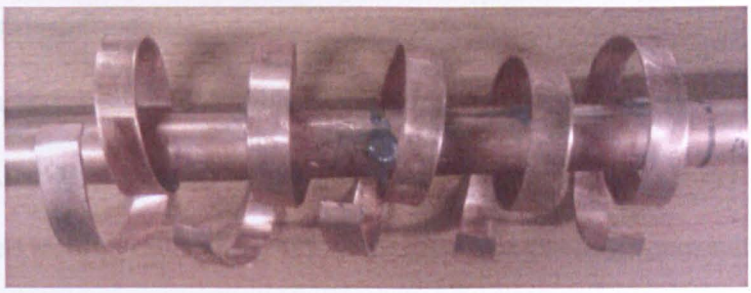

Figure 5-3 Photo of finned tube configuration

Table 5-1 Physical properties of PCM S15 product (provided by manufacturer: EPS Ltd.)

Physical properties	S15
Ingredient	Inorganic salts, nucleating agents and thickening agents
Melting point(°C)	15
Heat storage capacity (kJ/kg)	142
Density (liquid) (kg/m^3)	1488
Thermal conductivity (liquid) (W/mk)	0.43
Specific heat capacity (kJ/kgK)	0.67

Table 5-2 Container dimensions and parameters

	Straight tube	Finned straight tube
PF(-)	0.962	0.950
Heat transfer area (m^2)	0.0057	0.0131
PCM mass(kg)	0.20	0.198
Energy storage capacity (kJ)	28.4	28.1
Container diameter (m)	0.072	0.072
Container height (m)	0.135	0.135
HTF pipe internal diameter (m)	0.0135	0.0135

5.2.4 Experimental method

Before each test, non-condensable gases were removed from the ejector cycle using a vacuum pump. After that the generator heater was switched on until the water temperature reached the desired testing value (120oC). The condenser cooling water was then switched on and the evaporator–spray nozzle circulation pump was turned on. Once the flow reached a steady state, a shut-off valve connecting the steam generator to the primary nozzle was opened and the test started.

All the main components were insulated with 20mm thickness foil face mineral wool. The pipe works were insulated with15mm thickness armflex insulation. Different flow rates were tested for charging mode with generator temperature of 120°C and condenser temperature of 35°C. For discharging mode, the heat source temperature was 25°C. Two thermocouples were located inside the container to register the PCM temperature at two different positions (Figure 5-3) perpendicular to the HTF flow direction. K-type thermocouples were used to monitor the temperature, with a maximum error of ±0.5°C. The flow meter was calibrated at HTF temperature of 20°C to an accuracy of 0.2%. The flow rates were recorded periodically and temperatures were measured automatically by Datataker500 at 30s time interval until the test process ended.

5.3 Storage capacity calculation

It is important to determine the characteristics of PCM storage system during charging and discharging mode. The cold storage rate of the experimental system during charging/discharging mode can be calculated as,

$$Q_{st} = \dot{m} c_p |T_{out} - T_{in}| \qquad \text{Eq. (5.2)}$$

Where, Q_{st} is the cold storage rate or cold discharge rate (kW);

$\dot{m}$ is the mass flow rate of HTF for charging mode (kg/s);

c_p is the specific heat of HTF (kJ/Kg °C);

T_{in} is the inlet temperature of HTF to the PCM container (°C);

T_{out} is the outlet temperature of HTF to the PCM container (°C).

The inlet temperature of HTF T_{in} was measured at the central point (shown as A in Figure 5-2) of a 12mm stainless pipe, which was connected with the copper tube inlet via a T-piece. The distance between the central line of this stainless pipe and the bottom line of the PCM container (where PCM material first contacted with HTF) was 20mm. The distance between this central point A and the central line of the copper tube was 30mm.

The cold storage capacity of the PCM cold storage system during charging/discharging mode can be represented as,

$$Q_{tot,st} = \int_o^{t_{st}} Q_{st} \cdot dt \qquad \text{Eq. (5.3)}$$

Where, $Q_{tot,st}$ is the cold storage capacity (kJ);

t_{st} is the charging/discharging period (s).

5.4 Results and discussions

5.4.1 Preliminary test

Before coupling the PCM cool storage system with the ejector cooling system, it is worthwhile testing the material property of PCM S15 product separately. A preliminary test on the cold storage property of PCM S15 product was carried out in an ice-water mixture bath. A cylindrical plastic PCM container with diameter of 72mm and height of 135mm was filled with 0.202kg PCM S15 product. In order to compare the cold storage characteristics of PCM and water, 0.136kg of water was filled in another container with same size. These two containers were immersed inside a 5 litre ice-water mixture bath, which was insulated with one layer of armacel foam (thickness=15mm) inside and another layer of mineral wool (thickness =20mm) outside. Water was drained from the bottom of the bath and ice cubes were added into the bath every 20 minutes. In this case, the temperature of the ice-water

mixture can be maintained at approximately 0°C. This provided a constant cold source for the cold storage test.

The testing results of the PCM cold storage container and water container immersed in ice-water bath are shown in Figure 5-4. It can be seen from the diagram that it took around 60 minutes for the temperature of water container to drop below 3°C. While the PCM container spent more than 250 minutes to cool down to the same temperature. Although the heat can be stored by PCM during latent heat storage process is larger compared with that of water, the total heat energy (latent heat and sensible heat) stored by PCM could only be 2-3 times as much as that stored by water. The reason that PCM took more than four times to cool down to the same temperature as water could be due to the following reasons: when the temperature of PCM material was beyond the melting point (15°C), the PCM material showed a semi-solid state. This made the PCM material demonstrating relatively high viscosity (higher than water). Hence, the frictions between molecular layers will be higher than other materials with lower viscosity. As the PCM material was in contact with HTF through the longitudinal direction of the PCM container, the molecular movement would be faster near the axis of the container and very slow near the walls. Therefore, larger driving force would be needed in order to overcome the frictions between the molecules and keep the fluid moving. This potentially slowed down the solidifying process.

During the phase change process, the temperature at the centre of the PCM container remained almost constant around 13.9°C. However, this latent heat storage process (shown in Figure 5-4) lasted for 35 minutes, which accounted for only 14% for the entire storage process. Similarly, the temperature profile of the PCM (Figure 5-5) obtained by the manufacturer during discharging process hardly showed any significant latent heat discharge process. For ideal PCM product, the latent heat charge/discharge process should be the major part of the charging/discharge process. Hence, the PCM S15 product used in our test could not provide

satisfying characteristics, which brought out difficulties for distinguishing the latent heat charge/discharge processes clearly from the entire testing processes.

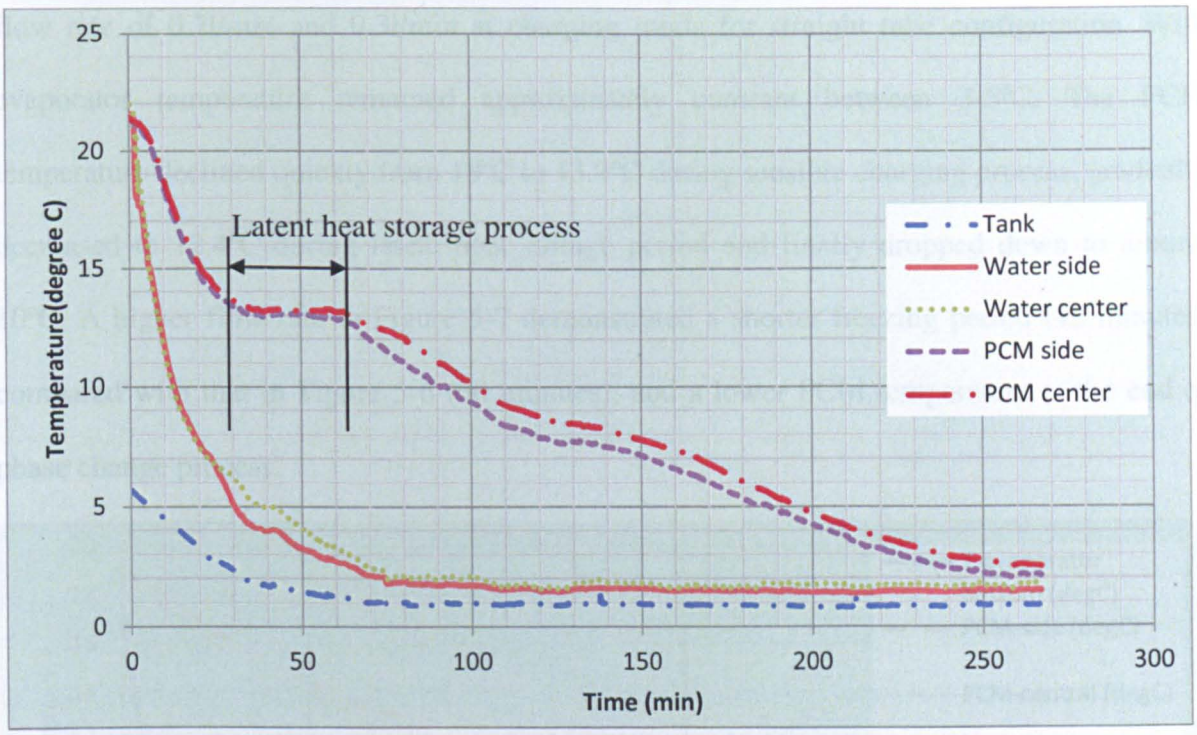

Figure 5-4 Preliminary testing results of PCM storage container and water container in ice-water bath

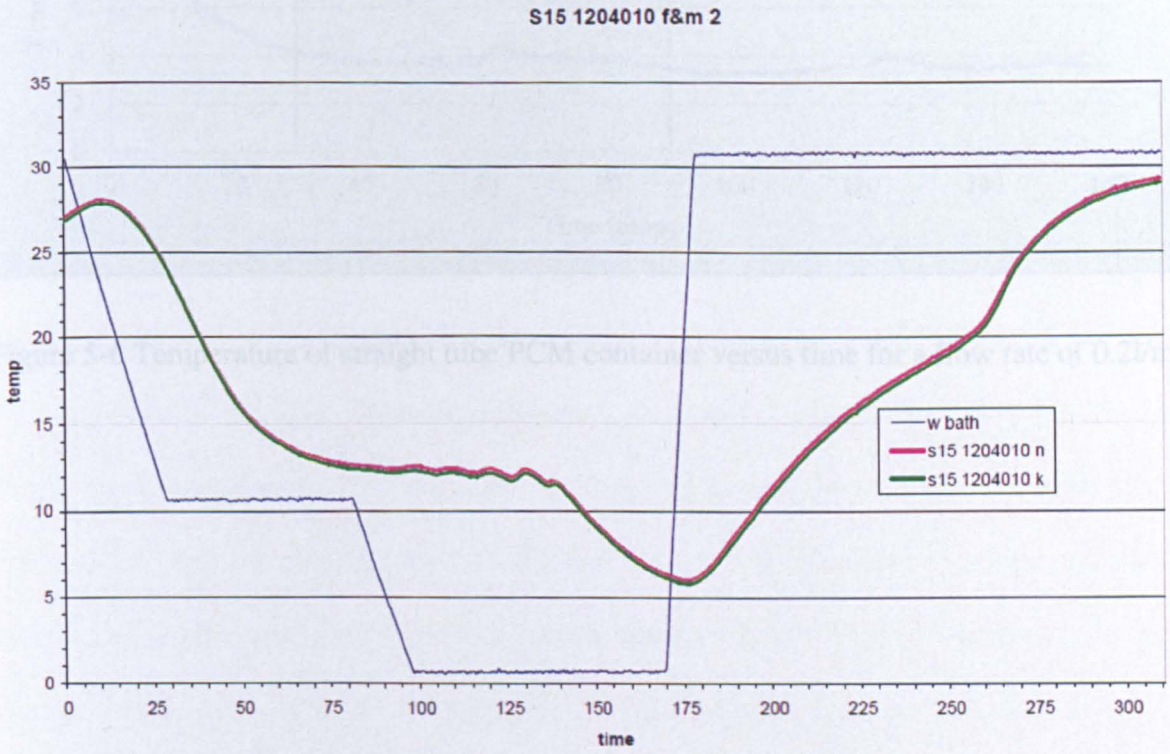

Figure 5-5 Charging and discharging results for PCM S15 product (from the manufacturer)

5.4.2 Straight tube charging mode

Figure 5-6 and Figure 5-7 indicate the evaporator and PCM temperature measurements for flow rate of 0.2l/min and 0.3l/min at charging mode for straight tube configuration. With evaporator temperature remained approximately constant between 3-5°C, The PCM temperature declined quickly from 19°C to 13.9°C during sensible charging process, gradually decreased to 12.4°C during latent heat storage period and finally dropped down to around 10°C. A higher flow rate in Figure 5-7 demonstrated a shorter freezing period (45 minutes) compared with that in Figure 5-6 (60 minutes), and a lower PCM temperature at the end of phase change process.

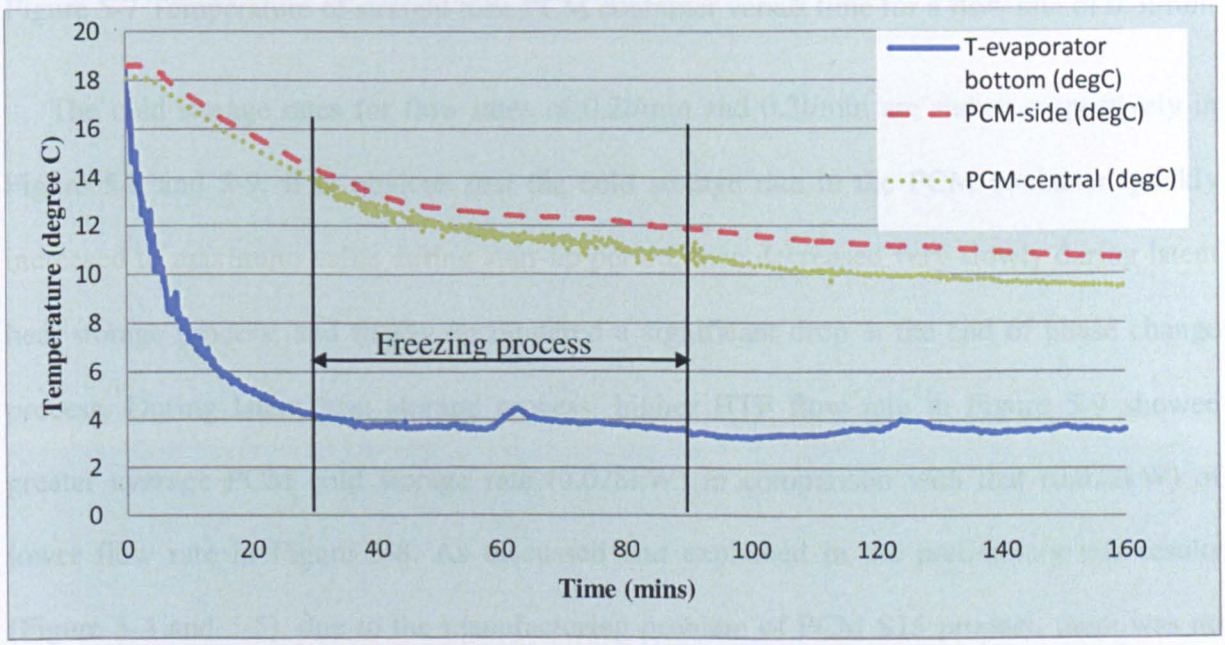

Figure 5-6 Temperature of straight tube PCM container versus time for a flow rate of 0.2l/min

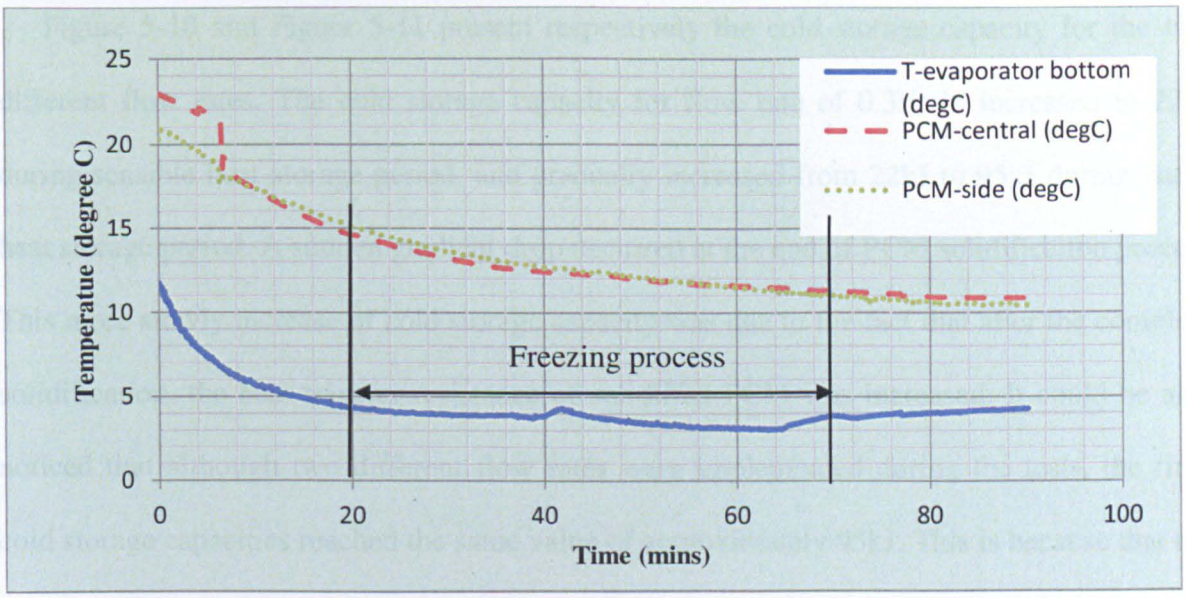

Figure 5-7 Temperature of straight tube PCM container versus time for a flow rate of 0.3l/min

The cold storage rates for flow rates of 0.2l/min and 0.3l/min are shown respectively in Figure 5-8 and 5-9. It is obvious that the cold storage rate in the PCM container quickly increased to maximum value during start-up period, then decreased very slowly during latent heat storage process, and finally encountered a significant drop at the end of phase change process. During latent heat storage process, higher HTF flow rate in Figure 5-9 showed greater average PCM cold storage rate (0.028kW) in comparison with that (0.022kW) of lower flow rate in Figure 5-8. As discussed and explained in the preliminary test results (Figure 5-4 and 5-5), due to the manufacturing problem of PCM S15 product, there was no significant latent heat storage process during which the temperature of PCM remained almost constant most of the time. The identification of the phase change starting time and finishing time were based on examining the gradient change of both PCM temperature profile (Figure 5-6 and 5-7) and the cold storage rate (Figure 5-8 and 5-9). The phase change process was considered to start when the PCM temperature dropped below 13.9°C, which was the phase change temperature shown in the preliminary test (Figure 5-4). A sudden drop of the cold storage rate indicated the finishing of latent heat storage process.

Figure 5-10 and Figure 5-11 present respectively the cold storage capacity for the two different flow rates. The cold storage capacity for flow rate of 0.3l/min increased to 22kJ during sensible heat storage period, and gradually increased from 22kJ to 95kJ during latent heat storage period. A sudden gradient drop occurred at the end of PCM solidification process. This more slowly increase of cold storage capacity was due to the fact that after the complete solidification, the heat transfer resistance of solidified PCM was increased. It could be also noticed that although two different flow rates were implemented during the tests, the final cold storage capacities reached the same value of approximately 95kJ. This is because that the cold storage capacity depends mainly on the amount of PCM used in the container. The various flow rates therefore can only affect the storage rate, not the storage capacity.

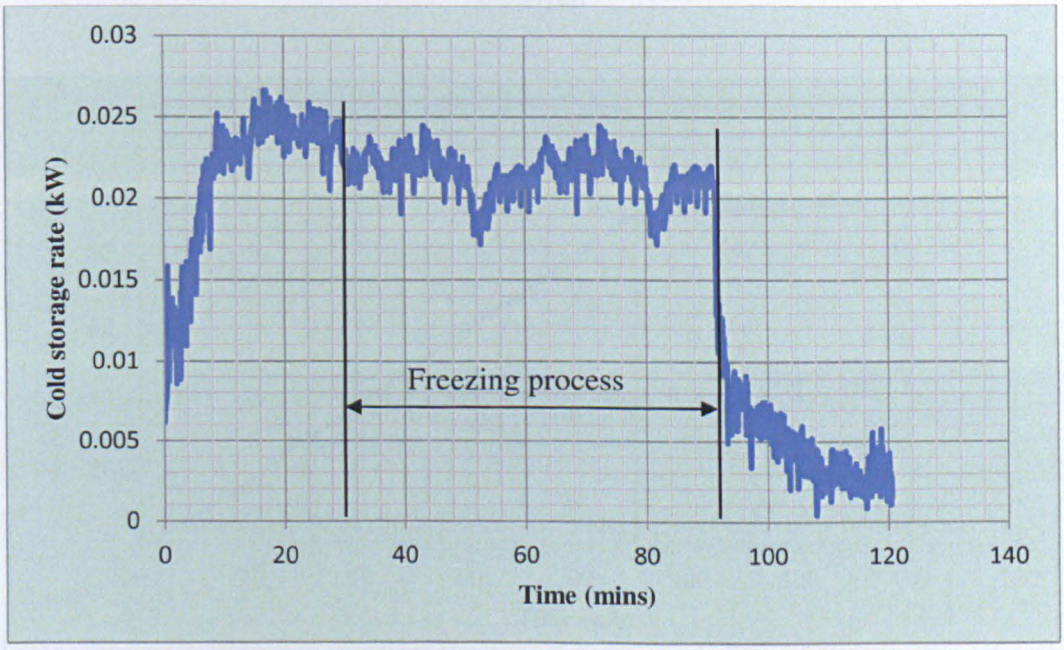

Figure 5-8 Cold storage rate of straight tube PCM container versus time for a flow rate of 0.2l/min

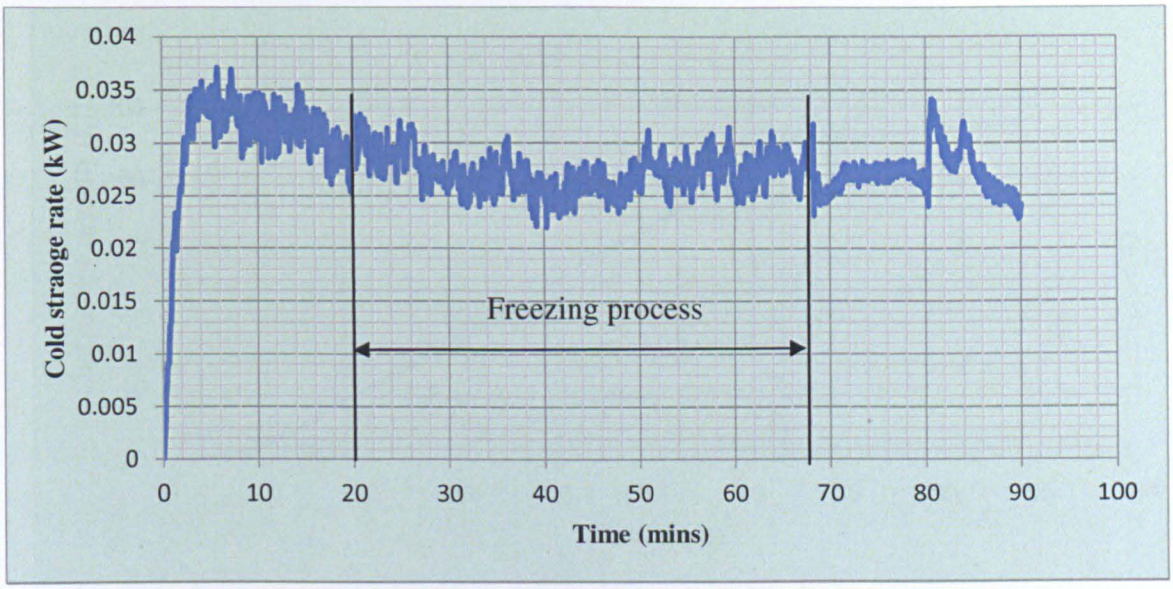

Figure 5-9 Cold storage rate of straight tube PCM container versus time for a flow rate of 0.3l/min

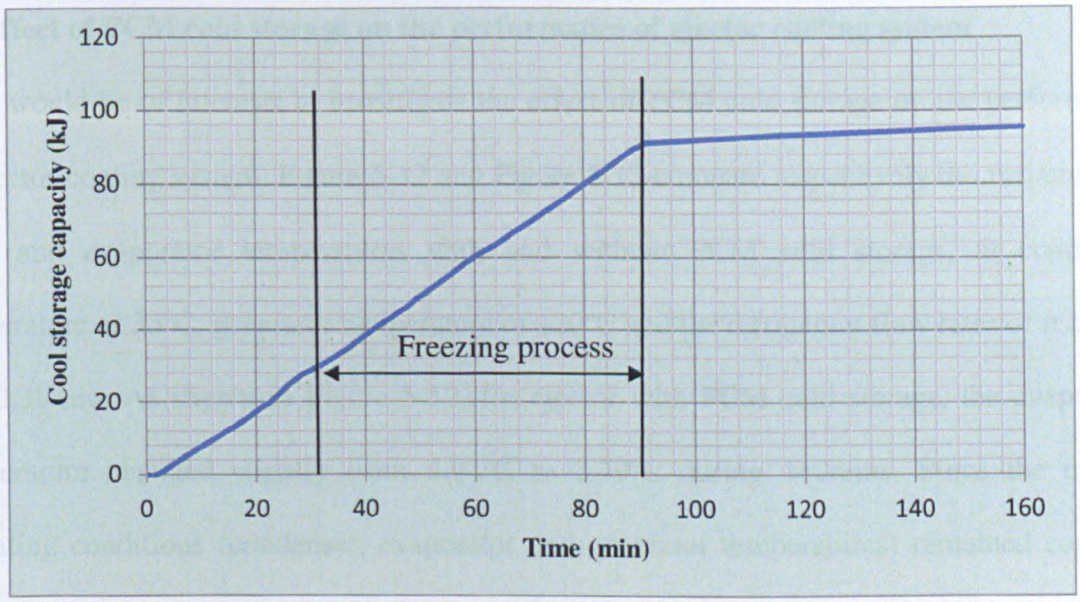

Figure 5-10 Cold storage capacity of straight tube PCM container versus time for a flow rate of 0.2l/min

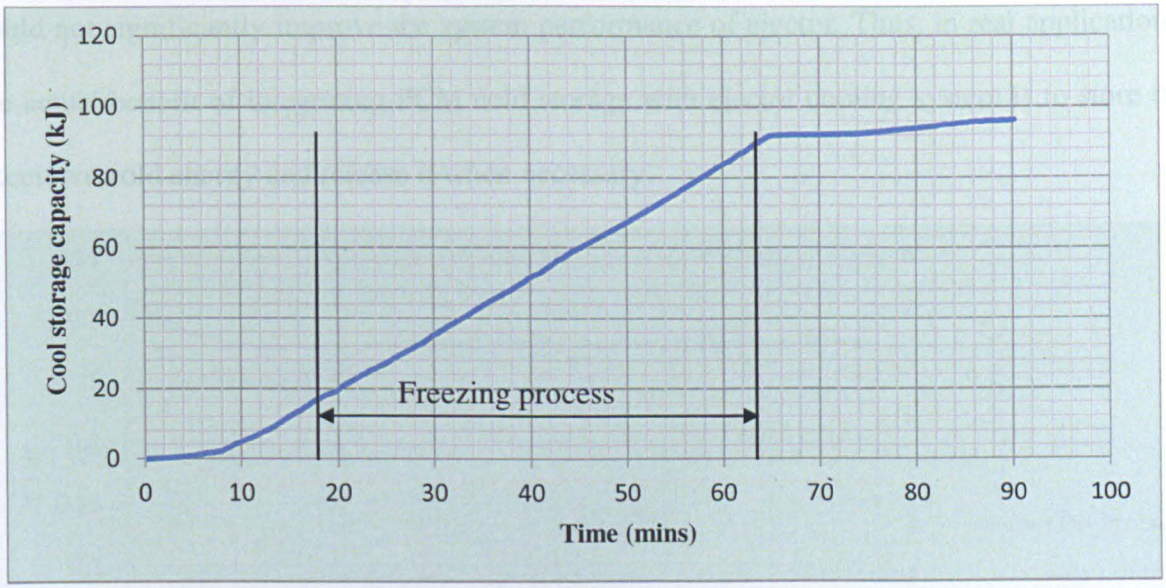

Figure 5-11 Cold storage capacity of straight tube PCM container versus time for a flow rate of 0.3l/min

Effect of PCM cold storage on the performance of ejector cooling system

It would be of interests to investigate the effect of PCM cold storage on the performance of ejector cooling system. Figure 5-12 and Figure 5-13 compare respectively the variations of COP and evaporator temperatures with and without PCM cold storage, at condenser temperature of 35°C, generator temperature of 120°C and the refrigerant flow rates of 0.2l/min and 0.3l/min. As shown in Figure 5-12, for ejector with PCM cold storage, the evaporator temperature changed slightly from 4.92°C to 3.79°C during 140mins. Since the ejector operating conditions (condenser, evaporator and generator temperatures) remained constant most of the time, the COP was kept at a constant value (around 0.28). While for the ejector without PCM cold storage system, the evaporator temperature decreased from 4.99°C to 0.98°C (around 80%), and the COP of the ejector reduced from 0.318 to 0.196 (about 38%). This further proved the conclusions obtained in Chapter 3 and Chapter 4 that the reduced evaporator temperature will lead to the decreasing of COP, which is disadvantageous to the system performance. It can be concluded that the integration of PCM cold storage system

could not significantly improve the system performance of ejector. Thus, in real applications, the actual benefit of integrating PCM cold storage with ejector cooling system is to store the excessive cold energy and release it when necessary.

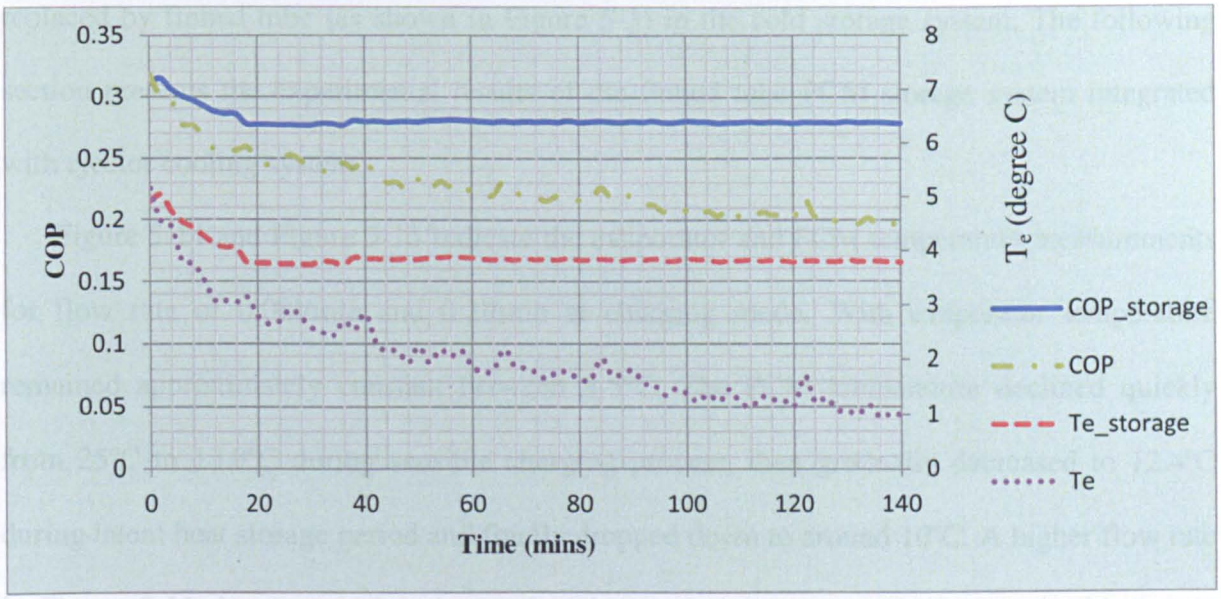

Figure 5-12 COP and evaporator temperature of ejector with and without PCM cold storage system (straight tube configuration, flow rate=0.2l/min)

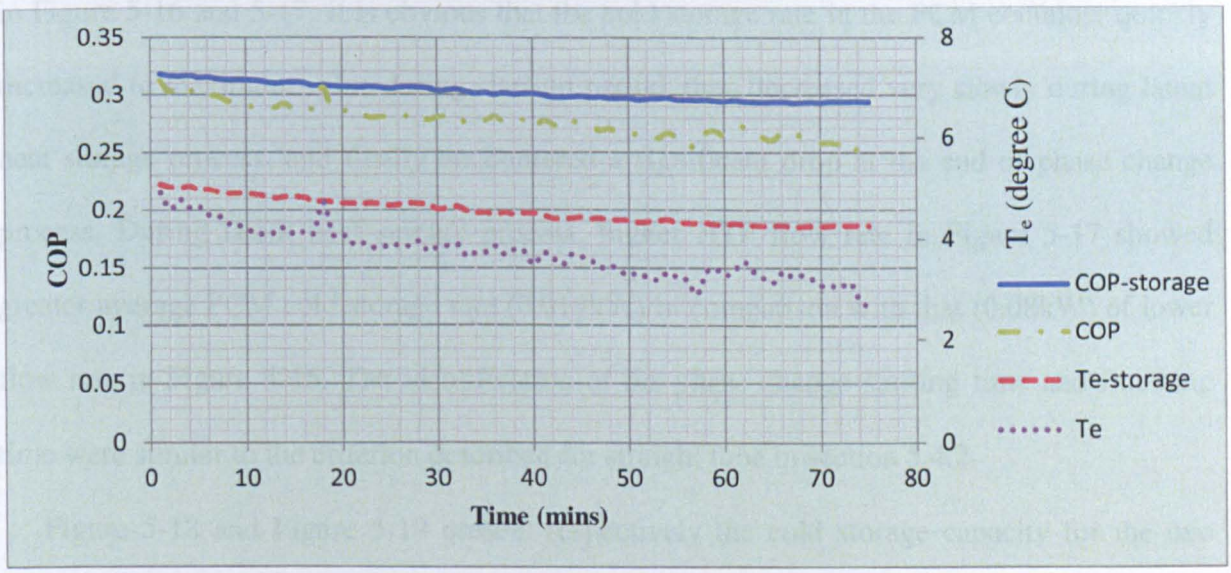

Figure 5-13 COP and evaporator temperature of ejector with and without PCM cold storage system (straight tube configuration, flow rate=0.3l/min)

5.4.3 Finned tube charging and discharging mode

5.4.3.1 Finned tube charging mode

In order to enhance the heat transfer between PCM and the HTF, the straight tube was replaced by finned tube (as shown in Figure 5-3) in the cold storage system. The following section presents the experimental results of the finned tube PCM storage system integrated with ejector cooling system.

Figure 5-14 and Figure 5-15 indicate the evaporator and PCM temperature measurements for flow rate of 0.08l/min and 0.2l/min at charging mode. With evaporator temperature remained approximately constant between 3-5°C, The PCM temperature declined quickly from 25°C to 13.9°C during sensible charging process, then gradually decreased to 12.4°C during latent heat storage period and finally dropped down to around 10°C. A higher flow rate in Figure 5-15 demonstrated a shorter freezing period (40 minutes) compared with that in Figure 5-14 (70 minutes), and a lower PCM temperature at the end of phase change process.

The cold storage rates for flow rates of 0.08l/min and 0.2l/min are illustrated respectively in Figure 5-16 and 5-17. It is obvious that the cold storage rate in the PCM container quickly increased to maximum value during start-up period, then decreased very slowly during latent heat storage process, and finally encountered a significant drop at the end of phase change process. During latent heat storage process, higher HTF flow rate in Figure 5-17 showed greater average PCM cold storage rate (0.018kW) in comparison with that (0.08kW) of lower flow rate in Figure 5-16. The identification of the phase change starting time and finishing time were similar to the criterion described for straight tube in section 5.4.2.

Figure 5-18 and Figure 5-19 present respectively the cold storage capacity for the two different flow rates. The cold storage capacity for flow rate of 0.2l/min increased to 27kJ during sensible heat storage period, and gradually increased from 27kJ to 80kJ during latent heat storage period. A sudden gradient drop occurred at the end of PCM solidification process.

This more slowly increase of cold storage capacity is due to the fact that after the complete solidification, the latent heat storage process is completed. After that, the cold energy is stored in the form of sensible heat, which has a much lower storage capacity than latent heat.

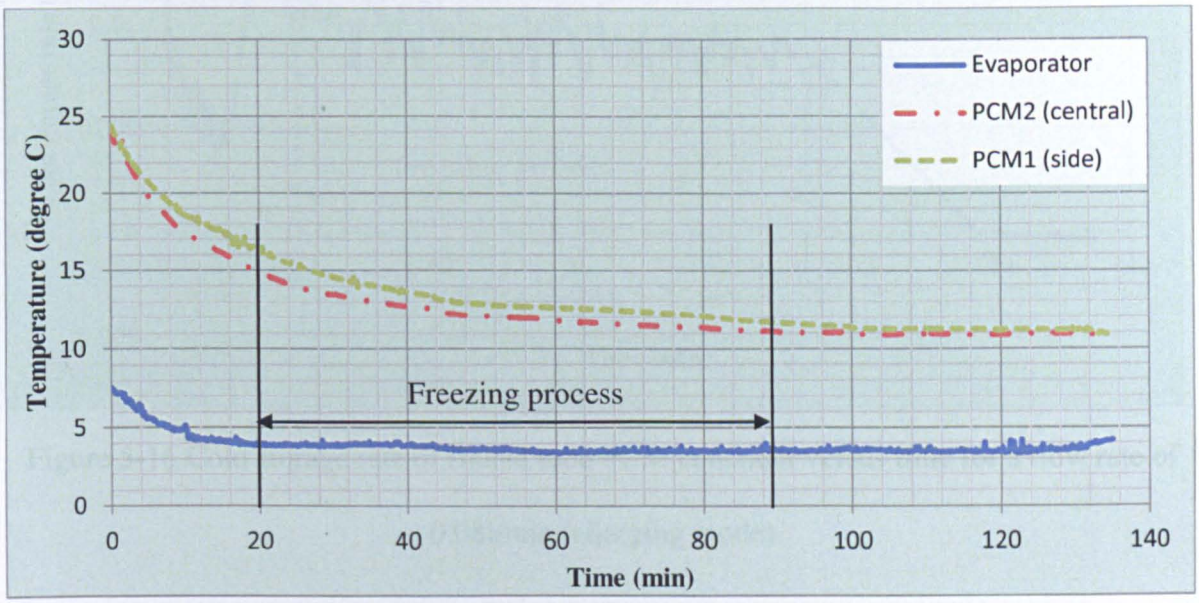

Figure 5-14 Temperature of finned tube PCM container versus time for a flow rate of 0.08l/min (charging mode)

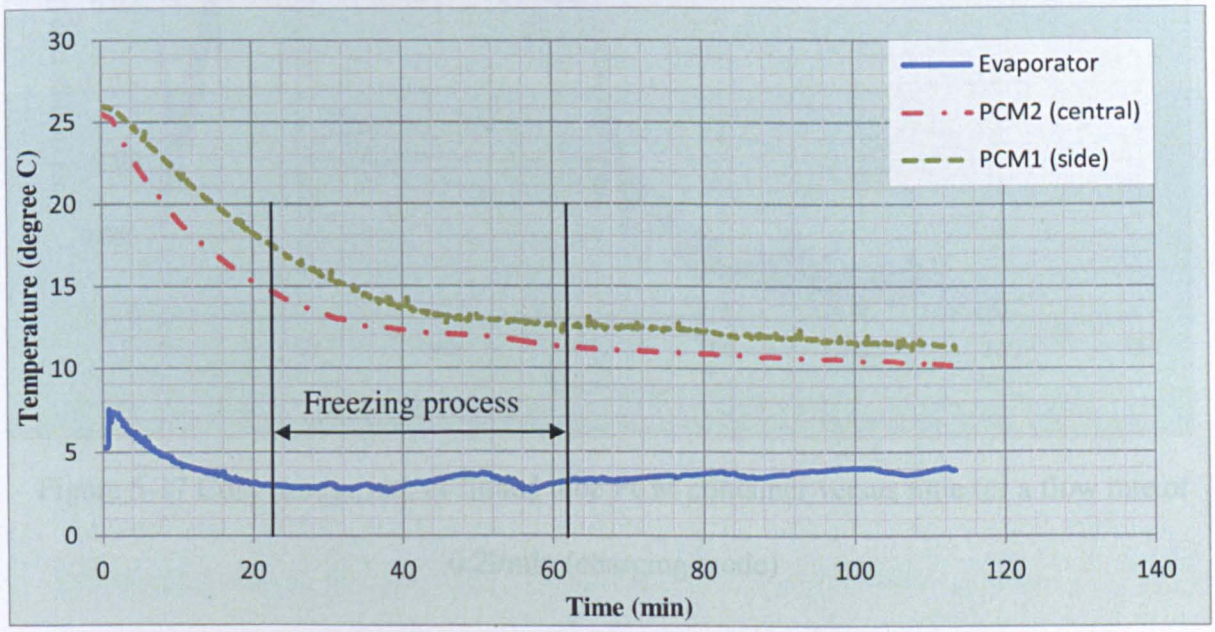

Figure 5-15 Temperature of finned tube PCM container versus time for a flow rate of 0.2l/min (charging mode)

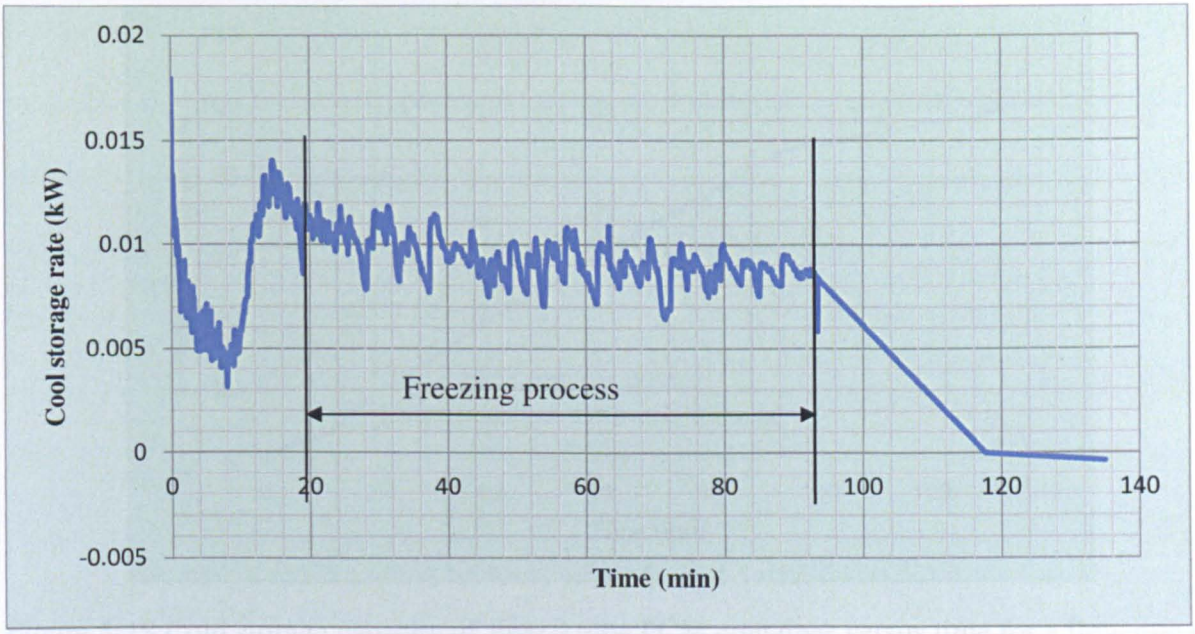

Figure 5-16 Cold storage rate of finned tube PCM container versus time for a flow rate of 0.08l/min (charging mode)

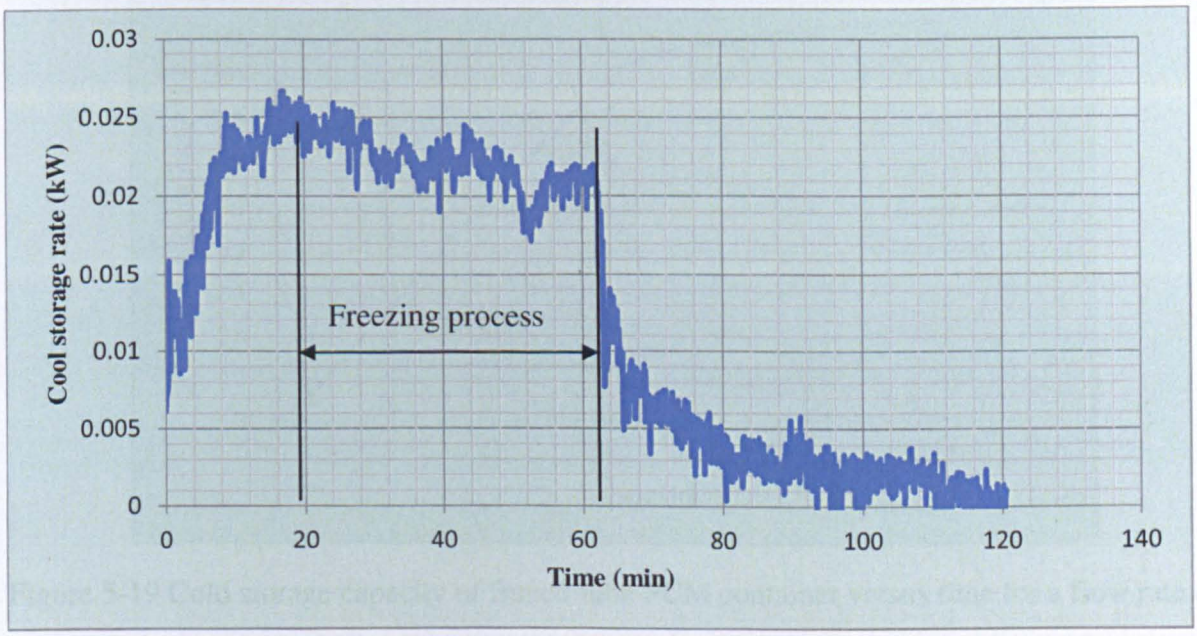

Figure 5-17 Cold storage rate of finned tube PCM container versus time for a flow rate of 0.2l/min (charging mode)

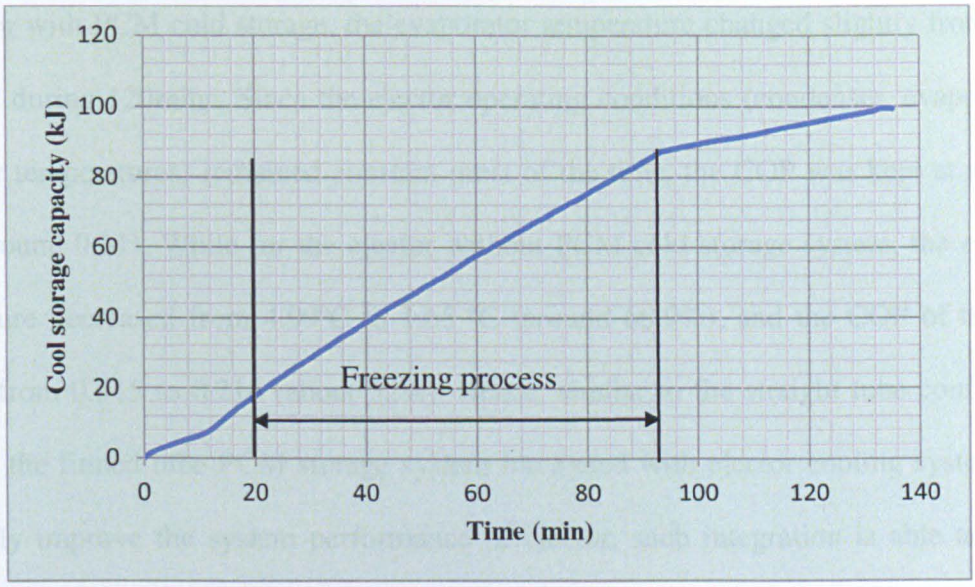

Figure 5-18 Cold storage capacity of finned tube PCM container versus time for a flow rate of 0.08l/min (charging mode)

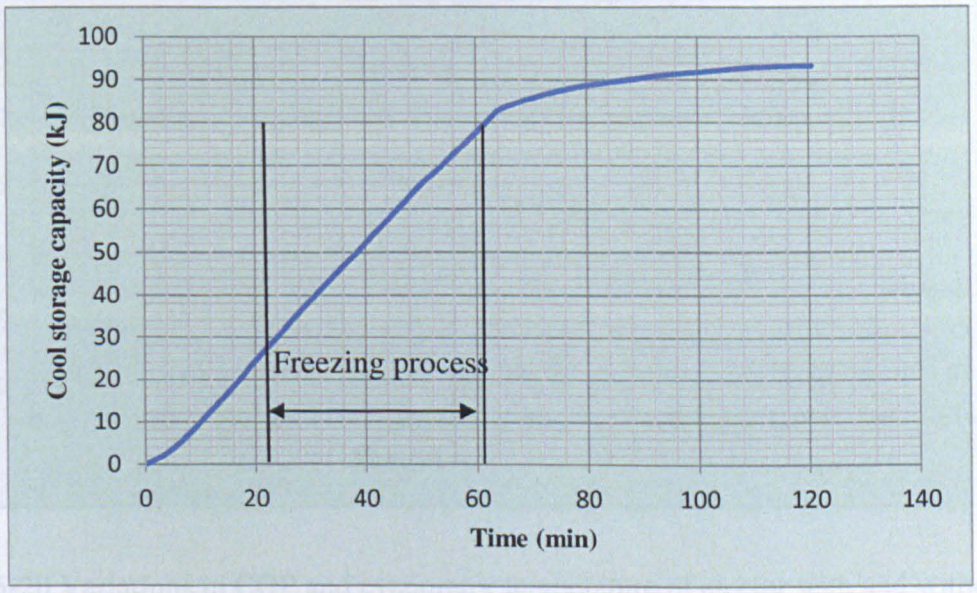

Figure 5-19 Cold storage capacity of finned tube PCM container versus time for a flow rate of 0.2l/min (charging mode)

Effect of PCM cold storage on the performance of ejector cooling system

Figure 5-20 and Figure 5-21 compare respectively the variations of COP and evaporator temperatures with and without PCM cold storage, at condenser temperature of 35°C, generator temperature of 120°C and the refrigerant flow rate of 0.08l/min. It can be found that

for ejector with PCM cold storage, the evaporator temperature changed slightly from 4.96 ℃ to 4.2 ℃ during 120mins. Since the ejector operating conditions (condenser, evaporator and generator temperatures) remained constant most of the time, the COP was kept at a constant value (around 0.31). While for the ejector without PCM cold storage system, the evaporator temperature decreased from 4.99℃ to 1.65 ℃ (around 66.9%), and the COP of the ejector reduced from 0.315 to 0.216 (about 32%). Hence, similar to the straight tube configuration, although the finned tube PCM storage system integrated with ejector cooling system cannot potentially improve the system performance of ejector, such integration is able to help the ejector to work under a more stable condition.

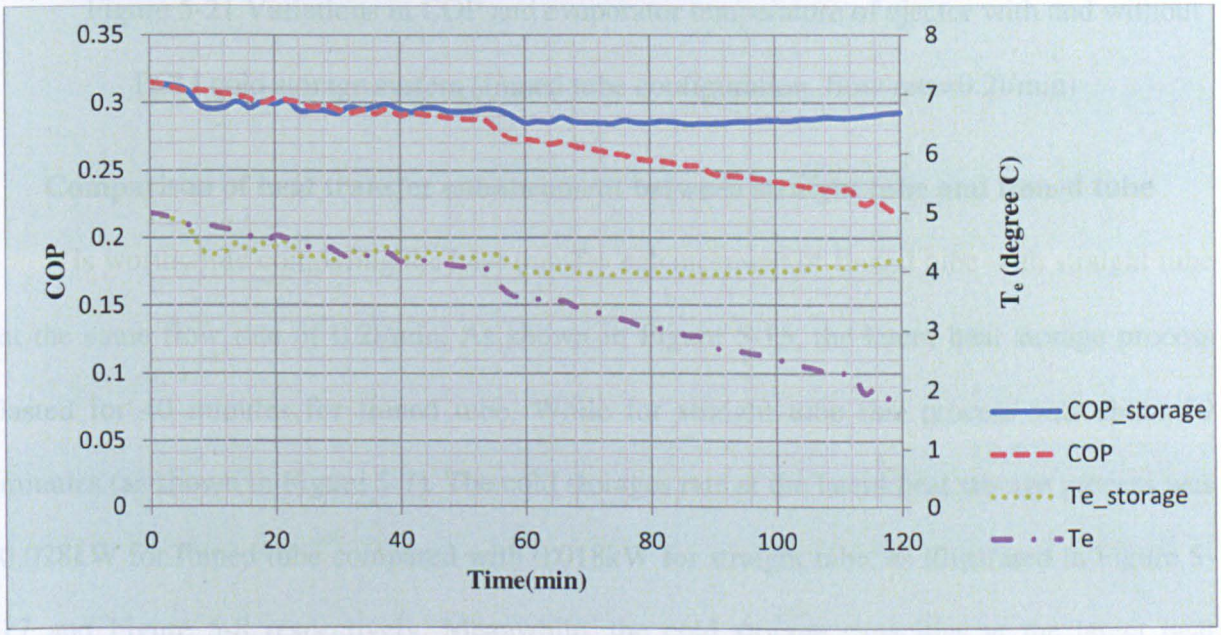

Figure 5-20 Variations in COP and evaporator temperature of ejector with and without PCM cold storage system (finned tube configuration, flow rate=0.08l/min)

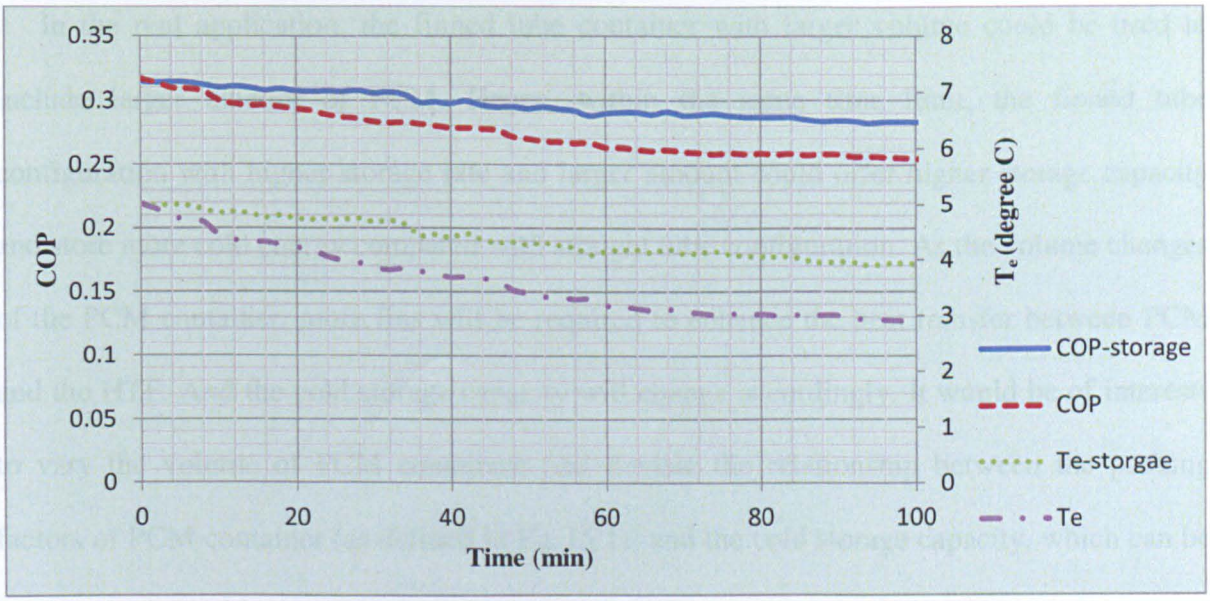

Figure 5-21 Variations in COP and evaporator temperature of ejector with and without PCM cold storage system (finned tube configuration, flow rate=0.2l/min)

Comparison of heat transfer enhancement between straight tube and finned tube

It is worthwhile comparing the heat transfer enhancement of finned tube with straight tube at the same flow rate of 0.2l/min. As shown in Figure 5-15, the latent heat storage process lasted for 40 minutes for finned tube. While for straight tube this process was about 50 minutes (as shown in Figure 5-7). The cold storages rate at the latent heat storage process was 0.028kW for finned tube compared with 0.018kW for straight tube, as illustrated in Figure 5-17 and Figure 5-8 respectively. Meanwhile, the cold storage capacities at the latent heat storage process were 85kJ for finned tube (Figure 5-19) and 95kJ for straight tube (Figure 5-10). It could be found that during latent heat storage process, finned tube could store the cold energy at a higher rate compared with straight tube. However, since both of the containers contained same amount of PCMs, the total amount of cold energy could be stored during this process remain approximately the same for finned tube and straight tube. In conclusion, finned tube with higher storage rate would offer shorter charge period, which was approximately 20% less than that of the straight tube.

In the real application, the finned tube container with larger volume could be used to include larger amount of PCM. Hence, within the same time limit, the finned tube configuration with higher storage rate and larger amount could offer higher storage capacity and store more cold energy compared with straight tube configuration. As the volume changes of the PCM container, more fins will be required to enhance the heat transfer between PCM and the HTF. And the cold storage capacity will change accordingly. It would be of interests to vary the volume of PCM containers and deviate the relationship between the packing factors of PCM container (as defined in Eq. (5.1)) and the cold storage capacity, which can be used as design guidance. This could be regarded as future research work.

5.4.3.2 Finned tube discharging mode

It has been proved that the finned tube is more effective compared with straight tube in terms of heat transfer enhancement. In order to analyze how effectively the cold energy could be released in the finned tube container, the experiments of the discharging mode were carried out at the heat source temperature of 25 °C for flow rate of 0.1l/min and 0.2l/min.

The HTF inlet and outlet temperatures and PCM temperature measurements for flow rate of 0.1l/min and 0.2l/min at discharging mode are shown in Figure 5-22 and Figure 5-23. For the flow rate of 0.1l/min, with HTF inlet temperature remained approximately constant at 25°C, the measured temperature in the side of the PCM container increased quickly from 11°C to 14.1°C during sensible charging process, then gradually changed from 14.1 to 17.4°C during latent heat storage period and went through a more significant temperature increase afterwards. A higher flow rate in Figure 5-23 demonstrated a shorter melting period (150 minutes) compared with that in Figure 5-22(200 minutes).

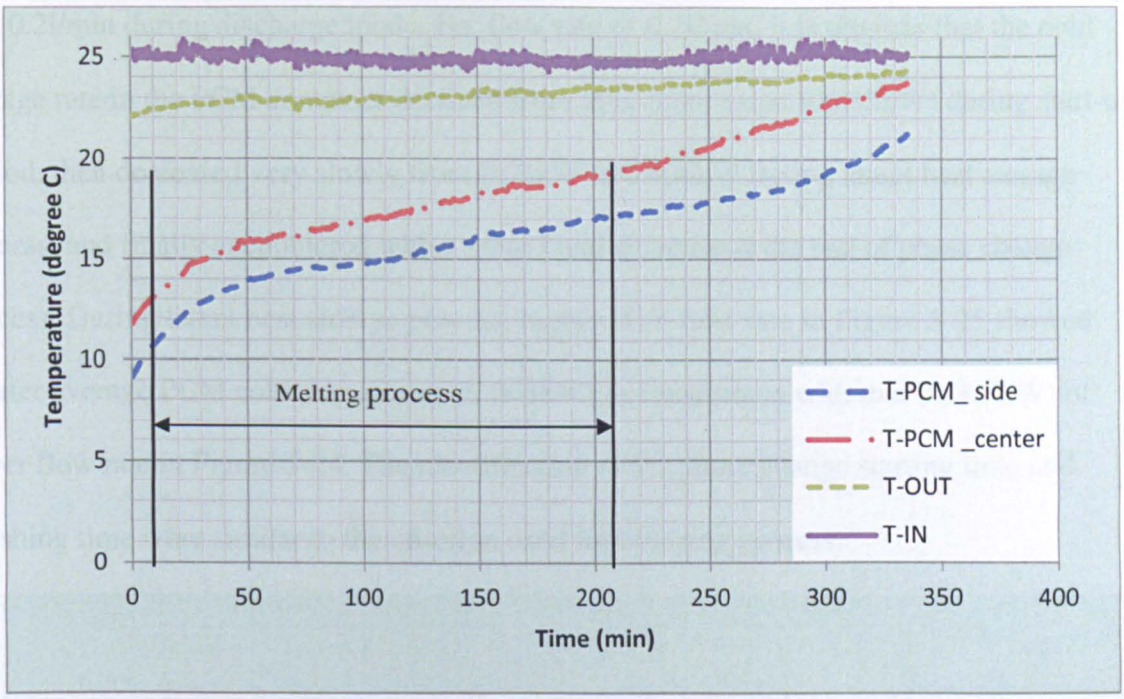

Figure 5-22 Temperature of finned tube PCM container versus time for a flow rate of 0.1l/min (Discharging mode)

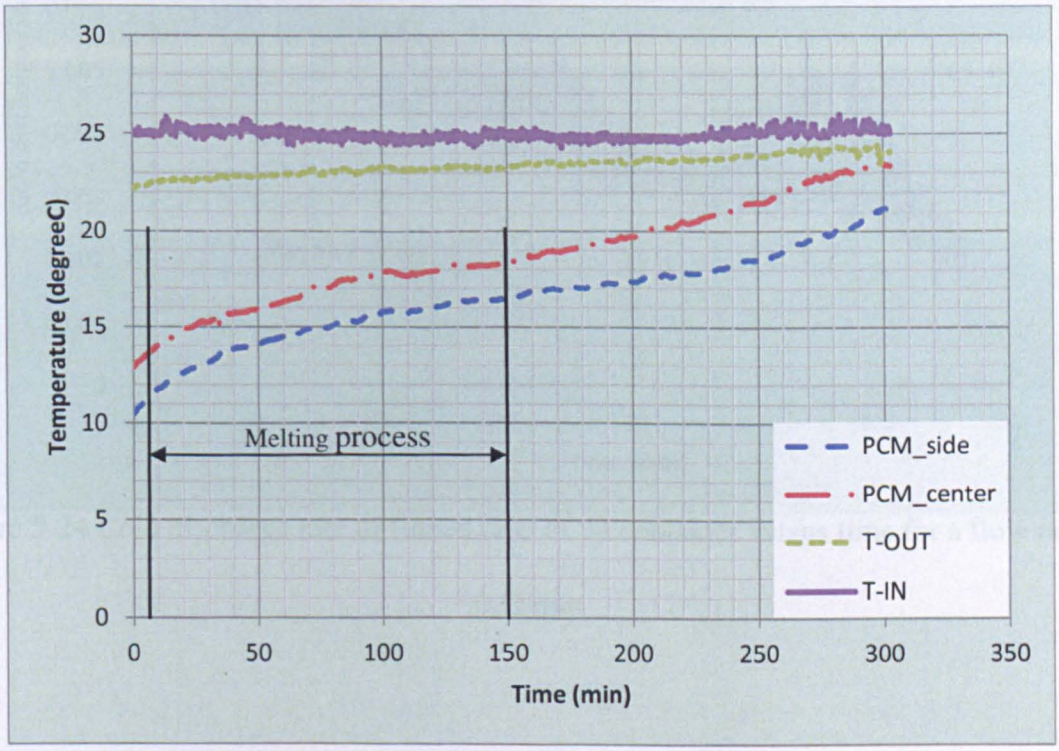

Figure 5-23 Temperature of finned tube PCM container versus time for a flow rate of 0.2l/min (Discharging mode)

Figure 5-24 and 5-25 illustrate respectively the cold storage rates for flow rate of 0.1l/min

and 0.2l/min during discharge mode. For flow rate of 0.2l/min, it is obvious that the cold storage rate in the PCM container declined from maximum value (0.012kW) during start-up period, then decreased very slowly from 0.01kW to 0.006kW during latent heat storage process, and finally encountered with a more rapid decrease at the end of phase change process. During latent heat storage process, higher HTF flow rate in Figure 5-25 showed greater average PCM cold storage rate (0.008kW) in comparison with that (0.005kW) of lower flow rate in Figure 5-24. The identification of the phase change starting time and finishing time were similar to the criterion used for charging process.

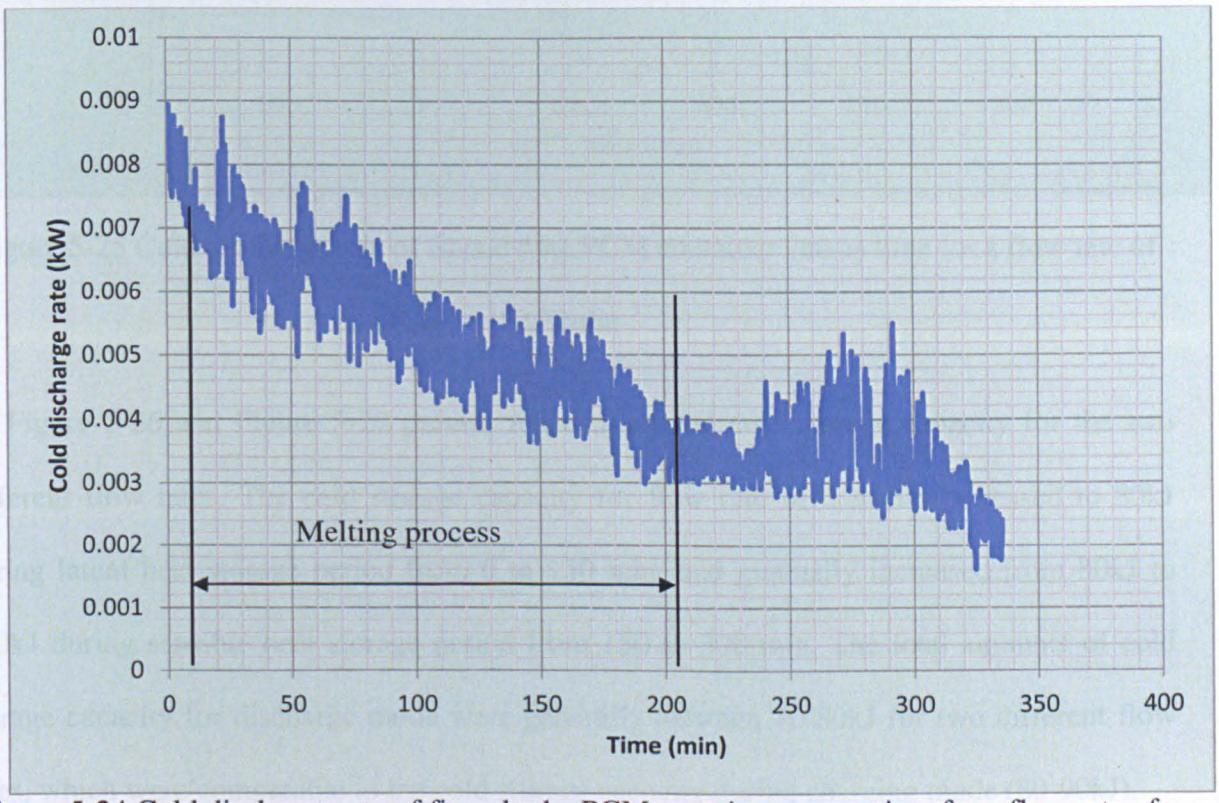

Figure 5-24 Cold discharge rate of finned tube PCM container versus time for a flow rate of 0.1l/min

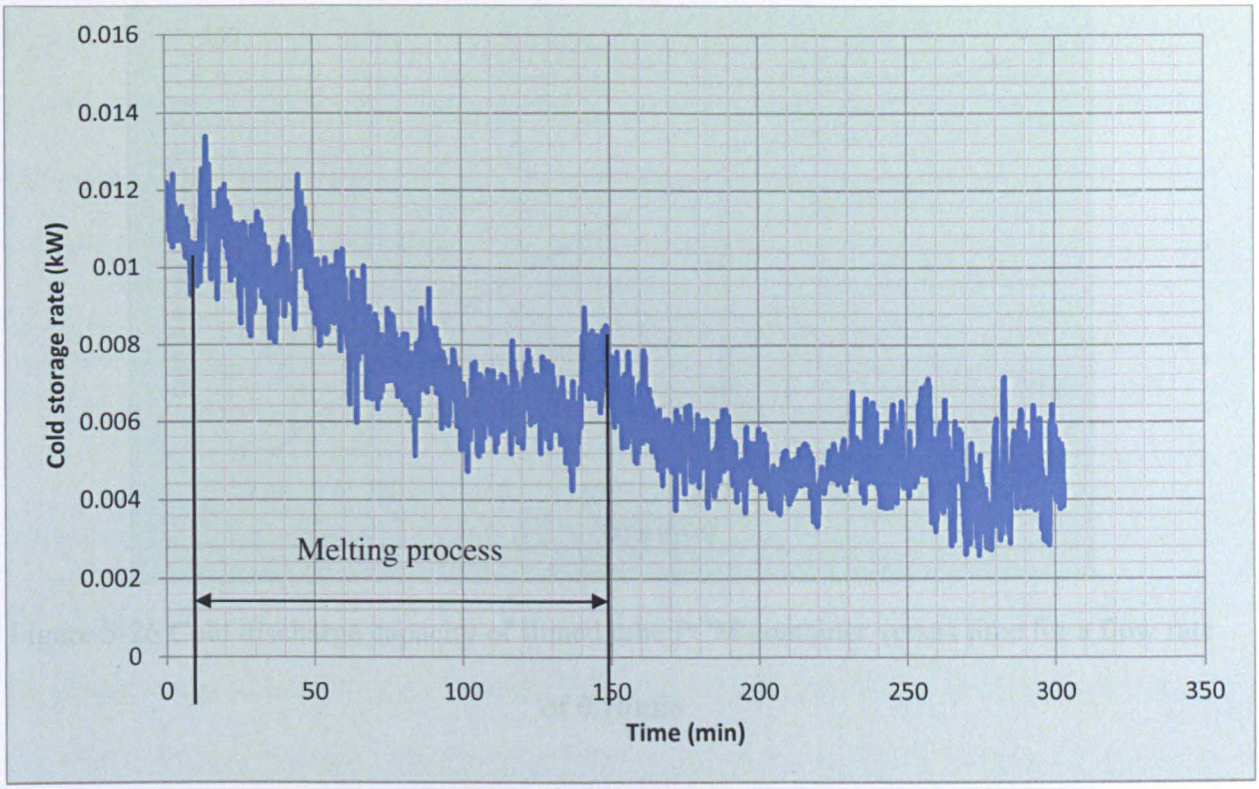

Figure 5-25 Cold discharge rate of finned tube PCM container versus time for a flow rate of 0.2l/min

Figure 5-26 and Figure 5-27 present respectively the cold storage capacity for the two different flow rates. The cold storage capacity for flow rate of 0.2l/min increased to 80kJ during latent heat storage period from 0 to 150 min, and gradually increased from 80kJ to 120kJ during sensible heat storage period from 150 to 300 min. The total amounts of cold storage capacity for discharge mode were generally between 70-80kJ for two different flow rates, which were comparable to the cold storage capacity during charging mode (80-90kJ).

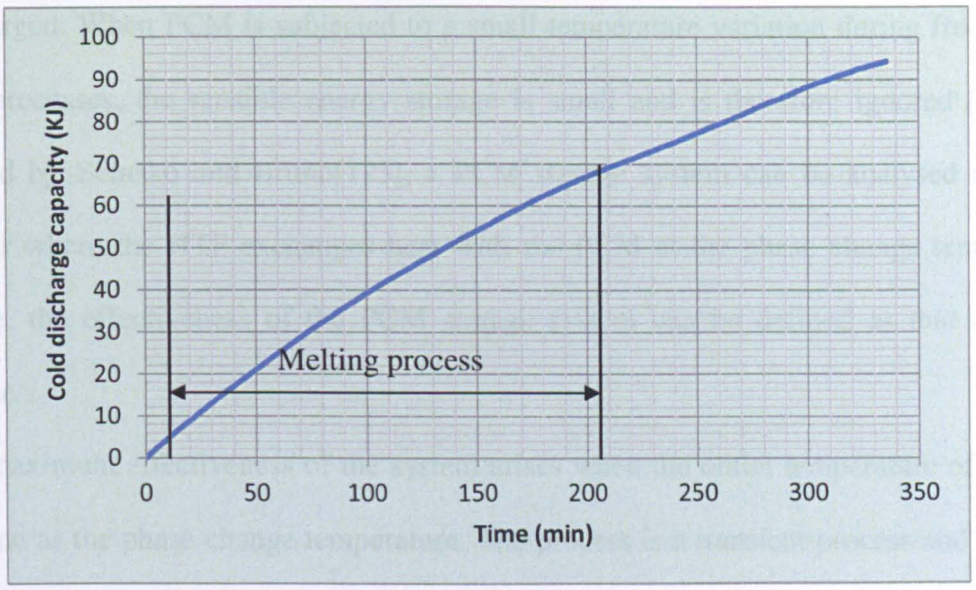

Figure 5-26 Cold discharge capacity of finned tube PCM container versus time for a flow rate of 0.1l/min

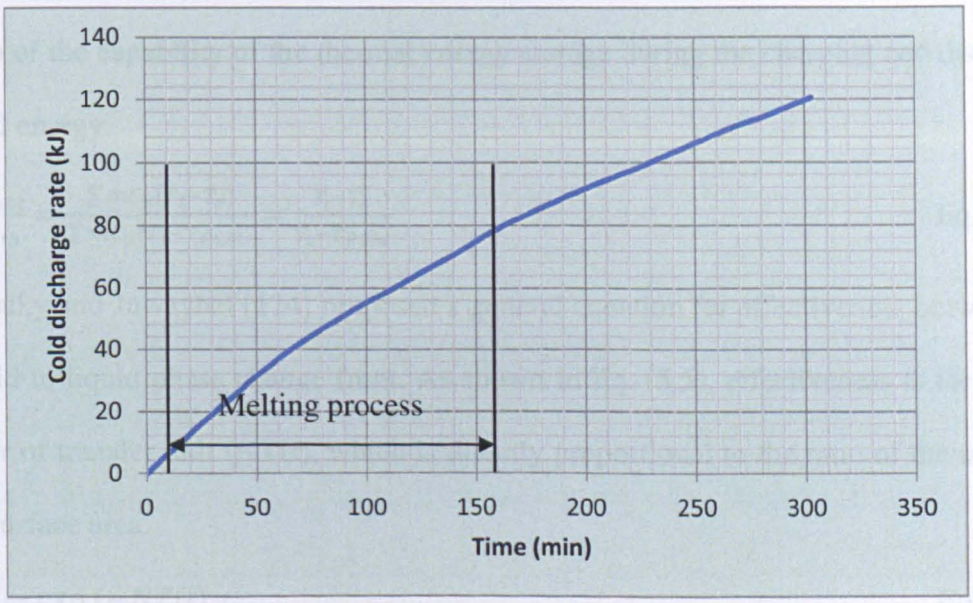

Figure 5-27 Cold discharge capacity of finned tube PCM container versus time for a flow rate of 0.2l/min

5.5 Effectiveness of PCM cold storage system

The objective of the cold storage thermal process is for the heat transfer fluid to reach the PCM temperature, hence, effectiveness is an applicable parameter[122]. The effectiveness is described as the ratio of the actual heat obtained over the theoretical maximum heat that can

be discharged. When PCM is subjected to a small temperature variation during freezing and melting processes, the sensible energy storage is small and is therefore ignored [122]. As mentioned by Belusko and Bruno[123], a PCM storage system can be analysed as a heat exchanger where the HTF exchanges heat with the PCM at the phase change temperature. Therefore, the effectiveness of the PCM storage system can be defined as that of a heat exchanger.

The maximum effectiveness of the system arises when the outlet temperature of the HTF is the same as the phase change temperature. The process is a transient process and therefore the heat exchanger effectiveness is bounded between 0 and 1. The average effectiveness over the phase change process can be determined by the average inlet and outlet temperature over the phase change process. The average effectiveness (as shown in E.q.(5.4)) gives an indication of the capability of the thermal energy storage during the charging and discharging of thermal energy.

$$\varepsilon = \frac{Q_{act}}{Q_{th}} = \frac{\sum mC_p(T_i - T_o)}{\sum mC_p(T_i - T_{PCM})} = \frac{\overline{T_i} - \overline{T_o}}{\overline{T_i} - \overline{T_{PCM}}} \qquad \text{Eq. (5.4)}$$

Dessouky and Juwayhel [124] proposed a general equation for effectiveness between HTF and a solid to liquid phase change front. As shown in Eq. (5.5), effectiveness is the function of number of transfer unit (NTU), which is directly proportional to the ratio of the mass flow rate and surface area.

$$\varepsilon = 1 - \exp(-NTU) \qquad \text{Eq. (5.5)}$$

Phase change effectiveness for charging process of PCM cold storage system is measured using Eq. (5.4) with T_{PCM} fixed at 13.9°C, which is the phase change temperature obtained in the preliminary test (Figure 5-4). In Figure 5-14, the charging effectiveness was measured to be 0.286 with mass flow rate of 0.08l/min. With higher flow rate of 0.2l/min, the charging effectiveness dropped to 0.125. In Figure 5-22 and 5-23, the discharging effectiveness was 0.144 and 0.089 for mass flow rate of 0.1l/min and 0.2l/min respectively.

For charging and discharging tests, flow rates were varied between 0.05l/min and 0.4l/min. The experimental results of these different flow rates were similar to those presented in previous section, hence, were not included in the thesis. Figure 5-28 and 5-29 illustrate the average effectiveness with respect to various flow rates for charging and discharging modes of PCM cold storage system. During the charging and discharging process, the PCM material inside the container is at stagnant state, which is different from conventional heat exchanger. Therefore a lower flow rate will result in longer contacting time of the HTF inside the container. This will lead to a better heat transfer between the PCM material and the HTF.

Effectiveness is the function of the number of transfer units which will be affected by the amount of natural convection in the PCM during charging and discharging processes. Since the difference between the inlet temperature of HTF and PCM phase change temperature is the main driving force for natural convection, an increase in the temperature difference will lead to a higher effectiveness. In our experiments, the inlet temperature of HTF for charging and discharging processes were chosen to be 5°C and 25°C respectively, and the ideal transient phase change temperature of PCM was 15°C. Therefore, the freezing and melting processes for finned tube PCM container were conducted under the same driving forces. For charging and discharging processes, the same impacts of the temperature differences on effectiveness can be expected. However, it can be noticed from Figure 5-28 and 5-29 that the effectiveness of charging process is higher than that of discharging process. The reason is that the thermal conductivity of solidified PCM (1.92 W/mk) is higher than that of the liquid one (0.43W/mk), which offers better heat transfer in charging process.

Two experimental derived formulas for the calculation of the average effectiveness for both charging and discharging process of the cold storage system based on the ratio of mass flow rate are shown in Eq. (5.6) and Eq. (5.7). These formulas act as characteristic curves for the PCM storage container design, which will be discussed in next section.

$$\varepsilon = 1 - \exp\left(-0.0256\left(\frac{A}{\dot{m}}\right)\right) \quad \text{Eq. (5.6)}$$

$$\varepsilon = 1 - \exp\left(-0.0168\left(\frac{A}{\dot{m}}\right)\right) \quad \text{Eq. (5.7)}$$

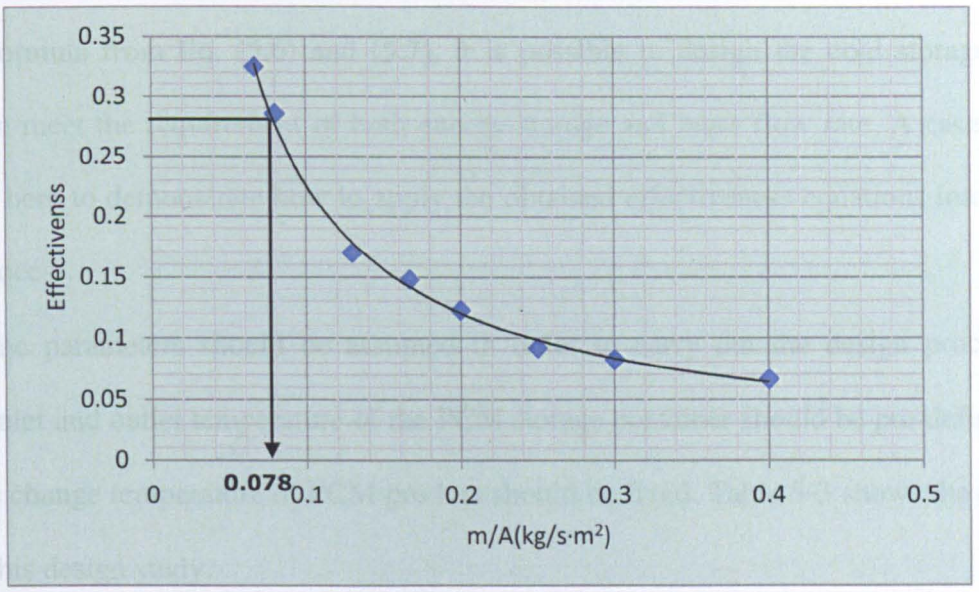

Figure 5-28 Charging effectiveness of finned tube PCM container over the operating mass flow rates

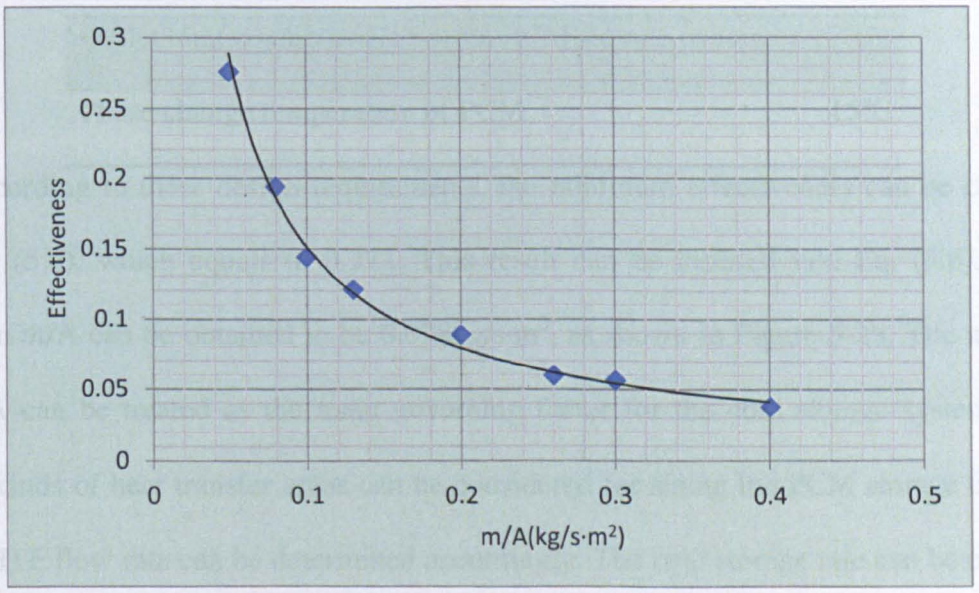

Figure 5-29 Discharging effectiveness of finned tube PCM container over the operating mass flow rates

5.6 Case study of PCM cold storage container design

The effectiveness of charging and discharging process gives an indication of how much energy can be extracted from the thermal energy storage system. With the experimental derived formula from Eq. (5.6) and (5.7), it is possible to design the cold storage system which can meet the requirement of both energy storage and mass flow rate. A case study is proposed here to demonstrate how to apply the obtained effectiveness equations into the real design process.

Some parameters should be assumed in order to carry out the design process. The average inlet and outlet temperature of the PCM storage container should be pre-defined. And the phase change temperature of PCM product should be fixed. Table 5-3 shows the specified data for this design study.

Table 5-3 Predefined data for the case study

Inlet temperature of HTF to PCM storage container	4°C
Outlet temperature of HTF from PCM storage container	7°C
Phase change temperature of PCM	15°C

According to these design requirements, the minimum effectiveness can be calculated from Eq. (5.4), which equals to 0.273. This result can be inserted into Eq. (5.6), and the maximum $\dot{m}/A$ can be obtained to be 0.078kg/s·m^2, as shown in Figure 5-28. The maximum ratio $\dot{m}/A$ can be treated as the main governing factor for the cold storage system design. Various kinds of heat transfer areas can be considered for sizing the PCM storage container, and the HTF flow rate can be determined accordingly. The cold storage rate can be calculated using the dimension of the storage unit and specific heat capacity of HTF. Considering the cold storage system operational time, in this case, 8 hours, the mass of PCM required can be computed with the calculated effectiveness from Eq. (5.4). Table 5-4 demonstrates the basic design parameters for sizing of the PCM storage container.

Table 5-4 Basic design parameters for sizing of the PCM storage container (with $\dot{m}$/A=0. 078kg/s·m^2)

Heat transfer area A (m^2)	Flow rate $\dot{m}$ (kg/s)	Average cold storage rate (kW)	Amount of PCM (kg)
0.08	$6.24*10^{-3}$	0.264	195.8
0.16	0.013	0.527	391.6
0.24	0.019	0.789	586.7

5.7 Conclusions

This chapter experimentally investigates the system performance of PCM cold storage system integrated with ejector cooling system. The ejector cooling system was able to provide a cooling load at temperatures between 3°C and 5°C. The PCM container, coupled with the evaporator, could store the excess cooling capacity of the ejector and provide cooling effect when the heat input is not sufficient. Medium temperature source (from solar collector or industrial waste) at temperature of 120 °C could be the main driving force for the system. Cold storage charging and discharging processes were performed with various mass flow rates, at the HTF inlet temperatures of 5°C and 25°C respectively. The following conclusions can be drawn from the experimental results:

(1) The cold storage/discharge rate decreased rapidly during the sensible cooling period, then remained more or less constant during the latent heat storage process, and dropped to a minimum value at the end of PCM solidification process. The cold storage/discharge capacity increased dramatically during the sensible cooling period, then increased gradually during the latent heat storage process, and finally reached a stable value.

(2) The integration of PCM cold storage with ejector cooling system could not improve the system performance of ejector. However, it can help to maintain a more stable evaporator temperature, and thus a more reliable ejector system performance.

(3) In order to analysis the heat transfer enhancement, finned tube and straight tube were studied and compared as two different heat exchangers between PCM and the HTF. The experimental results of charging mode indicated that during latent heat storage process, the charging period of PCM container with finned tube was 20% less than that with straight tube. At the flow rate of 0.2l/min, the cold storage rate of finned tube was 0.028kW, which was 56% higher than that of the straight tube. It could be concluded that the finned tube was more effective than the straight tube in terms of improving the heat transfer.

The PCM storage container was analyzed as a heat exchanger between the HTF and a constant temperature heat sink/source at the phase change interface in the PCM, and the average effectiveness of the storage container were calculated at various mass flow rates. The testing results indicated that a lower flow rate will result in longer contacting time of the HTF inside the container, which leads to a better heat transfer between the PCM material and the HTF.

(4) The testing results allowed a direct derivation as the function of the average effectiveness and the mass flow rate. This was applied to the design of the storage container considering different working conditions. This equation can only be validated for maximum fin distance of 25mm, which suited the design condition in this experiment. For larger container, this equation will underestimate the heat transfer performance where the effect of natural convection is expected to increase.

Chapter 6 Theoretical and Experimental Investigations of Combined Power and Ejector Cooling System

6.1 Introduction

In the era of rapid global economic development, the electricity consumption is increasingly significant. According to European Community report [125], the world electricity demand is expected to rise by 38.9% from 2010 to 2020. Since most of the electricity is generated by the combustion of primary energy (coals and fossil fuels). The rising electricity demand will result in greater consumption of primary energy and larger emission of green house gases. The generation of electricity by renewable energy source is therefore a promising option.

In some tropical areas, the power generation capacity is still very low. The abundant solar energy throughout the year offers huge potentials for electricity production. Meanwhile, the cooling loads and solar radiations share the same pattern and both reach the summit at summer times. This enables the possibility of power the ejector cooling system by solar energy.

Thus, a combined power and ejector cooling system is presented in this chapter. This system could not only meet the cooling requirements in summer times but also generate power in the meantime. During winter season when cooling effect is not demanded, the great amount of low grade energy could still be converted into electricity for end-users. If the combined system could be further designed to gear with the electricity grid, the tight power supply during peak hours could be substantially alleviated.

As a kind of low grade energy, solar energy is intensively studied as the driving force for thermal power plants [126-128]. The thermal efficiency is uneconomically low when the steam temperature drops below 370 °C. Low grade energy can not be utilized directly in

thermal power[129]. Exploitation of using low grade energy (temperature less than 250 °C [130]) to generate electricity therefore becomes a promising research topic.

Roy et al. [131] carried out analysis of a Rankine cycle with ammonia absorption refrigeration system. The thermodynamic simulations based on heat source of 100°C and heat sink of 10°C revealed the maximum thermal efficiency was 11-12%. Godefroy et al. [68] presented a CHP-ejector tri-generation system which utilized the heat output from the CHP unit to drive an ejector cooling system. Four different scenarios were analyzed and compared, and an optimum system efficiency of 50% with cooling capacity of 2kW was achieved in the simulation. A similar combined ejector refrigeration and power cogeneration system was studied by Alexis [65]. The Rankine cycle produced electrical output of 2MW, and part of the steam was bleeded off from the turbine at 7bar to drive a steam ejector cycle. The parametric studies showed that the ratio between electrical power and heat was in the range of 0.1-0.4 with turbine inlet temperature of 360°C and pressure of 20bar, condenser temperature of 50 °C and evaporator temperature of 10°C. However, the turbine inlet temperature and pressure were relatively above the quality of low grade energy.

First and second law analysis on a combined power and ejector refrigeration system was performed by Wang et al.[132]. The simulation results indicated that turbine power output was in the range of 90-130kW with evaporator temperature of -5°C, condenser temperature of 25°C, turbine inlet temperature of 130°C and inlet pressure of 0.7MPa. The authors suggested that increasing the area of heat transfer in the generator, and design optimization of turbine and ejector could help to improve the system performance. Zheng and Weng [133] carried out theoretical investigation on an organic Rankine cycle (R245fa) combined with ejector refrigeration cycle. The simulation results demonstrated that a thermal efficiency of 34.1% could be achieved with generator temperature of 122°C, condenser temperature of 25 °C and evaporator temperature of 7 °C.

Recent years' researches are mostly focused on the combination between absorption/ejector refrigeration system with Rankine cycle to provide cooling and generate electricity. Most of the research works are only limited in theoretical studies, with few experimental work available. The properties of different working fluids would be of importance to the system performance, which are hardly revealed by researchers. This chapter presents thermodynamic study of a combined power and ejector refrigeration cycle. The performance of the combined system with different working fluids (water, ethanol, methanol, HFE7000 and HFE7100) is compared and analyzed. Preliminary experimental investigations on a steam turbine power generation cycle are carried out to verify the two possible system configurations.

6.2 Preliminary experimental investigations into the combined power and ejector cooling system

Preliminary experimental works were carried out in order to explore the capability of power generation for steam turbine under low temperature heat source (<132°C). Two system configurations (Figure 6-1and Figure 6-2) were tested respectively in the lab. Configuration A (Figure 6-1) shows the power generation cycle in series with the ejector cooling cycle, where the turbine exhaust is used to drive the ejector cycle. In this configuration, the power can be generated simultaneously when the ejector is providing cooling effect. Configuration B (Figure 6-2) shows the Rankine cycle in parallel to the ejector cooling cycle, with a heat exchanger (HX) as the main connection. In this configuration, the power generation cycle can run separately from the ejector cooling cycle, which is more flexible. The HX between these two cycles needs proper design and optimization in order to maximum the heat transfer between the working fluids in the two cycles.

In our test rig, the ejector nozzle is 1.5mm, which is manufactured to match with the designed cooling capacity of the system. Such small ejector nozzle resulted in reduced back

pressure at the turbine outlet. Hence, configuration A leads to unsuccessful preliminary tests. However, if the ejector is designed (with larger cooling capacity and nozzle size) specifically with the aim to offer enough back pressure to drive the turbine, this kind of configuration should be able to provide both power and cooling effect simultaneously.

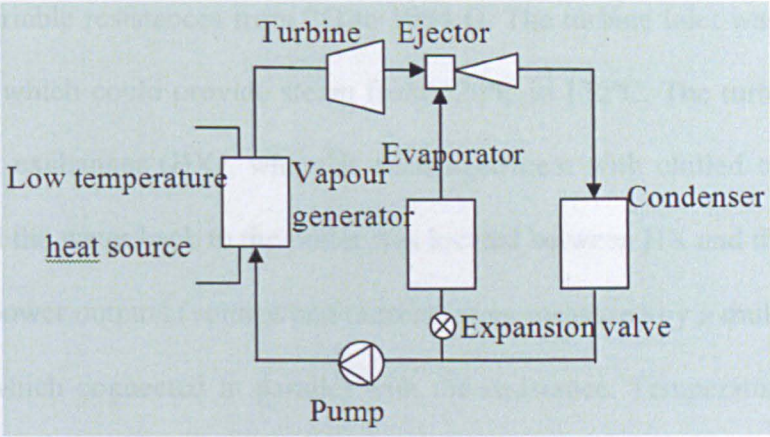

Figure 6-1Schematic diagram of combined power and ejector cooling system

—configuration A

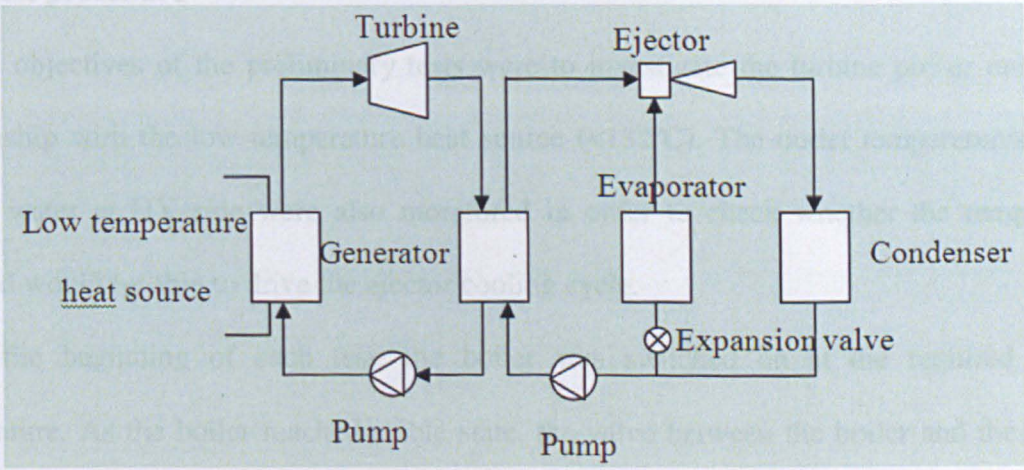

Figure 6-2 Schematic diagram of combined power and ejector cooling system

—configuration B

6.2.1 Test rig description

The test rig according to Configuration B was built up in lab. The turbine (as shown in Figure 6-3) is an air expander manufactured by Gast Group Ltd. It was connected with a 12V DC motor, which was wired with an adjustable resistance. The resistance had 12 channels, which offered variable resistances from 2Ω to 1084 Ω. The turbine inlet was connected to an electrical boiler, which could provide steam from 120°C to 132°C. The turbine exhaust went into a plate heat exchanger (HX), where it exchanged heat with chilled tap water. A gear pump which feed the water back to the boiler was located between HX and the boiler.

The turbine power outputs (voltage and current) were measured by a multimeter (ammeter, and voltmeter) which connected in parallel with the resistance. Temperatures at the turbine outlet, and the chilled water outlet in the heat exchange side were measured using K-type thermocouples. The pressures of the steam coming from the boiler were measured by pressure transducer. All the data were recorded by Datataker DT800.

6.2.2 Test procedure

The objectives of the preliminary tests were to investigate the turbine power outputs in relationship with the low temperature heat source (<132°C). The outlet temperatures of the chilled water at HX side were also monitored in order to check whether the temperature supplied would be able to drive the ejector cooling cycle.

At the beginning of each test, the boiler was switched on at the required testing temperature. As the boiler reached stable state, the valve between the boiler and the turbine inlet was opened, and the chilled tap water (13°C) at the HX side was turned on. Once the turbine reached steady state, the output current and voltage were measured by the multimeter and recorded manually. The resistance was varied from channel 12 to channel 1, with output current and voltage recorded each time. The outlet temperatures of the chilled water were monitored as well.

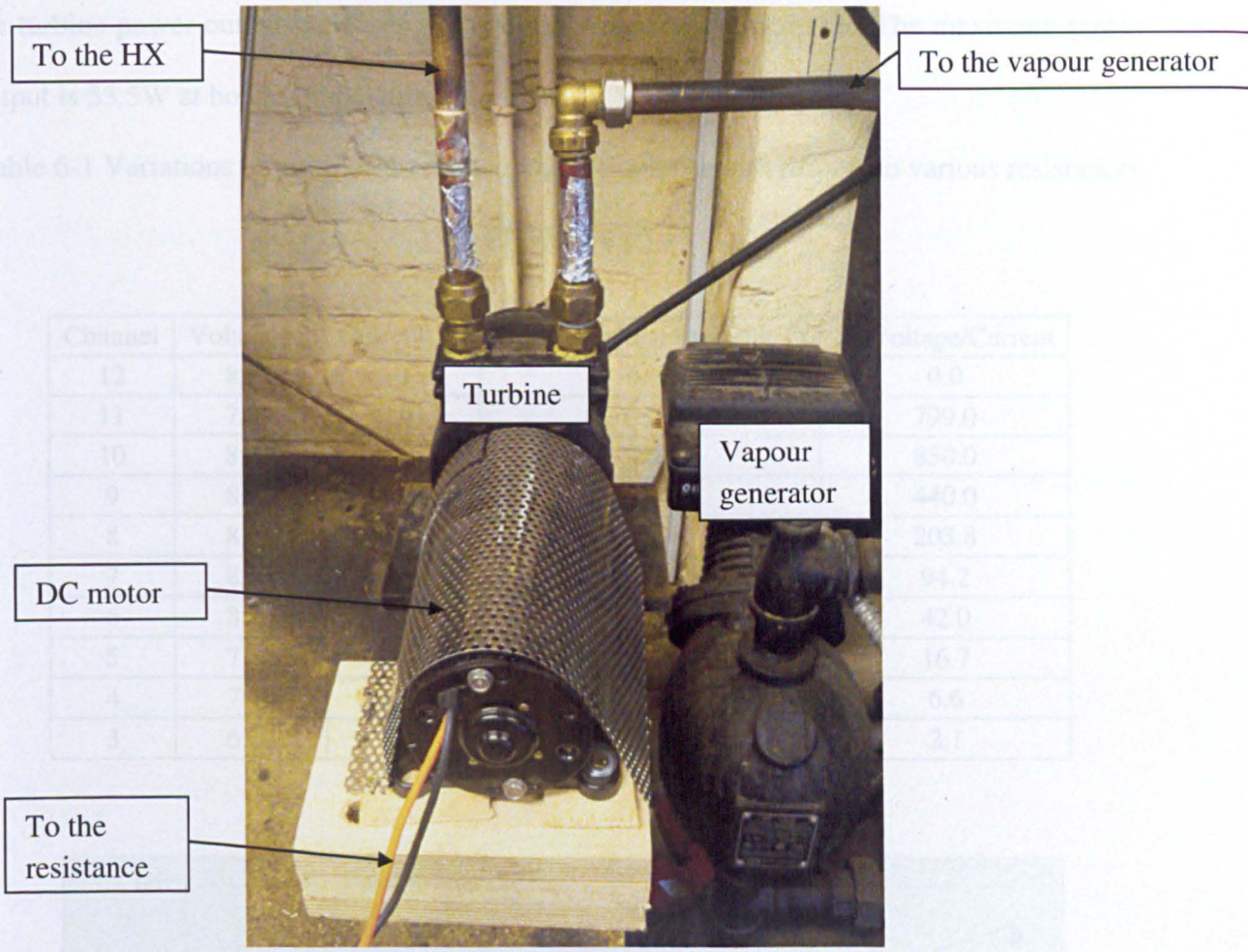

Figure 6-3 Photo of the turbine connected with the DC motor

6.2.3 Test results

6.2.3.1 Turbine power outputs

For a typical case (boiler temperature of 120°C), variations of turbine current and voltage outputs with respect to various resistances is shown in Table 6-1. It is obvious that resistance decreases by switching from Channel 12 to Channel 3. The reduced resistance results in the decreased voltage and the increased current. The total power output reaches the maximum value of 18.6W at channel 3.

By varying the boiler temperature from 120°C to 132°C, the maximum turbine power output could be achieved at channel 2 to channel 3. The variations of turbine power output with respect to different boiler temperatures are illustrated in Figure 6-4. It can be found that

the turbine power output increases as the boiler temperature increases. The maximum power output is 53.5W at boiler temperature of 132 ℃.

Table 6-1 Variations of turbine current and voltage outputs with respect to various resistances (T_b=120℃)

Channel	Voltage(v)	Current(A)	Power=Voltage*current(w)	R=Voltage/Current
12	8.55	0	0.00	0.0
11	7.99	0.01	0.08	799.0
10	8.50	0.01	0.09	850.0
9	8.80	0.02	0.18	440.0
8	8.15	0.04	0.33	203.8
7	8.48	0.09	0.76	94.2
6	8.40	0.2	1.68	42.0
5	7.50	0.45	3.38	16.7
4	7.10	1.08	7.67	6.6
3	6.20	3	18.60	2.1

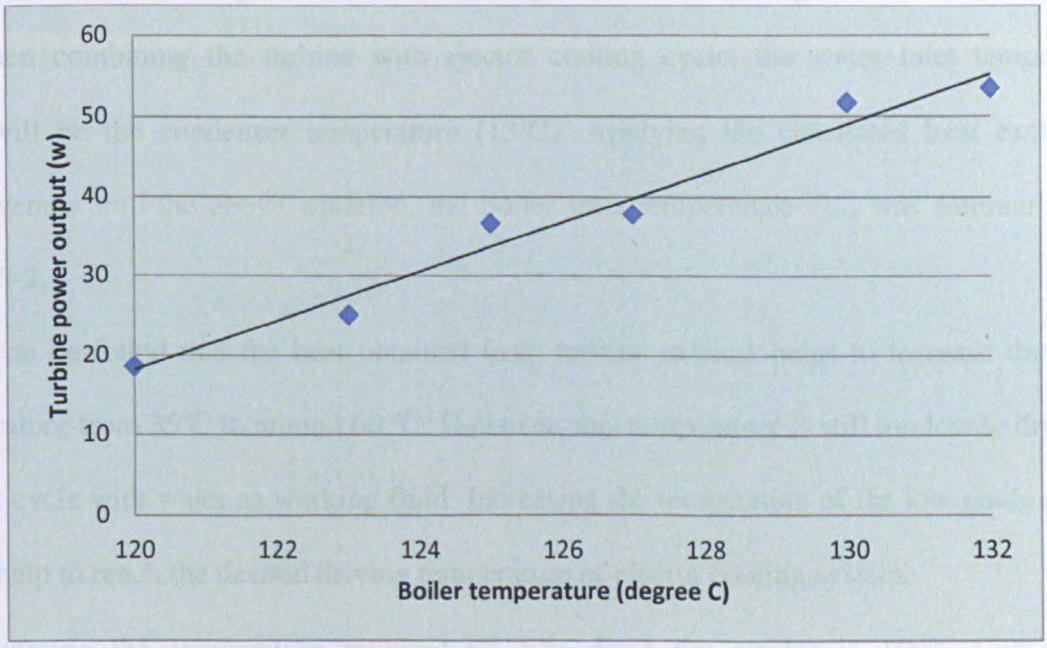

Figure 6-4 Variations of turbine power outputs with respect to different boiler temperature

6.2.3.2 Chilled water outlet temperature

As the boiler temperature varies from 120°C to 132°C, the measured chilled water outlet temperatures T_{H_out} are shown in Table 6-2. The heat exchanger effectiveness E_x is then calculated according to the following equation:

$$E_x = \frac{T_{H\_out} - T_{H-in}}{T_{t-in} - T_{H\_in}} \qquad \text{Eq. (6.1)}$$

Where T_{t-in} is turbine exhaust inlet temperature, T_{H-in} is the chilled water inlet temperature (tap water was used in the test, hence T_{H-in} =13 °C) and T_{H_out} is the chilled water outlet temperature.

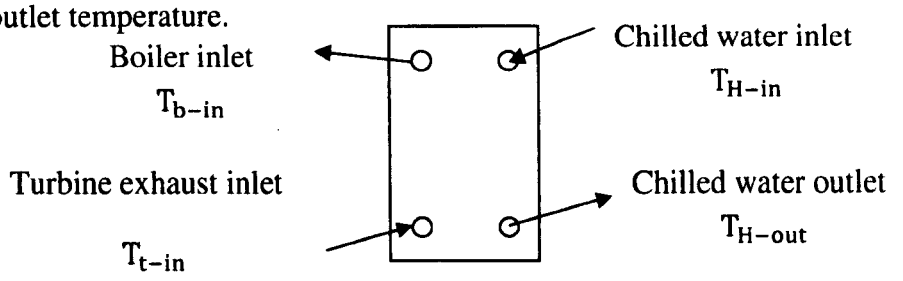

Figure 6-5 Schematic diagram of heat exchanger

When combining the turbine with ejector cooling cycle, the water inlet temperature T_{H-in} will be the condenser temperature (13°C). Applying the calculated heat exchanger effectiveness into the above equation, the boiler inlet temperature $T_{b\text{-}in}$ was summarized in Table 6-2.

It can be found that the heat obtained from turbine exhaust helps to increase the water temperature from 35°C to around 60 °C. However, this temperature is still too low to drive the ejector cycle with water as working fluid. Increasing the temperature of the low grade energy could help to reach the desired driving temperature of ejector cooling system.

Assuming the temperature required (T_b) to drive the ejector is 100°C-120°C, heat exchanger inlet temperature T_{H-in} =35 °C (condenser temperature) and heat exchanger efficiency E_x = 0.8 , the turbine inlet temperature T_{t_in} could be calculated according to Eq. (6.1). Assuming the turbine expansion ratio P_{t_in} / P_{t_out} = 2.5, thus the turbine outlet pressure and temperature could be obtained in Table 6-3. It could found that the turbine inlet

temperature is required in the range of 224 °C-281 °C, which is virtually above the range of the low grade energy. In this case, with low grade energy as heat source, additional heater or booster should be added between the ejector and HX to increase turbine exhaust temperature. This will involve in additional energy consumption. In order to avoid this, an improved system configuration is studied and analyzed in the following simulation section.

Table 6-2 Measured and calculated water outlet temperature

T_b (°C)/ P_b (bar)	T_{t-in}(°C)/ P_{t-in}(bar)	T_{H_out}(°C)	E_x(°C)	T_{b-in}(°C)
120/2.0	87.5/0.65	45.1	0.431	57.6
123/2.2	89.6/0.69	47.8	0.454	59.8
125/2.35	91/0.75	49.6	0.469	61.3
127/2.48	92.6/0.78	50.5	0.471	62.1
130/2.7	93.4/0.80	51.3	0.476	62.8
132/2.88	94.2/0.83	52.4	0.485	63.7

Table 6-3 Calculated turbine inlet/outlet temperature for ejector driving temperature 100 °C - 120 °C

T_b (°C)	T_{t_out} (°C)	P_{t-out} (bar)	P_{t_in}(bar)	T_{t-in}(°C)
100	181.25	10	25	224
105	192.5	13	32.5	239
110	203.75	17	42.5	254
115	215	21	52.5	265
120	226.25	26	65	281

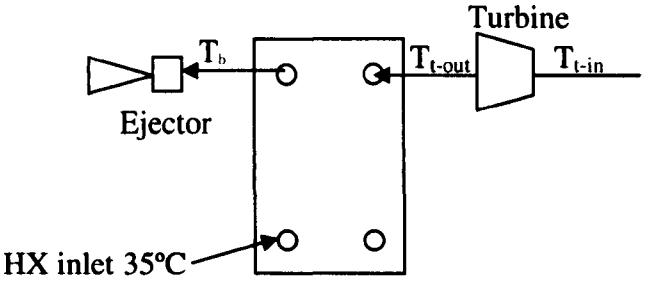

Figure 6-6 Schematic diagram for calculating turbine inlet/outlet temperature

6.3 Thermodynamic simulations of combined power and ejector cooling system

6.3.1 System description

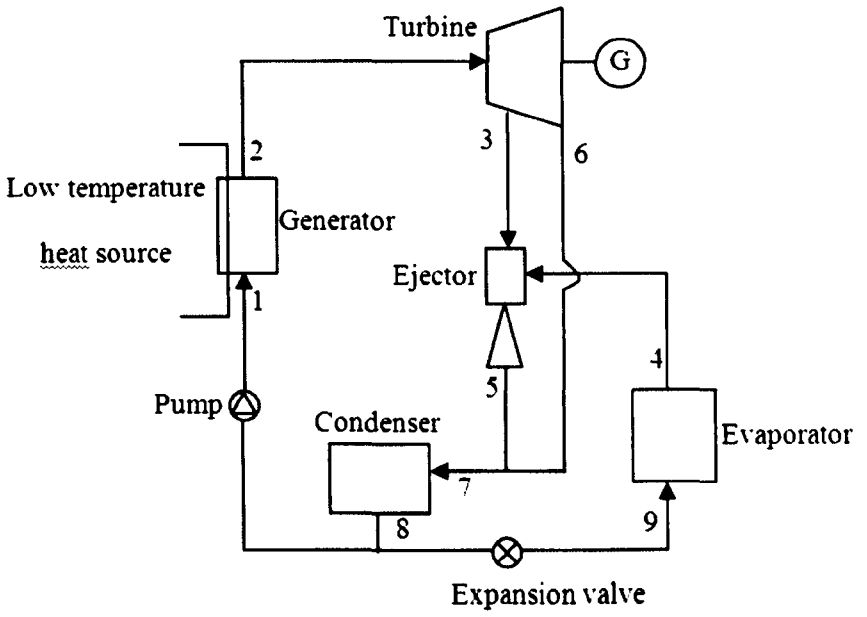

Figure 6-7 Schematic diagram of the combined power and ejector cooling system

According to the preliminary experimental results, if the turbine outlet is connected directly with the ejector inlet, the back pressure would be too low for the proper operation of turbine. In order to avoid this, part of the turbine exhaust is diverted into the condenser directly without going through the ejector nozzle. The schematic diagram of this modified system is shown in Figure 6-7. The saturated liquid from pump outlet (state 1) goes into the vapour generator where the working fluid absorbs heat from the low temperature heat source (industrial waste heat or solar energy). The liquid working fluid vaporizes and comes out from the vapour generator as high pressure steam (state 2) and enters the steam turbine, where the thermal energy is converted into mechanical energy in the turbine. The partially expanded vapour (state 3) acts as the primary fluids and enters into the ejector's convergent-divergent nozzle, where it expands to supersonic flow and create a low pressure region which entrains the secondary flow from the evaporator (state 4). The two flows are then mixed in the ejector mixing chamber, and finally leave the diffuser at state 5. The remaining fully expanded

vapour (state 6) from the turbine outlet together with the combined stream from ejector are all condensed in the condenser by rejecting heat to the chilled water. The liquid working fluid leaves the condenser as saturated liquid (state 8). A proportion of the condensate is returned to the evaporator through an expansion valve at state 9, while the remainder is re-circulated to the vapour generator by the pump.

6.3.2 Assumptions

Following assumption are made to simplify the simulation of the combined cycle:

1) System operates in steady state condition.

2) The turbine and ejector are at adiabatic conditions. No heat loss/gain is considered for the vapour generator, evaporator and condenser.

3) The potential, kinetic energies and friction losses are neglected, hence:

$$P_4 = P_9, P_2 = P_1, P_5 = P_6 = P_7 = P_8 \qquad \text{Eq. (6.2)}$$

3) Isentropic expansion process through expansion valve

$$h_8 = h_9 \qquad \text{Eq. (6.3)}$$

4) The high pressure steam in the turbine is expanded and the losses were taken into account by assuming an isentropic efficiency of 0.8.

6.3.3 Governing equations

Apply the principle of mass conservation of working fluids at different states identified in Figure 6-7, gives the following relationships:

$$\dot{m}_1 = \dot{m}_2 = \dot{m}_3 + \dot{m}_6 \qquad \text{Eq. (6.4)}$$

$$\dot{m}_5 = \dot{m}_3 + \dot{m}_4 \qquad \text{Eq. (6.5)}$$

$$\dot{m}_8 = \dot{m}_7 = \dot{m}_5 + \dot{m}_6 \qquad \text{Eq. (6.6)}$$

Apply the principle of energy conservation to each of the components in the system. Thus for vapour generator:

$$Q_g = \dot{m}_2(h_2 - h_1) \qquad \text{Eq. (6.7)}$$

According to [134], turbine expansion ratio was defined by,

$$\alpha = p_2/p_3 \qquad \text{Eq. (6.8)}$$

The high pressure steam in the turbine is expanded from state 2 to state 3, and the losses were taken into account by assuming an isentropic efficiency of η_t =0.8 [134]. The following equations could be obtained:

$$h_{3\_isen}=\text{enthalpy } (p=p_3, s=s_2) \qquad \text{Eq. (6.9)}$$

$$\eta_t=(h_2 - h_3)/(h_2 - h_{3\_isen}) \qquad \text{Eq.(6.10)}$$

The same process can be applied to obtain the properties at state 6.

The turbine mechanical work is calculated by:

$$W_{tu} = \dot{m}_2(h_2 - h_3) + \dot{m}_6(h_3 - h_6) \qquad \text{Eq. (6.11)}$$

All the ejector working mechanism and governing equations can be found in Chapter 3. The energy balance at the ejector diffuser:

$$\dot{m}_3 h_3 + \dot{m}_4 h_4 = \dot{m}_5 h_5 \qquad \text{Eq. (6.12)}$$

Ejector entrainment ratio $\omega = \dot{m}_4/\dot{m}_3$ Eq. (6.13)

The cooling effect obtained from the evaporator can be calculated by:

$$Q_e = \dot{m}_4(h_4 - h_9) \qquad \text{Eq. (6.14)}$$

The energy balance at condenser inlet:

$$(\dot{m}_2 - \dot{m})h_6 + (\dot{m}_4 + \dot{m}_3)h_5 = \dot{m}_7 h_7 \qquad \text{Eq. (6.15)}$$

The heat rejected to the chilled water from the condenser is determined by

$$Q_c = \dot{m}_7(h_7 - h_8) \qquad \text{Eq. (6.16)}$$

The remaining condensate from the condenser (state 8) is compressed and goes isentropically in the pump to the operating pressure of the boiler. The pump mechanical work is calculated by

$$W_{pum} = \dot{m}_2(h_1 - h_{10}) \qquad \text{Eq. (6.17)}$$

And the enthalpy at the state 1 is calculated by:

$$h_1 = h_8 + W_{net}$$ Eq. (6.18)

Where v_1 is the volumetric flow rate, which could be determined by state 2.

The net work output: $W_{net} = W_{tu} - W_{pum}$ Eq. (6.19)

The thermal efficiency of the system, defined as the ratio of the useful energy output to the total energy input, can be given by:

$$\eta = (W_{net} + Q_e)/Q_g$$ Eq. (6.20)

Where W_{net} is the net mechanical work defined in Eq. (6.17), Q_e is the cooling output and Q_g is the total heat absorbed from the low temperature heat source in the vapour generator.

6.3.4 Simulation procedure

Based on the above governing equations, computer simulation was carried out in the EES software, from whose database the thermodynamic properties of different working fluids could be obtained. The input parameters for the simulation are summarized in Table 6-4. The corresponding temperature, pressure, enthalpy and entropy at all the states identified in Figure 6-5 could be obtained as indicated in flow chart Figure 6-8.

Five different working fluids, methanol, ethanol, water, HFE7000 and HFE7100 are selected and compared in the simulation. The physical properties of these five working fluids could be found in Chapter 3 section 3.1.5.1.

Table 6-4 Simulation input parameters

Turbine expansion ratio	$\boldsymbol{\beta = P_2/P_3 = 2.5}$[134]
Turbine extraction ratio	$\lambda = \dot{m}_3/\dot{m}_2 = 0.3$[134]
Turbine/pump isentropic efficiency	$\eta_{tu} = \eta_{pum} = 0.8$
Evaporator temperature	$T_4 = 10\ ^oc$

Condenser temperature	$T_7 = 10\ ^oc$
Evaporator cooling capacity	0.5kW

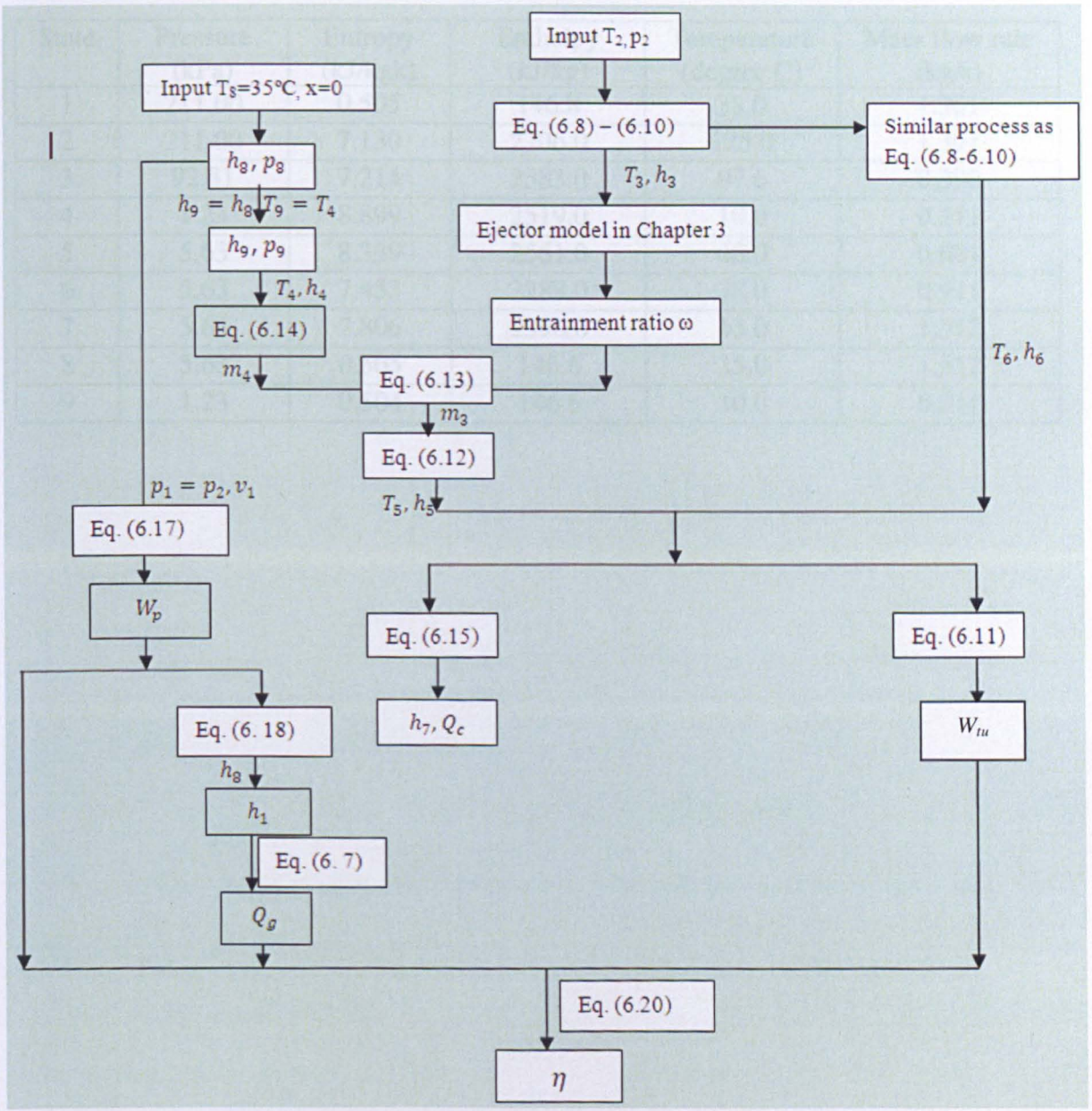

Figure 6-8 Flow chart for computer simulation

6.3.5 Simulation results and discussions

The thermodynamic properties and mass flow rates at each of the state points are indicated in Table 6-5 and the T-S diagram is shown in Figure 6-9. It should be pointed out that the

values of mass flow rates and thermodynamic properties have been rounded off. Hence, the variations between the two sides of Eq. (6.1)-Eq. (6.18) is around 0.5% of their average value in some cases.

Table 6-5 Simulation results with water as the working fluid

State	Pressure (kPa)	Entropy (kJ/kgk)	Enthalpy (kJ/kg)	Temperature (degree C)	Mass flow rate (kg/s)
1	211.00	0.505	146.8	38.0	1.301
2	211.00	7.130	2706.0	125.0	1.301
3	92.81	7.214	2583.0	97.6	0.390
4	1.23	8.899	2519.0	10.0	0.211
5	5.63	8.339	2561.0	48.0	0.601
6	5.63	7.453	2288.0	38.0	0.911
7	5.63	7.806	2396.0	43.0	1.512
8	5.63	0.505	146.6	35.0	1.512
9	1.23	0.504	146.6	10.0	0.211

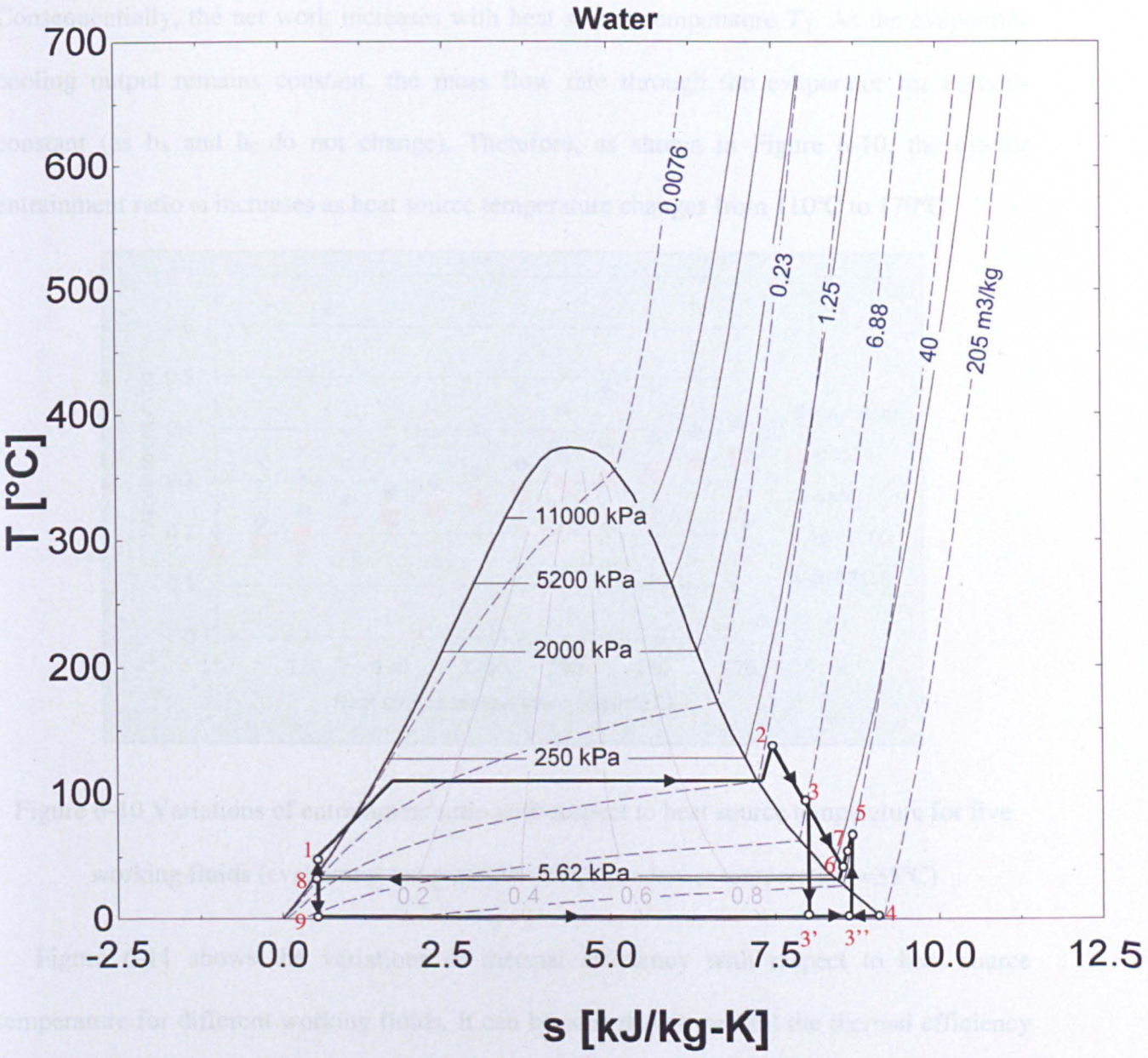

Figure 6-9 T-S diagram of combined power and ejector cooling system

6.3.5.1 Effect of heat source temperature

The heat source temperature T_2 is varied between 110°C and 170°C, while other input parameters are at fixed value as shown in Table 6-4. According to Eq. (6.8), the turbine inlet pressure increases as heat source temperature increases. Since the evaporator and the condenser temperature is fixed at 10 °C and 35 °C respectively, the thermodynamic conditions at state 1, 8, 9 and 10 remain constant. Hence the mechanical work consumed by the pump stays constant, while the turbine output work increases (according to Eq. (6.11)).

Consequentially, the net work increases with heat source temperature T_2. As the evaporator cooling output remains constant, the mass flow rate through the evaporator m_4 remains constant (as h_4 and h_9 do not change). Therefore, as shown in Figure 6-10, the ejector entrainment ratio ω increases as heat source temperature changes from 110°C to 170°C.

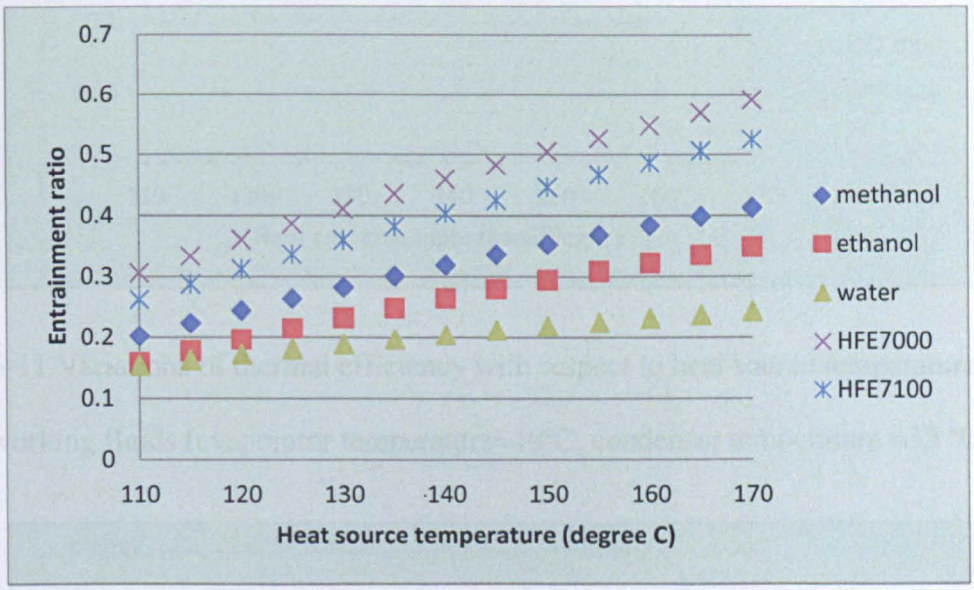

Figure 6-10 Variations of entrainment ratio with respect to heat source temperature for five working fluids (evaporator temperature=10°C, condenser temperature =35°C)

Figure 6-11 shows the variations of thermal efficiency with respect to heat source temperature for different working fluids. It can be seen that in general the thermal efficiency will increase as the heat source temperature increase from 110°C to 170°C. As discussed above, together with Eq.(6.19), it could be noted that as the heat source temperature increases, the increased net work is proportional larger than the increased vapour generator energy input, therefore the overall thermal efficiency is improved. It can be notified that the increase rate of thermal efficiency is highest for methanol, follow by water and ethanol, with HFE7000 and HFE7100 as the lowest.

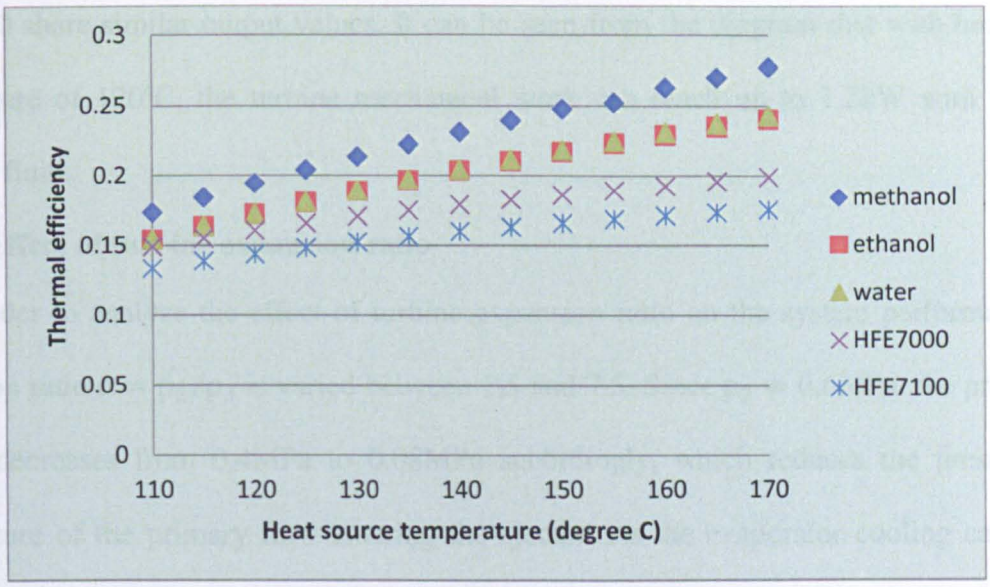

Figure 6-11 Variations of thermal efficiency with respect to heat source temperature for five working fluids (evaporator temperature=10°C, condenser temperature =35 °C)

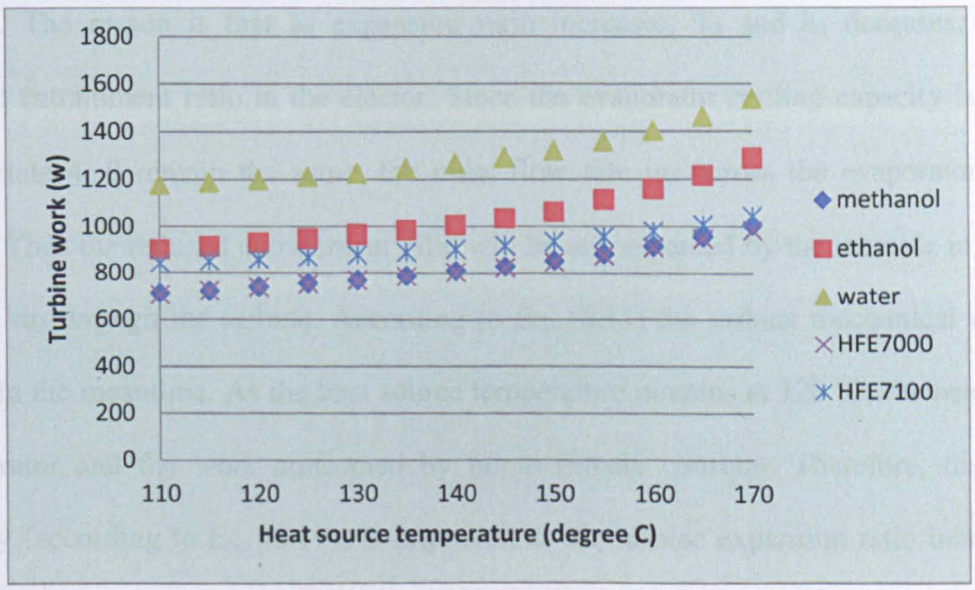

Figure 6-12 Variations of turbine work with respect to heat source temperature for five working fluids (evaporator temperature=10°C, condenser temperature =35°C)

Figure 6-12 shows that the turbine work output increases as the heat source temperature increases from 110°C to 170°C. Among all the compared working fluids, water demonstrates the highest turbine work output, followed by ethanol, while methanol, HFE7000 and

HFE7100 share similar output values. It can be seen from the diagram that with heat source temperature of 120°C, the turbine mechanical work can reach up to 1.2kW with water as working fluid.

6.3.5.2 Effect of turbine expansion ratio

In order to analyze the effect of turbine expansion ratio on the system performance, the expansion ratio $\alpha = p_2/p_3$ is varied between 1.5 and 7.5. Since $p_2 = 0.6$MPa, the pressure at state 3 decreases from 0.4MPa to 0.08MPa accordingly, which reduces the pressure and temperature of the primary flow entering the ejector. As the evaporator cooling capacity is constant, the secondary flow remains constant. Thus, the increased expansion ratio will lead to the decrease of entrainment ratio, as shown in Figure 6-13.

Figure 6-14 shows that the thermal efficiency increases as the turbine expansion ratio increases. The reason is that as expansion ratio increases, T_3 and h_3 deceases, resulting decreased entrainment ratio in the ejector. Since the evaporator cooling capacity is constant and the state 4, 9 remain the same, the mass flow rate m_4 across the evaporator remains constant. Thus the reduced entrainment ratio will be accompanied by the increase in the mass flow rate m_3 through the turbine. According to Eq. (6.11) the turbine mechanical work will increase in the meantime. As the heat source temperature remains at 120 °C, the heat input to the generator and the work consumed by pump remain constant. Therefore, the thermal efficiency (according to Eq. (6.19)) is improved as the turbine expansion ratio increases. At the same expansion ratio of 4, methanol demonstrates the highest thermal efficiency, followed by water and ethanol, with HFE7000 and HFE7100 at last.

Similar trend could be found in the variations of turbine work output in respect to expansion ratio. As shown in Figure 6-15 water has highest turbine work output, followed by ethanol and methanol, with HFE7100 and HFE7000 as the lowest. The reason is that

increased expansion ratio could be translated into larger pressure difference across turbine inlet and outlet, which virtually produces higher turbine mechanical work.

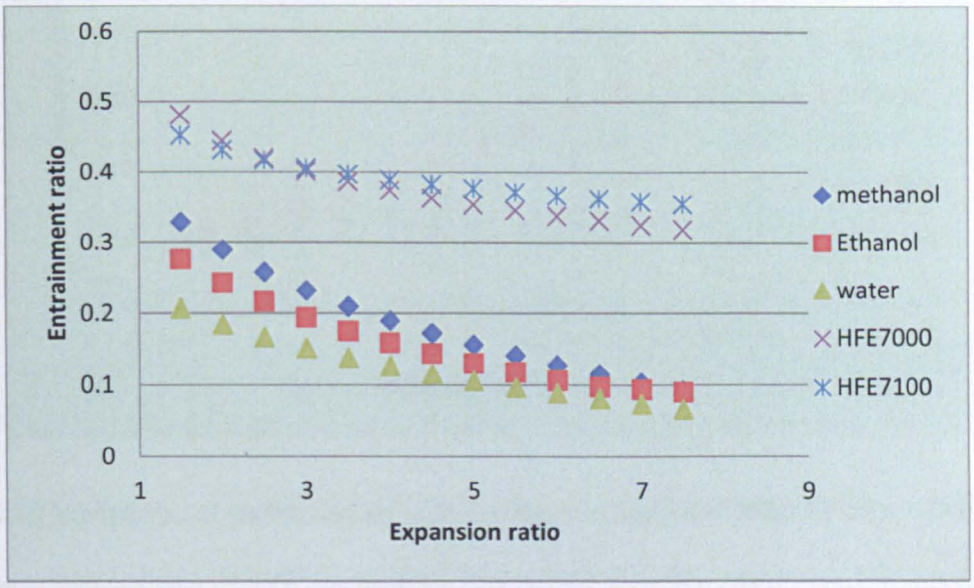

Figure 6-13 Variations of entrainment ratio with respect to expansion ratio for five working fluids (heat source temperature=120°C, evaporator temperature=10°C, condenser temperature =35°C)

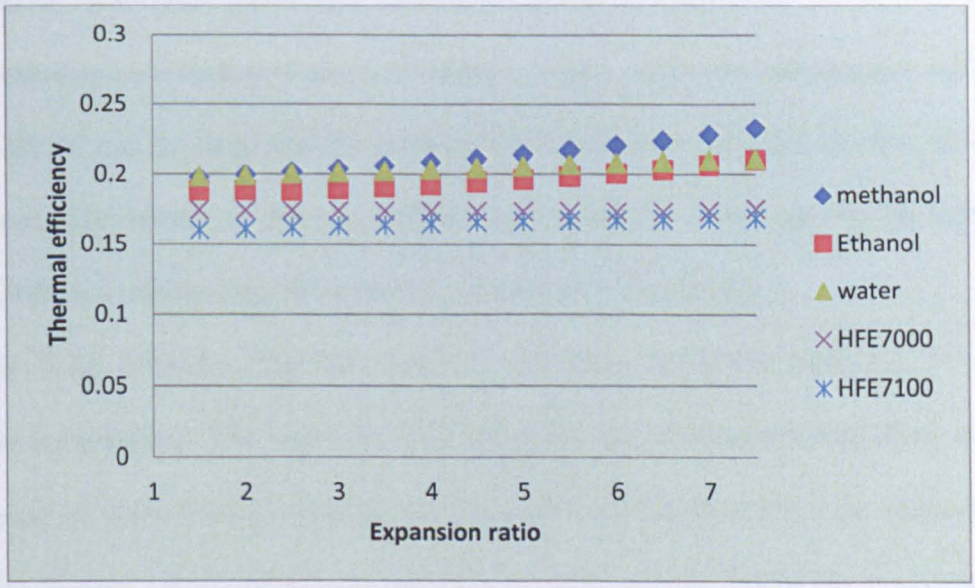

Figure 6-14 Variations of thermal efficiency with respect to expansion ratio for five working fluids (heat source temperature=120°C, evaporator temperature=10°C, condenser temperature =35 °C)

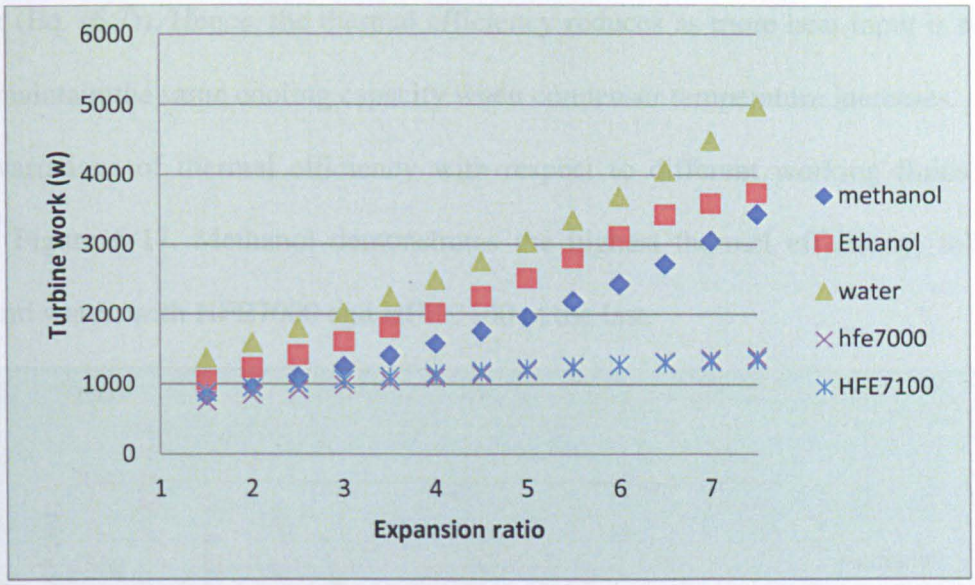

Figure 6-15 Variations of turbine work with respect to expansion ratio for five working fluids (heat source temperature=120°C, evaporator temperature=10°C, condenser temperature =35°C)

6.3.5.3 Effect of condenser temperature

In order to analyze the effect of condenser temperature on system performance, T_4 is varied from 30°C to 40 °C with heat source temperature of 120 °C, evaporator temperature of 10 °C, and the other input parameters constant as shown in Table 6-4.

The variations of turbine work with respect to the condenser temperature are shown in Figure 6-16. It can be seen that the turbine work decreases with the increase of condenser temperature. The reason is that the turbine work output is influenced by the turbine back pressure, which is affected by the increase of condenser temperature.

Figure 6-17 indicates that the thermal efficiency decreases with the increasing of condenser temperature. The reason is that increasing the condenser temperature will lead to the increase of ejector back pressure. As illustrated in Figure 6-18, with increasing of the condenser pressure, the ejector entrainment ratio will decline. Since the evaporator cooling capacity is defined as constant, according to Eq. (6.14), the secondary mass flow rate is always constant. Thus the decreasing of entrainment ratio will result in the increase of primary mass flow rate, which finally leads to the increase of the heat input in the vapour

generator (Eq. (6.7)). Hence, the thermal efficiency reduces as more heat input is required in order to maintain the same cooling capacity when condenser temperature increases.

The variations of thermal efficiency with respect to different working fluids could be found in Figure 6-17. Methanol demonstrates the highest thermal efficiency, followed by ethanol and water, with HFE7000 and HFE 7100 at the last.

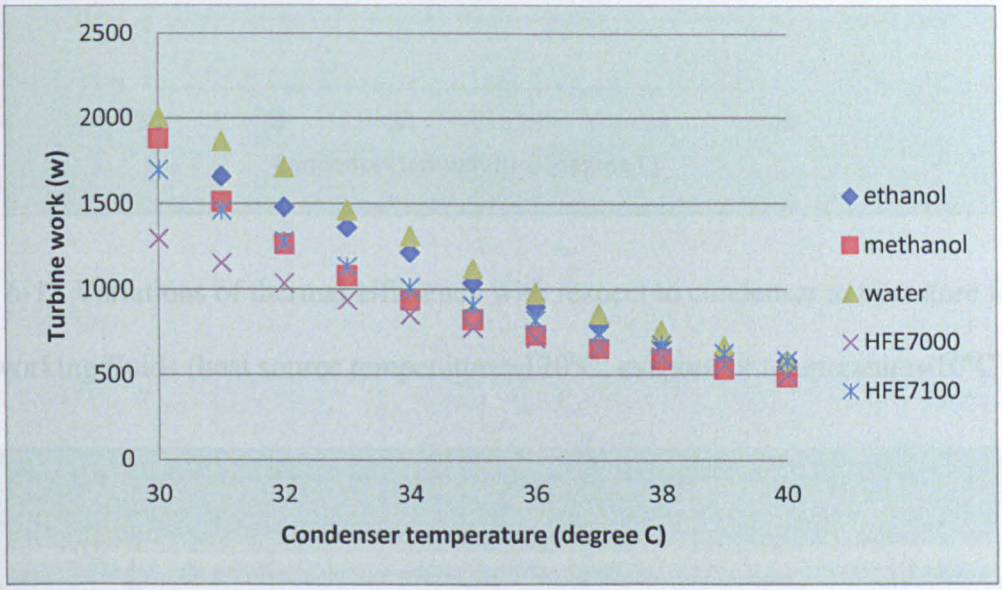

Figure 6-16 Variations of turbine work with respect to condenser temperature for five working fluids (heat source temperature=120°C, evaporator temperature=10°C)

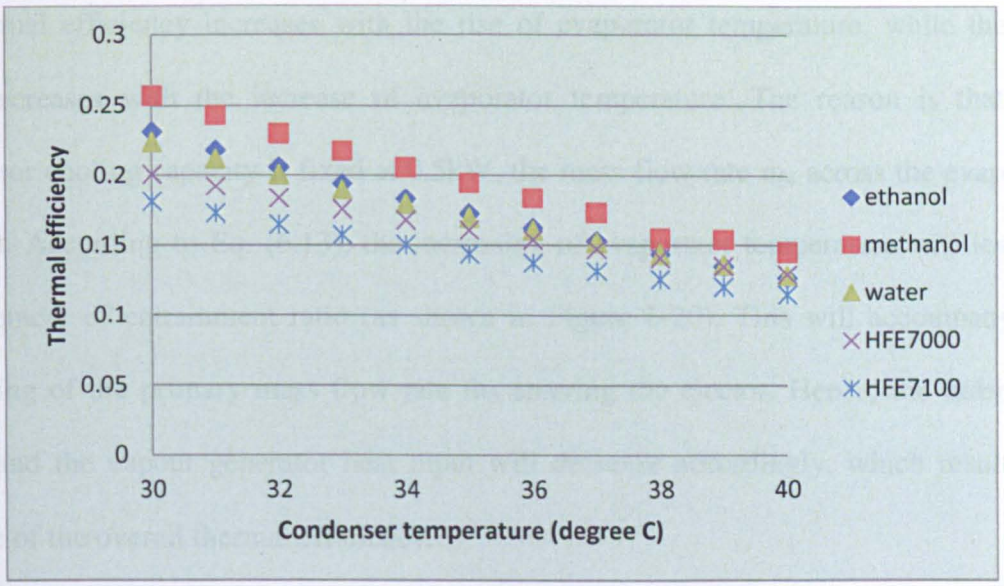

Figure 6-17 Variations of thermal efficiency with respect to condenser temperature for five working fluids (heat source temperature=120°C, evaporator temperature=10°C)

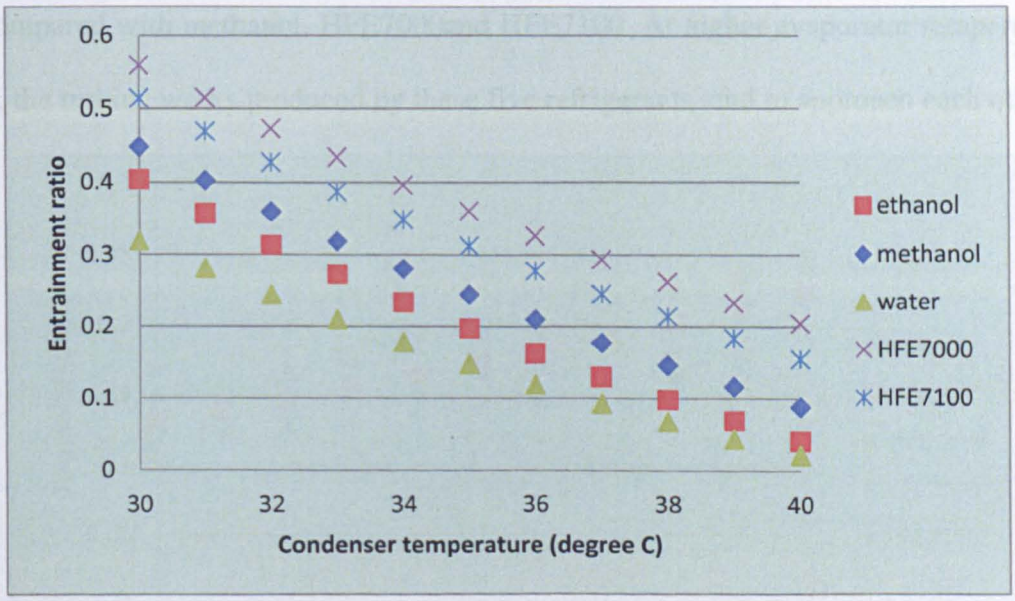

Figure 6-18 Variations of entrainment ratio with respect to condenser temperature for five working fluids (heat source temperature=120°C, evaporator temperature=10°C)

6.3.5.4 Effect of evaporator temperature

Figure 6-19 and Figure 6-20 show the effect of evaporator temperature on the system thermal efficiency and turbine work for five different working fluids. It could be found that

the thermal efficiency increases with the rise of evaporator temperature, while the turbine work decreases with the increase of evaporator temperature. The reason is that, as the evaporator cooling capacity is fixed at 0.5kW, the mass flow rate m_4 across the evaporator is constant. According to Eq. (6.13), the increasing of evaporator temperature will lead to the improvement of entrainment ratio (as shown in Figure 6-20). This will accompany by the decreasing of the primary mass flow rate m_3 entering the ejector. Hence, the turbine work output and the vapour generator heat input will decrease accordingly, which results in the increase of the overall thermal efficiency.

Figure 6-19 also demonstrates that the methanol shows the highest thermal efficiency, followed by ethanol and water, with HFE7000 and HFE 7100 at last. Figure 6-20 shows that at lower evaporator temperatures (5°C-8°C), water and ethanol can produce higher turbine work compared with methanol, HFE7000and HFE7100. At higher evaporator temperate (9°C -15 °C), the turbine works produced by these five refrigerants tend to approach each other.

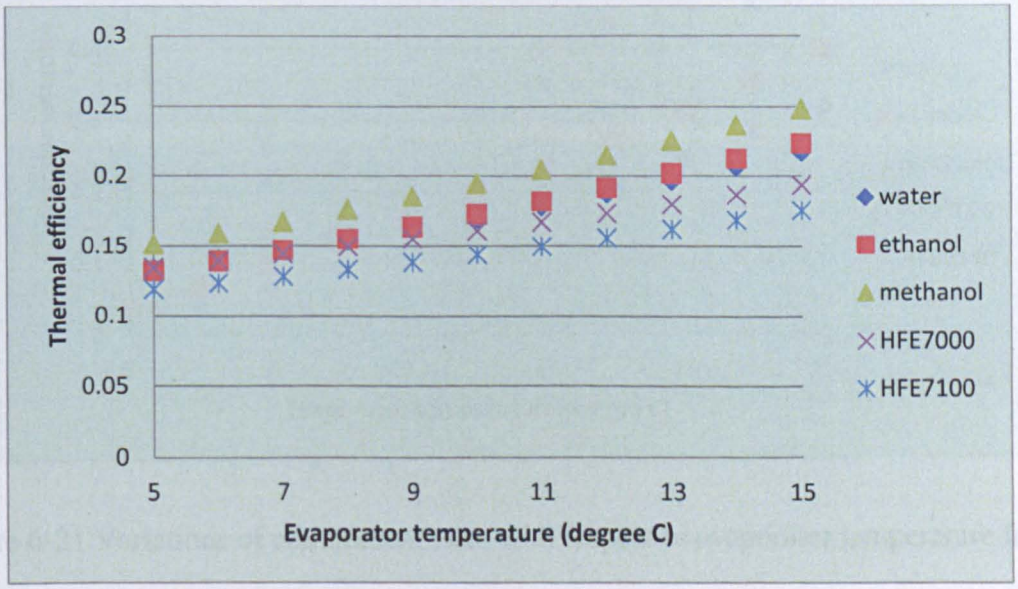

Figure 6-19 Variations of thermal efficiency with respect to evaporator temperature for five working fluids (heat source temperature=120°C, condenser temperature=35°C)

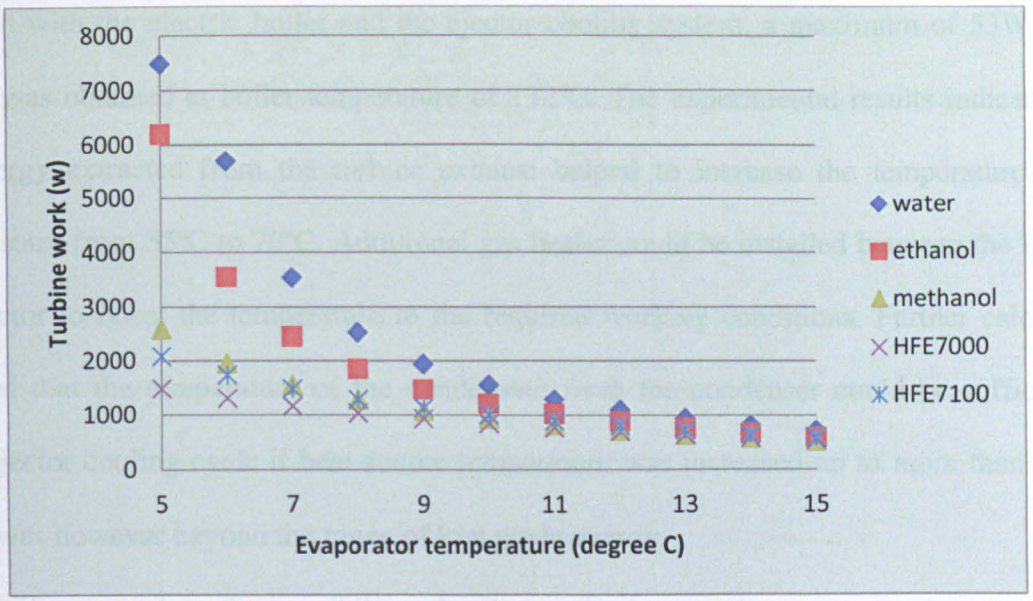

Figure 6-20 Variations of turbine work with respect to evaporator temperature for five working fluids (heat source temperature=120°C, condenser temperature=35°C)

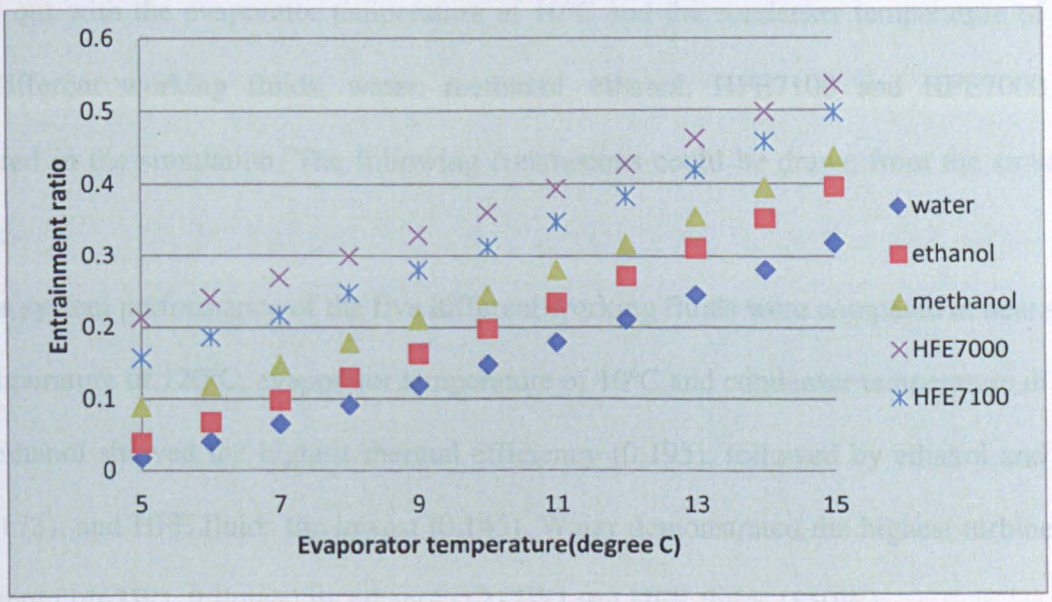

Figure 6-21 Variations of entrainment ratio with respect to evaporator temperature for five working fluids (heat source temperature=120°C, condenser temperature=35°C)

6.4 Conclusions

Two different configurations of combined power and ejector cooling system driven by low grade energy were experimentally investigated. Although the steam turbine was not perfectly

matched with the electric boiler and the ejector cooling system, a maximum of 53W power output was obtained at boiler temperature of 132°C. The experimental results indicated that the energy extracted from the turbine exhaust helped to increase the temperature of the condensates from 35°C to 70°C. Additional gas heater could be installed between the HX and the ejector to boost the temperature to the required working conditions. Further calculation revealed that the temperature of the condensate from the condenser could be sufficient to drive ejector cooling cycle if heat source temperature was increased up to more than 200°C, which was however beyond the range of low grade energy.

In order to explore the possibility of utilizing the low grade energy (temperature in the range of 110°C-170°C) as the heat source to drive turbine and ejector cooling system without any additional heater. A novel configuration was presented and the computer simulation was carried out with the evaporator temperature of 10°C and the condenser temperature of 35°C. Five different working fluids, water, methanol, ethanol, HFE7100 and HFE7000 were compared in the simulation. The following conclusions could be drawn from the simulation results:

1) The system performance of the five different working fluids were compared at heat source temperature of 120°C, evaporator temperature of 10°C and condenser temperature of 35°C. Methanol showed the highest thermal efficiency (0.195), followed by ethanol and water (0.173), and HFE fluids the lowest (0.145). Water demonstrated the highest turbine work output (1463W), followed by ethanol (1217W) and HFE fluids (850W).
2) With water as the working fluid, the thermal efficiency of the combined system improved from 0.15 to 0.25 and the turbine work output increased from 1200W to 1400W when the heat source temperature increased from 110 °C to 170 °C.
3) For all the five working fluids, an average 10 % thermal efficiency improvement could be achieved when the turbine expansion ratio increased from 1.5 to 7. In the meantime,

significant improvements (3-3.5 times) of turbine work output could be notified with water, methanol and ethanol as working fluids. However, ejector entrainment ratios decreased about 50% as the turbine expansion ratio raised from 1.5 to 7. It could be concluded that the increasing of turbine expansion ratio is beneficial to the turbine power output, but not helpful for the system performance improvement of the ejector.

4) When the condenser temperature increased from 30°C to 40°C, the thermal efficiency of the combined system reduced approximately by 40% and the turbine work output decreased about 60%. This means that the condenser temperature plays a crucial role in the overall system performance. If the ambient temperature goes beyond the design conditions (35 °C), the performance of the combined system drops dramatically.

5) When the evaporator temperature increased from 5°C to 15°C, the thermal efficiency of the combined system improved significantly (average 60% for five working fluids). However, the turbine work output decreased about 50% as the evaporator temperature increased from 10°C to 15°C. In this case, the evaporator temperature has to be selected properly in order to guarantee the thermal efficiency and the turbine work output at the designed conditions.

Chapter 7 Modelling and Economic Analysis of Solar-driven Ejector Cooling system with and without the Power Generation System in Shanghai

Approximately 15% of electricity consumption is used for driving air-conditioning and refrigeration systems[135]. Due to the rapid urbanisation, the metropolitan areas are usually warmer than their surrounding rural areas because of intensive human activities, known as the Urban Heat Island Effect (UHI). As one of the world lagest world-famous economic and financial centres, Shanghai experiences very hot and humid summer seasons, with peak temperature reaches up to 35°C or more. The cooling demand as well as the electricity consumption is soaring year by year. Sometimes, the electricity has to be cut off in some districts temporarily in order to mitigate the overburdening summer electricity condition in the city.

Although Shanghai is located in the subtropical area, the available solar radiation during summer seasons is potentially adequate. The utilization of available solar energy could be a practical method to meet with the increasing cooling demand in Shanghai. Ejector cooling system driven by solar energy can make use of the abundant solar energy and provide cooling effect. The low cost compared with other solar-driven systems (such as absorption system) makes it more attractive for cooling applications.

The combined power and ejector cooling system (discussed in Chapter 6) can provide both power and cooling effect at the same time. The summer cooling demands can be satisfied by powering the ejector with renewable solar energy. The consumption of primary energy (coal, fossil fuel etc) required by tradition air-conditioning system is therefore considerably avoided. Moreover, the generated power could be fed back into the grid. Thus, the combined system would be helpful to mitigate the summer electricity demands and offer cooling effect in a more environmental friendly way.

The hourly simulations of a solar-driven ejector cooling system suitable for Shanghai summer seasons are presented in section 7.2. Based on the previous simulation results in Chapter 6, the system performances of the combined power and ejector cooling system driven by solar energy are simulated and discussed in section 7.3. Various evacuated solar collector areas and storage tank volumes are compared. In order to determine the least cost to meet the energy demands, Life Saving Analysis is applied to optimize the system dimension.

7.1 Annual cooling load simulation of an office building in Shanghai

7.1.1 Shanghai climatic condition

As driven by the solar energy, the performance of the solar-driven ejector cooling system greatly depends on local climatic conditions. Shanghai has a humid climate and experiences four distinct seasons. Winters are chilly and damp, and cold northwesterly winds from Siberia can cause night time temperatures to drop below freezing. Summers are hot and humid, with an average of 18.7 days exceeding 35°C annually[136]; occasional downpours or freak thunderstorms can be expected. The city is also susceptible to typhoons in summer and the beginning of autumn. The city averages 4.2°C in January and 27.9°C in July, for an annual mean of 16.1°C. Shanghai experiences on average 1,878 hours of sunshine per year, with the hottest temperature ever recorded at 40.2°C, and the lowest at −12.1 °C. The following climate data (shown in Table 7-1) summarize the average temperature, precipitation, humidity, and mean monthly sunshine hours in Shanghai from 1971 to 2000, as obtained from China Meteorological Data Sharing Service System[136].

Although Shanghai is located at subtropical area, with latitude of 31°12'0'' and longitude of 121°13'00'', the solar irradiation is adequate during summer seasons. The total solar irradiation and hourly outdoor ambient temperature on a typical day on June 29th are shown in Figure 7-1 and 7-2 (obtained from the Ecotect database).

Table 7-1 Climate data for Shanghai (1971–2000)

Month	Jan	Feb	Mar	Apr	May	Jun	Jul	Aug	Sep	Oct	Nov	Dec	Year
Average high (°C)	8.1	9.2	12.8	19.1	24.1	27.6	31.8	31.3	27.2	22.6	17.0	11.1	20.2
Average low (°C)	1.1	2.2	5.6	10.9	16.1	20.8	25.0	24.9	20.6	15.1	9.0	3.0	12.9
Precipitation mm (inches)	50.6	56.8	98.8	89.3	102.3	169.6	156.3	157.9	137.3	62.5	46.2	37.1	1,164.7
% humidity	75	74	76	76	76	82	82	81	78	75	74	73	76.8
Avg. precipitation days (≥ 0.1 mm)	9.7	10.3	13.9	12.7	12.1	14.4	12.0	11.3	11.0	8.1	7.0	6.5	129.0
Mean monthly sunshine hours	123.0	115.7	126.0	156.1	173.5	147.6	217.8	220.8	158.9	160.8	146.6	147.7	1,894.5

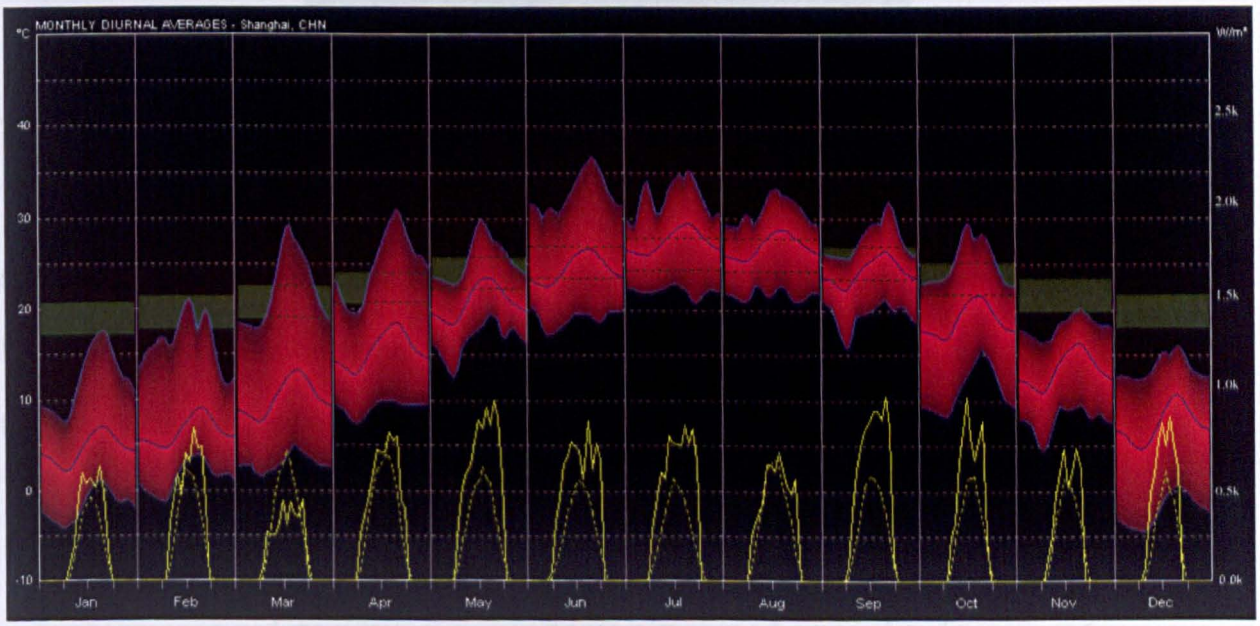

Figure 7-1Monthly average solar radiations in one year for Shanghai, China

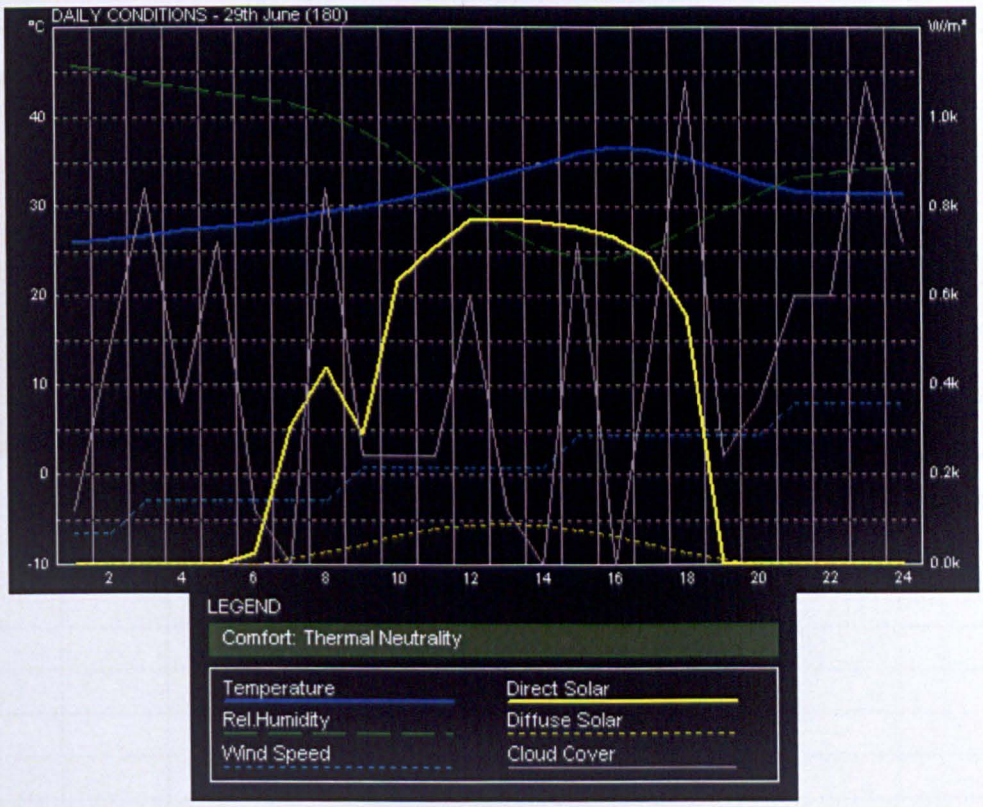

Figure 7-2 Hourly ambient temperatures and solar radiations on June 29th in Shanghai

7.1.2 Cooling load simulation for an office building in Shanghai

A model of an office building with the following details (shown in Table 7-2) was built up and simulated in Ecotect. The monthly heat and cooling load during a year was obtained in Figure 7-3, which indicated that the maximum cooling load occurred on June 29th. Therefore, the hourly cooling load on this typical day was calculated and shown in Figure 7-4.

Table 7-2 Office building simulation parameters

Floor area	50 m^2
Wall/Window area (North& South)	30/3 m^2
Wall/Window area (East& West)	15/1.5 m^2
Roof area	58.3 m^2
Total volume	150m^2
Maximum indoor temperature	26℃

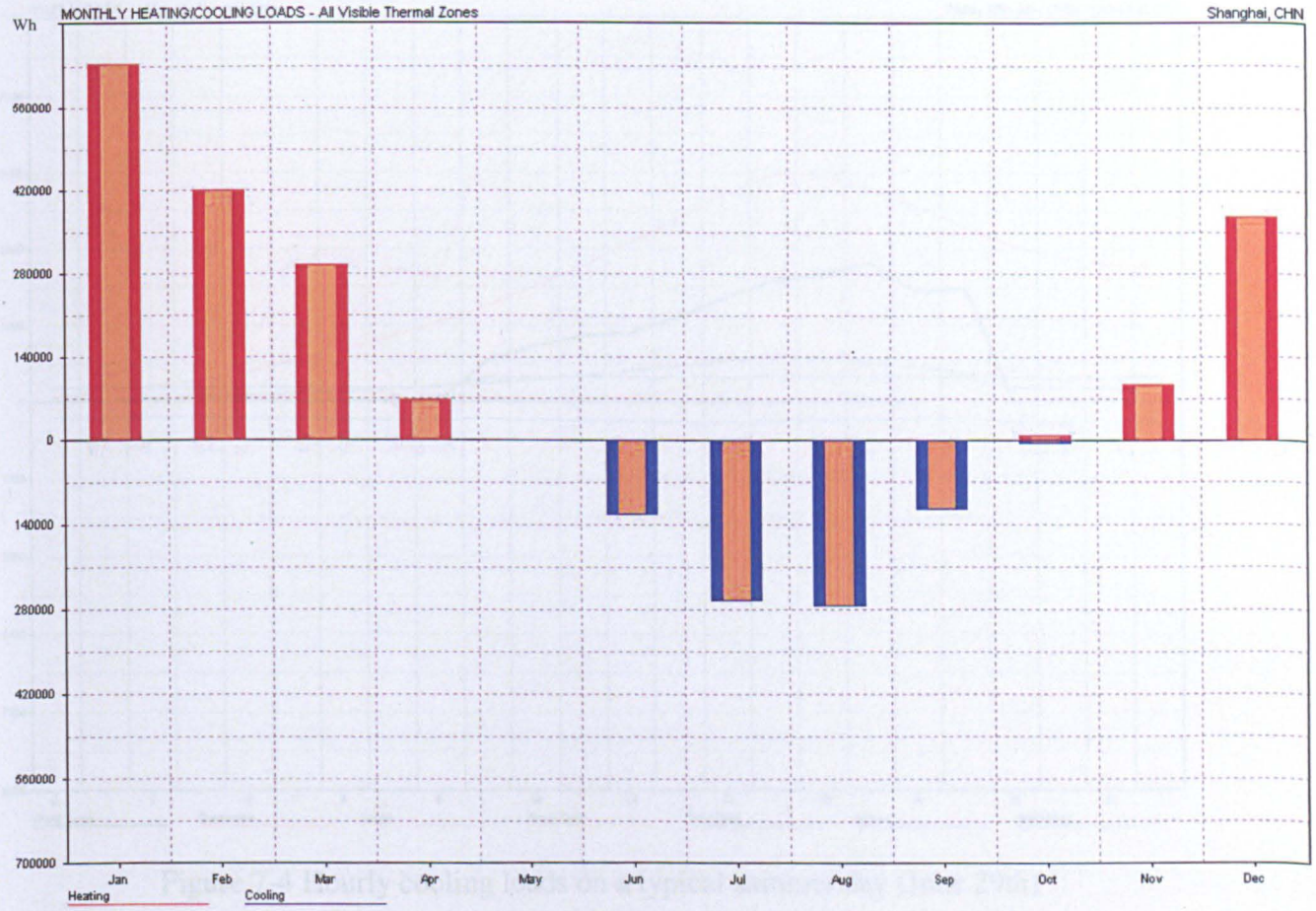

Figure 7-3 Hourly solar irradiation variations in Shanghai (July)

Figure 7-4 Hourly cooling loads on a typical summer day (June 29th)

7.2 Simulation of solar driven ejector cooling system for an office building in Shanghai

7.2.1 System description

The whole system (as shown in Figure 7-5) can be divided into two subsystems: the solar collector subsystem and the ejector cooling subsystem. The main connection between the solar collector and the ejector cooling device is via a storage tank. An auxiliary heater is fitted as the backup energy source.

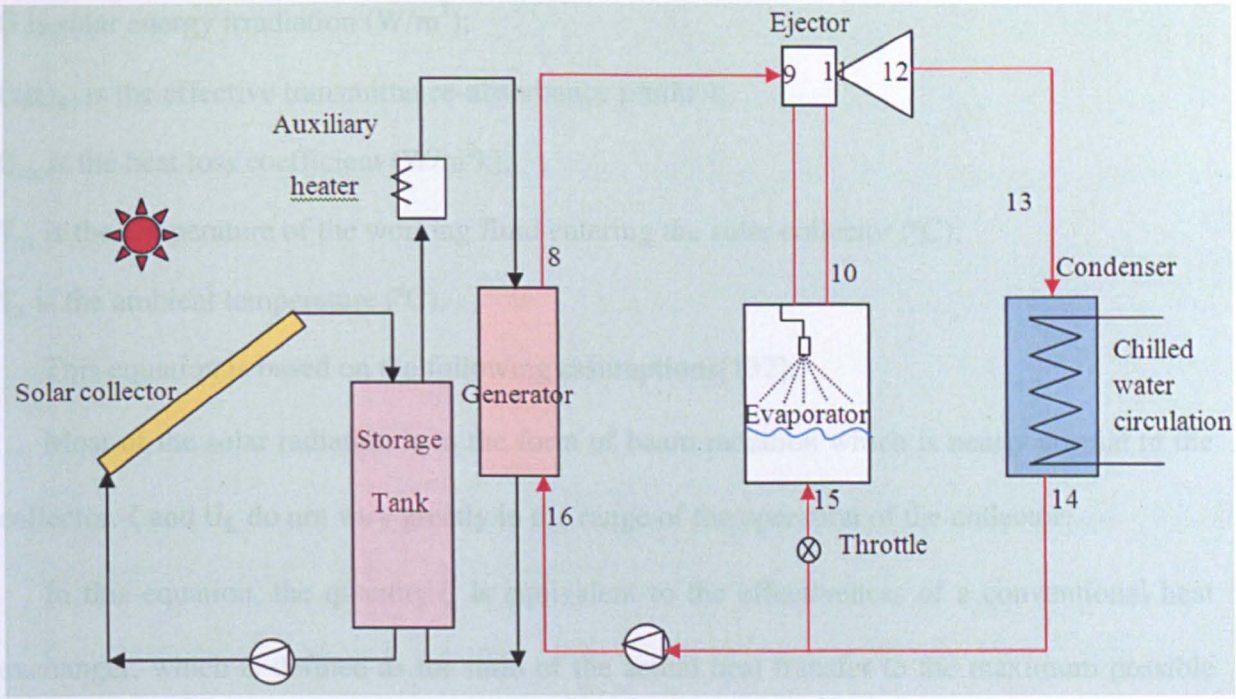

Figure 7-5 Schematic diagram of the experimental system on ejector cooling system

7.2.1.1 The solar collector subsystem

The solar collector subsystem is comprised of solar collectors, a storage tank and an auxiliary heater. The storage tank is used as the thermal storage when the solar radiation is sufficient. The auxiliary heater is placed between the storage tank and the generator of the ejector cooling subsystem. When solar radiation is fluctuating and the temperature of the fluid supplied from the storage tank is lower than the generator working temperature, the auxiliary heater can be switched on and provide additional heat source.

The actual heat gained by the solar collector, Q_c, can be calculated from the heat balance equation [137] as shown below,

$$Q_{cl} = \eta_{cl} Q_s = A_{cl}\zeta[G(\tau\alpha)_e - U_{ta}(T_{in} - T_a)] \quad \text{Eq. (7.1)}$$

Where, Q_{cl} is the actual heat gained by the solar collector (kW);

Q_s is the energy gain from solar radiation(kW);

η_{cl} is the solar collector efficiency;

A_{cl} is the solar collector area (m^2);

ζ is the solar collector heat removal factor;

G is solar energy irradiation (W/m^2);

$(\tau\alpha)_e$ is the effective transmittance-absorbance product;

U_{ta} is the heat loss coefficient (W/m^2k);

T_{in} is the temperature of the working fluid entering the solar collector (°C);

T_a is the ambient temperature (°C).

This equation is based on the following assumptions[137]:

Most of the solar radiation is in the form of beam radiation which is nearly normal to the collector. ζ and U_L do not vary greatly in the range of the operation of the collector.

In this equation, the quantity ζ is equivalent to the effectiveness of a conventional heat exchanger, which is defined as the ratio of the actual heat transfer to the maximum possible heat transfer. $\zeta(\tau\alpha)_e$ and ζU_{ta} are two parameters that describe how the collector works, where $\zeta(\tau\alpha)_e$ is an indication of how energy is absorbed and ζU_{ta} is an indication of how energy is lost.

The solar collector efficiency is defined as the ratio of the useful heat gain over any time period to the solar radiation over the same period. The instantaneous energy efficiency of the solar collector, as suggested by [137] can also be expressed in the form of $F_R(\tau\alpha)_e$ and $F_R U_L$ as shown below,

$$\eta_{cl} = \frac{Q_{cl}}{A_{cl}G} = \frac{\dot{m}c_p(T_{out}-T_{in})}{A_{cl}G} = \zeta(\tau\alpha)_e - \frac{\zeta U_{ta}(T_{in}-T_a)}{G} \qquad \text{Eq. (7.2)}$$

Thus, the actual solar energy gained by the collector can be calculated as shown below,

$$Q_{cl} = \eta_{cl}A_{cl}G \qquad \text{Eq. (7.3)}$$

Water is selected as the working fluid inside the solar collector subsystem. During a certain instant, the temperature difference of the circulated water at the solar collector inlet and outlet can be calculated from following equation,

$$(\dot{m}c_p)_{cl}(T_{out} - T_{in}) = Q_{cl} = \eta_{cl}A_{cl}G \qquad \text{Eq. (7.4)}$$

The heat loss of the tank is given by,

$$Q_{loss} = (A_{ta}U_{ta})(T_{ta} - T_a) \quad \text{Eq.(7.5)}$$

Where, A_{ta} is tank surface area (m^2);;

U_{ta} is tank heat loss coefficient ($U_t = 0.72 W/m^2k$ [137]);

T_{ta} is tank temperature.

The heat supplied to the generator to run the ejector subsystem is considered as the heat removed from the tank,

$$Q_{load} = Q_g = \dot{m}_p(h_8 - h_{16}) \quad \text{Eq. (7.6)}$$

Assuming the temperature remains the same inside the storage tank, the energy balance on the tank as suggested by [137], can be calculated as,

$$(\dot{m}c_p)_{tank}\frac{dT_{ta}}{dt} = Q_{cl} - Q_{loss} - Q_{load} \quad \text{Eq. (7.7)}$$

This equation is integrated over time to determine the long-term performance of the storage tank and the solar process. In order to solve this equation in finite differentiation form, the tank temperature is calculated at the end of a time increment (1 hour). The temperature at the end of an hour is assumed to be the same as that at the beginning.

The auxiliary heater is switched on when the temperature of the water in the storage tank is lower than 80°C, which is the minimum temperature for ejector operation. In this case, the auxiliary energy is calculated by,

$$Q_{aux} = (\dot{m}c_p)_{ta}(T_g - T_{ta}) \quad \text{Eq. (7.8)}$$

7.2.1.2 Ejector cooling subsystem

The pressure-enthalpy diagram of the ejector cooling subsystem is shown in Figure 7-6, according to the subsystem diagram in Figure 7-5.

Energy balance equation at the mixing point of the ejector,

$$\dot{m}_p h_8 + \dot{m}_s h_{10} = (\dot{m}_p + \dot{m}_s)h_{12} \quad \text{Eq. (7.9)}$$

The entrainment ratio is defined as the ratio of mass flow rate between secondary and primary flow,

$$\omega = \dot{m}_s/\dot{m}_p \quad \text{Eq. (7.10)}$$

The efficiency of the ejector cooling subsystem is generally expressed in terms of coefficient of performance (COP). The pump work input is relatively low compared with the heat required by the generator. Hence, it can be neglected in the calculation. And the system COP can be evaluated as the ratio between the cooling capacity and the heat required by the generator, as shown below,

$$COP_{ej}=\frac{Q_e}{Q_g}=\frac{\dot{m}_s(h_{10}-h_{15})}{\dot{m}_p(h_8-h_{16})} \quad \text{Eq. (7.11)}$$

The basic ejector working theory and mathematical model can be found in Chapter 3.

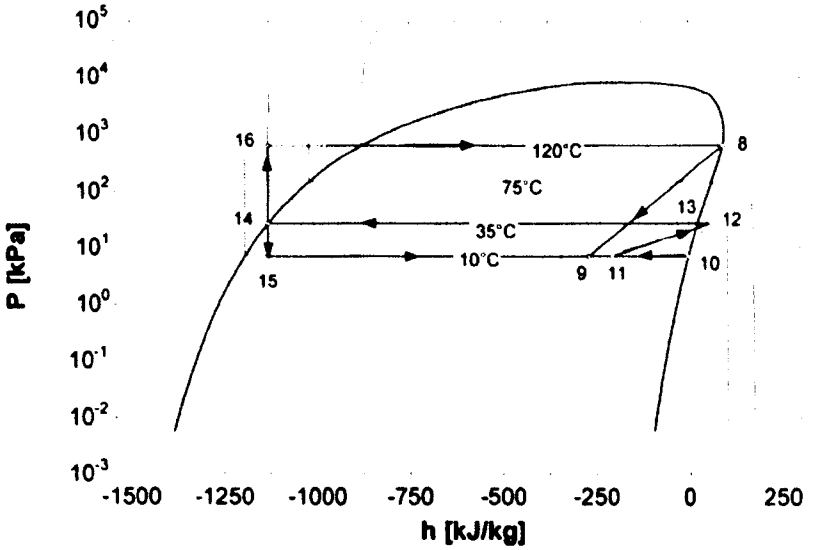

Figure 7-6 P-h diagram of ejector cooling subsystem

7.2.2 Modelling of the solar-driven ejector cooling system

7.2.2.1 System performance

Neglecting the power supply to the circulation pump, the overall system performance of solar-driven ejector cooling system can be evaluated as the product of the solar collector efficiency and the COP of the ejector subsystem, as shown below

$$COP = \eta_{cl} COP_{ej} \quad \text{Eq. (7.12)}$$

In case of the solar driven ejector cooling system, the solar fraction over a period represents the effectiveness of the system better than the conventional efficiency term. In this

case, the solar fraction is defined as the fraction of the solar energy supply to the cooling system to the total power supply to the generator to run the system,

$$SF = \frac{Q_{cl}}{Q_g} \qquad \text{Eq. (7.13)}$$

7.2.2.2 Simulation method

The performance of the systems was modelled by a simulation programme written in EES (Engineering Equation Solver). The calculation flow chart can be found in Figure 7-7. And the simulation parameters are summarized in Table 7-3.

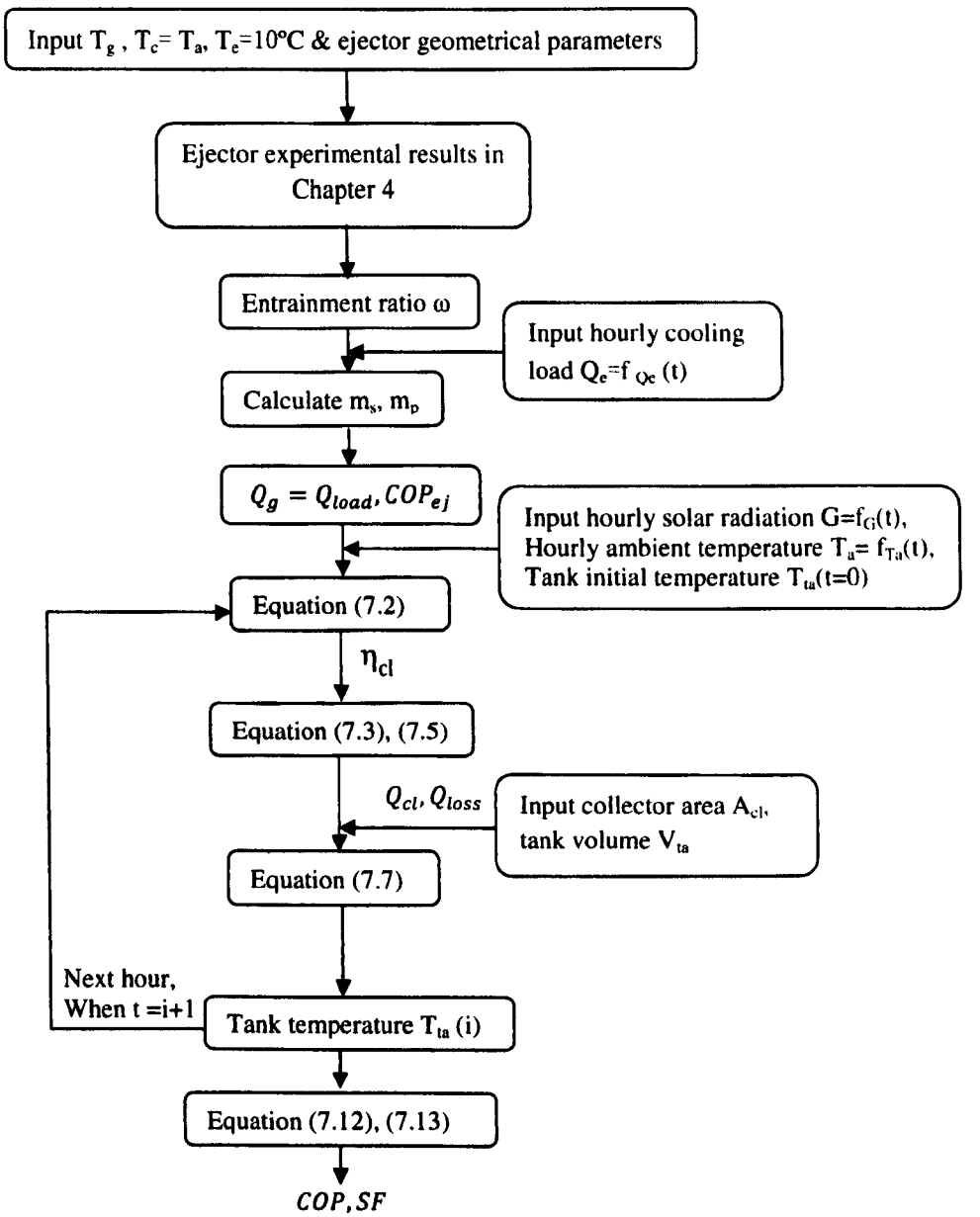

Figure 7-7 Calculation flow chart of solar driven ejector cooling system

Table 7-3 Simulation parameters

Climatic data	Location: Shanghai Latitude: 31°12'0'' Longitude: 121 ° 13'00''
Solar collector subsystem	Flat plat double glaze: $\eta_s = 0.8 - 3.5(\frac{T_{ta}-T_a}{G})$ [138]
Collector type	Storage tank heat exchanger efficiency: $\eta_{ta} = 0.8$
Storage tank	Storage tank volume: 0.5,1, 1.5, 2, 3, 4, 5 m^3
Auxiliary heater	Setting temperature: the heater starts when the water from the storage tank supplied to the generator goes below 80 °C
Ejector cooling subsystem	Refrigerant: water Operation period: 7:00-17:00, Monday to Friday Cooling capacity: calculated by Ecotect in Figure 7-4
Generator	Minimum driven temperature : 80°C Maximum driven temperature: 120 °C
Ejector	Design characteristic parameters as shown in Figure 4-7.
Condenser	Condenser temperature: 5 °C higher than ambient temperature
Evaporator	Evaporator temperature: 10 °C
Pump	Pump efficiency: 0.8

7.2.3 Simulation results

7.2.3.1 The effect of solar collector area

With storage tank volume fixed at 1.5 m^3, solar collector area of various values (10 m^2, 20 m^2, 30 m^2, 40 m^2 and 50 m^2) were investigated with respect to solar collector heat gains and auxiliary heater capacity as shown in Figure 7-8 and Figure 7-9. It is obvious that greater solar collector area will lead to higher heat gain and less auxiliary heat requirement. For instance, at 2 pm of a typical day in July, the heat gain (18812kWh) of collector area 50m^2 is

approximately 2.5 times than that of collector area $20m^2$ (7602kWh). The auxiliary heater does not need to be switched on from 8am to 1pm for solar collector area of $50m^2$. While for the collector area of 20 m^2, the auxiliary heater has to work all through the day.

The effect of solar collector area on solar fraction is shown in Figure 7-10. It can be observed that for a given collector area, the maximum of solar fraction occurs at around 1pm. According to Eq.(6.14), this means that at mid-day, the ratio between the available solar energy and the required energy by generator reaches the peak value. It is obvious that larger collector area will lead to higher solar fraction, which is another way of demonstrating that larger collector area will produce more useful heat gain from collector.

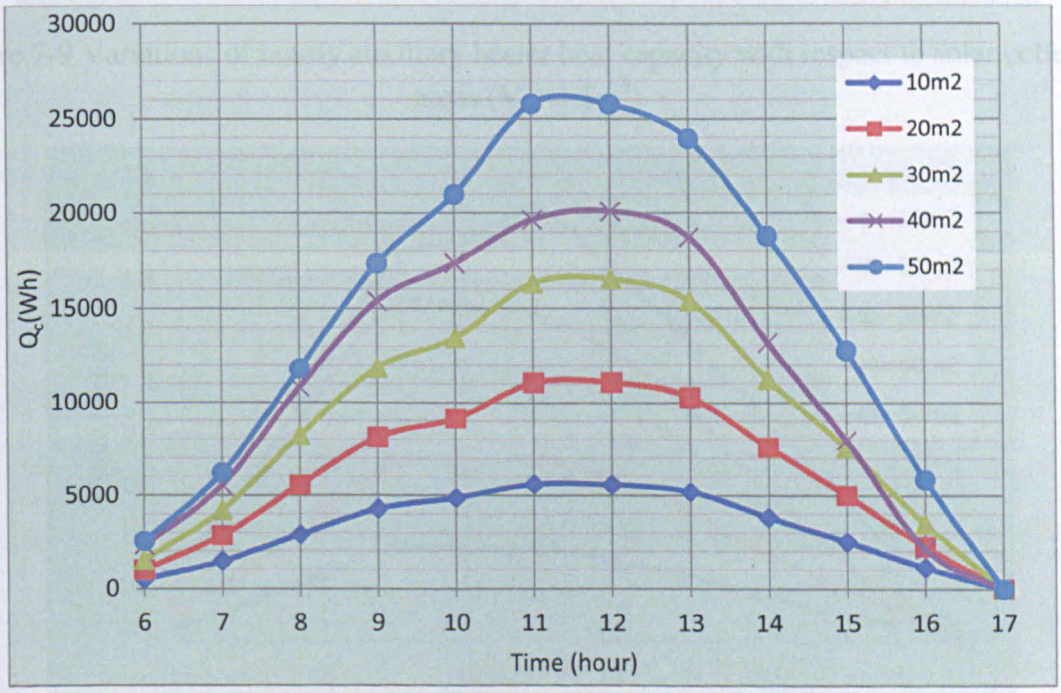

Figure 7-8 Variations of hourly solar collector heat gain with respect to solar collector areas (V_{ta}=1.5 m^3)

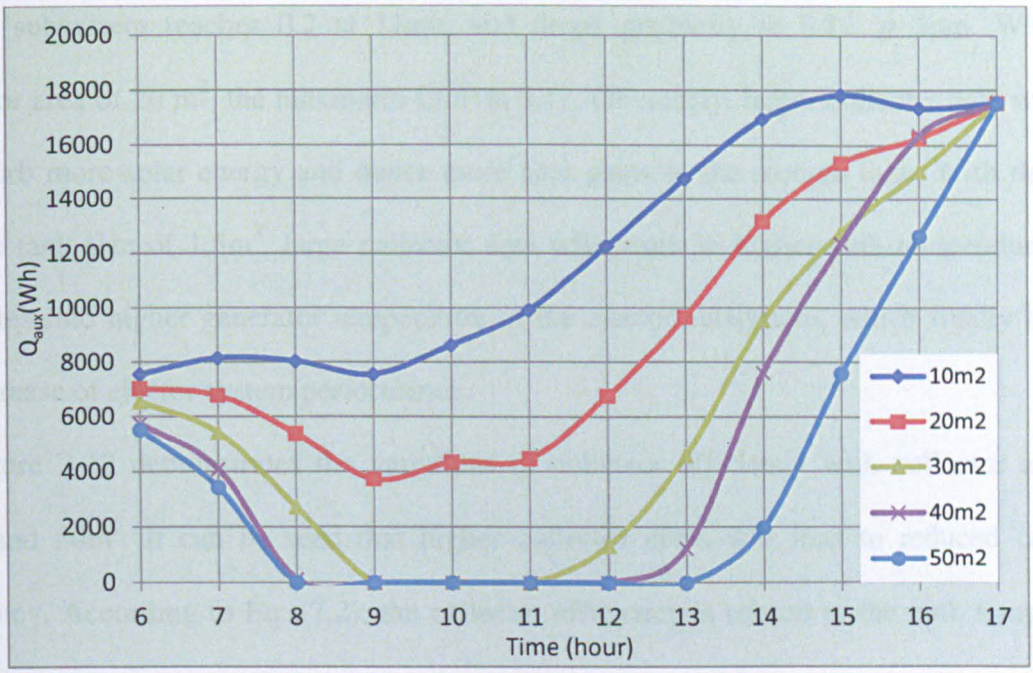

Figure 7-9 Variations of hourly auxiliary heater heat capacity with respect to solar collector areas (V_{ta}=1.5m^3)

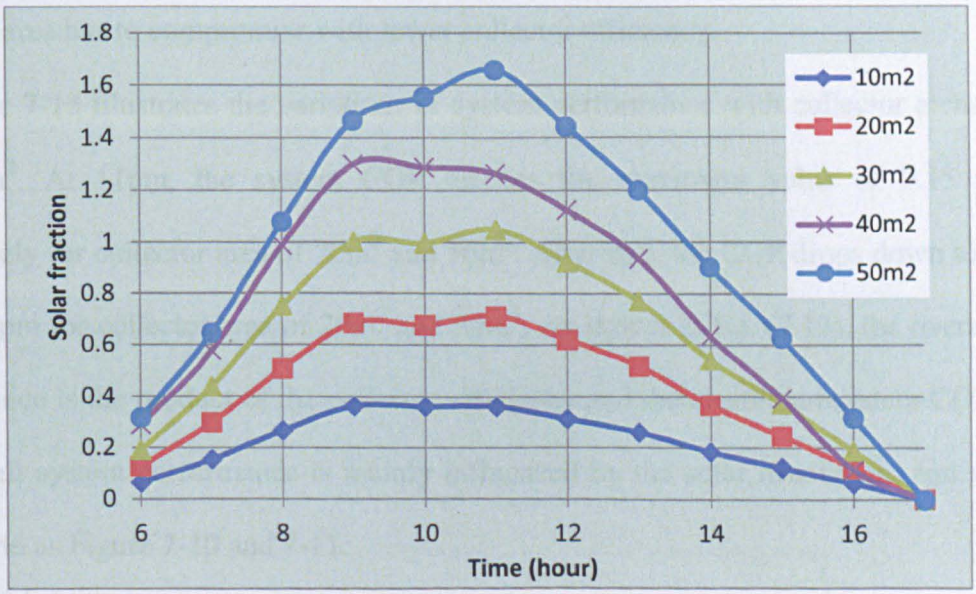

Figure 7-10 Variations of solar fraction with respect to solar collector areas (V_t=1.5m^3)

The variations of ejector subsystem COP, collector efficiency and overall system efficiency with respect to collector areas are shown in Figure 7-11, 7-12 and 7-13 respectively. It can be found that the ejector subsystem performance and overall system efficiency for collector areas of 50 m^2 surpass these for collector areas of 20 m^2 for most of the period from 6am to 5pm in a typical summer day. In Figure 7-11, with collector area of 50 m^2, COP of

ejector subsystem reaches 0.2 at 11am, and drops gradually to 0.12 at 5pm. While for collector area of 20 m^2, the maximum COP is 0.17. Obviously, larger collector area will help to absorb more solar energy and hence more heat gains to the storage tank. With the same storage tank size of 1.5m^3, large collector area will result in higher tank temperature. This translates into higher generator temperature in the ejector subsystem, which finally leads to the increase of ejector system performance.

Figure 7-12 demonstrates the variations of collector efficiency with collector areas of 20m^2 and 50m^2. It can be seen that higher collector areas will lead to reduced collector efficiency. According to Eq. (7.2), the collector efficiency is related to the tank temperature with all the other parameters being constant values. Larger collector area contributes to higher tank temperature, which translates into lower solar efficiency. Hence, the choice of larger collector area has to compromise with lower collector efficiency.

Figure 7-13 illustrates the variations of system performance with collector areas of 20m^2 and 50m^2. At 11pm, the system COP reaches the maximum value of 0.15 and 0.10 respectively for collector area of 20m^2 and 50m^2. After that, the COP drops down to 0.06 and 0.05 at 5pm for collector area of 20m^2 and 50m^2. As shown in Eq. (7.13), the overall system performance is the product of the collector efficiency and the ejector subsystem COP. Hence, the overall system performance is mainly influenced by the solar irradiation, and shares the same trend as Figure 7-10 and 7-11.

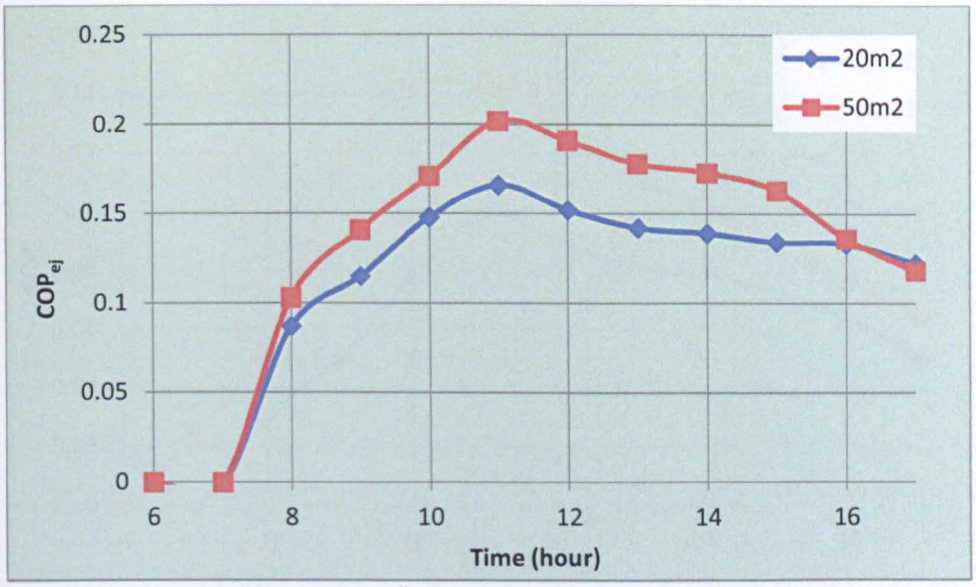

Figure 7-11 Variations of COP_{ej} with solar collector areas of $20m^2$ and $50m^2$(V_{ta}=1.5m^3)

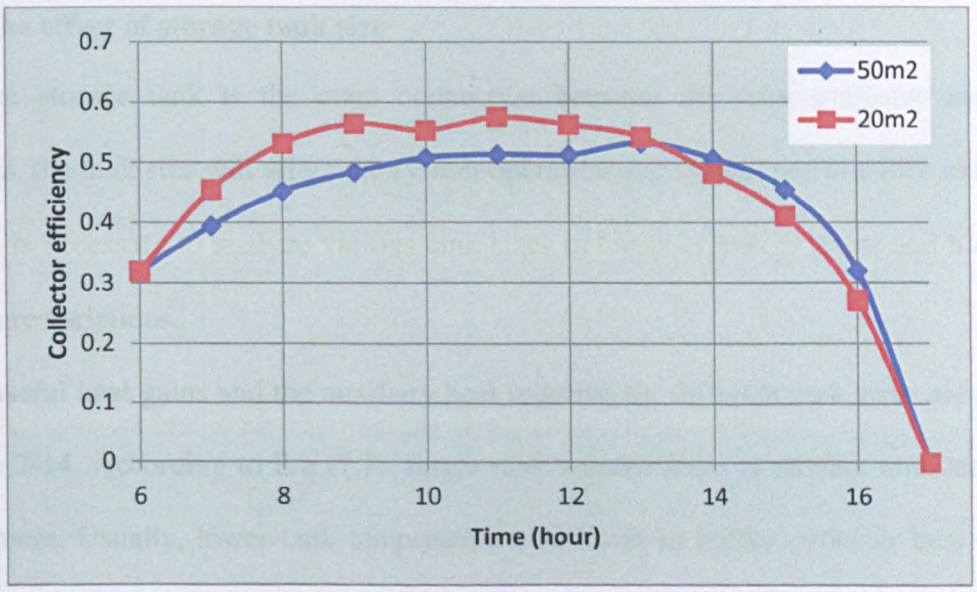

Figure 7-12 7-12 Variations of collector efficiency with solar collector areas of $20m^2$ and $50m^2$(V_{ta}=1.5m^3)

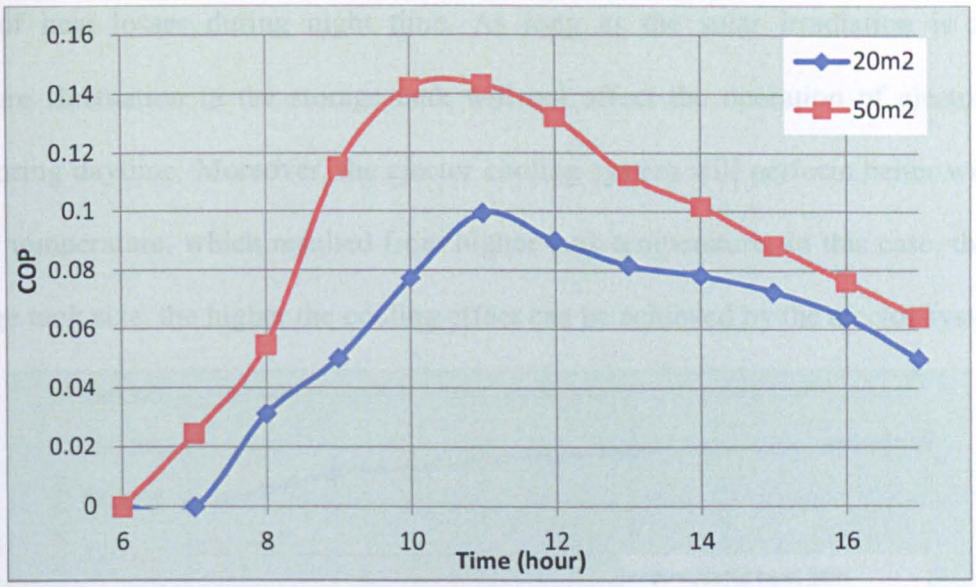

Figure 7-13 Variations of COP with solar collector areas of $20m^2$ and $50m^2$ (V_{ta}=$1.5m^3$)

7.2.3.2 The effect of storage tank size

As the storage tank is the main connection between the solar collector and ejector subsystem, the tank size will affect the system operation and system performance extensively. Hence, it is necessary to analyze various tank sizes in terms of energy gains and hourly tank temperature variations.

The useful heat gains and the auxiliary heat required for different tank sizes are presented in Figure 7-14. According to E.q (7.7), larger tank volume leads to smaller tank temperature improvement. Usually, lower tank temperature will result in higher collector heat gain (E.q (7.1)). Hence, the increase of tank volume demonstrates a slight increase of useful heat gains. It can be noticed from Figure 7-14 that auxiliary heat requirements approach close to each other. It reaches a minimum value for 3.5 m3 storage tank, which is 10000kWh less than that for 1.0 m3 storage tank.

The effect of various tank volumes on the tank temperature is shown in Figure 7-15. It is obvious that tank temperature becomes more stable with larger tank volume. When the tank volume decreases to $1m^3$, greater temperature fluctuation will occur during a typical day. The tank temperature can reach up to 110℃ when the solar radiation is strong and drops to 65 ℃

because of heat losses during night time. As long as the solar irradiation is abundant, temperature fluctuation in the storage tank will not affect the operation of ejector cooling system during daytime. Moreover, the ejector cooling system will perform better with higher generator temperature, which resulted from higher tank temperature. In this case, the smaller the storage tank size, the higher the cooling effect can be achieved by the ejector system.

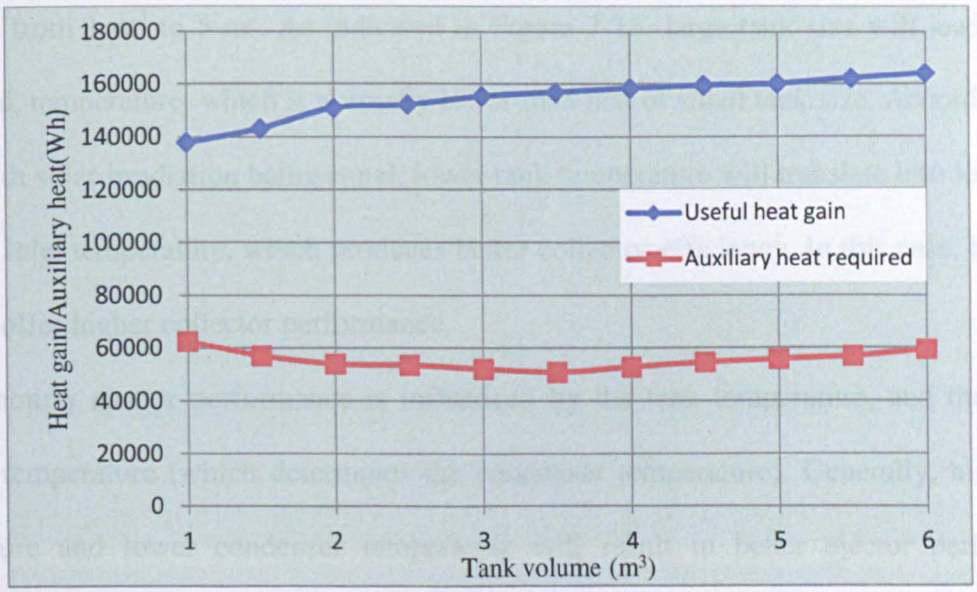

Figure 7-14 Effect of various tank sizes on useful heat gain and auxiliary heat required (A_{cl}=40 m^2)

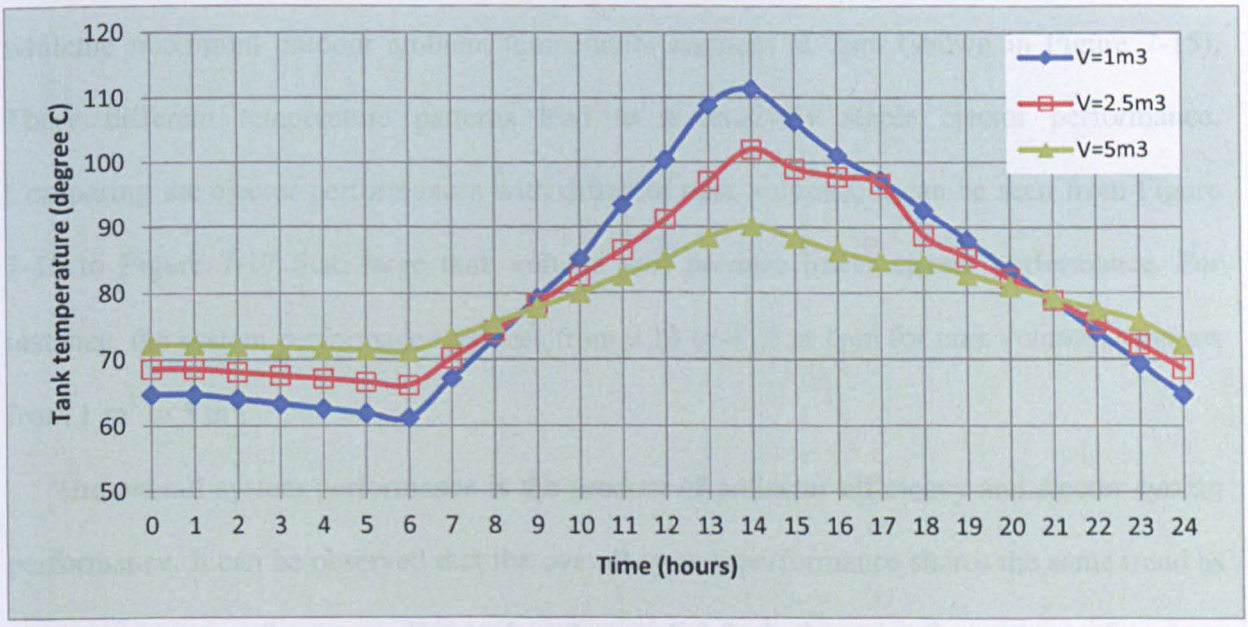

Figure 7-15 Effect of various tank sizes on the tank temperature during a normal weather condition (Acl=40 m^2)

Figure 7-16 to Figure 7-18 illustrate the performance variations of solar collector, ejector subsystem and the overall system with different tank volumes. It can be found that the performance variations share the same trend for various tank volumes. For tank volume of $1m^3$, collector efficiency increases to around 0.6 at 11am and drops down to 0 at 5pm. The maximum value of the collector efficiency increases from 0.6 to 0.65 as the tank size increases from 1 m^3 to 5 m^3. As indicated in Figure 7-15, large tank size will lead to more stable tank temperature, which is normally lower than that of small tank size. According to Eq. (7.2,), with solar irradiation being equal, lower tank temperature will translate into lower solar collector inlet temperature, which produces better collector efficiency. In this case, large tank size will offer higher collector performance.

The hourly ejector performance is influenced by the tank temperature, and the outdoor ambient temperature (which determines the condenser temperature). Generally, higher tank temperature and lower condenser temperature will result in better ejector performance. However, the tank temperature and the condenser temperature do not reach the summit at the same moment. The maximum tank temperature occurs at 11am (shown in Figure 7-15), whilethe maximum outdoor ambient temperature happens at 2pm (shown in Figure 7-15). These different temperature patterns lead to a relatively stable ejector performance. Comparing the ejector performances with different tank volumes, it can be seen from Figure 7-15 to Figure 7-17 that, large tank volume will produce lower ejector performance. For instance, the system performance reduces from 0.13 to 0.85 at 1pm for tank volume increases from 1 m^3 to 5 m^3.

The overall system performance is the product of collector efficiency and ejector system performance. It can be observed that the overall system performance shares the same trend as ejector system performance. For tank volume of $2.5m^3$, the overall system performance

fluctuates around 0.6 from 10am to 3pm, and drops to 0 at 5pm. The average overall system performance reduces from 0.113 to 0.046, as the tank volume increases from 1 m^3 to 5 m^3.

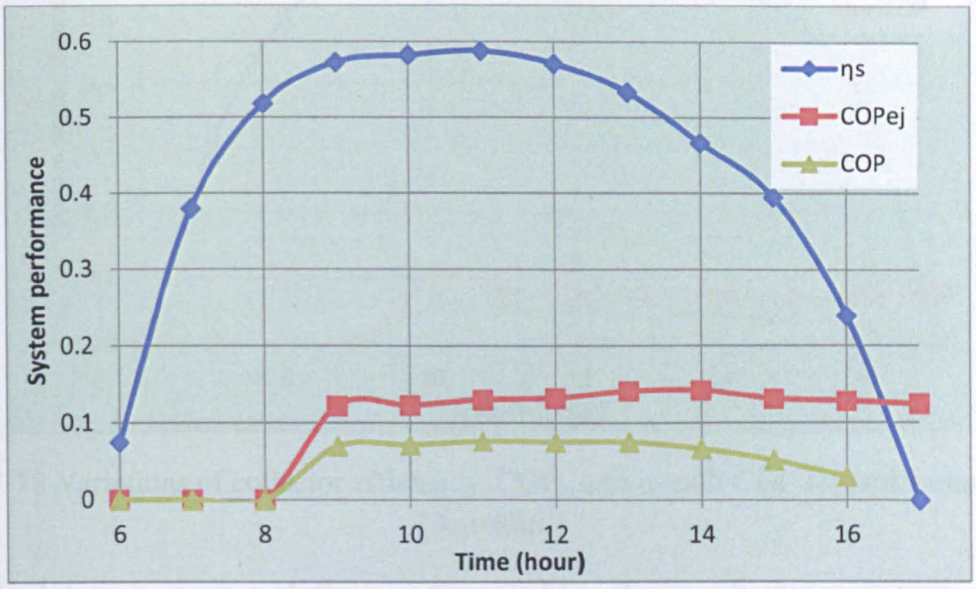

Figure 7-16 Variations of collector efficiency, COP_{ej} and overall COP for tank volume=1 m^3 (A_{cl}=40m^2)

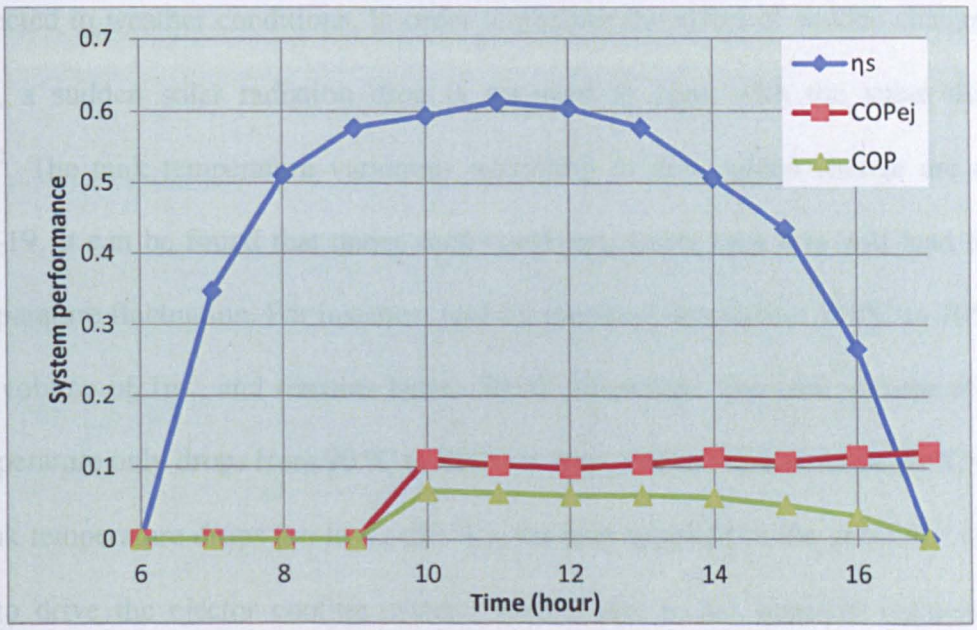

Figure 7-17 Variations of collector efficiency, COP_{ej} and overall COP for tank volume=2.5 m^3 (A_{cl}=40m^2)

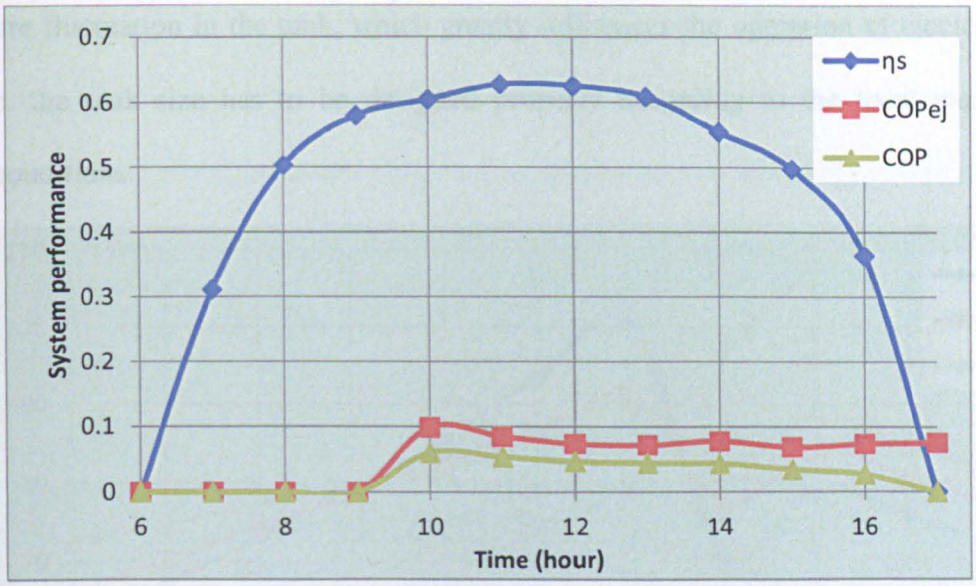

Figure 7-18 Variations of collector efficiency, COP_{ej} and overall COP for tank volume=5 m^3 (A_{cl}=40m^2)

7.2.3.3 Tank temperature variations under a sudden change of solar radiation

Although the solar radiation is abundant and free during summer times, it can be transient and subjected to weather conditions. In order to analyze the effect of sudden change of solar radiation, a sudden solar radiation drop is assumed at 1pm, with the value declines to 750W/m^2. The tank temperature variations according to this sudden change are shown in Figure 7-19. It can be found that under such condition, larger tank size will lead to smaller tank temperature fluctuation. For instance, tank temperature drops from 110℃ to 70℃ at 1pm for tank volume of 1m^3, and remains below 80 ℃ afterwards. For tank volume of 5m^3, the tank temperature only drops from 90 ℃ to 82 ℃ at 1pm, and maintains above 80 ℃ until 4pm. If the tank temperature drops too low (<80 ℃), the heat supplied to the generator will not be enough to drive the ejector cooling system. Hence, due to the transient features of solar energy, the tank size should be relatively large in order to maintain the system in a more stable way.

As discussed before, the storage tank with smaller size will result in higher tank temperature, which is beneficial to the overall system performance. However, considering the transient features of solar energy, storage tank with smaller size will lead to larger

temperature fluctuation in the tank, which greatly influences the operation of ejector system. Therefore, the tank size has to be designed properly according to the local weather and climatic conditions.

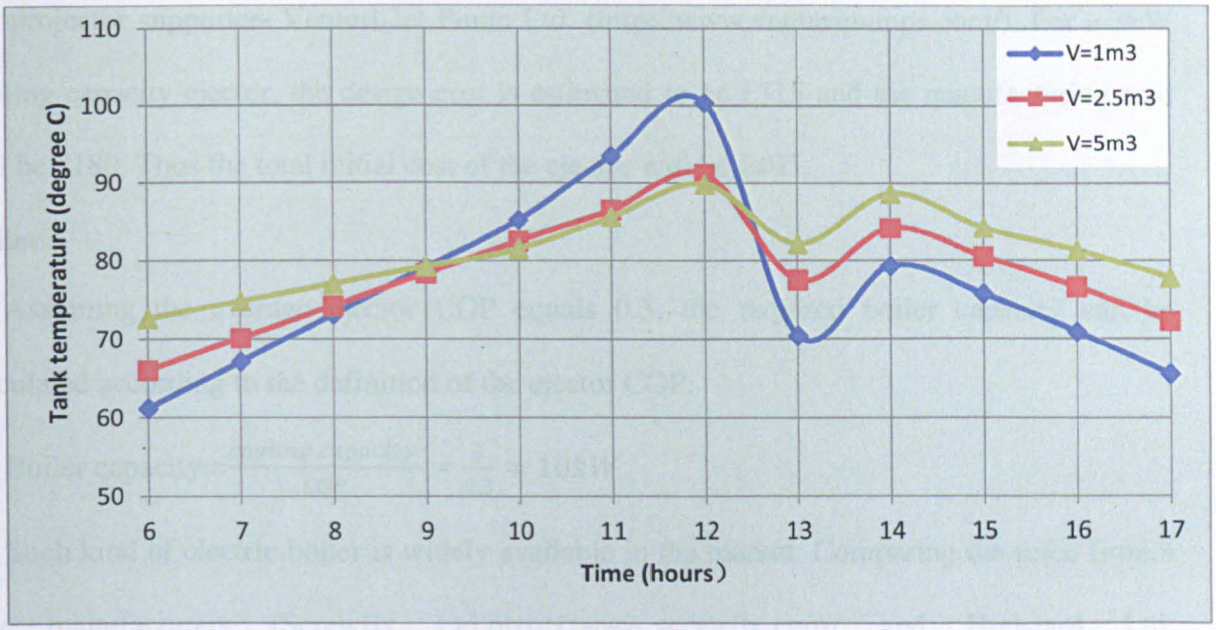

Figure 7-19 Effect of various tank sizes on the tank temperature when a sudden drop of solar irradiation occurs (A_{cl}=40 m^2)

7.2.4 Economic analysis

As discussed in previous section, the solar collector area is closely related to the useful heat gain from solar energy and auxiliary heat input required to run the ejector cooling system. Although larger collector area will produce higher useful heat gain and require less auxiliary heat input, the initial costs will be higher. In order to determine the least cost of the solar collector during a life cycle, economic analysis of the solar-driven ejector system is implemented in this section.

7.2.4.1 Cost analysis of ejector cooling system

7.2.4.1.1 Main components initial costs

The costs of the main components in the ejector cooling systems are estimated as following:

Ejector

The initial costs of ejector involve two parts, the design cost and manufacturing cost. Commercial ejector components are very few at the moment. The quote was obtained from our projector supporter- Venturi Jet Pump Ltd. (http://www.venturipumps.com/). For a 3kW cooling capacity ejector, the design cost is estimated to be £315 and the manufacturing cost will be £180. Thus the total initial cost of the ejector will be £495.

Boiler

Assuming the average ejector COP equals 0.3, the required boiler capacity can be calculated according to the definition of the ejector COP:

$$\text{Boiler capacity} = \frac{cooling\ capacity}{COP} = \frac{3}{0.3} = 10kW$$

Such kind of electric boiler is widely available in the market. Comparing the price from a few manufacturers (Screwfix Ltd.http://www.screwfix.com/ and Highcard Ltd. http://www.radiantheatproducts.com), the estimated price for a 10kW boiler is about £520.

Condenser/Evaporator

As described in Chapter 3, cylindrical stainless steel vessels can be used as the main housing for the condenser and the evaporator. For the evaporator of 200mm diameter and 350mm height, the overall area of the material required = $(2\pi r^2+\pi dh)$ = $(2*3.14*0.1^2+3.14*0.2*0.35)$ =0.691m^2. As the density of stainless steel is 8.0kg/m^3, and the thickness of the cylindrical vessel is 3.5mm, the overall weight of the material =0.691*8.0*0.035=0.19kg. As the stainless steel price is £1800/tonne (http://www.meps.co.uk/Stainless%20Prices.htm), the overall cost of the material for the evaporator =0.19*1800/1000=£0.342. The manufacturing process of the evaporator vessel is about one day for a skilled technician, which is about £35. Thus, the total initial cost for the evaporator will be £35.34.

The same calculation could be implemented for the condenser, and all the detailed parameters are listed in the following table:

Table 7-4 Cost estimations for evaporator and condenser vessels

Vessel	Diameter (mm)	Height (mm)	Thickness(mm)	Total area (m^2)	Weight (kg)	Cost of material	Cost of labour	Total Cost
Evaporator	200	350	3.5	0.691	0.19	£0.34	£35	£35.34
Condenser	500	800	3.5	4.082	1.63	£2.94	£35	£37.94
							Sum	£73.28

Pump

A centrifugal pump produced by RS Ltd.(http://uk.rs-online.com) is used to circulate the refrigerant in the cycle. The estimated price for such pump is £125.

The main components cost and the total investment costs of the ejector cooling system are summarized in Table 7-5:

Table 7-5 Summary of the investment costs for ejector's main components

	Investment cost (3kW cooling capacity)
Ejector	£495
Boiler	£520
Evaporator	£35.34
Condenser	£37.94
Pump	£125
Total investment costs	£1213.3
Main components costs (excludes boiler)	£693.3

7.2.4.1.2 Investment cost comparisons of ejector cooling system with vapour compression system

The general cost and performance comparisons for ejector cooling system and vapour compression system are summarized in Table 7-6. Due to decades of research and commercialization, the price and the COP of vapour compression system surpass the ejector cooling system. However, vapour compression system can cause environmental pollutions and ozone depletion if conventional refrigerants are used. Moreover, as the system is mainly driven by electricity, the primary energy costs during a life cycle are significantly high. Although the COP of the ejector system is relatively low. Its ability of utilizing low grade energy makes it less dependent on primary energy and contributes greatly to energy saving. Since the available manufacturer of the ejector in the market are of limited numbers, current price of the ejector are relatively high. From long term point of view, as the technology of the ejector is further developed, mass production can be expected in the market. Thus, the price and the competitiveness of the ejector cooling system can be more attractive in the near future.

Table 7-6 Comparisons between ejector and vapour compression systems

Type		Ejector cooling system	Vapour compression system[139]
Cooling performance	Cooling capacity (kW)	3	2.6
	COP	0.3-0.5	2.6-3.0
	Cooling temperature(°C)	≤20	18-45
Noise (Db) (indoor)		23-35	39
Size (mm^3) (indoor)		1200*850*300	815*298*194
Life expectancy (year)		≤15	≤25
Initial equipment cost (£)		£1213	£518

7.2.4.2 Payback period

Payback period in capital budgeting refers to the period of time required for the return on an investment to "repay" the sum of the original investment.

Payback Period = Amount to be Invested/Estimated Annual Net Cash Flow

The total investment varies as the solar collector size increases. According to [140, 141], for flat plat double glaze collector, the price of the collector is the sum of two parts:

Area dependent cost=£250/m^2;

Area independent cost=£1000.

For instance, with collector area of $30m^2$, the collector investment cost = 250*30+1000=£8500. The total investment cost equals to the main components cost (excluding the boiler) and the solar collector cost. Thus, the total investment cost=£8500+£693=£9193.

The annual profit obtained from this system is mainly due to the cooling effect provided by solar energy which can be calculated as gas savings in terms of solar collector heat gains. Take the collector area equals to $30m^2$ as the example, the calculations are shown below:

According to Figure 7-8, for $A_c=30m^2$, the daily useful heat gain is equal to 109861Wh.

Assuming the annual cooling requirements is from June to September, the annual heat gain from the solar energy=$109861*4*30=13.183*10^3$kWh

The same amount of heat could be provided by gas with the volume=

$13.183*10^3*3.6*10^6/(7.5*10^7)=6.33*10^3\ m^3$

Where, the combustion value of gas=$7.5*10^7$ J/Kg.

As the gas price is £0.72/m^3 (according to gas price from Shanghai Gas Company Ltd.: http://www.shgas.com.cn/), such amount of gas=$6.33*10^3*0.72$=£459

Hence, the payback period of different sizes of solar collector are calculated and shown in Table 7-7. It could be found that for collector areas between 10-$50m^2$, payback period is very close to a normal life cycle of 20 years. This means that although the initial investment cost is high, the system is still worth investing as the profit will eventually meet with the investment after a life cycle. If we consider that the solar collector can also provide domestic hot water all throughout the year, the solar saving would be greatly increased and the payback period should be reduced significantly.

Table 7-7 Summary of payback period for various collector areas

Collector Area (m^2)	Investment Cost (£)	Solar saving (£)	Payback period (year)
10	4193	159	26.37
20	6693	309	21.66
30	9193	459	20.03
40	11693	557	20.99
50	14193	718	19.77

7.2.4.3 Introduction of Life Saving Analysis

The method applied for the economic analysis is called the Life Saving Analysis, which takes into considerations of time value of money and allows detailed consideration of the complete range of costs[142]. Solar process is generally featured by high initial cost and low operation cost. Thus, the basic analysis method is to compare the initial investment with estimated future operating costs.

Life Saving Cost (LSC) is the sum of all the costs associated with an energy delivery system over its lifetime in today's currency, and takes into account of the money deflation[142]. Life Saving Analysis (LSA), for a solar system plus auxiliary device, is defined as the difference between the life cycle cost of a conventional gas-only system and the life cycle cost of the solar plus auxiliary system. This is equivalent to the total present worth of the gains from the solar system compared to the gas-only system.

7.2.4.4 Discounting and inflation

The most complete approach of economic analysis for solar process is to use LSC methods which take into account all future expenses. This method provides a means of comparison of future costs with today's costs. This is achieved by discounting all anticipated costs to the common basis of present worth (or present value), that is, what would have to be invested today at the best alternative investment rate to have the funds available in the future

to meet all the anticipated expenses. Hence, the results obtained from analyses of this type usually depend very much in the predictions of future costs.

It must be noted that the case flow of money at hand is worth less than the same amount in the future, because the money at hand can be invested at some compounding interest to generate a bigger sum in the future. A case flow F occurring N years from now can be discounted to its present value P by [142]:

$$P = \frac{F}{(1+d)^N} \qquad \text{Eq. (7.15)}$$

Where, d is market discount rate.

Similarly, the amount of money needed to purchase an item is increasing because the value of money is inflating. With an annual inflation rate i, a purchase cost C at the end of year N will become a future cost F according to [142]:

$$F = C(1+i)^{N-1} \qquad \text{Eq. (7.16)}$$

If an obligation recurs each year and inflates at a rate i per period, a present worth factor, PWF, of the series of N such payments can be found by,

$$PWF = \sum_{j=1}^{N} \frac{(1+i)^{j-1}}{(1+d)^j} = \begin{cases} \frac{1}{d-i}\left[1 - \left(\frac{1+i}{1+d}\right)^N\right] & \text{if } i \neq d \\ \frac{N}{i+1} & \text{if } i = d \end{cases} \qquad \text{Eq. (7.17)}$$

7.2.4.5 Life cycle saving method description

Excel document is applied to calculate the life cycle saving, with the life cycle of 20 years. The Excel spreadsheet is divided into two areas, the input parameters area and the calculation area. The parameters used in the calculation are shown in Table 7-8.

With reference to Table 7-8, for collector area of $30m^2$, by multiplying the area dependent cost with the solar collector area will give a cost related to the size of the system.

Table 7-8 List of input parameters (A_c=30m^2)

Input parameters	Value	Units
Ejector system main component costs	693	£
First year gas savings	459	£
Gas inflation rate	7	%
Collector area	30	m^2
Area dependent cost	250	£/m^2
Area independent cost	1000	£
Annual market discount rate	8	%
Maintenance in first year	2	% of total system cost
Annual increase in maintenance	2	%
Pump electrical load	0.2	kW
Price of electricity	0.245	£/kWh
Annual increase in electricity cost	3	%
Down payment &Resale value	20	%
PWF for mortgage payment	9.1285	

The analysis is performed annually, as shown in Table 7-9, for which the following amounts are calculated:

1) Gas savings (column B)

Detailed calculation is shown in Section 7.2.4.1. This value is increased by gas inflation rate as shown in Table 7-8.

2) Extra mortgage payment (column C)

The mortgage payment is the annual value of money required to cover the funds borrowed at the beginning to install the system. This includes interest and principal payment. The estimation of the annual mortgage payment can be found by dividing the amount borrowed by

the present worth factor (PWF). The PWF is estimated by using the inflation rate equal to zero (equal payments) and with the market discount rate equal to the mortgage rate (9%). According to Eq. (7.17), the PWF can be calculated for 20 years' period with the value of 9.1285. In order to find the annual mortgage payment, the amount borrowed is divided by this number, with the results shown in column C.

3) Extra maintenance cost (column D)

The total system cost can be obtained by adding the area independent cost. The system maintenance cost is initially estimated at 2% of the initial system cost and is increased annually by 2% as the system becomes older.

4) Extra parasitic cost (column E)

The parasitic cost is obtained by multiplying the pump power by the operation hours and by the price of electricity (according to shanghai electricity 2012 price: http://www.dfdaily.com/html/21/2012/7/3/818095.shtml). For instance, for collector area of $30m^2$, the pump is estimated to be 0.31kW, the annual electricity cost to run the pump=0.31*3600*0.245=£27.34.

This cost is also increased at an inflation rate over the period of economic analysis by using Eq. (7.16), with "i" equals to the annual increase of electricity price shown in Table 7-9.

5) Solar savings (column F)

Solar savings for each year are the sums of the items in columns B to columns E. In equation form, the solar savings of the system can be expressed as,

Solar savings= Extra mortgage payment + Extra maintenance cost+ Extra parasitic cost+ Gas savings Eq. (7.18)

6) PW of solar savings (column G)

The present worth (PW) of each year's solar savings is determined by using Eq. (7.15). The results are added up to give the total PW of the system over its life time.

All the savings are positive and the costs are negative. In this case appropriate signs have been used in Table 7-9. On the contrary, the signs of the various parameters in Eq. (7.18) should be changed accordingly.

7.2.4.6 Solar-driven ejector cooling system example

Solar-driven ejector cooling system with collector areas of $30m^2$ is considered. The proposed collector area and associated equipment will supply energy equivalent to £459 in the first year. The total cost of the equipment will be £9193 and is to be 80% financed over 20 years at an interest rate of 9%. The mortgage that has to be paid during 20 years is equal to the borrowed amount by the present worth factor, which is £805.65. Gas costs are expected to rise at 7% per year. It is expected that the equipment will have a resale value at the end of 20 years of 20% of original cost. The power consumption of the solar circulation pump is 0.31kW and is estimated to work for 3600 hours per year. The price of the electricity cost is £0.245/kWh and its price is expected to rise at 3% per year. Finally the market discount rate is 8%.

The objective here is to establish the present worth of solar savings for this system over a 20 years period. Table 7-9 shows the yearly incremental costs and savings. Year zero shows only the 20% down payment (£1838.6) of the system total cost, which is a negative present worth of solar savings. Each year's solar savings is brought to a present worth using Eq. (7.15) with annual market discount rate of 8%. The resale value of the equipment after 20 years is shown as a secondary entry in year 20, and is positive as it contributes to savings. The sum of the numbers in column G, £738.4, is the total present worth of the gains from the solar system compared to the gas-only system and is called "life cycle solar savings".

Table 7-9 Economic analysis calculation example for collector area=30 m^2

A	B	C	D	E	F	G	H	I	J
							Supplementary information		
Year	Gas saving	Extra mortgage payment	Extra mainte-nance cost	Extra parastic cost	Solar savings	PW of solar savings	Mortgage	interest	Remaining
0				**Down payment**	**-1838.6**	**-1838.6**			**7354.4**
1	459.00	-805.65	183.86	-27.34	-190.13	-176.05	805.65	661.90	7210.64
2	491.13	-805.65	187.54	-28.16	-155.15	-133.01	805.65	648.96	7053.95
3	525.51	-805.65	191.29	-29.01	-117.86	-93.56	805.65	634.86	6883.15
4	562.29	-805.65	195.11	-29.88	-78.12	-57.42	805.65	619.48	6696.98
5	601.66	-805.65	199.02	-30.77	-35.75	-24.33	805.65	602.73	6494.06
6	643.77	-805.65	203.00	-31.69	9.42	5.94	805.65	584.47	6272.87
7	688.84	-805.65	207.06	-32.65	57.59	33.61	805.65	564.56	6031.78
8	737.05	-805.65	211.20	-33.62	108.97	58.88	805.65	542.86	5768.98
9	788.65	-805.65	215.42	-34.63	163.78	81.93	805.65	519.21	5482.54
10	843.85	-805.65	219.73	-35.67	222.26	102.95	805.65	493.43	5170.32
11	902.92	-805.65	224.12	-36.74	284.65	122.08	805.65	465.33	4829.99
12	966.13	-805.65	228.61	-37.84	351.24	139.48	805.65	434.70	4459.04
13	1033.76	-805.65	233.18	-38.98	422.30	155.28	805.65	401.31	4054.70
14	1106.12	-805.65	237.84	-40.15	498.16	169.60	805.65	364.92	3613.97
15	1183.55	-805.65	242.60	-41.35	579.14	182.57	805.65	325.26	3133.57
16	1266.40	-805.65	247.45	-42.59	665.60	194.28	805.65	282.02	2609.94
17	1355.04	-805.65	252.40	-43.87	757.92	204.84	805.65	234.89	2039.18
18	1449.90	-805.65	257.45	-45.19	856.50	214.34	805.65	183.53	1417.06
19	1551.39	-805.65	262.60	-46.54	961.79	222.86	805.65	127.54	738.94
20	1659.99	-805.65	267.85	-47.94	1074.24	230.48	805.65	66.50	-0.21
20				Resale value	1838.6	394.47			
				Total PW of solar savings		**738.40**			

7.2.4.7 Solar-driven ejector cooling system optimisation example

The system optimization is carried out by employing different collector areas in Excel spreadsheet and by plotting the PW of the solar savings against the collector areas. The optimum collector area, i.e, the area at which the solar savings is at maximum value, can then be determined. Table 7-10 shows gas savings and pump power consumption for various collector areas. By inserting various collector area values, the calculations can be repeated

accordingly. Since the results are greatly affected by the market discount rates and interest rates, it could be of interest to analyze the optimization results in relationship to these two rates. The results of the optimisation for various interest rates and market discount rates are shown graphically in Figure 7-20 and Figure 7-21. It could be found that lower interest rates and market discount rates will always yield to higher life cycle savings. As it can be observed that the economically viable solution is to use collector area of $30m^2$, which yields the maximum life cycle savings for all the cases. It should be pointed out that a larger collector area does not necessarily lead to higher life cycle savings, due to the increase in equipment installation costs.

Table 7-10 Collector area related parameters for system optimization

Collector area(m^2)	Gas savings(£)	Pump power (kW)
10	159	0.18
20	310	0.25
30	477	0.31
40	636	0.38
50	795	0.45

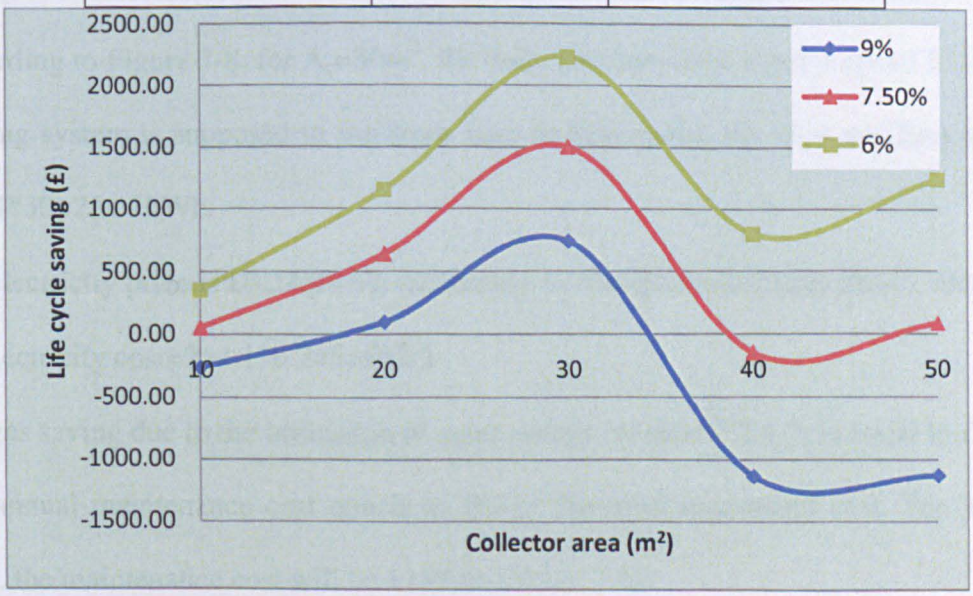

Figure 7-20 Life cycle savings with various interest rates

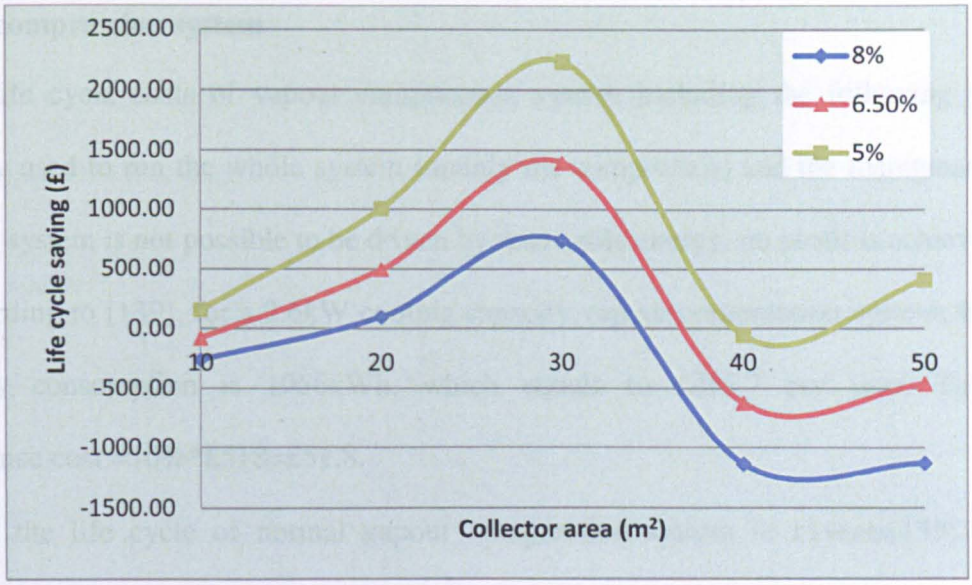

Figure 7-21 Life cycle savings with various market discount rates

7.2.5 Life cycle analysis comparisons between solar driven ejector and vapour compression system

Solar driven ejector cooling system

The life cycle costs of solar driven ejector cooling system including the following parts: the electricity costs for running the auxiliary heater when the solar radiation is low and the maintenance costs (mainly for the solar collector). These two parts are negative values. The gas saving due to the utilization of solar energy is considered as the profit to the system.

According to Figure 7-8, for A_c=30m^2, the daily auxiliary heat input is about 211.8Wh. As the cooling system is supposed to run from June to September, the total auxiliary heat input =211.8*4*30=254.1kWh.

The electricity price is £0.245/kWh (according to Shanghai electricity price), therefore the annual electricity cost=254.1*0.245=£62.3.

The gas saving due to the utilization of solar energy (section 7.2.4.2) is equal to £459.

The annual maintenance cost equals to 2% of the total investment cost. For 30m^2 solar collector, the maintenance cost will be £183.86 (Table 7-9).

Vapour compression system

The life cycle costs of vapour compression system including the following parts: the electricity used to run the whole system (mainly the compressor) and the maintenance costs. Since the system is not possible to be driven by renewable energy, no profit is achieved.

According to [139], for a 2.6kW cooling capacity vapour compression system, the annual electricity consumption is 1056kWh, which equals to £258.7 per year. The annual maintenance cost =10%*£518=£51.8.

Since the life cycle of normal vapour compression system is 11years[139]. We will compare the life cycle costs within 11 years for both the ejector and vapour compression system. Table 7-11 shows the summarized results for this comparison. The annual increase in electricity and maintenance are 3% and 2% respectively, the same value as applied in previous section.

Table 7-11Life cycle cost comparisons between ejector and vapour compression system

Items	Solar driven Ejector	Vapour compression [139]
Annual electricity requirement (kWh)	254.1	1056.0
Annual electricity cost (£)	62.3	258.7
Annual gas saving (£)	459.0	0
Annual maintenance cost (£)	183.8	51.8
Total electricity cost for 11 years(£)	797.9	3313.3
Total maintenance cost for 11 years (£)	2237.3	630.3
Total gas saving for 11 years(£)	5049.0	0
Initial investment cost (£)	9193.0	518.0
Life cycle cost (£)	7179.2	4461.7

It can be seen from Table 7-11, the initial investment cost of the solar driven ejector cooling system is about 18 times than that of the vapour compression system. After 11 years life cycle, the total life cycle cost of the solar driven ejector cooling system is about 1.6 times than that of the vapour compression system. The contributions of annual gas saving because of using the solar energy potentially narrow this price gap in the long term. Hence, in viewing

the entire life cycle, the energy saving and environmental benign feature makes the solar driven ejector system more comparable with vapour compression system.

7.2.6 Global warming impact

The global warming was considered as the main environmental problem during the last several decades, and is believed to be the result of the depletion of the stratospheric ozone layer. The leakage of the refrigerants from air conditioners and refrigerating machines are thought to be major sources for the ozone layer depletion.

Both direct and indirect effects have to be considered in order to investigate the global warming effect. The direct effect includes the release of refrigerants that are greenhouse gases, and the indirect effect is the carbon dioxide production in powering the equipment. The combined effect can be evaluated by the total equivalent warming impact (TEWI). In this expression, the direct effect is defined in relation to the global warming potential (GWP) of the emitted gas, which is a ratio of how strong a greenhouse gas is, in comparison with carbon dioxide. GWP is dependent on the greenhouse gas characteristic, and is usually used in a 100 year integrated time. Hence the direct effect can be defined with respect to an equivalent released amount of CO_2, as below,

Direct effect (kg CO_2) = [(mark-up rate*service life) +end-of-life loss]*charge*GWP

Eq. (7.19)

Where, charge is the initial charge of refrigerant in the system (kg), make-up rate is the percent refrigerant charge lost per year (averaged over the entire equipment life), service life is the number of years that the system is under operation and GWP is the global warming potential of the gas.

The indirect effect is due to the emission of CO_2 from power plants, which generate the electrical power required by the operation of the system, and is shown as follow,

Indirect effect (kg CO_2) = operation power *service life *emitted CO_2 Eq. (7.20)

Where operation power is the annual power needed by the system (kWh/year), emitted CO_2 is the amount CO_2 emitted from the power plant per kWh received by the system.

For the case of the solar-driven ejector cooling system, since no HFC refrigerants are used, only the indirect effect needs to be estimated by Eq. (7.20). In this case, for a life cycle of 20 years, the amount of CO_2 emitted from the auxiliary heater is about 14305.6kg, which can be calculated as following,

As shown in Figure 7-9, the required auxiliary heater input for collector area of $30m^2$=110543*30*4/1000=13265.2kWh;

Auxiliary heater efficiency =85% resulting in 15606.1kWh to be supplied by gas;

Calorific value of gas =60.0 MJ/kg, resulting in 260.1kg of gas consumption;

Every kg of gas produces about 2.75kg CO_2;

The indirect effect, that is the overall CO_2 emitted because of using the auxiliary heater across a life cycle=2.75*260.1*20=14305.6kg.

In the case of a conventional R410a air-conditioner with 0.5kW cooling capacity, the direct effect for a life cycle of 20 years, as calculated from Eq. (7.19), is 3591kg CO_2. The calculation process is as below,

Charge of R410a =2 kg (average figure from manufacturers catalogues);

Assumed make-up rate =4%, end-of-life loss=15%;

GWP for R410a for a 100-year period =1890;

The direct effect, that is the overall CO_2 emitted because of leakage of refrigerant across a life cycle= (4%*20+15%)*2*1890=3591kg.

The indirect effect for the conventional R410a air-conditioner covering the annual cooling load for 20-year period would be 34560kg of CO_2. 3kW cooling capacity, which works 8 hours per day from June to September, the summer cooling load can be calculated as below,

The hourly cooling load (Figure7-4), for a typical day equals to 10622kWh. Hence, the summer cooling load=10622*30*4=8497.6kWh

Assuming the energy efficiency ratio (the ratio between cooling capacity and power consumption) for air-conditioner is 3, the annual power consumption=8497.6/3=2832.5kWh

Assuming world average value of CO_2 release from electric energy production of 0.6kg/kWh, the overall indirect CO_2 emitted because of electricity consumption=2832.5*20*0.6=33990kg

Therefore the TWEI for a conventional R410a air-conditioner would be= 33990+3591=37581kg of CO_2, which is 2.63 times greater than that using the solar-driven ejector cooling system (collector area of $30m^2$). If solar collector with larger size is applied, the amount of CO_2 emitted because of using auxiliary heat could be reduced to a greater extent, which would be much beneficial to the global environment. Hence, the global warming impact produced by the solar driven ejector cooling system is much less than that of the conventional air-conditioning system.

7.3 Simulation of solar-driven combined power and ejector cooling system for an office building in Shanghai

7.3.1 System description

Last section investigated the system performance of ejector cooling system under the influences of intermittent solar radiation. In the tropical rural areas of some developing countries, the weather is extremely hot during summer seasons and the solar energy is abundant over the year. However, because of the poor development in the electricity infrastructure, the access to electricity is hardly available. The combined power and ejector cooling system driven by solar energy would be much beneficial to such rural areas, which could provide both cooling and power with the abundant solar energy.

The performance of combined power and ejector cooling system was discussed in Chapter 6. This section mainly investigates the intermittent effects of solar radiation on the performance of the combined system.

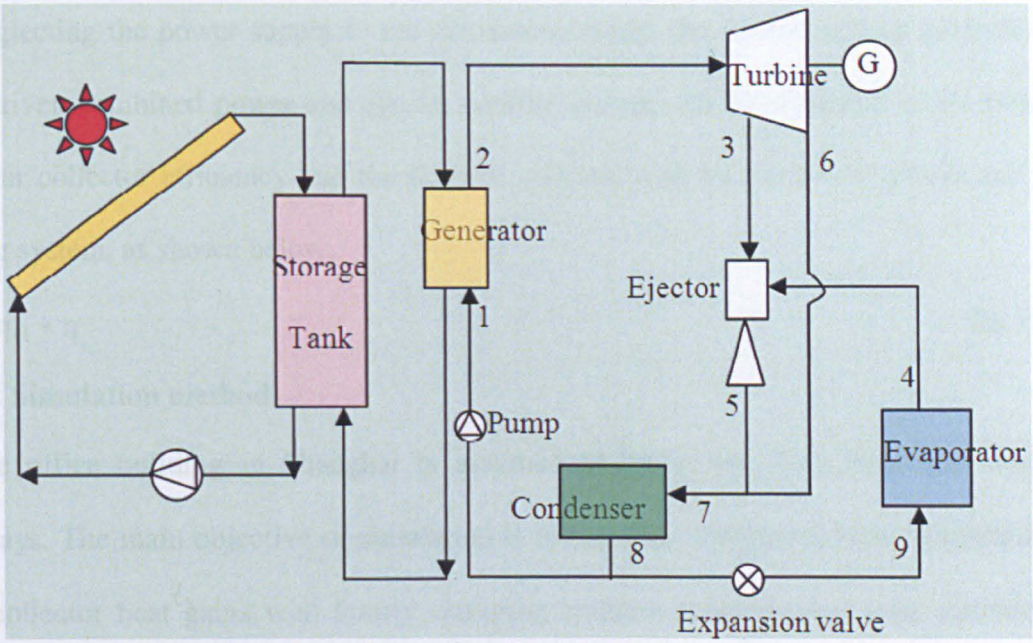

Figure 7-22 Schematic diagram of solar driven combined power and ejector cooling system

As shown in Figure 7-22, the whole system consists of two subsystems: the solar collector subsystem and the combined power and ejector cooling subsystem, of which the main connection is via a storage tank.

The working principle and governing equations of solar collector subsystem and combined power and ejector cooling subsystem have been discussed in section 7.2.1.1. and section 6.3.3.

7.3.2 Modelling of the solar-driven combined power and ejector cooling system

7.3.2.1 System performance

The solar-driven combined power and ejector cooling system is the combination of solar collector and combined power and ejector cooling system. The collector efficiency is defined in Eq. (7.2). For different types of solar collector, the collector efficiencies η_s are specified in Table 7-3. In Chapter 6, the thermal efficiency of combined power and ejector cooling system is defined as the ratio of the useful energy output to the total energy input, given by:

$$\eta = (W_{net} + Q_e)/Q_g \quad \text{Eq. (7.21)}$$

Where, W_{net} is the net mechanical work defined in Eq. (5.18), Q_e is the cooling output and Q_g is the total heat absorbed from the low temperature heat source in the vapour generator.

Neglecting the power supply to the circulation pump, the overall system performance of solar-driven combined power and ejector cooling system can be evaluated as the product of the solar collector efficiency and the thermal efficiency of the combined power and ejector cooling system, as shown below:

$$COP=\eta_{cl} * \eta \quad \text{Eq. (7.22)}$$

7.3.2.2 Simulation method

The office building in Shanghai is assumed to be in use from 8am-5pm during the weekdays. The main objective of simulation is to calculate the hourly tank temperatures and solar collector heat gains with hourly changing ambient temperatures, solar radiations and cooling loads. According to the energy balance in the tank (Eq. (7.8)), the collector hourly heat gain is affected by the tank heat loss (Eq. (7.6)), the required generator heat input for the combined system (Eq. (7.7)) and the tank temperature variation.

The simulation input parameters are solar radiation, the ambient temperature, the hourly cooling load, the volume of storage tank and the collector area. The time step for calculation is set to 1 hour, and the results are given with daily solution. The governing equations are described in section 7.2.1.1 for solar collector system and section 6.3.3 for combined power and ejector cooling system. The performance of the systems was modelled by a simulation programme written in EES (Engineering Equation Solver). The calculation flow chart can be found in Figure 7-23.

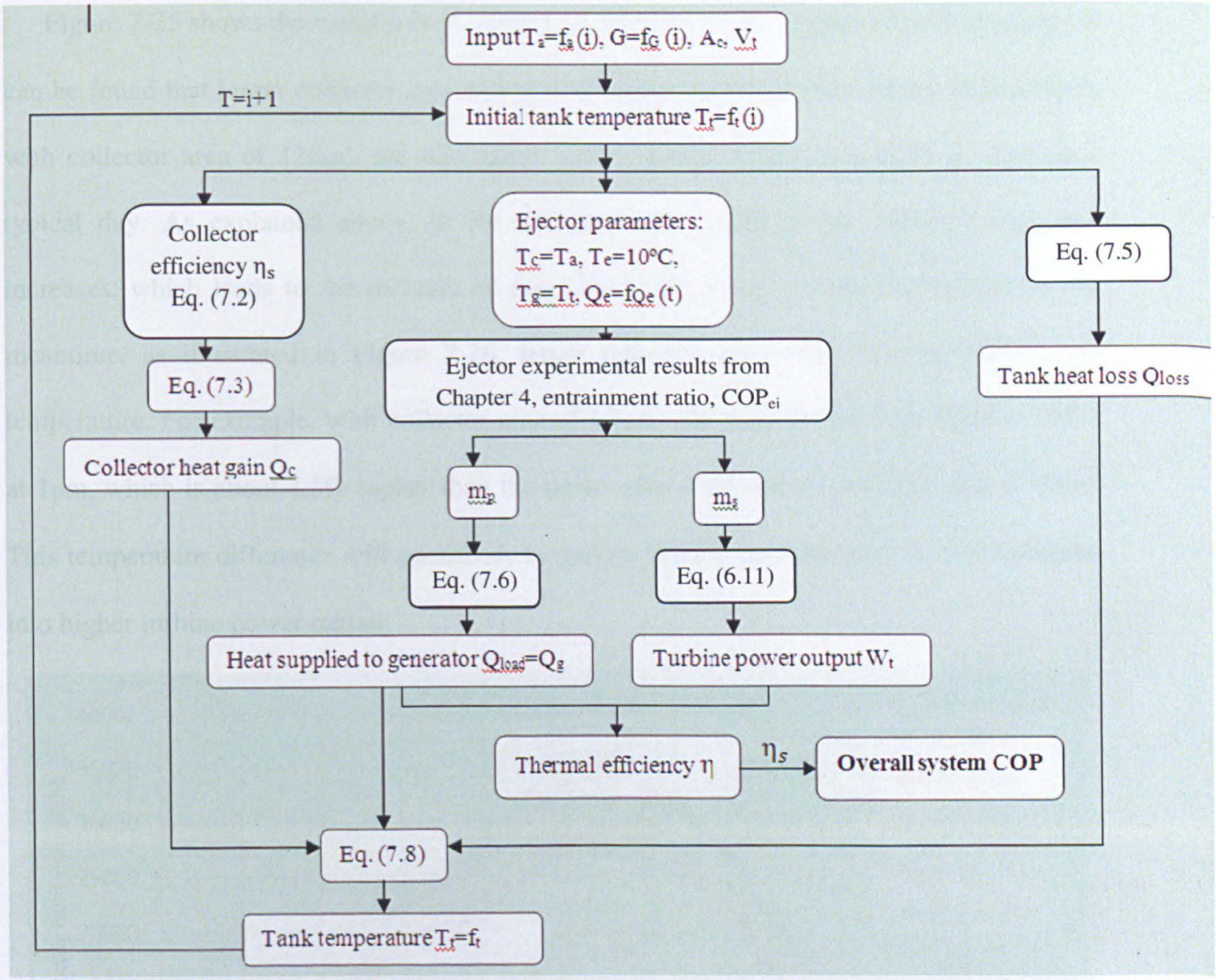

Figure 7-23 Calculation flow chart of solar driven combined power and ejector cooling system

7.3.3 Simulation results and discussions

7.3.3.1 The effect of solar collector area

For solar-driven combined power and ejector cooling system, with storage tank volume fixed at 1.0 m^3, solar collector area of various values (80m^2, 90 m^2, 100 m^2, 110 m^2 and 120 m^2) are investigated with respect to solar collector heat gains as shown in Figure 7-24. It is obvious that greater solar collector area will lead to higher heater gain. According to Eq. (7.3), when the collector area is fixed, the collector heat gain is mainly influenced by the solar radiation. Since the solar radiation normally reaches the peak value during the mid of the day, the maximum solar collector heat gain occurs around 11-12am in the day.

Figure 7-25 shows the variations of turbine power output with respect to collector areas. It can be found that larger collector area will lead to higher turbine power output. For instance, with collector area of $120m^2$, the maximum turbine power output is 4112W at 11am in a typical day. As explained above, as the collector area improves the collector heat gain increases, which leads to the increase of mass flow rate going through the turbine. In the meantime, as illustrated in Figure 7-26, larger collector area will result in higher tank temperature. For example, with collector area of $120m^2$, the tank temperature reaches 190°C at 1pm, which is about 4.5% higher than the peak value achieved by collector area of $80m^2$. This temperature difference will contribute to greater turbine inlet pressure, which translates into higher turbine power output.

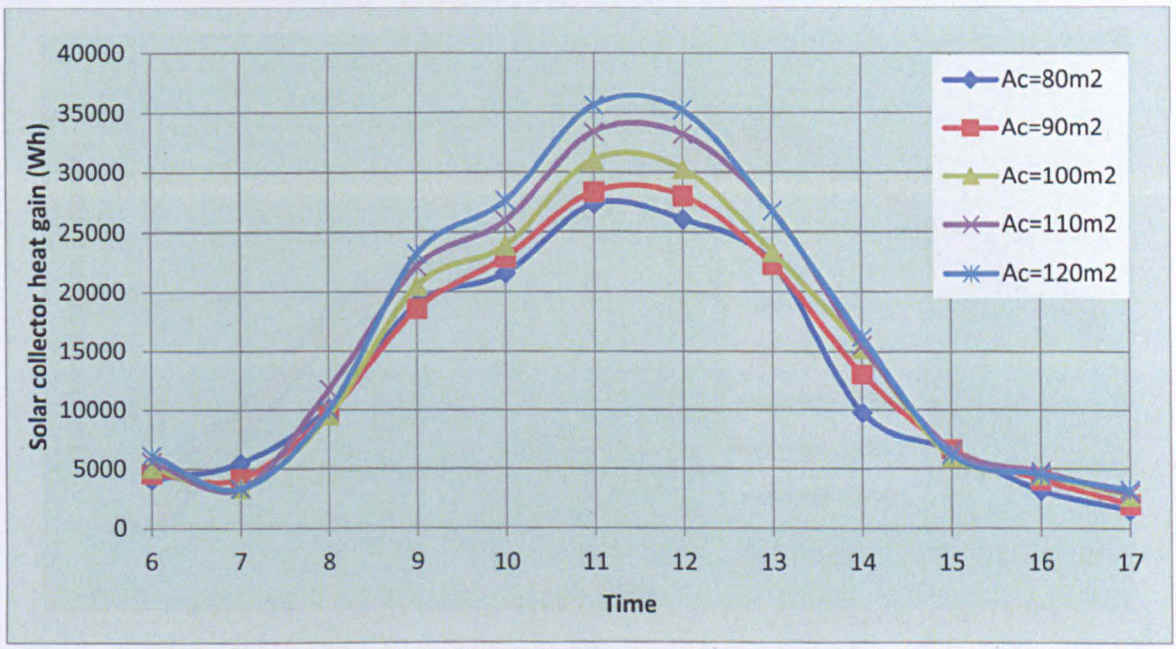

Figure 7-24 Variations of on hourly solar collector heat gain with respect to solar collector areas (V_{ta} =1.0m^3)

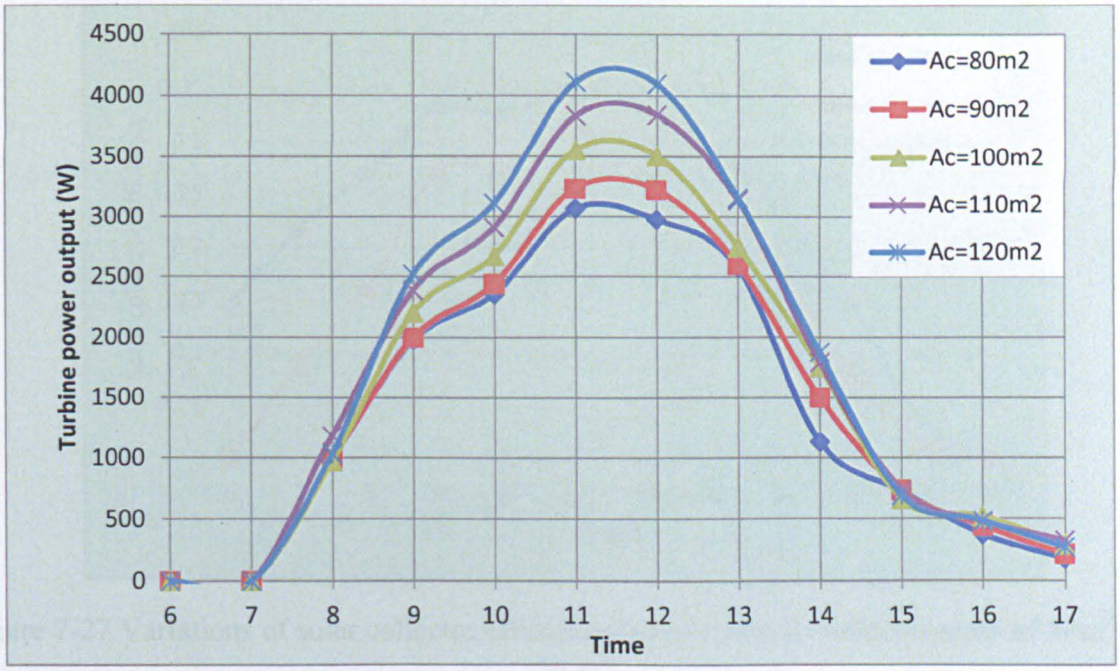

Figure 7-25 Variation of turbine power output with respect to solar collector area (V_{ta} =1.0m^3)

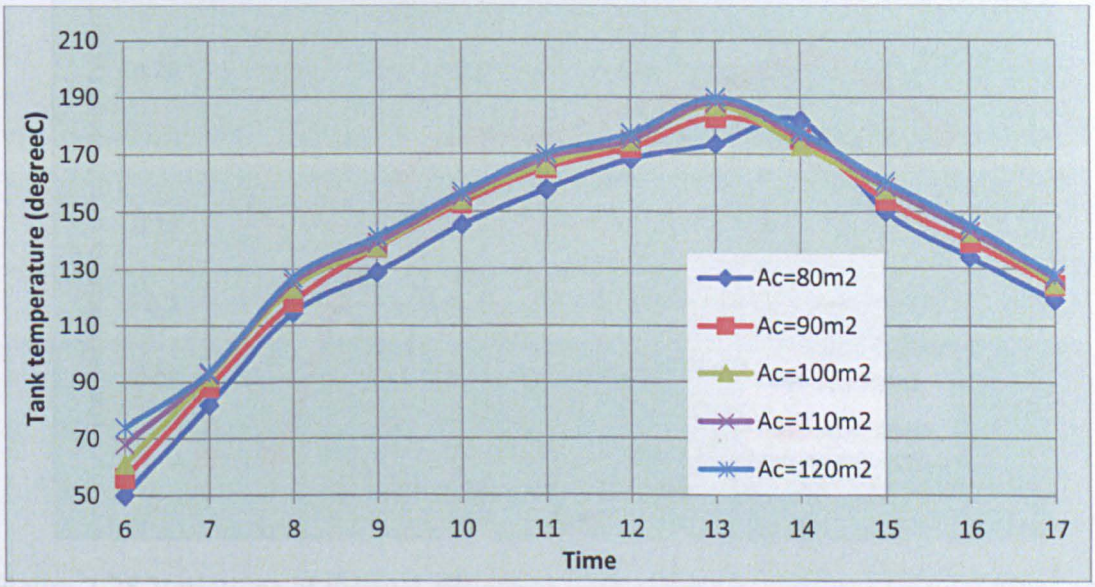

Figure 7-26 Tank temperature variations with respect to solar collector area (V_{ta}=1.0m^3)

The system performance of solar collector, combined power and ejector cooling system and the overall system are compared and shown in Figure 7-27 to Figure 7-29 with respect to collector areas of 80m^2 and 120 m^2. The effect of solar collector area on solar collector efficiency is shown in Figure 7-27. As concluded from Figure 7-26, larger collector area will accompany by higher tank temperature. According to Eq. (7.2), with all the other parameters being constant, higher tank temperature will contribute to lower collector efficiency.

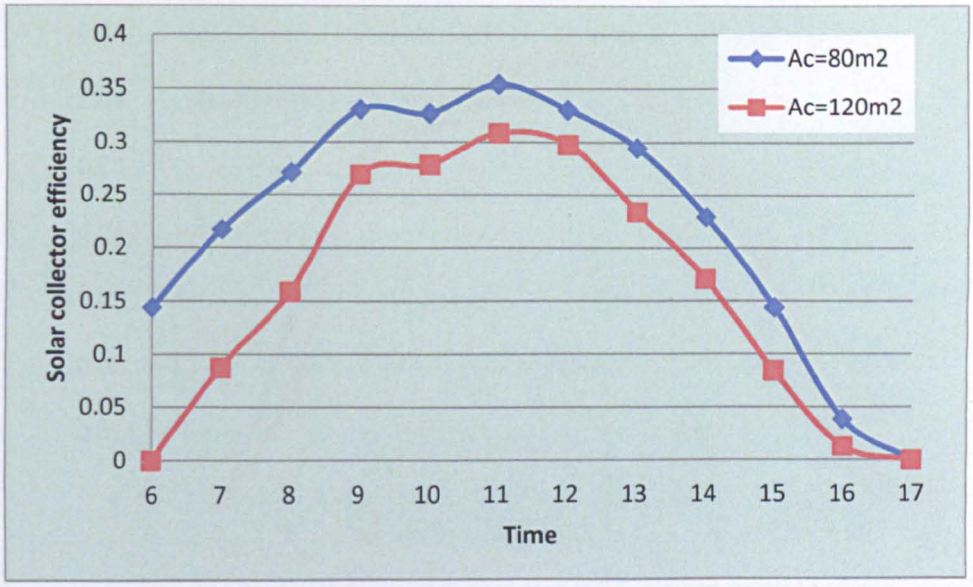

Figure 7-27 Variations of solar collector efficiency with respect to collector areas of 80m^2 and 120 m^2

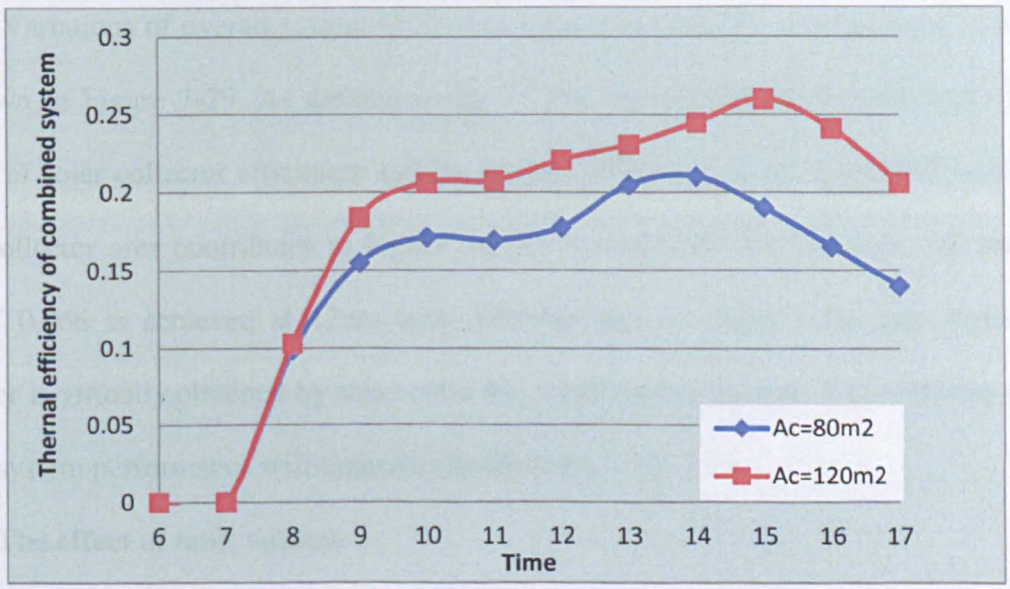

Figure 7-28 Variations of thermal efficiency with respect to collector areas of 80m^2 and 120m^2

Figure 7-28 illustrates the variations of thermal efficiency of the combined system with respect to collector areas. As defined in Eq. (7.21), the thermal efficiency of the combined system is the ratio between the useful energy output (cooling capacity Q_e and turbine power output) to the total energy input (generator heat input Q_g). It can be seen from Figure 7-28 that the thermal efficiency increases as the collector area increases from 80 m^2 to 120 m^2, mainly due to the reason that larger collector area leads to higher turbine output.

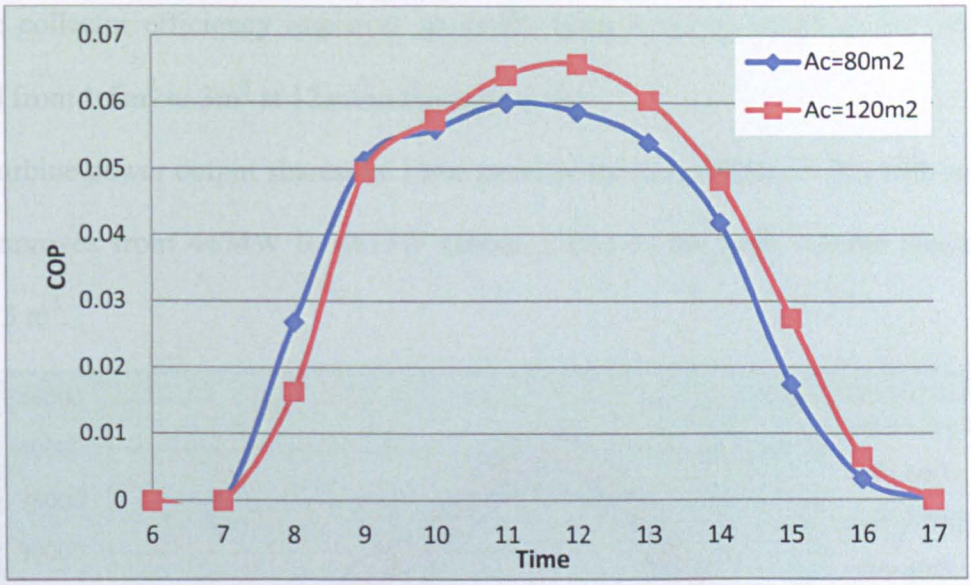

Figure 7-29 Variations of overall system COP with respect to collector areas of $80m^2$ and $120m^2$

The Variations of overall system COP with respect to collector areas of $80m^2$ and $120m^2$ are shown in Figure 7-29. As defined in Eq. (7.22), the overall system performance is the product of solar collector efficiency and the thermal efficiency of the combined system. The larger collector area contributes to higher overall system COP. For instance, the maximum COP of 0.066 is achieved at 12am with collector area of $120m^2$. The heat input to the generator is virtually obtained by solar collector, which is free energy. If considering this, the overall system performance will improve significantly.

7.3.3.2 The effect of tank volume

As discussed in section 7.2.3.2, the storage tank with larger volume needs to absorb larger amount of heat, which leads to reduced tank temperature compared with small tank volume. This will result in the improvement of solar collector efficiency (Eq. (7.2)), and consequentially contribute to larger collector heat gains (Eq. (7.4)). This can be proved by Figure 7-30 and Figure 7-31, which shows that the increase of tank volume will lead to slight increase of solar heat gains and solar collector efficiency. For instance, the peak heat gains increases from 37194W to 40386W (about 8.6%) as the tank volume increases from $1.5m^3$ to

$3m^3$. The collector efficiency improves gradually from 0.322 to 0.354 as the tank volume increased from $1.5m^3$ to $3m^3$ at 12am in the typical day.

The turbine power output shares the same trend as shown in Figure 7-32, with peak power output improves from 4474W to 4613W (about 3.1%) as the tank volume increases from $1.5m^3$ to $3\ m^3$.

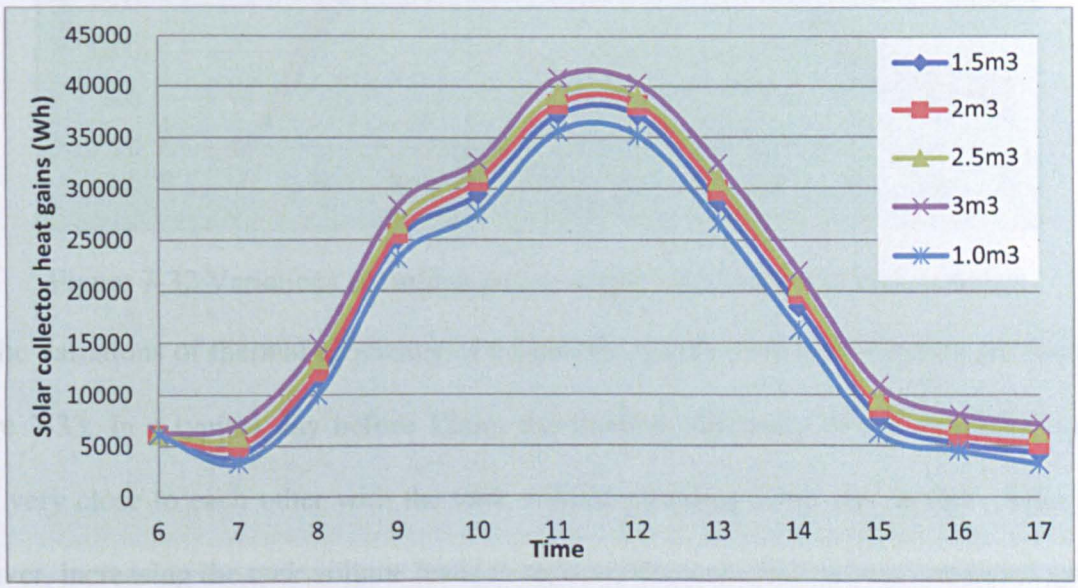

Figure 7-30 Variations of solar collector heat gains with respect to tank volumes

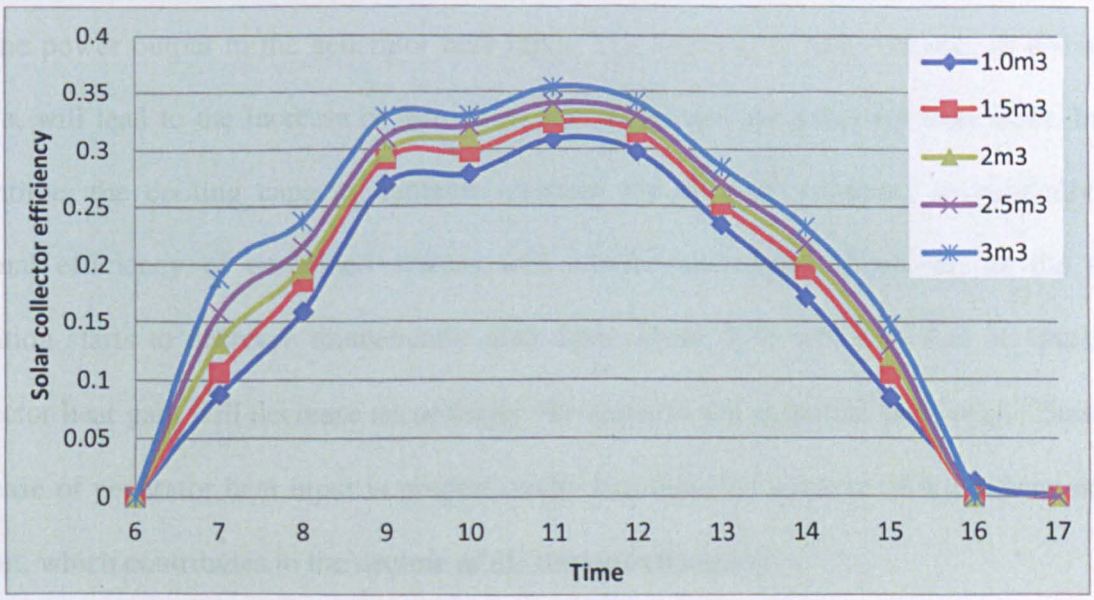

Figure 7-31 Variations of solar collector efficiency with respect to tank volumes

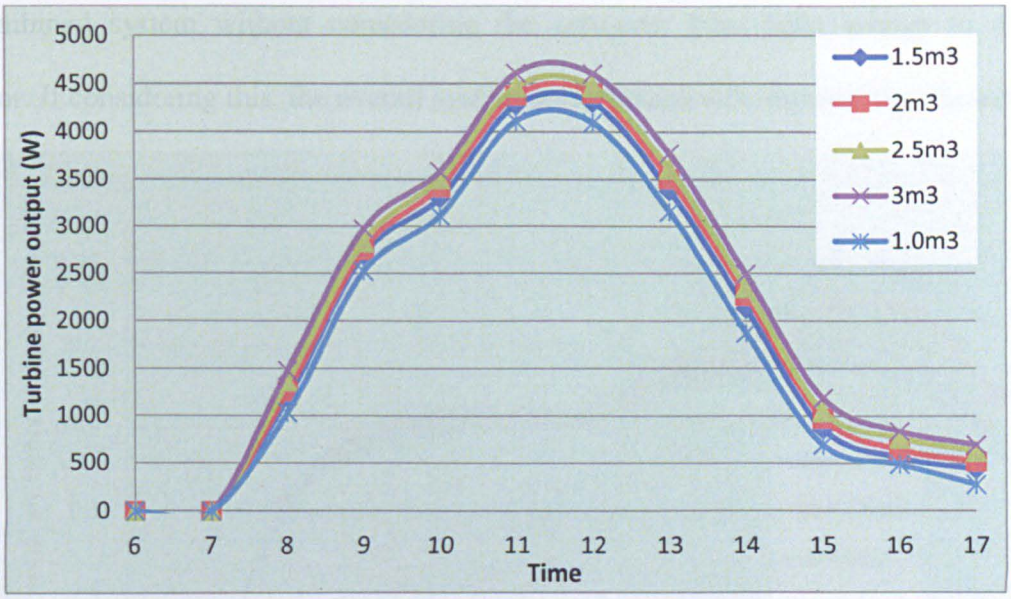

Figure 7-32 Variations of turbine power output with respect to tank volumes

The variations of thermal efficiency of combined system with tank volumes are shown in Figure 7-33. In a typical day before 12am, the thermal efficiency of the combined system stays very close to each other with the tank volume changing from $1m^3$ to $3m^3$. After 1pm, however, increasing the tank volume leads to reduced thermal efficiency of combined system. According to Eq. (7.21), thermal efficiency is defined as the ratio of cooling capacity and turbine power output to the generator heat input. The increase of tank volume, as discussed above, will lead to the increase of turbine power output and the generator heat input. In the meantime, the cooling capacity remains constant for all tank volumes, so generally the thermal efficiency of combined system will remain unchanged. However, as the solar radiation starts to decrease dramatically after 2pm (about 17% less than that at 1pm), the collector heat gain will decrease accordingly, the same as the generator heat input. Thus, the increase of generator heat input is proportionally less than the increase of the turbine power output, which contributes to the decline of the thermal efficiency.

Figure 7-34 shows the variations of overall COP with respect to various tank volumes. As defined in Eq. (7.22), the overall COP is the product of system performances of solar collector

and combined system without considering the zero-cost from solar energy to drive the generator. If considering this, the overall system performance will improve significantly.

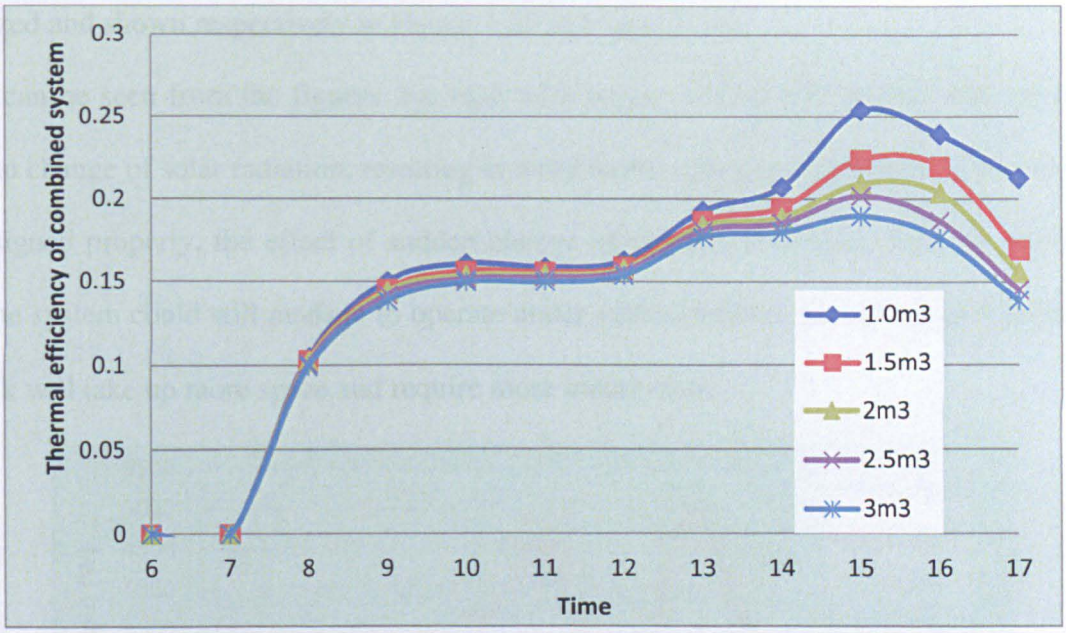

Figure 7-33 Variations of thermal efficiency with respect to tank volumes

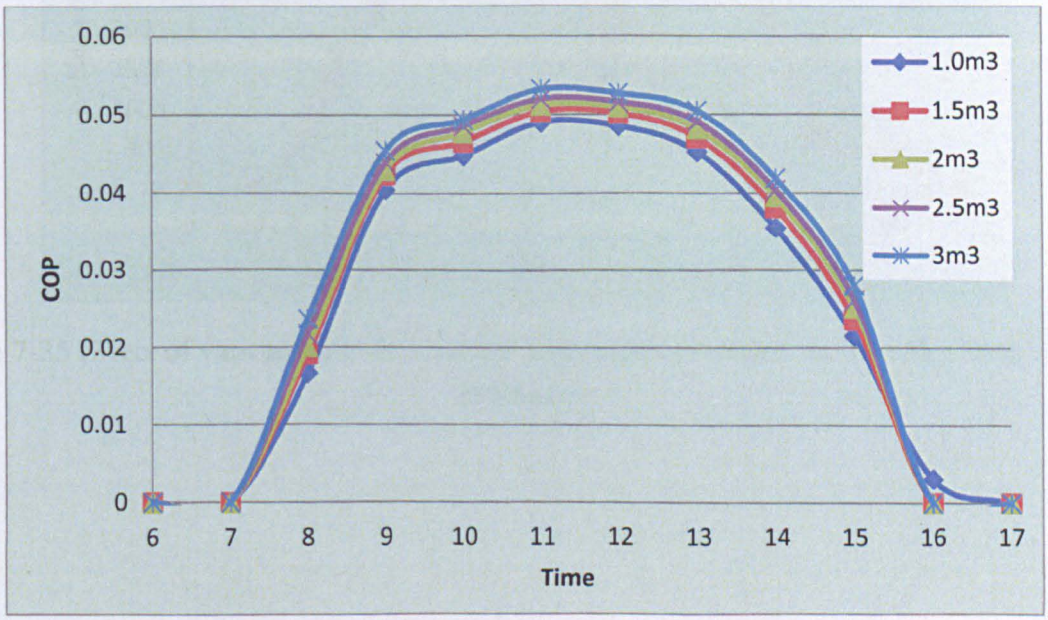

Figure 7-34 Variations of overall system performance with respect to tank volumes

7.3.3.3 System performance under a sudden change of solar radiation

The performance of solar driven system is greatly affected by the intermittent solar energy. Any sudden change of climatic conditions will influence the solar collector heat gains. Assuming a sudden reduce of solar radiation at 12am ($G=750w/m^2$), the effects of three

different tank sizes ($1.0m^3$, $2.5m^3$ and $5m^3$) with respect to turbine power output, solar collector efficiency, thermal efficiency of the combined system and overall system COP are analyzed and shown respectively in Figure 7-35 to Figure 7-38.

It can be seen from the figures that tank with larger volume will be less affected by the sudden change of solar radiation, resulting in more stable system performance. If the tank size is designed properly, the effect of sudden change of climatic condition could be minimized and the system could still manage to operate under such condition. However, such larger size of tank will take up more space and require more initial costs.

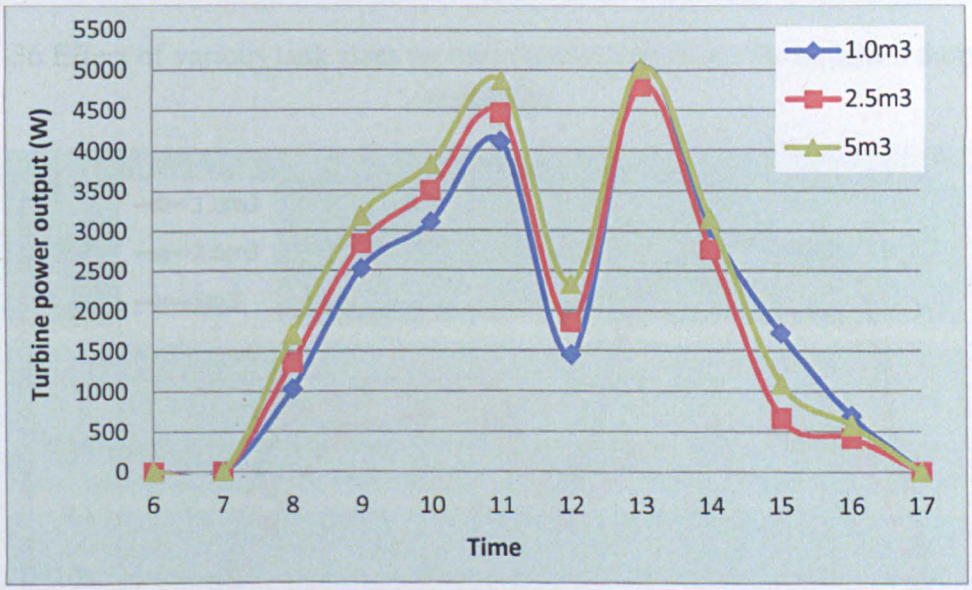

Figure 7-35 Effect of various tank sizes on the turbine power output for a sudden drop of solar irradiation

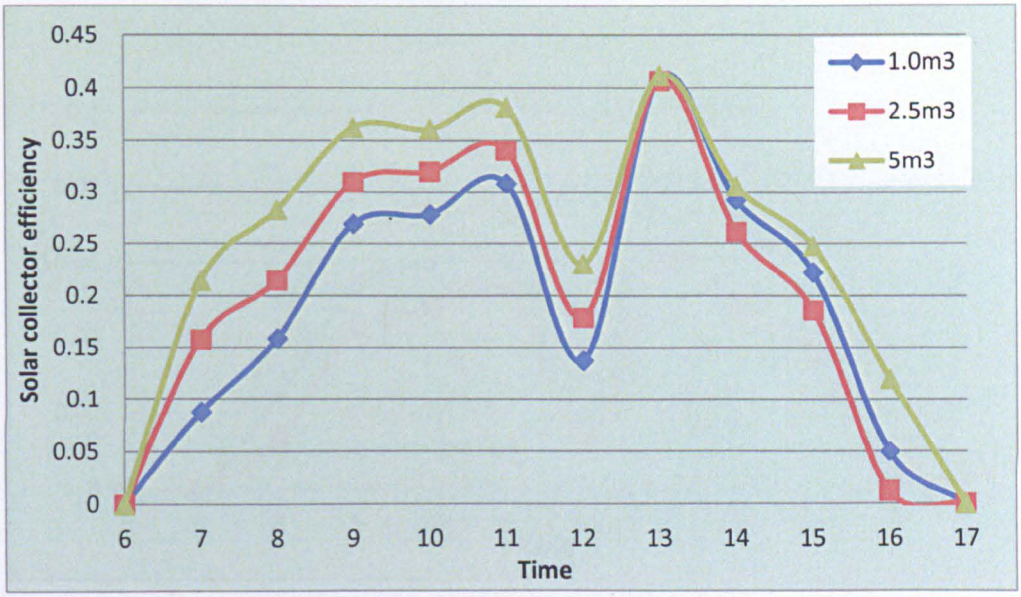

Figure 7-36 Effect of various tank sizes on the collector efficiency for a sudden drop of solar irradiation

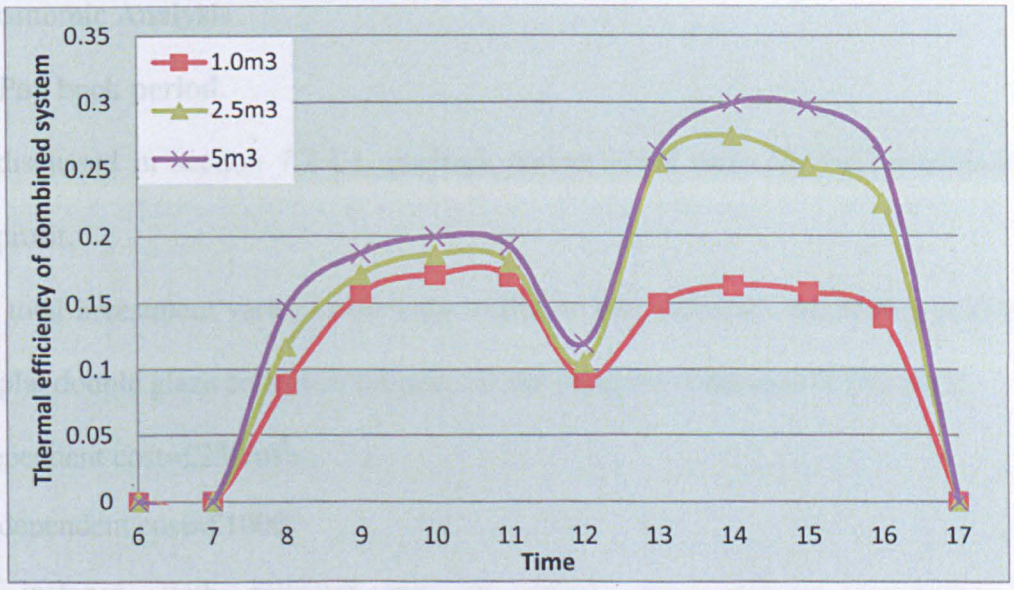

Figure 7-37 Effect of various tank sizes on the thermal efficiency of combined system for a sudden drop of solar irradiation

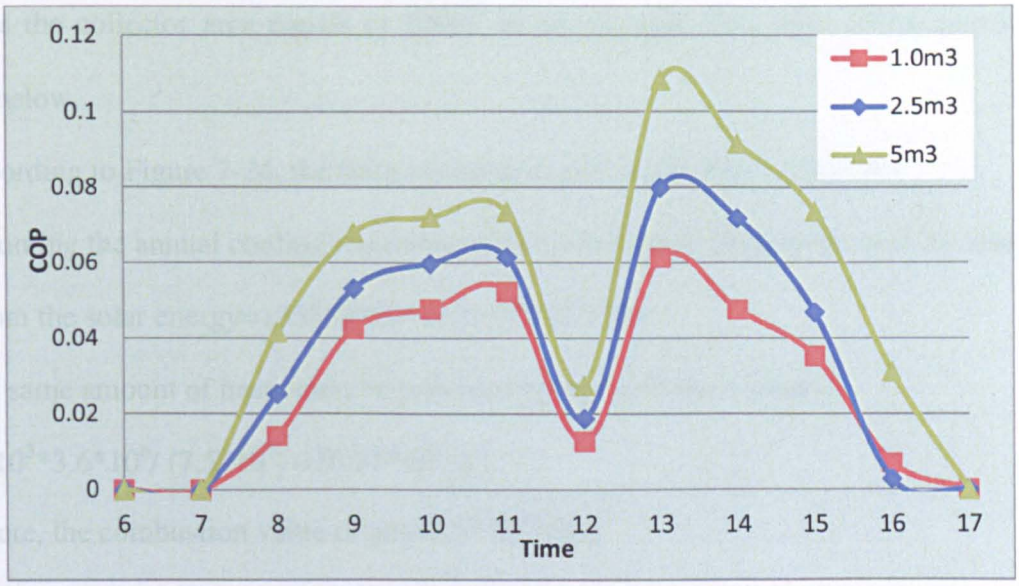

Figure 7-38 Effect of various tank sizes on the overall COP for a sudden drop of solar irradiation

7.3.4 Economic Analysis

7.3.4.1 Pay back period

As discussed in section 7.2.4.1, payback period is the ratio of total investment to the annual profit.

The total investment varies as the solar collector size increases. According to [140, 141], for flat plat double glaze collector, the price of the collector is the sum of two parts:

Area dependent cost=£250/m^2;

Area independent cost=£1000.

For instance, with collector area of 100m^2, the collector investment cost = 100*250+1000=£26000. The total investment cost= collector cost + ejector main component cost=£26000+£693=£26693.

The annual profit obtained from this system is mainly two parts: one is due to the utilizations of solar energy which can be calculated as gas savings in terms of solar collector heat gains. Another part is the power generated by combined power system. This can be used to provide electricity for the office building, which could be considered as an additional income to the system.

Take the collector area equals to $100m^2$ as an example, the solar saving calculation is shown below,

According to Figure 7-24, the daily useful heat gain is equal to 175559Wh.

Assuming the annual cooling requirements is from June to September, and the annual heat gain from the solar energy=$175559*30*4=21.07*10^3$kWh;

The same amount of heat could be provided by gas with the volume= $21.07*10^3*3.6*10^6/(7.5*10^7)=10.11*10^3\ m^3$;

Where, the combustion value of gas=$7.5*10^7$ J/Kg;

As the gas price is £0.72/m^3 (according to Shanghai gas price), such amount of gas=$10.11*10^3*0.72$=£728.

The power generation calculation is shown in the following,

According to Figure 7-25, the daily power output is equal to 18883W;

If considering the power generation efficiency of 30% for the small-scale turbine, the summer power generation=$18883*30\%*120/(3.6*10^6)$=1886kWh;

The electricity price is £0.245/kWh (according to Shanghai electricity price), therefore the total annual power income=1886*0.245=£462.

Hence, the payback period of different sizes of solar collector are calculated and shown in Table 7-12. It could be found that payback period increases from 20 to 23 years as the collector area increases from $80m^2$ to $120m^2$. The average payback period is 22.2 years. This means that although the initial investment cost is high, the system is still worth investing as the profit will eventually meet with the investment after a life cycle.

Table 7-12 Summary of payback period for various collector areas

Collector Area (m^2)	Investment Cost (£)	Annual profit (£)	Payback period (year)
80	21693	1039	20.8
90	24193	1108	21.8
100	26693	1190	22.4
110	29193	1300	22.4
120	31693	1343	23.5

7.3.4.2 Life cycle saving method description

The same as section 7.2.4, Life Saving Analysis is employed for economic analysis. Most of the calculation methods and the parameters definition are the same as described previously. The only difference lies in that the generated power from solar driven combined power and ejector system is considered as an additional income for the system. Excel document is applied to calculate the life cycle saving, with the life cycle of 20 years. The Excel spreadsheet is divided into two areas, the input parameters area and the calculation area. The parameters used in the calculation are shown in Table 7-13.

With reference to Table 7-13, for collector area of $100m^2$, by multiplying the area dependent cost with the solar collector area will give a cost related to the size of the system.

The analysis is performed annually, as shown in Table 7-14, for which the following amounts are calculated:

Gas savings (column B)

Power generation income (Column C)

Both of these two calculations could be found in section 7.3.4.1

The calculations in other columns are preceded in the same ways as in section 7.2.4.

Table 7-13 Lists of input parameters

Input parameters	Value	Units
Ejector main component cost	693	£
First year gas savings	728	£
Gas inflation rate	7	%
First year power generation income	462	£
Power inflation rate	7	%
Collector area	100	m2
Area dependent cost	250	£/m2
Area independent cost	1000	£/m2
Annual market discount rate	8	%
Maintenance in first year	2	% of total system cost
Annual increase in maintenance	2	%
Pump electrical load	1.08	kW
Operation hours	3600	hours
Price of electricity	0.245	£/kWh
Annual increase in electricity cost	3	%
Down payment	20	%
Resale value	20	%
PWF for mortgage payment	9.1285	

7.3.4.3 Solar-driven combined power and ejector cooling system example

Solar-driven combined power and ejector cooling system with collector areas of 100 m^2 is considered. The proposed collector area and associated equipment will supply energy equivalent to £728 in the first year, and the power generated by the turbine will bring in £462 income. The total cost of the equipment will be £26693 and is to be 80% financed over 20

years at an interest rate of 9%. The mortgage that has to be paid during 20 years is equal to the borrowed amount by the present worth factor, which is £636.78. Gas costs are expected to rise at 7% per year. It is expected that the equipment will have a resale value at the end of 20 years of 20% of original cost. The power consumption of the solar circulation pump is 1.08kW and is estimated to work for 3600 hours per year. The price of the electricity cost is £0.245/kWh and its price is expected to rise at 3% per year. Finally the market discount rate is 8%.

Table 7-14 Economic analysis calculation example for collector area=100 m^2 (units: pound)

A	B	C	D	E	F	G	H	I	J	K
Year	Gas saving	Power income	Extra mortgage payment	Extra mainte -nance cost	Extra parastic cost	Solar savings	PW of solar savings	Supplementary information		
								Mortgage	interest	Remaining
0					Down payment	-5338.6	-5338.6			21354.4
1	728.00	462.00	-2278.58	520.00	-68.20	-636.78	-589.61	2278.58	1872.00	20393.42
2	778.96	494.34	-2278.58	530.40	-70.25	-545.12	-467.36	2278.58	1835.41	19950.25
3	833.49	528.94	-2278.58	541.01	-72.35	-447.49	-355.23	2278.58	1795.52	19467.20
4	891.83	565.97	-2278.58	551.83	-74.52	-343.47	-252.46	2278.58	1752.05	18940.67
5	954.26	605.59	-2278.58	562.86	-76.76	-232.63	-158.32	2278.58	1704.66	18366.75
6	1021.06	647.98	-2278.58	574.12	-79.06	-114.48	-72.14	2278.58	1653.01	17741.18
7	1092.53	693.34	-2278.58	585.60	-81.43	11.46	6.69	2278.58	1596.71	17059.30
8	1169.01	741.87	-2278.58	597.32	-83.88	145.74	78.74	2278.58	1535.34	16316.06
9	1250.84	793.80	-2278.58	609.26	-86.39	288.93	144.54	2278.58	1468.45	15505.93
10	1338.40	849.37	-2278.58	621.45	-88.99	441.65	204.57	2278.58	1395.53	14622.89
11	1432.09	908.82	-2278.58	633.88	-91.66	604.55	259.28	2278.58	1316.06	13660.37
12	1532.33	972.44	-2278.58	646.55	-94.40	778.35	309.09	2278.58	1229.43	12611.22
13	1639.60	1040.51	-2278.58	659.49	-97.24	963.78	354.38	2278.58	1135.01	11467.66
14	1754.37	1113.35	-2278.58	672.68	-100.15	1161.66	395.50	2278.58	1032.09	10221.17

15	1877.17	1191.28	-2278.58	686.13	-103.16	1372.85	432.78	2278.58	919.91	8862.50
16	2008.57	1274.67	-2278.58	699.85	-106.25	1598.27	466.52	2278.58	797.62	7381.54
17	2149.18	1363.90	-2278.58	713.85	-109.44	1838.90	497.00	2278.58	664.34	5767.30
18	2299.62	1459.37	-2278.58	728.13	-112.72	2095.81	524.48	2278.58	519.06	4007.78
19	2460.59	1561.53	-2278.58	742.69	-116.11	2370.12	549.19	2278.58	360.70	2089.90
20	2632.83	1670.84	-2278.58	757.54	-119.59	2663.04	571.35	2278.58	188.09	-0.58
Sum					Resale value	5200	1115.65			
					Total PW of solar savings		-1185.38			

7.3.4.4 Solar-driven combined power and ejector cooling system optimization example

The system optimization is carried out by employing different collector areas in Excel spreadsheet and by plotting the PW of the solar savings against the collector area. The optimum collector area, i.e, the area at which the solar savings is at maximum value, can then be determined. Table 7-15 shows the gas savings, power generation income with respect to various collector areas. By inserting various collector area values, the calculation can be repeated accordingly. And the results of the optimisation are shown graphically in Figure 7-39 and Figure 7-40.

For interest rate of 9% and market discount rate of 8%, the life cycle savings of the combined power and ejector cooling system with collector area of 80-120m^2 are all negative values. This means that over 20 years' life cycle, the income from the system (gas savings+ power generation income) could not meet up with the initial investment cost. Thus, compared with the life cycle analysis applied for solar-driven ejector cooling system in section 7.2.4, the solar-driven combined power and ejector cooling system is less competitive from economic points of view.

However, this conclusion is based on many assumptions. For instance, the electricity rate for the power generation income calculation is the same rate as that supplied by national grid in Shanghai. If considering from sustainable energy point of view, the government could wish to promote this application. Thus the rate of the electricity generated by the combined system would be higher than current value, and the total savings across the lift cycle would be increased. Similarly, with decades of development and improvement in the technology of solar collector production, the initial cost of the collector would drop down gradually. Moreover, since the results are greatly affected by the market discount rates and interest rates. It could be interesting to analyze the optimization results in relationship to these rates, which are shown graphically in Figure 7-39 and Figure 7-40. It could be found that lower interest rates and market discount rates will always yield to higher life cycle savings. With interest rates lower than 7.5% and market discount rate lower than 6.5%, it would be economically viable to use collector area of $90m^2$, which yields a positive life cycle savings. Hence, the total life cycle savings are significantly influenced by the technology development and changing market conditions.

Table 7-15 Collector area related parameters for system optimization

Collector area(m^2)	Gas savings(£)	Power generation income (£)	Pump power(kW)
80	652	387	0.78
90	682	426	0.9
100	728	462	1.08
110	796	504	1.23
120	821	522	1.42

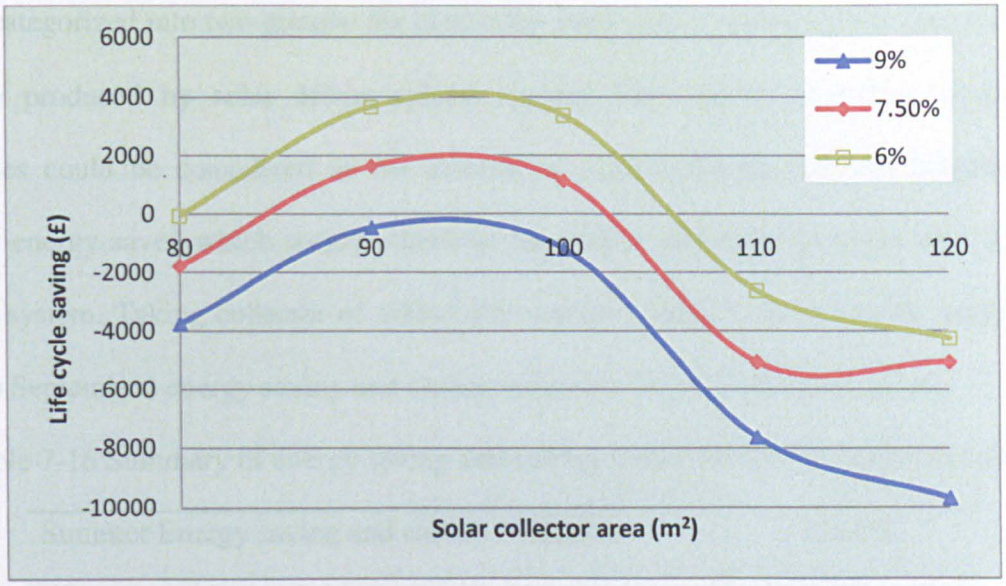

Figure 7-39 Life cycle savings with various interest rates

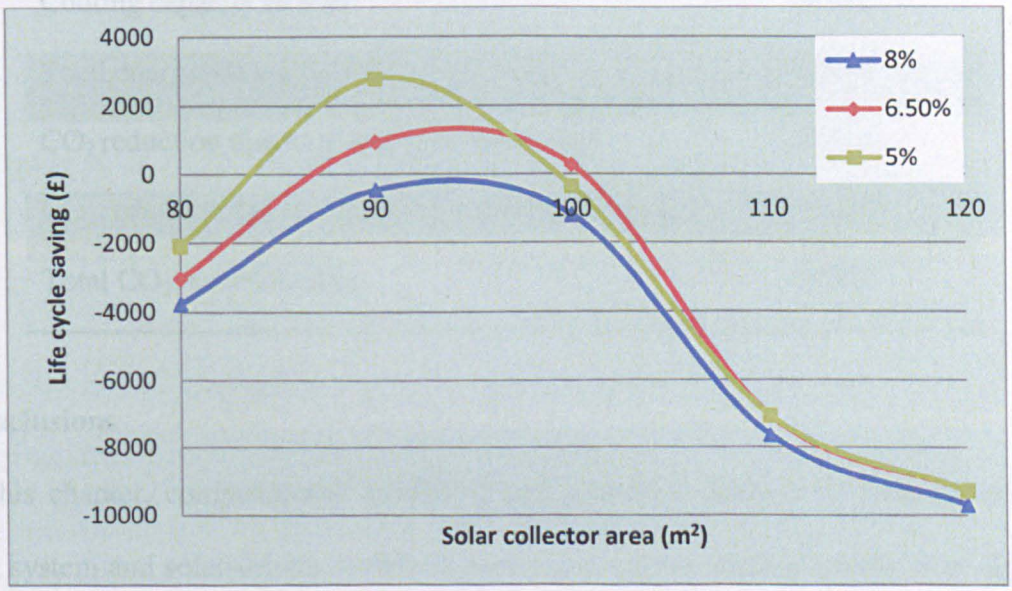

Figure 7-40 Life cycle savings with various market discount rates

7.3.5 Energy saving and carbon reduction

Compared the optimisation result of solar driven combined power and ejector system with that of solar driven ejector cooling system (discussed in section 7.2), it is obvious that solar driven combined power and ejector system requires larger size collector. This will cause larger installation costs, but also rewarded with higher savings throughout the life cycle.

As larger size collector is able to provide abundant heat input for the combined system, no additional auxiliary heater will be required. The overall energy saved by the combined system

can be categorized into two groups: the electricity generated by steam turbine and the cooling capacity produced by solar driven ejector system. The carbon reduction of these two categories could be considered as the amount of carbon dioxide reduced because of the primary energy saved which would otherwise be used to generate electricity and power the cooling system. Taking collector of $100m^2$ for example, Table 7-16 shows the summer time (June to September) energy saving and carbon reduction for the combined system.

Table 7-16 Summary of energy saving and carbon reduction for the combined system

Summer Energy saving and carbon reduction	Amount
Power generation (kWh)	1888.6
Cooling capacity (kWh)	2915.6
Total energy saving (kWh)	4804.2
CO_2 reduction due to power generation (kg)	2001.9
CO_2 reduction due to the ejector cooling effect (kg)	1164.8
Total CO_2 reduction (kg)	3166.7

7.4 Conclusions

In this chapter, computational modelling and economic analysis of solar-driven ejector cooling system and solar-driven combined power and ejector cooling system were developed based on climatic conditions of Shanghai, China. The system performances (solar fraction, overall thermal efficiency and turbine power output) of the two systems were evaluated respectively under various collector areas, storage tank sizes and storage tank temperatures. The following conclusions can be obtained:

Solar collector system with larger collector area will lead to higher useful heat gain from solar energy, less auxiliary heat input and higher solar fraction. However, this has to be compromised with greater equipment costs. For solar-driven combined power and ejector

cooling system with collector area of $80m^2$ and storage tank volume of $1m^3$, the peak turbine work output was 3000W at 11pm and the maximum thermal efficiency was 0.2 at 1pm.

The increasing of storage tank volume helps to the improve the solar collector efficiency and increase the collector heat gains, which generally leads to higher thermal efficiency of combined system and larger turbine work output. Smaller storage tank size results in higher tank temperature, which might be beneficial to the COP of ejector cooling system. Considering the transient features of solar energy, storage tank with smaller size would lead to larger temperature fluctuation in the tank, which greatly influences the proper operation of the ejector system. Therefore, the tank size has to be properly designed according to the local weather and climatic conditions.

Economic analysis has been implemented in order to optimise the system. The initial investment cost of single ejector cooling system is estimated to be £1213.3. The payback periods were 19–26 years and 20-23 years respectively for solar-driven ejector cooling system without and with power generation. The life cycle savings of these two systems for various collector areas were evaluated. For solar-driven ejector cooling system without and with power generation, the economically viable solution is to use collector area of $30m^2$ and $90m^2$ respectively, which yielded the maximum life cycle savings. Comparing solar driven ejector and vapour compression systems, the life cycle costs of solar driven ejector system is about 1.6 times than that of vapour compression system.

The environmental impacts of the two systems have been discussed as well. Compared with conventional R410a air conditioning system, solar-driven ejector cooling system did not contribute to the release of HFC refrigerants. During 20 years' life cycle, the total equivalent warming impact of a solar-driven ejector cooling system was 14305.6kg CO2, which was about 38% of that from a conventional R410a air conditioning system. For the solar-driven combined power and ejector cooling system, the annual energy saving was 10763.5kWh,

which was equivalent to 3058.9kg of CO_2 emission avoidance. Hence, in terms of environmental impact, the characteristics of energy saving and carbon reduction make the solar driven ejector cooling systems more competitive than other air conditioning systems.

Chapter 8 Conclusions and Future Works

8.1 Conclusions

This research works investigated various kinds of ejector cooling systems, which can supply cooling effects in sustainable ways. Simulations were conducted on a single ejector cooling system in order to analyze the effects of various working conditions on the system performance. Experimental investigations were carried out on the ejector cooling system under different generator, evaporator and condenser temperatures. The effects of nozzle exit planes on the system performance were also evaluated. The experimental results are compared and verified with simulation outcomes.

The innovations of the research works lie on two sides, the cold side (evaporator) and the hot side (heat source). From the cold side, the aim is to investigate the possibility of storing the excessive cold energy from the evaporator, and re-use it whenever required. A case study of a hybrid ejector and CO_2 vapour compression system was presented, with the aim to explore the potential of sub-cooling vapour compression system with the help of the ejector. From the hot side, explore the possibility of utilizing low grade energy (such as solar energy) to drive the ejector. In the rural tropical area where the solar energy is abundant throughout the year and the electricity generation capacity is very low, a solar-driven combined power and ejector cooling system could be applied to offer both electricity and cooling effect.

8.1.1 Computer simulations on the ejector cooling system and a case study

Thermodynamic simulations were carried out on ejector cooling system based on 1-D simplified model. Five different refrigerants (water, methanol, ethanol, HFE7000 and HFE7100) were compared to identify the most appropriate working fluid for use in the ejector system. Under the same working conditions, HFE fluids demonstrated the highest COP, followed by methanol and ethanol, and water as last. However, due to high GWP (GWP>150),

HFE fluids were unacceptable for cooling system. Because of the toxic, explosive and flammable features of methanol, it was phased out as well. Ethanol was much less toxic and flammable and had superior properties to water. Water was the safest but had the poorest performance and would require large heat transfer area, with the subsequent increase in weight and reduction in space. It was concluded that for small scale cooling system, water could be used successfully. But for higher cooling requirements ethanol would be a better candidate.

The effects of various operating conditions on the ejector system performance were studied numerically. The system COP varied at different operating conditions. At evaporator temperature of 10°C, condenser temperature of 35°C and generator temperature of 120°C, the COP of the ejector system was estimated to be larger than 0.45. For a designed ejector cycle, any increase in generator temperature and evaporator temperature and decrease in condenser temperature would lead to the improvement in entrainment ratio, and hence higher system COP.

A case study of a novel hybrid ejector and CO_2 vapour compression system was performed. The purpose was to utilise the waste heat from exhaust gas and the vapour compression sub-system to drive the ejector system, whose cooling effect will be employed to sub-cool the vapour compression sub-system. Thermodynamic simulations of two sub-systems and the hybrid system were presented. The results showed that, at boiler temperature of 120°C, evaporator temperature of 10°C, COP of the hybrid system was 0.584, i,e about 22% improvement compared with COP of 0.479 for single ejector cycle. Exploitation of the energy consumption ratio between ejector sub-system and CO_2 VC sub-system indicated that as the energy extracted from the exhausted gases increased, the performance of the CO_2 VC sub-system improved, and hence higher cooling effect.

8.1.2 Experimental investigations on ejector cooling system

Laboratory evaluations of the ejector cooling system were carried out with boiler temperatures between 115°C and 130°C, and evaporator temperatures between 5°C and 10°C. For a given boiler temperature, an increase in evaporator temperature improved the system performance and produced a higher critical condenser pressure. With boiler temperature of 120°C, 36.8% COP improvement could be achieved when evaporator temperature was increased from 5°C to 10°C. This further proved that in the hybrid system, the ejector operating in higher evaporator temperature would contribute to the improvement in overall system performance.

For a given constant evaporator temperature, increasing the boiler temperature resulted in a reduction in COP but an increase in critical condenser pressure. At evaporator temperature of 5°C, with 10°C increase of boiler temperature from 120°C to 130°C, COP decreased by 30.8% whilst critical condenser pressure increased by 20%.

Two different nozzle exit position (NXP=0 and NXP=4.4mm) were investigated with respect to the system performance. It was found that nozzle exit position only had a small influence on the system performance. When nozzle was positioned 0.44mm further inside the mixing chamber, 6% COP variations were obtained.

The measured COPs of the system from experiments were in the range of 0.2 to 0.5, which were approximately 85% compared with the simulation results. In order to eliminate the discrepancies between experimental and theoretical results, a three dimensional model which considering the friction losses and the dynamic mixing process should be applied. A more accurate pressure sensor should be used in the test to minimize the test uncertainty.

8.1.3 Experimental investigations on PCM cold storage system integrated with ejector cooling system

Experimental investigations were conducted on the PCM cold storage system integrated with ejector cooling system. The PCM container, coupled with the evaporator, could store the excessive cooling capacity of the ejector and release it when the heat input is not sufficient. Cold storage charging and discharging processes were performed with various mass flow rates, at the heat transfer fluid inlet temperatures of 5°C and 25°C respectively.

The integration of PCM cold storage with ejector cooling system could not improve the system performance of the ejector. However, it can help to maintain a more stable evaporator temperature, and thus a more reliable ejector system performance.

In order to analyze the heat transfer enhancement, finned tube and straight tube were studied and compared as two different heat exchangers between PCM and the HTF. The experimental results of charging mode indicated that during latent heat storage process, the charging period of PCM container with finned tube was 20% less than that of straight tube. At the flow rate of 0.2l/min, the cold storage rate of finned tube was 0.028kW, which was 56% higher than that of the straight tube. Hence, finned tube configuration was more effective than the straight tube configuration in terms of improving heat transfer.

The effectiveness-NTU method was applied for characterizing the tube-in-container PCM storage system. The testing results indicated that an increase in the mass flow rate would lead to the decrease of the storage effectiveness. The correlation of effectiveness as the function of ratio m^*/A was derived from experimental data, and was used as a design parameter for the PCM cold storage system. The equations can only be validated for maximum fin distance of 25mm, which suited the design condition in this experiment. For larger container, this equation will underestimate the heat transfer performance where the effect of natural convection is expected to increase.

8.1.4 Combined power and ejector cooling system

Two different configurations of combined power and ejector cooling system were experimentally investigated. Although the steam turbine was not perfectly matched with the electric boiler and the ejector cooling system, a maximum of 53W power output was obtained at boiler temperature of 132°C. In order to explore the possibility of using the low grade energy (temperature in the range of 110°C-170°C) to drive the turbine and ejector cooling system without any additional heater, a novel configuration was presented and the computer simulation was carried out.

The system performance of the five different working fluids were compared at heat source temperature of 120°C, evaporator temperature of 10°C and condenser temperature of 35°C. Methanol showed the highest thermal efficiency (0.195), while water demonstrated the highest turbine work output (1463W).

For the five compared working fluids, an average 10% of thermal efficiency improvement could be achieved when the turbine expansion ratio increased from 1.5 to 7. In the meantime, significant improvements (3-3.5 times) of turbine work output could be notified with water, methanol and ethanol as the working fluids.

When the condenser temperature increased from 30°C to 40°C, the thermal efficiency of the combined system reduced approximately by 40% and the turbine work output decreased by about 60%. This indicates that if the ambient temperature goes beyond the design condition (35 °C), the performance of the combined system will drop dramatically.

When the evaporator temperature increased from 5°C to 15°C, the thermal efficiency of the combined system improved significantly (average 60% for the five working fluids), while the turbine work output decreased by about 50%. Hence, the evaporator temperature has to be selected properly in order to guarantee the thermal efficiency and the turbine work output at the designed conditions.

8.1.5 Solar-driven ejector cooling system with and without power generation

Computational modelling and economic analysis of the solar-driven ejector cooling system and solar-driven combined turbine and ejector cooling system have been developed based on climatic conditions of Shanghai.

Solar collector system with larger collector area would lead to higher useful heat gain from solar energy, less auxiliary heat input and higher solar fraction. However, this had to be compromised with greater equipment costs. For the solar-driven combined power and ejector cooling system with collector area of $80m^2$ and storage tank volume of $1m^3$, the peak turbine work output was 3000W at 11pm and the maximum thermal efficiency was 0.2 at 1pm.

The increasing of storage tank volume would help to improve the collector heat gain, which leaded to higher thermal efficiency of combined system and larger turbine work output. Considering the intermittence of solar energy, storage tank with smaller size would result in temperature fluctuation in the tank, which influenced the proper operation of ejector system. Therefore, the tank size has to be properly designed according to the local climatic conditions.

Economic analysis was implemented in order to optimise the system. For solar-driven ejector cooling system without and with power generation, the economically viable solution was to use collector area of $30m^2$ and $90m^2$ respectively, which yields the maximum life cycle saving.

The environmental impacts of the two systems were discussed. During 20 years' life cycle, the total equivalent warming impact of the a solar-driven ejector cooling system was about 14305.6kg CO_2, which was about 38% of that from a conventional R410a air conditioning system. For the solar-driven combined power and ejector cooling system, the annual energy saving was 10763.5kWh, which was equivalent to 3058.9kg of CO_2 emission avoidance. Hence, in terms of environmental impact, the characteristics of energy saving and carbon

reduction make the solar driven ejector cooling systems more competitive than conventional air conditioning systems.

8.2 Potential improvement and future works

The ejector cooling system was proved to function well during the experiments. The test results being lower than the theoretical values indicated that in the simulation process, instead of using 1-D model with ideal fluid assumptions, 3-D model which considering the friction losses and the dynamic mixing process should be applied. This refinement could provide more accurate simulation results, which is helpful for ejector system design.

The simulation of the hybrid ejector and CO_2 vapour compression system demonstrated that with the help of ejector to sub-cool the vapour compression system, the performance of the two sub-systems improved significantly compared with single cycles. It would be worth building the prototype of the hybrid system and experimentally analyze the feasibility and working mechanism of these two sub-systems. If the hybrid system proves to work properly during the tests, economic analysis and manufacturing studies should be followed on. As the hybrid system is designed to be driven by vehicle exhaust gases, one possible application is to design the system miniature and explore the possibility of implementing it into the transport system. Since the temperature and quantity of the vehicle exhausts depends greatly on the vehicle moving speed, which is always changing during the journey. The key research challenge is how to match the ejector with the changing vehicle speed to provide stable and reliable cooling effect.

Two configurations of combined power and ejector cooling system were tested experimentally. Although the turbine was not greatly matched with the ejector system, 53W electricity power output was obtained. It would be interesting to design the combined system with proper turbine and suitable ejector nozzle size and explore the potentials of driving the ejector by the turbine exhaust. If low grade energy is chosen as the main driving force to

power the turbine, the appropriate matching between the turbine exhausts and the ejector system remains to be the research hot point. Turbine exhausts with properly designed temperature and mass flow rate will be crucial to run the ejector cooling system. Moreover, other organic fluids, like R143a and R142b, can be tested as the working fluids for the combined system. Their working performance could be compared with that of water, and a better candidate can be determined for the combined system. If the combined power system proved to function stably in the lab, it is worth building up the full size model on site. The cooling effect and power generation condition can be monitored under the scenario of daily building energy requirements. The pros and cons of the combined system incorporated with the building service systems can offer better guidance for the further system design and improvement.

One obstacle which brings forward to the researchers is the relatively low compression ratio (2-3) of the ejector. Some of the working fluids which require higher compression ratio can thus barely apply their applications in the ejector system. In order to improved the performance of ejector system, binary fluids ejector (BFE) was introduced by Ralph and Schlichtig[143] half a century ago. BFE with azeotropic mixtures is believed to achieve 30-50% performance improvement compared with conventional single fluid ejector [144, 145]. However, the working mechanism and the mixing process of the two fluids inside ejector are hardly studied by researchers. The experimental results of binary ejector are hardly available from the literature. These areas remain to be interesting topics for future research.

REFERENCES

[1] Adnott J. Energy Efficiency of Room Air-Conditioners (EERAC) Study. Directorate General for Energy (DGXVII) of the Commission of the European Communities. 1999.

[2] wallonne LRg. La consommation e´nerge´ tique de nos ba^timents, un enjeu crucial pour l'avenir. http://energiewalloniebe. 2006.

[3] (IEA) IEA. Climate policy uncertainty and investement risk,. Paris: International Energy Agency. 2007a.

[4] L. Zhang, Akiyama T. How to recuperate industrial waste heat beyond time and space. International Journal of Exergy. 2009;6:214-27.

[5] Gosney W. Principle of refrigeration. Cambridge University Press. 1982.

[6] Chen X, Omer S, Worall M, Riffat S. Recent developments in ejector refrigeration technologies. Renewable and Sustainable Energy Reviews. 2013;19:629-51.

[7] El-Dessouky H, Ettouney H, Alatiqi I, Al-Nuwaibit G. Evaluation of steam jet ejectors. Chemical Engineering and Processing: Process Intensification. 2002;41:551-61.

[8] Pianthong K, Seehanam W, Behnia M, Sriveerakul T, Aphornratana S. Investigation and improvement of ejector refrigeration system using computational fluid dynamics technique. Energy Conversion and Management. 2007;48:2556-64.

[9] Chunnanond K, Aphornratana S. An experimental investigation of a steam ejector refrigerator: the analysis of the pressure profile along the ejector. Applied Thermal Engineering. 2004;24:311-22.

[10] Selvaraju A, Mani A. Experimental investigation on R134a vapour ejector refrigeration system. International Journal of Refrigeration. 2006;29:1160-6.

[11] Sankarlal T, Mani A. Experimental investigations on ejector refrigeration system with ammonia. Renewable Energy. 2007;32:1403-13.

[12] Chaiwongsa P, Wongwises S. Experimental study on R-134a refrigeration system using a two-phase ejector as an expansion device. Applied Thermal Engineering. 2008;28:467-77.

[13] YapIcI R. Experimental investigation of performance of vapor ejector refrigeration system using refrigerant R123. Energy Conversion and Management. 2008;49:953-61.

[14] Ma X, Zhang W, Omer SA, Riffat SB. Experimental investigation of a novel steam ejector refrigerator suitable for solar energy applications. Applied Thermal Engineering. 2010;30:1320-5.

[15] Cizungu K, Mani A, Groll M. Performance comparison of vapour jet refrigeration system with environment friendly working fluids. Applied Thermal Engineering. 2001;21:585-98.

[16] YapIcI R, Ersoy HK, Aktoprakoglu A, HalkacI HS, Yigit O. Experimental determination of the optimum performance of ejector refrigeration system depending on ejector area ratio. International Journal of Refrigeration. 2008;31:1183-9.

[17] Sun D-W. Variable geometry ejectors and their applications in ejector refrigeration systems. Energy. 1996;21:919-29.

[18] Ersoy HK, Yalcin S, Yapici R, Ozgoren M. Performance of a solar ejector cooling-system in the southern region of Turkey. Applied Energy. 2007;84:971-83.

[19] YapIcI R, Ersoy HK. Performance characteristics of the ejector refrigeration system based on the constant area ejector flow model. Energy Conversion and Management. 2005;46:3117-35.

[20] Rusly E, Aye L, Charters WWS, Ooi A. CFD analysis of ejector in a combined ejector cooling system. International Journal of Refrigeration. 2005;28:1092-101.

[21] Nehdi E, Kairouani L, Elakhdar M. A solar ejector air-conditioning system using environment-friendly working fluids. International Journal of Energy Research. 2008;32:1194-201.

[22] Vidal H, Colle S. Simulation and economic optimization of a solar assisted combined ejector-vapor compression cycle for cooling applications. Applied Thermal Engineering.30:478-86.

[23] Huang BJ, Chang JM, Petrenko VA, Zhuk KB. A SOLAR EJECTOR COOLING SYSTEM USING REFRIGERANT R141b. Solar Energy. 1998;64:223-6.

[24] Khaliq A, Agrawal BK, Kumar R. First and second law investigation of waste heat based combined power and ejector-absorption refrigeration cycle. International Journal of Refrigeration. 2012;35:88-97.

[25] Elakhdar M, Nehdi E, Kairouani L, Tounsi N. Simulation of an ejector used in refrigeration systems. International Journal of Refrigeration. 2011;34:1657-67.

[26] Huang BJ, Chang JM, Wang CP, Petrenko VA. A 1-D analysis of ejector performance. International Journal of Refrigeration. 1999;22:354-64.

[27] Aidoun Z, Ouzzane M. The effect of operating conditions on the performance of a supersonic ejector for refrigeration. International Journal of Refrigeration. 2004;27:974-84.

[28] Selvaraju A, Mani A. Analysis of an ejector with environment friendly refrigerants. Applied Thermal Engineering. 2004;24:827-38.

[29] Jia Y, Wenjian C. Area ratio effects to the performance of air-cooled ejector refrigeration cycle with R134a refrigerant. Energy Conversion and Management. 2012;53:240-6.

[30] Alexis GK, Karayiannis EK. A solar ejector cooling system using refrigerant R134a in the Athens area. Renewable Energy. 2005;30:1457-69.

[31] Hernandez JI, Dorantes RJ, Best R, Estrada CA. The behaviour of a hybrid compressor and ejector refrigeration system with refrigerants 134a and 142b. Applied Thermal Engineering. 2004;24:1765-83.

[32] Yu J, Chen H, Ren Y, Li Y. A new ejector refrigeration system with an additional jet pump. Applied Thermal Engineering. 2006;26:312-9.

[33] Yu J, Du Z. Theoretical study of a transcritical ejector refrigeration cycle with refrigerant R143a. Renewable Energy.35:2034-9.

[34] Kairouani L, Elakhdar M, Nehdi E, Bouaziz N. Use of ejectors in a multi-evaporator refrigeration system for performance enhancement. International Journal of Refrigeration. 2009;32:1173-85.

[35] Yu J, Zhao H, Li Y. Application of an ejector in autocascade refrigeration cycle for the performance improvement. International Journal of Refrigeration. 2008;31:279-86.

[36] Gould D. Theoretical Analysis of the Steam Pressure Exchange Ejector for an Automotive Air Conditioning Application. PhD thesis, University of Vermont, USA. 2009.

[37] Khalil A, Fatouh M, Elgendy E. Ejector design and theoretical study of R134a ejector refrigeration cycle. International Journal of Refrigeration. 2011;34:1684-98.

[38] Roman R, Hernandez JI. Performance of ejector cooling systems using low ecological impact refrigerants. International Journal of Refrigeration. 2011;34:1707-16.

[39] Pridasawas W, Lundqvist P. A year-round dynamic simulation of a solar-driven ejector refrigeration system with iso-butane as a refrigerant. International Journal of Refrigeration. 2007;30:840-50.

[40] Boumaraf L, Lallemand A. Modeling of an ejector refrigerating system operating in dimensioning and off-dimensioning conditions with the working fluids R142b and R600a. Applied Thermal Engineering. 2009;29:265-74.

[41] Butterworth MD, Sheer TJ. High-pressure water as the driving fluid in an ejector refrigeration system. Applied Thermal Engineering. 2007;27:2145-52.

[42] Varga S, Oliveira AC, Diaconu B. Numerical assessment of steam ejector efficiencies using CFD. International Journal of Refrigeration. 2009;32:1203-11.

[43] Varga S, Oliveira A, Diaconu B. Analysis of a solar-assisted ejector cooling system for air conditioning. Int J Low-Carbon Tech. 2009;4:2-8.

[44] Eames IW, Aphornratana S, Haider H. A theoretical and experimental study of a small-scale steam jet refrigerator. International Journal of Refrigeration. 1995;18:378-86.

[45] Cizungu K, Groll M, Ling ZG. Modelling and optimization of two-phase ejectors for cooling systems. Applied Thermal Engineering. 2005;25:1979-94.

[46] Sozen A, Ozalp M, Arcaklioglu E. Prospects for utilisation of solar driven ejector-absorption cooling system in Turkey. Applied Thermal Engineering. 2004;24:1019-35.

[47] Wang J, Dai Y, Zhang T, Ma S. Parametric analysis for a new combined power and ejector-absorption refrigeration cycle. Energy. 2009;34:1587-93.

[48] Eames IW, Ablwaifa AE, Petrenko V. Results of an experimental study of an advanced jet-pump refrigerator operating with R245fa. Applied Thermal Engineering. 2007;27:2833-40.

[49] Holton WC. Effect of molecular weight of entrained fluid on the performance of steam-jet ejector. ASME Trans October. 1951:905-10.

[50] Riffat SB, Gan G, Smith S. Computational fluid dynamics applied to ejector heat pumps. Applied Thermal Engineering. 1996;16:291-7.

[51] Riffat SB, Omer SA. CFD modelling and experimental investigation of an ejector refrigeration system using methanol as the working fluid. Int J Energy Res. 2001;25:115-28.

[52] Bartosiewicz Y, Aidoun Z, Desevaux P, Mercadier Y. Numerical and experimental investigations on supersonic ejectors. International Journal of Heat and Fluid Flow. 2005;26:56-70.

[53] Sriveerakul T, Aphornratana S, Chunnanond K. Performance prediction of steam ejector using computational fluid dynamics: Part 1. Validation of the CFD results. International Journal of Thermal Sciences. 2007;46:812-22.

[54] Riffat SB, Everitt P. Experimental and CFD modelling of an ejector system for vehicle air conditioning. J Inst Energy. 1999;72:41-7.

[55] Varga S, Oliveira AC, Diaconu B. Influence of geometrical factors on steam ejector performance - A numerical assessment. International Journal of Refrigeration. 2009;32:1694-701.

[56] Zhu Y, Cai W, Wen C, Li Y. Numerical investigation of geometry parameters for design of high performance ejectors. Applied Thermal Engineering. 2009;29:898-905.

[57] Aphornratana S, Eames IW. A small capacity steam-ejector refrigerator: experimental investigation of a system using ejector with movable primary nozzle. International Journal of Refrigeration. 1997;20:352-8.

[58] Guo J, Shen HG. Modeling solar-driven ejector refrigeration system offering air conditioning for office buildings. Energy and Buildings. 2009;41:175-81.

[59] Bejan A, Vargas JVC, Sokolov M. Optimal allocation of a heat-exchanger inventory in heat driven refrigerators. International Journal of Heat and Mass Transfer. 1995;38:2997-3004.

[60] Diaconu BM, Varga S, Oliveira AC. Numerical simulation of a solar-assisted ejector air conditioning system with cold storage. Energy.36:1280-91.

[61] Dennis M, Garzoli K. Use of variable geometry ejector with cold store to achieve high solar fraction for solar cooling. International Journal of Refrigeration. 2011;34:1626-32.

[62] Mark Worall IWE. An experimental investigation of a jet-pump thermal (ice) storage system powered by low-grade heat. Proceedings of the 3rd International Conference on Sustainable Energy Technologies, Nottingham, UK, 28-30 June. 2004.

[63] Eames IW, Worall M, Wu S. An experimental investigation into the integration of a jet-pump refrigeration cycle and a novel jet-spay thermal ice storage system. Applied Thermal Engineering.

[64] Zhang N, Lior N. Methodology for thermal design of novel combined refrigeration/power binary fluid systems. International Journal of Refrigeration. 2007;30:1072-85.

[65] G.K A. Performance parameters for the design of a combined refrigeration and electrical power cogeneration system. International Journal of Refrigeration. 2007;30:1097-103.

[66] Zheng B, Weng YW. A combined power and ejector refrigeration cycle for low temperature heat sources. Solar Energy.84:784-91.

[67] Wang J, Dai Y, Gao L. Parametric analysis and optimization for a combined power and refrigeration cycle. Applied Energy. 2008;85:1071-85.

[68] Godefroy J, Boukhanouf R, Riffat S. Design, testing and mathematical modelling of a small-scale CHP and cooling system (small CHP-ejector trigeneration). Applied Thermal Engineering. 2007;27:68-77.

[69] Shen S, Qu X, Zhang B, Riffat S, Gillott M. Study of a gas-liquid ejector and its application to a solar-powered bi-ejector refrigeration system. Applied Thermal Engineering. 2005;25:2891-902.

[70] Wang F, Shen S. A novel solar bi-ejector refrigeration system and the performance of the added injector with different structures and operation parameters. Solar Energy. 2009;83:2186-94.

[71] Sokolov M, Hershgal D. Enhanced ejector refrigeration cycles powered by low grade heat. Part 1. Systems characterization. International Journal of Refrigeration. 1990;13:351-6.

[72] Sokolov M, Hershgal D. Solar-powered compression-enhanced ejector air conditioner. Solar Energy. 1993;51:183-94.

[73] Arbel A, Sokolov M. Revisiting solar-powered ejector air conditioner--the greener the better. Solar Energy. 2004;77:57-66.

[74] Zhu Y, Jiang P. Hybrid vapor compression refrigeration system with an integrated ejector cooling cycle. International Journal of Refrigeration. 2012;35:68-78.

[75] Chen S-L, Wang P-P, Lee T-S. An experimental investigation of nucleation probability of supercooled water inside cylindrical capsules. Experimental Thermal and Fluid Science. 1998;18:299-306.

[76] Fukai J, Kanou M, Kodama Y, Miyatake O. Thermal conductivity enhancement of energy storage media using carbon fibers. Energy Conversion and Management. 2000;41:1543-56.

[77] Alvarado JL, Marsh C, Sohn C, Phetteplace G, Newell T. Thermal performance of microencapsulated phase change material slurry in turbulent flow under constant heat flux. International Journal of Heat and Mass Transfer. 2007;50:1938-52.

[78] Diaconu BM, Varga S, Oliveira AC. Experimental assessment of heat storage properties and heat transfer characteristics of a phase change material slurry for air conditioning applications. Applied Energy. 2010;87:620-8.

[79] Inaba H, Zhang Y, Horibe A, Haruki N. Numerical simulation of natural convection of latent heat phase-change-material microcapsulate slurry packed in a horizontal rectangular enclosure heated from below and cooled from above. Heat and Mass Transfer/Waerme- und Stoffuebertragung. 2007;43:459-70.

[80] Zhang Y, Hu X, Wang X. Theoretical analysis of convective heat transfer enhancement of microencapsulated phase change material slurries. Heat and Mass Transfer/Waerme- und Stoffuebertragung. 2003;40:59-66.

[81] Marín JM, Zalba B, Cabeza LF, Mehling H. Improvement of a thermal energy storage using plates with paraffin–graphite composite. International Journal of Heat and Mass Transfer. 2005;48:2561-70.

[82] Erek A, Ilken Z, Acar MA. Experimental and numerical investigation of thermal energy storage with a finned tube. International Journal of Energy Research. 2005;29:283-301.

[83] Ermis K, Erek A, Dincer I. Heat transfer analysis of phase change process in a finned-tube thermal energy storage system using artificial neural network. International Journal of Heat and Mass Transfer. 2007;50:3163-75.

[84] Zhou G, Zhang Y, Zhang Q, Lin K, Di H. Performance of a hybrid heating system with thermal storage using shape-stabilized phase-change material plates. Applied Energy. 2007;84:1068-77.

[85] Zhou G, Yang Y, Wang X, Zhou S. Numerical analysis of effect of shape-stabilized phase change material plates in a building combined with night ventilation. Applied Energy. 2009;86:52-9.

[86] Martin V, He B, Setterwall F. Direct contact PCM–water cold storage. Applied Energy. 2010;87:2652-9.

[87] Chen B, Wang X, Zeng R, Zhang Y, Wang X, Niu J, et al. An experimental study of convective heat transfer with microencapsulated phase change material suspension: Laminar flow in a circular tube under constant heat flux. Experimental Thermal and Fluid Science. 2008;32:1638-46.

[88] Felix Regin A, Solanki SC, Saini JS. An analysis of a packed bed latent heat thermal energy storage system using PCM capsules: Numerical investigation. Renewable Energy. 2009;34:1765-73.

[89] Ismail KAR, Moraes RIR. A numerical and experimental investigation of different containers and PCM options for cold storage modular units for domestic applications. International Journal of Heat and Mass Transfer. 2009;52:4195-202.

[90] Diaconu BM. Energy analysis of a solar-assisted ejector cycle air conditioning system with low temperature thermal energy storage. Renewable Energy. 2012;37:266-76.

[91] Fang G, Wu S, Liu X. Experimental study on cool storage air-conditioning system with spherical capsules packed bed. Energy and Buildings. 2010;42:1056-62.

[92] Helm M, Keil C, Hiebler S, Mehling H, Schweigler C. Solar heating and cooling system with absorption chiller and low temperature latent heat storage: Energetic performance and operational experience. International Journal of Refrigeration. 2009;32:596-606.

[93] Omer SA, Riffat SB, Ma X. Experimental investigation of a thermoelectric refrigeration system employing a phase change material integrated with thermal diode (thermosyphons). Applied Thermal Engineering. 2001;21:1265-71.

[94] Riffat SB, Omer SA, Ma X. A novel thermoelectric refrigeration system employing heat pipes and a phase change material: an experimental investigation. Renewable Energy. 2001;23:313-23.

[95] Henning HM, Erpenbeck T, Hindenburg C, Santamaria IS. The potential of solar energy use in desiccant cooling cycles. International Journal of Refrigeration. 2001;24:220-9.

[96] Halliday SP, Beggs CB, Sleigh PA. The use of solar desiccant cooling in the UK: a feasibility study. Applied Thermal Engineering. 2002;22:1327-38.

[97] Mei L, Infield D, Eicker U, Loveday D, Fux V. Cooling potential of ventilated PV façade and solar air heaters combined with a desiccant cooling machine. Renewable Energy. 2006;31:1265-78.

[98] Gommed K, Grossman G. Experimental investigation of a liquid desiccant system for solar cooling and dehumidification. Solar Energy. 2007;81:131-8.

[99] Yadav YK. Vapour-compression and liquid-desiccant hybrid solar space-conditioning system for energy conservation. Renewable Energy. 1995;6:719-23.

[100] Jia CX, Dai YJ, Wu JY, Wang RZ. Analysis on a hybrid desiccant air-conditioning system. Applied Thermal Engineering. 2006;26:2393-400.

[101] Fathalah K, Aly SE. Study of a waste heat driven modified packed desiccant bed dehumidifier. Energy Conversion and Management. 1996;37:457-71.

[102] Ma Q, Wang RZ, Dai YJ, Zhai XQ. Performance analysis on a hybrid air-conditioning system of a green building. Energy and Buildings. 2006;38:447-53.

[103] Zadpoor AA, Golshan AH. Performance improvement of a gas turbine cycle by using a desiccant-based evaporative cooling system. Energy. 2006;31:2652-64.

[104] Sözen A, Altıparmak D, Usta H. Development and testing of a prototype of absorption heat pump system operated by solar energy. Applied Thermal Engineering. 2002;22:1847-59.

[105] De Francisco A, Illanes R, Torres JL, Castillo M, De Blas M, Prieto E, et al. Development and testing of a prototype of low-power water–ammonia absorption equipment for solar energy applications. Renewable Energy. 2002;25:537-44.

[106] Syed A, Izquierdo M, Rodríguez P, Maidment G, Missenden J, Lecuona A, et al. A novel experimental investigation of a solar cooling system in Madrid. International Journal of Refrigeration. 2005;28:859-71.

[107] Liu YL, Wang RZ. Performance prediction of a solar/gas driving double effect LiBr–H2O absorption system. Renewable Energy. 2004;29:1677-95.

[108] Keenan J, Neumann E, F. L. . An investigation of ejector design by analysis and experiment. ASME J Appl MechTrans. 1950;72.

[109] Munday J, Bagster D. A new theory applied to steamjet refrigeration. Ind Eng Chem Process Des Dev. 1977;16:442-51.

[110] DEFRA. Greenhous gas impacts of food retailing. Final report, FO405. 2008.

[111] Devotta S, Sicars S. Special Report: Safeguarding the Ozone Layer and the Global Climate System: Refrigeration. Cambridge University Press. 2005.

[112] IPCC. Climate Change: The Scientific Basis, Chapter 6. Cambridge University Press. 2001.

[113] Koehler J, Tegethoff W, Westphalen D. Absorption refrigeration system for mobile applications utilizing exhaust gases. Heat and Mass Transfer. 1997;32:333-40.

[114] Boatto P, Boccaletti C, Cerri G. Absorption refrigeration system for mobile applications utilizing exhaust gases part 1: tests on the exhaust system for a spark-ignition system. Proc Inst Mech Eng D. 2000;214:979-82.

[115] Boatto P, Boccaletti C, G C. Absorption refrigeration system for mobile applications utilizing exhaust gases part 2: the automotive absorption system. Proc Inst Mech Eng D. 2000:983-89.

[116] Izquierdo M, Arostegui J, Martin L. Mobile water-lithium bromide absorption machine using the engine exhaust gases as energy source. IIR-B2 Conference: New Applications of Natural Working Fluids in Refrigeration and Air-Conditioning, Hannover, Germany. 1994.

[117] H.Inokuty. Graphical method of finding compression pressure of CO2 refrigerating machine for maximum coefficient of performance. The Fifth International Congress of Refrigeration, Rome. 1928:p.p. 185-92.

[118] Worall M, Omer S, Riffat SB. A hybrid jet-pump CO2 compression system for transport refrigeration. International Journal of Low-Carbon Technologies. 2011;6:249-54.

[119] Klein S. Engineering equation solver, version 8.400, F-Chart Software, Middleton, WI, USA. 2008.

[120] Boatto P, Boccaletti C, Cerri G, Malvicino C. Internal combustion engine waste heat potential for an automotive absorption system of air conditioning Part 1: tests on the exhaust system of a spark-ignition engine. Proceedings of the I MECH E Part D Journal of Automobile Engineering. 2000:979-82.

[121] Daly S. Automotive air conditioning and climate control systems. Elsevier's Science & Technology Rights. 2006.

[122] Sari A, Kaygusuz K. Thermal performance of palmitic acid as a phase change energy storage material. Energy Conversion and Management. 2002;43:863-76.

[123] Belusko M BF. 140 – Design methodology of PCM thermal storage systems with parallel plates. 1st International congress on heating, cooling, and buildings, EUROSUN2008 Lisbon, Portugal. 2008.

[124] El-Dessouky H, Al-Juwayhel F. Effectiveness of a thermal energy storage system using phase-change materials. Energy Conversion and Management. 1997;38:601-17.

[125] POLES. Prospective outlook on long-term energy systems. Office for official oublications of the European Communities, Report EUR 17358 EN. 1996.

[126] Schnatbaum L. Solar thermal power plants. Eur Phys J Spec Top. 2009;176:127-40.

[127] Kaltschmitt M, Streicher W, Wiese A. Solar Thermal Power Plants. In: Kaltschmitt M, Streicher W, Wiese A, editors. Renewable Energy: Springer Berlin Heidelberg; 2007. p. 171-228.

[128] McVeigh JC. Sun power. An introduction to the applications of solar energy1977.

[129] Hung TC, Shai TY, Wang SK. A review of organic rankine cycles (ORCs) for the recovery of low-grade waste heat. Energy. 1997;22:661-7.

[130] Y. Ammar, S. Joyce, R. Norman, Y. Wang, Roskilly AP. Low grade thermal energy sources and uses from the process industry in the UK. Sustainable Thermal Energy Management in the Process Industries International Conference: Newcastle upon Tyne, UK. 2011.

[131] Roy P, Désilets M, Galanis N, Nesreddine H, Cayer E. Thermodynamic analysis of a power cycle using a low-temperature source and a binary NH3–H2O mixture as working fluid. International Journal of Thermal Sciences. 2010;49:48-58.

[132] Wang J, Dai Y, Sun Z. A theoretical study on a novel combined power and ejector refrigeration cycle. International Journal of Refrigeration. 2009;32:1186-94.

[133] Zheng B, Weng YW. A combined power and ejector refrigeration cycle for low temperature heat sources. Solar Energy. 2010;84:784-91.

[134] Habibzadeh A, Rashidi MM, Galanis N. Analysis of a combined power and ejector-refrigeration cycle using low temperature heat. Energy Conversion and Management. 2013;65:381-91.

[135] L. Lucas. IIR News. International Journal of Refrigeration. 1988;21:88.

[136] China Meteorological Data Sharing Service System. http://cdccmagovcn/shuju/index3jsp?tpcat=SURF&dsid=SURF_CLI_CHN_MUL_MMON_19712000_CES&pageid=3.

[137] Duffie. A, I D. Solar enegineering of thermal processes. 2006:P291.

[138] Atmaca I, Yigit A. Simulation of solar-powered absorption cooling system. Renewable Energy. 2003;28:1277-93.

[139] Riffat SB, Qiu G. Comparative investigation of thermoelectric air-conditioners versus vapour compression and absorption air-conditioners. Applied Thermal Engineering. 2004;24:1979-93.

[140] Mateus T, Oliveira AC. Energy and economic analysis of an integrated solar absorption cooling and heating system in different building types and climates. Applied Energy. 2009;86:949-57.

[141] Oliveira AC, Afonso C, Matos J, Riffat S, Nguyen M, Doherty P. A combined heat and power system for buildings driven by solar energy and gas. Applied Thermal Engineering. 2002;22:587-93.

[142] J.A. Duffle, Beckman WA. Solar engineering of Thermal Processes, second ed. John Wiley and Sons Inc, New York. 1991.

[143] Ralph C, Schlkmig R. Ejector type refrigeration system. Patent of United State, 3,199,310. 1965.

[144] Boumaraf L, Lallemand A. Performances d'une machine tritherme à éjecteur utilisant des mélanges de fluides frigorigènes. International Journal of Refrigeration. 1999;22:580-9.

[145] Dorantès R, Lallemand A. Influence de la nature des fluides, purs ou en mélanges non-azéotropiques, sur les performances d'une machine de climatisation à éjecto-compresseur. International Journal of Refrigeration. 1995;18:21-30.

LIST OF PUBLICATIONS

Published paper:

X. Chen, S.A. Omer, M. Worall, S.B. Riffat. Recent developments in ejector refrigeration technologies. *Renewable and Sustainable Energy Reviews*, Vol. 19, March 2013, pages 629-651.

X. Chen, M. Worall, S.A. Omer, Y. Su, S.B. Riffat. Theoretical studies of a hybrid ejector CO_2 compression cooling system for vehicles and preliminary experimental investigations of an ejector cycle. *Applied Energy*, Vol. 102, February 2013, pages 931-942.

X. Chen, M. Worall, S.A. Omer, Y. Su, S.B. Riffat. A theoretical and experimental study of a steam ejector refrigeration system. *11th International Conference on Sustainable Energy Technologies*, Canada, 2012

X. Chen, S.A. Omer, Y. Su, S.B. Riffat. Simulations of solar-driven combined power and ejector system and economic analysis. *12th International Conference on Sustainable Energy Technologies*, Hongkong, 2013

X. Chen, S.A. Omer, Y. Su, S.B. Riffat. Experimental investigation on finned tube PCM cold storage systems integrated with ejector cooling system. *12th International Conference on Sustainable Energy Technologies*, Hongkong, 2013

Submitted paper:

X. Chen, M. Worall, S.A. Omer, Y. Su, S.B. Riffat. Experimental investigation on PCM cold storage integrated with ejector cooling system. *Applied Thermal Engineering*. Under review.